Resistive states of superconducting channels in an alternating electromagnetic field (Review)

V. M. Dmitriev*

B. Verkin Institute for Low Temperature Physics and Engineering, National Academy of Sciences of Ukraine, pr. Lenina 47, 61164 Kharkov, Ukraine; International Laboratory of High Magnetic Fields and Low Temperatures, 95 Gajowicka Str., 53421 Wroclaw, Poland

I. V. Zolochevskiĭ and E. V. Khristenko

B. Verkin Institute for Low Temperature Physics and Engineering, National Academy of Sciences of Ukraine, pr. Lenina 47, 61164 Kharkov, Ukraine

(Submitted November 7, 2000)
Fiz. Nizk. Temp. **27**, 227–252 (March 2001)

The processes that determine the structure and properties of the resistive state of superconducting channels having a uniform distribution of the current and order parameter over their transverse cross section are discussed. Particular attention is devoted to the resistive state arising when an external alternating electromagnetic field is applied to the superconductor. The current, temperature, frequency, and power characteristics of the resistive state are examined. The necessary information about the NS boundary and phase-slip centers is given, and the known results for high-T_c superconducting materials are presented. © *2001 American Institute of Physics.* [DOI: 10.1063/1.1355514]

INTRODUCTION

The term ''superconducting channels'' is commonly applied to superconducting samples whose transverse dimensions are smaller than the Ginzburg–Landau coherence length $\xi(T)$ and the magnetic field penetration depth $\lambda(T)$. When these conditions are satisfied, the electric current density and order parameter are uniformly distributed over the cross section of the sample. These requirements are satisfied by thin films $\sim$100 nm thick and about one micron wide or by whiskers ~ 1 μm in diameter. The length of the samples is ordinarily much larger than $\xi(T)$ and $\lambda(T)$ and ranges from tens to hundreds of microns. These are in essence quasi-one-dimensional structures, which are interesting primarily in that magnetic flux vortices cannot form in them, and so they are free of the resistivity due to the motion of vortices in the direction transverse to the sample. This raises the question of the nature of the resistivity that arises in such samples when direct (dc) or alternating (ac) currents greater than the critical values are passed through them. Studies of the resistive states due to the passage of dc current have yielded unexpected information about the very nature of superconductivity and have revealed the essence of many phenomena of nonequilibrium superconductivity. Good reviews are available on some of this research (see, e.g., Refs. 1–4).

Research on the resistive states arising upon the passage of ac current is no less interesting and has also yielded unexpected results. As far as we know, the results obtained in this area of research have as yet to be systematized in a published review. The present article was undertaken to fill this gap.

Since the exposition of the problems due to the flow of ac currents along a channel require information about the effects due to dc current, the necessary information on that topic will be included. In this review preference will be given to experimental results, particularly since in many cases the theory does not completely describe the experimental results or is lacking altogether. One of the goals of this review is precisely to get theorists interested in the ac problem.

1. THEORY OF THE RESISTIVE CURRENT STATE OF A SUPERCONDUCTING CHANNEL

1.1. Charge imbalance and the penetration depth of a longitudinal dc electric field in a superconductor

In elucidating the structure and properties of the resistive current state we will require certain concepts that are best introduced by considering the passage of current through the boundary between a normal metal and a superconductor (an NS boundary). The features of such a boundary were first pointed out in Refs. 5 and 6 in a study of the resistance of a superconductor in an intermediate state.

The excited states of a superconductor, unlike those of the electronic system of a metal in the normal state, are separated from the ground state (condensate) by an energy gap Δ. The energy of a quasiparticle in a state with momentum $\mathbf{k}$ can be written[7,8]

$$E_k=(\varepsilon_k^2+\Delta^2)^{1/2}, \tag{1.1}$$

where $\varepsilon_k=\hbar^2(k^2-k_F^2)/2m=[(\hbar^2k^2/2m)-E_F]$ is the energy of a quasiparticle excitation (electron or hole) in the normal metal, measured from the Fermi level E_F. Since the energy E_k for any type of excitation in a superconductor is positive, the spectrum of excitations can be represented in the form an electronlike branch ($k>k_F$) and a holelike branch ($k<k_F$). The symmetry of the occupation of the branches of the spectrum (an imbalance of the charge of the branches) can be broken by an outside influence that leads to injection of quasiparticles into the superconductor. Let us consider the case

when a dc current is flowing through an NS boundary. Here the electrons having energies higher than Δ penetrate into the superconductor, disrupting the balance of the occupation of the branches of the quasiparticle spectrum by overpopulating the electron branch, which leads to an excess quasiparticle charge Q in the superconductor. By virtue of the overall electrical neutrality of the metal, this charge is compensated by a decrease of the charge of the condensate, which leads to a shift of the chemical potential μ_s of the Cooper pairs relative to the Fermi energy by an amount proportional to this charge:[7]

$$Q=2N(0)(E_F-\mu_s), \tag{1.2}$$

where $N(0)$ is the density of states at the Fermi level.

Since the excess quasiparticle charge Q is a function of the spatial coordinate x, it is clear that the chemical potential μ_s will also depend on x. It follows that a superconductor can support the existence of an electric field **E** that can be written in gradient-invariant form as[9,10]

$$\mathbf{E}=\frac{1}{e}\frac{\partial \mathbf{p}_s}{\partial t}-\frac{1}{e}\nabla\Phi. \tag{1.3}$$

Here $\mathbf{p}=m\mathbf{v}_s=1/2\hbar\nabla\chi-e\mathbf{A}/c$ is the momentum of the superconducting condensate, $\Phi=1/2\hbar(\partial\chi/\partial t)+e\varphi$ is the gradient-invariant potential, which is the difference of the chemical potential of the quasiparticles $\mu_n=E_F+e\varphi$ and the pair chemical potential $\mu_s=E_F-(1/2)\hbar(\partial\chi/\partial t)$; χ is the phase of the complex superconducting order parameter, and **A** and φ are the usual electromagnetic potentials. The first term in (1.3) is due to the inertia of the electrons of the condensate and is important in in the case of ac currents or inductive excitation of the field. When a specified dc current is flowing through an NS boundary, one can limit consideration to the second term in (1.3):

$$\mathbf{E}=-\frac{1}{e}\nabla\Phi. \tag{1.4}$$

In the neighborhood of the critical temperature T_c, where the gap is small ($\Delta<k_BT$, k_BT is the characteristic energy of the quasiparticles), one can neglect the change in the chemical potential of the quasiparticles in comparison with the change in the chemical potential of the superconducting electrons. Since for $T\to T_c$ there are few paired electrons and a great many normal electrons, removing a certain number of pairs from the condensate and transferring them to the collective of normal electrons will cause a much greater change in the properties of the condensate than in the properties of the collective of normal electrons. Therefore, using (1.2), we can write expression (1.4) for **E** in the form:

$$\mathbf{E}=-\frac{1}{2eN(0)}\nabla Q. \tag{1.5}$$

Thus an electric field arises in a superconductor under nonequilibrium conditions in the presence of a gradient of the quasiparticle charge; however, this field will not accelerate the condensate, since it is compensated by the gradient of the invariant potential Φ. The presence of a steady-state nonequilibrium quasiparticle charge in a certain region of the superconductor means that a flux of quasiparticles is continuously entering this region, carrying a certain charge which, on relaxing, passes over into the condensate. This condition is expressed by the simple relation

$$\operatorname{div} j_n=-eQ/\tau_Q, \tag{1.6}$$

where j_n is the normal component of the total current density, and τ_Q is the relaxation time of the charge imbalance. In the case when the temperature is close to T_c, one can write Ohm's law for the quasiparticles in the usual form:

$$\mathbf{j}_n=\sigma\mathbf{E}, \tag{1.7}$$

where σ is the normal conductivity at low temperatures. Formulas (1.5)–(1.7) lead to a closed equation for Q:

$$\nabla^2Q=\frac{1}{l_E^2}Q. \tag{1.8}$$

Here

$$l_E^2=\sigma\tau_Q/2e^2N(0). \tag{1.9}$$

Since the conductivity σ of the normal metal can be written in the form[11]

$$\sigma=\frac{2}{3}e^2N(0)l_iv_F, \tag{1.10}$$

where l_i is the mean free path of an electron and v_F is the velocity of an electron at the Fermi surface, we finally get

$$l_E=\left(\frac{v_Fl_i\tau_Q}{3}\right)^{1/2}=(D\tau_Q)^{1/2}. \tag{1.11}$$

Here $D=(1/3)v_Fl_i$ is the diffusion coefficient of electrons with mean free path l_i. The depth l_E to which normal electrons are drawn into the superconductor by the electric field from the normal metal is called the diffusion length or penetration depth of the longitudinal electric field. This gives rise to an additional resistance which for $\Delta<k_BT$ has the form[12–14]

$$R=\rho l_E/S, \tag{1.12}$$

where $\rho=\sigma^{-1}$ is the normal resistivity at low temperatures, and S is the cross-sectional area of the channel. The quantity τ_Q, which determines the penetration depth l_E, was first estimated theoretically and measured experimentally in Refs. 8 and 15. In Refs. 8 and 16, τ_Q was measured using a normal metal–insulator–superconductor tunnel junction. When current is passed through the junction from the normal metal region, nonequilibrium electrons are injected into the superconducting electrode, leading to a difference in the populations of the branches of the excitation spectrum. The value of τ_Q was calculated from the potential difference between a point above the tunnel junction and a remote part of the superconducting region.

The process restoring the balance of populations between the branches of the quasiparticle spectrum in the absence of magnetic impurities is governed by the elastic (on impurities) and inelastic (on phonons) scattering of excitations. However, not all scattering events (elastic or inelastic) lead to charge relaxation. The most important events are those for excitations with energies E_k in the interval $\Delta\leqslant E_k\leqslant 2\Delta$. This leads to a difference between τ_Q and τ_ε by a factor of Δ/k_BT, since the total number of excitations is of

the order of k_BT. A more precise calculation of the relaxation time of the quasiparticle charge gives[17,18]

$$\tau_Q=\frac{4k_BT}{\pi\Delta}\left(\frac{\tau_\varepsilon}{2\Sigma}\right)^{1/2}. \tag{1.13}$$

Here

$$\Sigma=\frac{1}{2\tau_\varepsilon}+\frac{D}{2}\left(\frac{4m^2v_s^2}{\hbar^2}-\frac{1}{\Delta}\frac{\partial^2\Delta}{\partial\mathbf{r}^2}\right); \tag{1.14}$$

τ_ε is the inelastic scattering time for electrons on the Fermi surface, $2mv_s$ is the superconducting momentum, and $\mathbf{r}$ is the spatial variable.

If the relaxation of the charge imbalance is governed by inelastic scattering, then[12,13]

$$\tau_Q=\frac{4k_BT}{\pi\Delta}\tau_\varepsilon, \tag{1.15}$$

and, consequently, at temperatures close to critical, where $\Delta\approx 3.16k_BT_c(1-T/T_c)^{1/2}$, $\tau_Q\propto(1-T/T_c)^{-1/2}$. An estimate of the superfluid velocity in the case when the superconducting current assumes the critical value gives[17,18]

$$\tau_Q(j_c)=(4k_BT/\pi\Delta)(3\tau_\varepsilon\tau_{GL})^{1/2}, \tag{1.16}$$

where $\tau_{GL}=\hbar/8k_B(T_c-T)$ is the Ginzburg–Landau time, which is related to the coherence length $\xi=(D\tau_{GL})^{1/2}$. If the bias current is set at the critical level for each temperature, then, as we see from (1.15), the relaxation time has the following temperature dependence:

$$\tau_Q\propto(1-T/T_c)^{-1}.$$

Let us consider the last term in (1.14). If the spatial dependence of the order parameter has the form $\Delta=\Delta_0[1-\exp(-x/\xi)]$ and the relaxation rate is given by $\Sigma_\xi=(2\tau_{GL})^{-1}$, then

$$\tau_Q=(4k_BT/\pi\Delta)(\tau_\varepsilon\tau_{GL})^{1/2}. \tag{1.17}$$

In this case the temperature dependence of τ_Q is the same as that given by expression (1.16). The temperature dependence of l_E will be discussed in more detail in Sec. 2.3.

Thus the passage of electric current through the boundary between a normal metal and a superconductor will give rise to an electric field in the superconductor which is damped over a distance l_E. Within a region of length l_E in the superconductor near the NS boundary the normal current will be converted to supercurrent, and the order parameter Δ is restored at a depth of the order of $\xi(T)$ in the superconductor.[19]

1.2. Models for the phase-slip centers

1.2.1. Phenomenological model of the resistive current state of a superconducting channel

The resistive state brought on in a superconducting channel by the passage of a dc current has by now been studied quite well experimentally and, thanks to the one-dimensionality of the problem, in which all of the quantities depend only on the coordinate along the sample, also theoretically.

Let us now give a brief chronology of the research topic dealing with the resistive current state of superconducting channels.

In a study of the influence of thermodynamic fluctuations on the critical current and critical temperature of superconducting tin whiskers in 1968, Webb and Warburton[20,21] observed a stepped character of the resistive transition. Regular voltage steps on the current–voltage (I–V) characteristics were also observed on uniform tin whiskers in Refs. 22 and 23 and on narrow tin strips in Ref. 24.

Three important features of the stepped I–V characteristics were noted: the values of the dynamic resistance on the sloped parts of the I–V characteristic are multiples; the continuations of the sloped parts of the I–V characteristic intersect at a single point on the current axis; and, there is no hysteresis, a fact which indicates that the stepped structure of the I–V characteristic is of the nature of a loop. In 1969, a new effect was reported: the generation of electromagnetic oscillations of relatively low frequencies ($\sim 10^7$ Hz) compared to those for the Josephson oscillations ($\sim 10^{10}$ Hz) by thin, narrow superconducting tin films (channels) when a dc electric current is passed through them.[25] This generation was observed when the film was in a resistive current state, and there was no current hysteresis at the point of generation on the I–V characteristic.

Thus by 1973 there had been observations of previously unknown properties of the resistive current state of superconducting channels which were in need of explanation. In that year Galaĭko, Dmitriev, and Churnilov[26] proposed the concept of dynamic phase separation of a current-carrying superconducting channel into quasinormal and superconducting regions. It was emphasized that this phase separation is of a dynamic and nonequilibrium nature. The resistivity exists over a wide range of currents, between the Ginzburg–Landau depairing current I_c and a certain upper critical current $I_{cn}\gg I_c$ at which the sample undergoes a transition to the normal state.

Here we should mention the large contributions to subsequent developments which were produced independently by groups at the B. Verkin Institute for Low Temperature Physics and Engineering in Kharkov, Ukraine and at Harvard University, in papers published in 1974–75 which contained the microscopic[10,27,28] and phenomenological[24] concepts concerning the basic features of the resistive state arising in a superconducting channel when a dc current is passed through it.

It was shown that the resistivity is a consequence of the formation and development, at currents $I_c<I<I_{cn}$, of a system of superconducting and quasinormal regions alternating along the sample. The latter are specific dynamic formations known as phase-slip centers (PSCs).

A characteristic feature of the I–V characteristics of superconducting channels is the presence of voltage jumps, at which the resistance of the sample changes by a multiple:

$$R=R_{d1}n, \tag{1.18}$$

where R_{d1} is the dynamic resistance on the linear I–V segment corresponding to the first PSC, and n is the number of PSCs in the channel. Figure 1 shows a typical I–V characteristic of a superconducting channel; it is characterized by the following main parameters: the critical current I_c, the

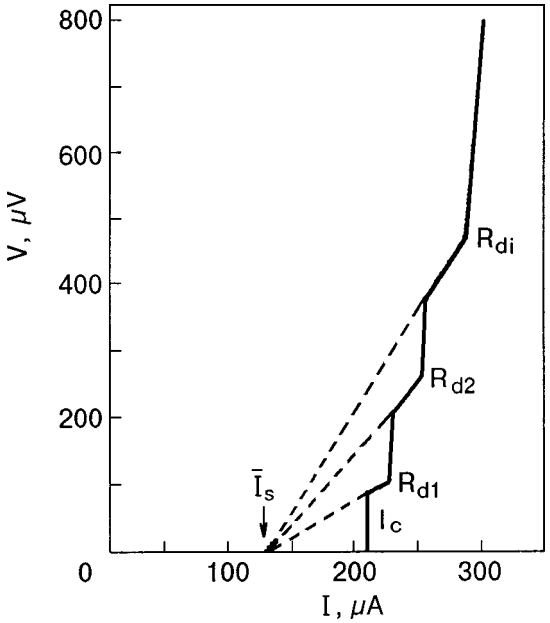

FIG. 1. Typical current–voltage characteristic of a homogeneous film superconducting channel (Sn-4) at a temperature $T/T_c=0.98$.

dynamic resistance R_{di} of the PSCs (here i is the number of the PSC, $i=1,2,3\ldots$), the cutoff current $\overline{I_s}$ at zero voltage, and the excess current $I_{\rm exc}$ at high voltages.

A phenomenological model of the resistive current state (the SBT model) was proposed in Ref. 24; this model united the idea of the quasiparticle diffusion[6] and the idea of phase-slip processes[29–31] into a picture of the PSCs. According to this model, a PSC consists of a core, with a size of the order of the coherence length $\xi(T)$, and diffusion tails extending away from it on both sides. In the core of the PSC the order parameter Δ and superconducting current oscillate, so that Δ goes to zero at certain points and the phase simultaneously jumps by 2π. The period of the oscillations is given by the Josephson relation[32]

$$\omega_J=2eV/\hbar, \tag{1.19}$$

as was confirmed experimentally in Refs. 24,33, and 34. When narrow tin films[24] and tin whiskers[33] were irradiated by an rf electromagnetic field, their I–V characteristics exhibited not only the voltage jumps typical of PSCs but also current steps at voltages related to the irradiation frequency by the Josephson relation (1.19). It should be noted that the size of the main current step decreased as the irradiation frequency was increased: while the I–V characteristic of a whisker clearly exhibited the main current step during irradiation at a frequency of 500 MHz, when the irradiation frequency was increased to 900 MHz for the same sample, the step was much smaller.[33] At irradiation frequencies of 10 GHz and higher it became difficult to discern the main current step, and the subharmonic steps had the same size as the main step.[24] The presence of the subharmonic current steps is indicative of anharmonicity in the oscillations of the order parameter and supercurrent. The time-averaged supercurrent flowing through the nonequilibrium region in which the voltage arises is equal to 0.5–0.8 times the local critical current of the superconducting channel, i.e., $\overline{I_s}=\beta I_c$. Here the normal current I_n flowing through a PSC is $I-\overline{I_s}=I-\beta I_c$. The nonequilibrium quasiparticles formed in the core of the PSC diffuse to a depth l_E, making for a quasiparticle distribution that is exponentially damped over a distance l_E. In this respect a PSC is analogous to an SNS structure.[34,35] Thus the dynamic resistance of the PSC is given by

$$R_{d1}=dV/dI=2l_E\rho/S. \tag{1.20}$$

The total voltage drop across one PSC, according to Ref. 24, is

$$V=2l_E\rho(I-\beta I_c)/S. \tag{1.21}$$

Numerous experiments done on narrow aluminum strips,[36–38] tin channels,[22,39–41] a tin–indium alloy,[42] and indium[43] have confirmed the basic ideas of the phenomenological model of the PSCs.[24] The value of l_E determined from the dynamic resistance of the PSC has the theoretically predicted dependence on the electron mean free path: $l_E\propto l_i$ (Ref. 43).

In Ref. 44 the spatial distribution of the chemical potentials of pairs μ_s and quasiparticles μ_n in the neighborhood of a PSC were measured by means of normal and superconducting tunnel probes placed close together in a tin superconducting channel. As expected, μ_s changed abruptly (jumped), since $\xi(T)$ was smaller than the distance between probes, whereas μ_n changed over a distance l_E from the center of the PSC by an exponential law. The predicted temperature dependence $l_E\propto(1-T/T_c)^{-1/4}$ was found, but because of thermal effects it was not always observed when l_E was determined from the dynamic resistance of the PSC. The value of l_E was in good agreement with the calculated value.

1.2.2. Microscopic theory of the phase-slip centers

The first microscopic theory of the resistive state of narrow superconducting channels was proposed in Refs. 10, 28, and 45–50. The general theoretical concepts from which this theory follows were first stated in Ref. 10, even before the advent of the phenomenological models; these concepts imply that, despite the absence of vortices, a resistive region should exist even in narrow superconducting channels, since, first, there exists a maximum uniform supercurrent I_c, and second, decreasing the current below a certain critical value I_{cn} in the normal state of the sample should lead to the Cooper instability and superconductive pairing of electrons. Because the mechanisms governing I_c and I_{cn} are different, these currents in general do not coincide. In Ref. 28 the kinetic equations were used to study the structure of the current state in a superconducting channel in a model based on microscopic phase separation with alternating superconducting and quasinormal regions along the channel. The values of the chemical potentials μ_s of neighboring superconducting segments differ by the potential difference $\delta\varphi$ between these segments. Thus in each superconducting part $\mathbf{E}=\nabla\Phi/e$ and $\mu_s=$const. The potential Φ is limited by compensation of the potential difference $\delta\varphi$ by the difference between the chemical potentials of pairs in neighboring superconducting segments. At points where the order parameter equals zero the phase coherence is disrupted, and μ_s, and with it Φ, undergoes a jump. This picture is illustrated schematically in Fig. 2. We see that the superconducting

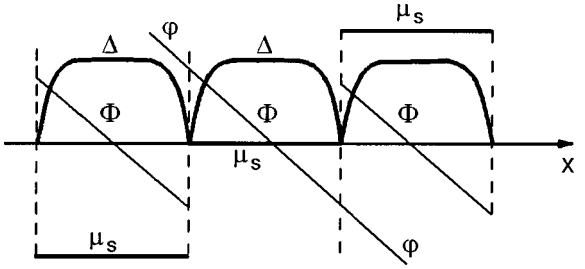

FIG. 2. Behavior of the order parameter Δ and potentials μ_s and Φ in the resistive current state model of Ref. 28.

parts have different pair chemical potentials μ_s. This means that the phase difference between neighboring segments will grow with time. Since the transition region between these segments, where $\Delta \approx 0$, has a width of the order of ξ, Josephson oscillations of the order parameter and supercurrent will arise.

In the dynamic model of a PSC[51–54] the nonstationary picture is considered right from the start. In this case the microscopic theory is based on analysis of the time-dependent microscopic equations of superconductivity. In the region of Josephson frequencies lower than $\Delta/\hbar$ and the energy relaxation rate, these equations were first obtained by Kramer and Watts-Tobin.[55,56] They have the form

$$-\frac{\pi}{8T}\sqrt{(4\tau_\varepsilon^2\Delta^2+\hbar^2)}\frac{\partial\Delta}{\partial t}+\frac{\pi\hbar}{8T}D\nabla^2\Delta + \frac{\pi\hbar}{8T}D\left(\frac{2e}{\hbar c}Q^*\right)^2\Delta+\frac{T_c-T}{T}\Delta-\frac{7\zeta(3)}{8\pi^2}\frac{\Delta^3}{T^2}=0; \tag{1.22}$$

$$\frac{1}{e\sqrt{(4\tau_\varepsilon^2\Delta^2+\hbar^2)}}\Delta^2\Phi-\frac{D}{\hbar c}\mathrm{div}(\Delta^2 Q^*)=0; \tag{1.23}$$

$$j=\varphi E+\frac{\sigma\pi\Delta^2}{2\hbar cT}Q^*, \tag{1.24}$$

where

$$E=\frac{1}{c}\frac{\partial Q^*}{\partial t}-\frac{1}{e}\nabla\Phi; \tag{1.25}$$

$$Q^*=(\hbar c/2e)\nabla\chi-A. \tag{1.26}$$

The solution of equations (1.22)–(1.26) and their analysis and subsequent experimental study have led to the following conclusions.[1,34,35,51,53,57] In the region of a PSC of length $2\xi\Gamma^{1/2}$, where $\Gamma=\hbar/2\tau_\varepsilon\Delta_0$ is the depairing factor, the supercurrent and the order parameter undergo substantial oscillations. At points where Δ goes to zero the phase χ jumps by 2π, and $\Phi(x=0)$ goes to infinity. The amplitude of the oscillations of Δ is of the order of $\Delta_0\Gamma^{1/2}$, where Δ_0 is the equilibrium value of the order parameter. The oscillations of Δ are rapidly damped with distance from the PSC, and at distances $x>x_2=\xi\Gamma^{1/2}$ the order parameter is practically independent of time. For $x\gg\xi$ the order parameter assumes its equilibrium value Δ_0. The supercurrent oscillates but remains small, so that all of the current is transported by normal excitations. At distances $x_1=(\xi l_E)^{1/2}<x\leqslant l_E$ the oscillations of all of the quantities are negligible. In this region a relaxation of the disequilibrium of Φ arising in the core of the PSC occurs. As Φ falls off, there is a decrease in the normal current, and increase in the supercurrent, and a decrease in Δ. Figure 3 shows the structure of a PSC, according to the dynamic model. Comparing it with Fig. 2, which illustrates the static model, we see that the behavior of the order parameter Δ and potential Φ in the two cases is analogous almost over the entire span between PSCs except for a narrow region in the immediate vicinity of each PSC. The process of formation of the voltage across the PSC in the static model has the same physical nature as in the dynamic model.

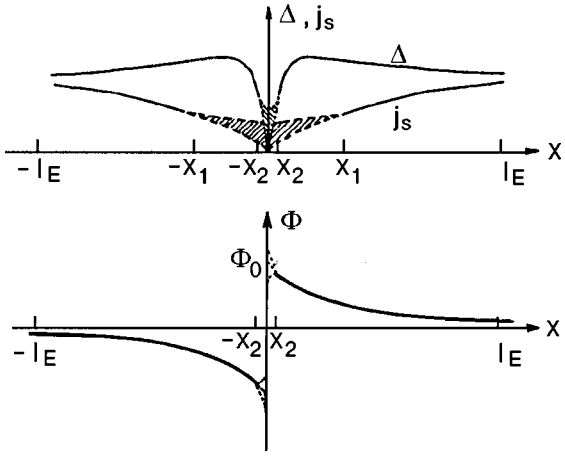

FIG. 3. Behavior of the order parameter Δ, supercurrent density j_s, and potential Φ in the static (solid curves) and dynamic (dashed curves) regions. The shaded regions are values that can be assumed by Δ and j_s in the process of oscillation.

As we have said, the I–V characteristics of superconducting channels exhibit voltage jumps. They are due to the appearance of new PSCs in the channel as the current increases. A qualitative picture of the voltage jumps, based on the SBT model,[24] is considered in Paragraph 1.2.1. A more consistent approach is based on the microscopic theory.[47] We note that the numerical value obtained for the dynamic resistance due to a single isolated PSC in the microscopic theory is equal to $2.06 l_E\rho/S$, in surprisingly good agreement with the phenomenological result obtained in the SBT model [see Eq. (1.20)].

Thus it can be surmised that the resistive current state of superconducting channels has by now been adequately studied experimentally and that it can be explained by the existing theory. However, it is still too early to speak of numerical agreement. Since the phase-slip processes are by nature substantially nonlinear, it is hardly possible to obtain a mathematically exact analytical solution of the dynamical equations (1.22)–(1.24). Nevertheless, the main qualitative characteristics of the resistive state are undoubtedly described correctly by the theory.

2. RESISTIVE STATE OF A SUPERCONDUCTING CHANNEL BROUGHT ON BY AN ALTERNATING ELECTROMAGNETIC FIELD

It is natural to suppose that under the influence of some external perturbation the equilibrium distribution function of

the quasiparticles in a superconductor will acquire a nonequilibrium admixture. Depending on the parity of this admixture to the quasiparticle distribution function with respect to ε_k, one can divide the nonequilibrium phenomena in superconductors into two types.[17]

The first type of disequilibrium is characterized by a symmetric change in the distribution function of electronlike and holelike excitations and generally comes about when a superconductor is irradiated by an external electromagnetic field. In a certain range of frequency and powers this disequilibrium leads to an increase in the gap and an increase in the critical parameters of a superconducting sample, i.e., to stimulation of superconductivity.[58,59] This effect can be explained in the theory proposed in Ref. 60.

The second type of nonequilibrium effects are those in which the admixture to the distribution function is odd, in which case the symmetry of the number of quasiparticles over the branches of the excitation spectrum is broken (imbalance of the charge of the branches). This situation is observed when a dc current is passed through an NS boundary, in the injection of nonequilibrium quasiparticles in SIN tunnel junctions, and also in a homogeneous superconductor with a temperature gradient or with $I > I_c$ (PSCs).

For a long time after the discovery of superconductivity stimulated by microwave radiation it was assumed that the electromagnetic field produced only a symmetric change in the quasiparticle distribution function and, consequently, did not lead to a population imbalance of the branches of the quasiparticle spectrum. However, in 1976 it was conjectured[61] that microwave irradiation of a superconductor gives rise to a dc electric field, i.e., leads to imbalance of the quasiparticle charge. The resulting imbalance of the populations of the branches of the quasiparticle spectrum was attributed in that paper,[61] and also in a later paper,[62] to the thermoelectric effect, and its value turned out to be rather small, of the order of ε^*/E_F ($\varepsilon^* \sim \Delta$). In Refs. 63 and 64 it was shown theoretically that the homogeneous state of a superconductor becomes unstable under the influence of an electromagnetic field, and a transition can occur to a spatially inhomogeneous state, the structure of which, however, remained undetermined. In Ref. 65 it was observed experimentally that under electromagnetic irradiation at a power P greater than the critical value P_c (P_c is the minimum power of electromagnetic radiation at which the critical current I_c of the channel is equal to zero) the superconducting channel undergoes NS phase separation, the physical nature of which remained unclear for some time. In this connection we should also mention the results of studies in which stepped structures were observed on the characteristics at superconducting transitions of narrow films of tin[66] and aluminum[67] in a microwave radiation field and also at transitions to the resistive state in wide superconducting films of tin[68] and aluminum[69,70] under the influence of an electromagnetic field.

2.1. Discreteness of the change in resistance of a superconducting channel irradiated by electromagnetic fields at powers greater than the critical

Let us consider the structure of the resistive state arising in a channel under the influence of an electromagnetic field. Figure 4 shows families of I–V characteristics and their derivatives for sample Sn-14 at different power levels of the

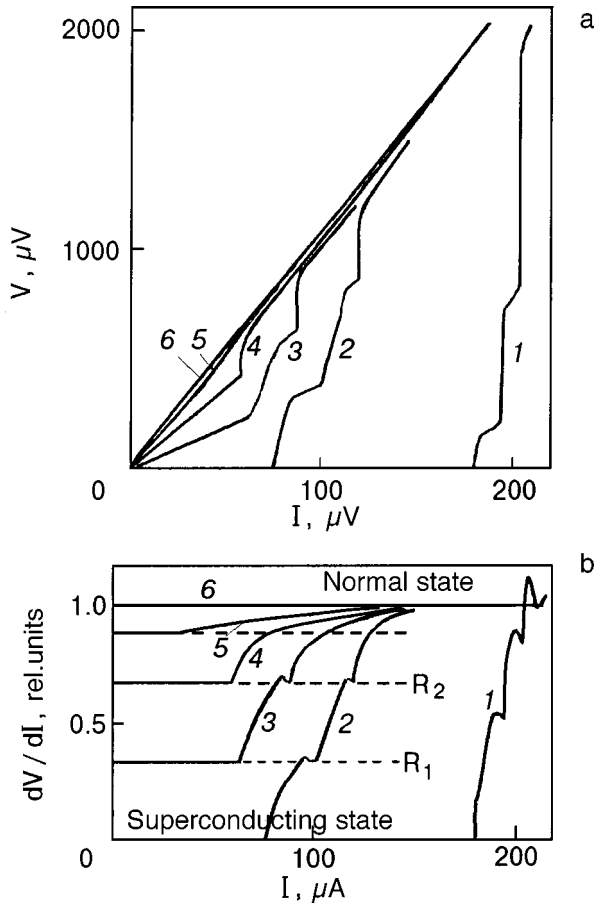

FIG. 4. Families of I–V characteristics (a) and their derivatives (b) for the superconducting channel Sn-14 at various irradiation power levels, $f = 6.3$ GHz, $T = 3.719$ K.

irradiation at a frequency $f = 6.3$ GHz.[71] For the first I–V characteristic and its derivative the power of the radiation was zero, and the other curves are labeled in order of increasing power. The parameters of all of the samples discussed in this review are presented in Table I.

It is seen from Fig. 4a that as the power of the irradiation increases, PSCs caused by the electromagnetic radiation (ac PSCs) arise in the sample, as distinct from those caused by dc current (dc PSCs). As the power of the rf field is increased monotonically, the channel resistance R_i ($i = 1,2,3 \ldots$) determined from the slope of the initial parts of the I–V characteristics changes discretely. Results analogous to those

TABLE I. Parameters of the film samples.

Sample	l, μm	w, μm	d, nm	$R_{4.2}$, Ω	R_{300}, Ω	T_c, K
Sn-2	80	1.0	175	6.85	67.74	3.763
Sn-3	25	1.0	73	5.50	51.20	3.821
Sn-4	30	1.0	199	1.45	21.50	3.783
Sn-5	21	1.5	70	4.26	30.91	3.860
Sn-6	30	1.0	100	4.33	39.32	3.733
Sn-8	33	1.0	88	5.87	51.33	3.821
Sn-10	53	1.5	86	5.13	60.02	3.842
Sn-12	35	1.0	71	5.48	64.73	3.812
Sn-13	35	1.0	88	4.08	52.08	3.820
Sn-14	75	1.0	117	10.5	95	3.781
Sn-15	20	1.0	50	9.32	63.05	3.830

Note: l is the length, w the width, and d the thickness of the sample.

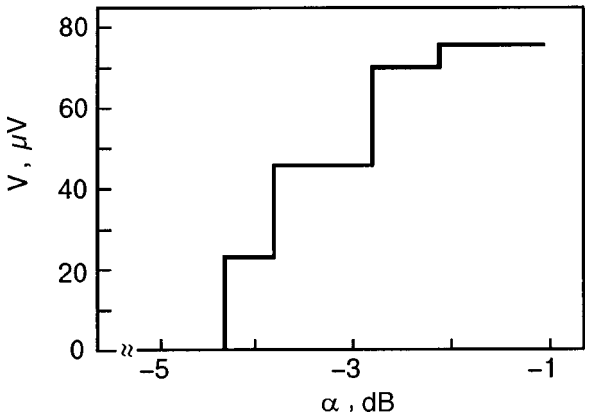

FIG. 5. Voltage arising across the ends of sample Sn-2 versus the power of the electromagnetic irradiation at $f=8.9$ GHz, $I_{tr}=11$ μA, and $T=3.650$ K.

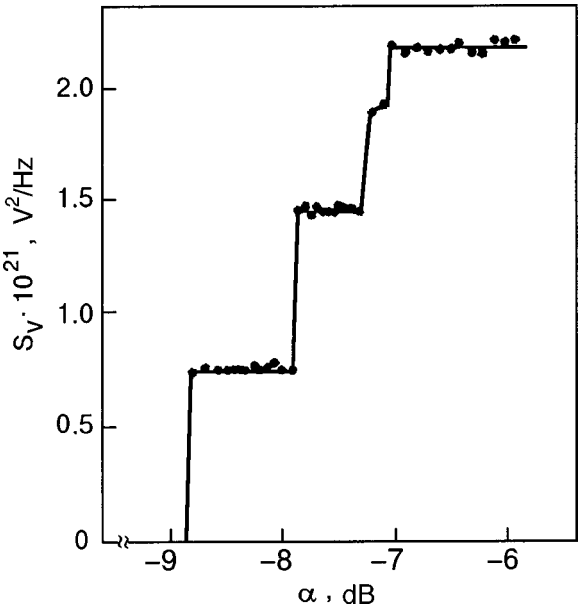

FIG. 6. Spectral noise density S_V of superconducting channel Sn-14 versus the power of the electromagnetic irradiation at $f=6.3$ GHz and $T=3.719$ K.

shown in Fig. 4a were also obtained in Ref. 72 for aluminum samples irradiated at a frequency of 25 GHz. The value of the resistance of an ac PSC can also be determined from Fig. 4b, since dV/dI at $I_{tr}=0$ is also the resistance of an ac PSC measured in alternating current (at a signal modulation frequency $f_m \sim 1$ kHz).

It is seen in Fig. 4a that for irradiation at a frequency of 6.3 GHz the resistance of the first ac PSC is $R_1=3.5$ Ω (curve *3*). With increasing irradiation power the number of PSCs arising under the influence of the electromagnetic field increases, and the resistance of the sample increases by a multiple: $R=R_1 n$, where R_1 is the resistance of one ac PSC, $n=1,2,3 \ldots N$ (N is the largest number of ac PSCs in the sample for the given irradiation frequency). Since the dimensions of the samples ($\sim 10^4$ m) are small compared with the wavelength of the electromagnetic field ($\sim 10^{-2}$ m), we can assume that a uniform rf current $I_{fr} \propto \sqrt{P}$ flows through the sample, although its value was not measured directly. As we see in Fig. 4, the resistance R_1 of each ac PSC that arises remains constant as the irradiation power is increased, i.e., the heating effect that would exist if the resistance R_1 were due to a normal domain with a length of the order of l_E is not observed. Figure 5 shows how the dc voltage arising between the ends of the superconducting channel (sample Sn-2) depends on the power of the electromagnetic irradiation $\alpha=10\log(P/P_0)$ at a low measuring current ($I_{tr}=11$ $\mu A \ll I_c$). For $0 \leqslant P < P_c$ the sample is found in the superconducting state, and no voltage drop between its ends is observed. As the rf current through the channel increases, ac PSCs arise in it, and the $V(\alpha)$ curves exhibit related voltage jumps. Results analogous to those shown in Fig. 5 were also obtained in Refs. 70 and 72 for aluminum samples irradiated at a frequency of 25 GHz.

Thus in the case when the irradiation power is above the critical level, the resistance of a superconducting channel changes discretely by multiples.

It should be noted, however, that the aforementioned techniques for determining the resistance of the ac PSCs presuppose the presence of dc (in the case of the I–V characteristics) or low-frequency (in the case of their derivatives) measuring currents. There is therefore some doubt as to whether the change in resistance of a superconducting channel in the resistive state in an electromagnetic field remains discrete in the absence of these currents.

It is known that the thermal motion of the current carriers in a conductor gives rise to thermal or resistance noise.[73,74] In accordance with the Nyquist theorem, the effective voltage of the thermal noise as a result of the presence of a resistance R is given by[75]

$$V=(4k_B TR\delta f)^{1/2}, \tag{2.1}$$

where δf is the frequency bandwidth of the circuit for the noise measurements. Since Eq. (2.1) is valid for any resistance R, regardless of its nature,[74] one expects the appearance of jumps in the noise voltage across the ends of a sample in the resistive state by amounts proportional to the square root of the resistances of the ac PSCs.

Figure 6 shows a plot of the spectral density of the noise, $S_V=V^2/\delta f=4k_B TR$, versus the power of the electromagnetic irradiation $\alpha=10\log(P/P_0)$ ($f=6.3$ GHz) for sample Sn-14 in the case of conventional methods of study (see Fig. 4).[71] We see that increasing the power of the electromagnetic field results in discrete increases in the voltage between the ends of the channel in the resistive state. It is important to note that the values of the noise voltage obtained in Ref. 71 are in quite good agreement with the values calculated according to formula (2.1) on the assumption that the sources of this noise are the ac PSCs whose resistances were determined (see Fig. 4). It can also be assumed that in the experiments investigating the noise of the Sn-14 superconducting channel the PSCs appear as a result of the flow of a parasitic dc current arising as a result of rectification of the microwave signal. However the rectification effect was not observed in Ref. 71. The presence of segments with a constant noise voltage on the $S_V(\alpha)$ curve (see Fig. 6) and the absence of excess noise suggest that the microwave signal ($f=6.3$ GHz) does not contain a parasitic current having a frequency lying within the frequency bandwidth of the noise measurements.[71]

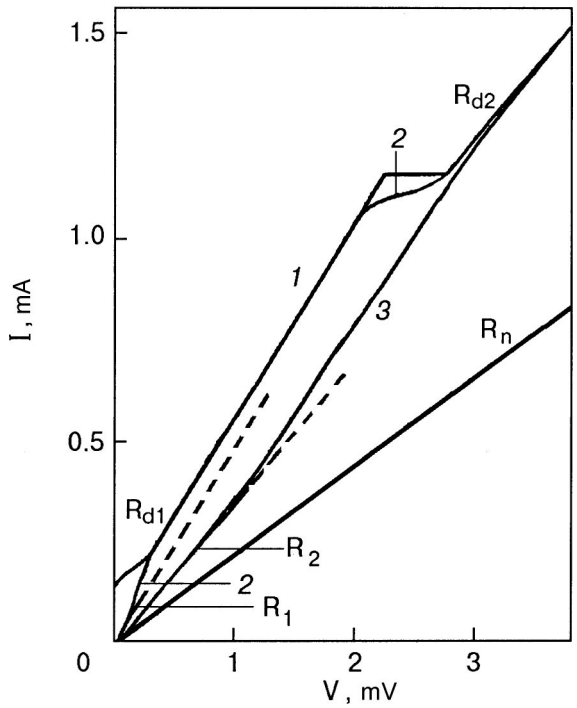

FIG. 7. Family of current–voltage characteristics of sample HS-7 at various levels of attenuation of the power of the external irradiation ($f=16.2$ GHz), P [dB]: -100 (*1*), -26 (*2*), -3 (*3*). $T=5$ K.

Measurements of the resistance of a channel in ac current ($f_m \sim 1$ kHz) at $I_{tr}=0$ and studies of the noise have thus shown that ac PSCs arise in a narrow channel under irradiation by an electromagnetic field with $P>P_c$ in the absence of a dc current.

A similar picture is observed in studies of high-temperature samples. Figure 7 shows a family of I–V characteristics for a $YBa_2Cu_3O_{7-x}$ sample (HS-7) for various power levels of the external radiation.[76] For the first I–V characteristic the irradiation power was equal to zero, and the rest are numbered in order of increasing power. We see from the figure that under microwave irradiation, as in the case of tin superconducting channels, the resistance of a high-temperature sample changes in a discrete manner (see the initial segments of the I–V characteristics in Fig. 7). First the sample undergoes an abrupt transition from the superconducting state to a state with resistance $R_1=1.88\ \Omega$, and upon further continuous increase in the power a transition to a state with $R_2=3.14\ \Omega$ occurs, and only then, as the power is increased further, does the sample go to the normal state with resistance $R_n=4.50\ \Omega$. This provides grounds for asserting that ac PSCs also arise in high-temperature samples under the influence of a microwave field, just as in the case of tin superconducting channels. The fact that the resistances of the PSCs deviate slightly from exact multiples (by $\sim 10\%$) can be attributed to nonideality of the channel and the its small length, which can accomodate only two ac PSCs. Interesting, in this experiment the irradiation frequency was such (see Sec. 2.2) that the dynamic resistances of the PSCs induced by the dc current are equal to the resistances of the ac PSCs: $R_{d1}=R_1$, $R_{d2}=R_2$, with $R_{d1}(P=0)=R_{d1}(P>P_c)$, $R_{d2}(P=0)=R_{d2}(P>P_c)$ (see Fig. 7).[76]

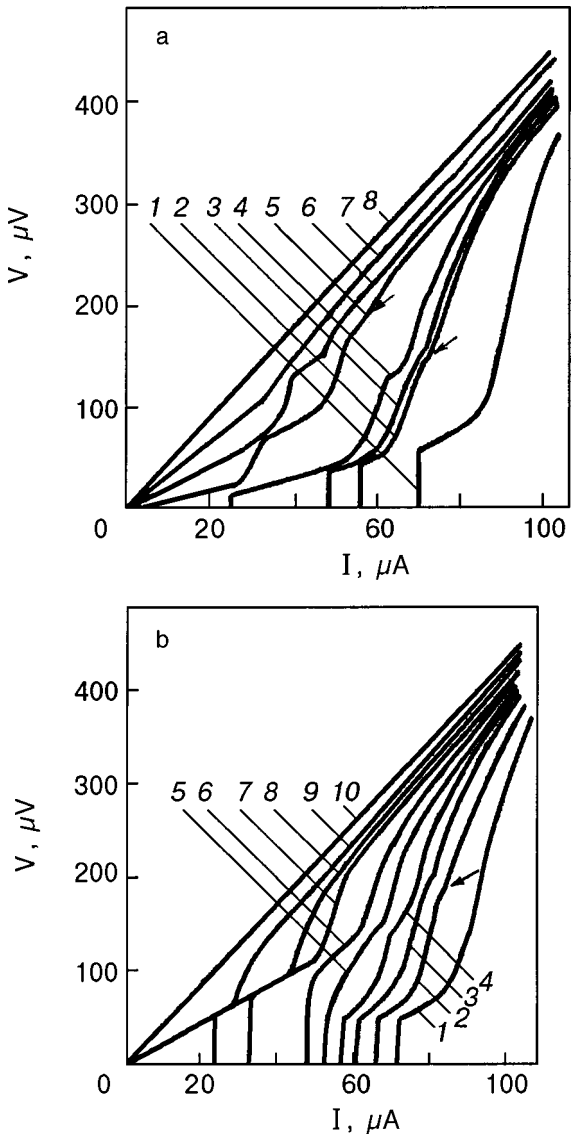

FIG. 8. Families of current–voltage characteristics of channel Sn-5 for various irradiation power levels at $T=3.821$ K: $f=1.5$ GHz (a) and $f=5.025$ GHz (b).

2.2. Nonmonotonic frequency dependence of the resistance of a phase-slip center caused by an electromagnetic field

Let us consider the frequency dependence of the penetration depth of a longitudinal electric field into a superconductor. Figure 8 shows families of I–V characteristics of sample Sn-5 at various power levels of irradiation at frequencies of 1.5 and 5.025 GHz.[77] For the first I–V characteristic the irradiation power is equal to zero, and the remaining curves (*2–10*) are labeled in order of increasing power. It follows from Fig. 8 that in the case when $P>P_c$, increasing the power of the electromagnetic field in the sample gives rise to ac PSCs, the resistance of which R_1 is different for different frequencies. In studying the resistivity arising in superconducting channels upon the formation of PSCs in them, one can determine the penetration depth of a longitudinal electric field into the superconductor [see (1.20)] as:

$$l_E(\omega=0)=lR_{d1}(P=0)/2R_n;$$
$$l_E(\omega)=lR_{d1}(P\geqslant P_c)/2R_n. \qquad (2.2)$$

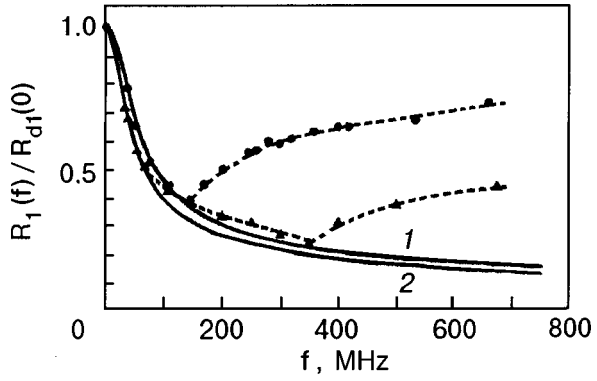

FIG. 9. Resistance of an rf phase-slip center $R_1(f)/R_{d1}(P=0)$ versus the frequency of the irradiation for samples Sn-3 (●) and Sn-4 (▲) at $T=3.742$ K.

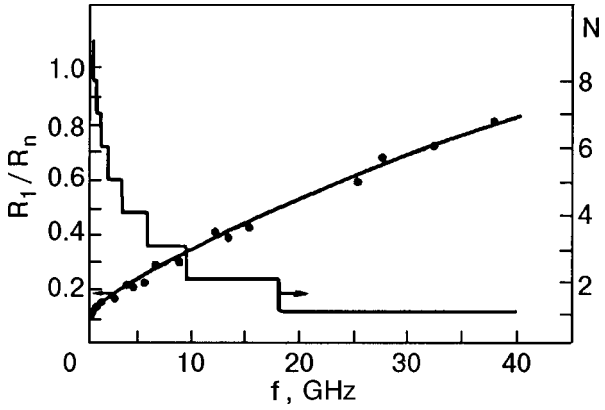

FIG. 10. Resistance R_1/R_n and maximum number N of rf phase-slip centers as a function of irradiation frequency for sample Sn-2 at $T=3.650$ K.

Here l is the length of the channel, R_n is its normal resistance at low temperature, and $\omega=2\pi f$ is the irradiation frequency. It will be shown in Sec. 3.1 that for $P>P_c$ the resistance of an ac PSC is equal to the resistance of a dc PSC.

As was shown in Sec. 1.1, in our understanding of the penetration of a longitudinal electric field into a superconductor an important role is played by the concepts of imbalance of the branches of the quasiparticle spectrum and of the mechanisms equalizing the populations of the electron and hole subsystems. The simplest mechanism for relaxation of the charge imbalance near T_c involves inelastic electron–phonon collisions.[9,78] In that case the frequency dependence $l_E(\omega)$ is given by the expression[9,79,80]

$$l_E(\omega)/l_E(0)=[(1-i\omega\tau_1)(1-i\omega\tau_\Delta)]^{-1/2}, \tag{2.3}$$

where $\tau_1=\tau_\varepsilon$ is the inelastic relaxation time for homogeneous samples, τ_Δ is the relaxation time of the phase of the order parameter:

$$\tau_\Delta=\begin{cases}\tau/2(1-T/T_c) & \text{``clean'' limit}\\ 2\hbar k_BT/\pi\Delta^2 & \text{``dirty'' limit;}\end{cases}$$

τ is the relaxation time in scattering on impurities.

In Ref. 81 the frequency dependence of l_E was considered with allowance for the relaxation mechanism involving collective oscillations. An expression for the penetration depth of a longitudinal electric field in that case has the same form as for the electron–phonon relaxation mechanism, only now τ_1 in formula (2.3) equals τ_s, the relaxation time on collective oscillations. In a thin film this relaxation time τ_s can be estimated by the an expression of the form:[81]

$$\tau_s\sim\frac{\Delta}{k_BT}\left(\frac{\varepsilon_F}{T^3}\right)^{1/2}p_Fd(p_Fl_i)^{1/2}, \tag{2.4}$$

where d is the thickness of the film, $l_i=l_{\rm ph}(R_{300}/R_{4.2}-1)$ is the mean free path of the electrons in respect to impurity scattering,[82] and $l_{\rm ph}$ is the mean free path of the electrons in respect to the phonon scattering mechanism ($T=300$ K).

Figure 9 shows the frequency dependence of the ratio $R_1(f)/R_{d1}(f=0)=l_E(\omega)/l_E(0)$ for samples Sn-3 and Sn-4.[83] It is seen that as the frequency is increased, the value of $R_1(f)$ [and, hence, $l_E(\omega)$] initially decreases and then begins to increase. The solid curves in Fig. 9 represent the real parts of the ratio $l_E(\omega)/l_E(0)$ calculated according to formula (2.3) for $\tau_1=5\times10^{-9}$ s (curve *1*) and $\tau_1=6.5\times10^{-9}$ s (curve *2*). It is seen that the curves conform well to the descending parts of the experimental curves, and that τ_1 is greater for sample Sn-4 than for sample Sn-3. In the framework of the model proposed in Ref. 81, this can be explained as follows. According to Eq. (2.4), the relaxation time τ_s for relaxation on collective oscillations is proportional to d and l_i, and the mean free path and thickness are greater for sample Sn-4 than for Sn-3 (see Table I). It is also important to note that for samples with larger d and l_i the deviation from the theoretical predictions begins at higher irradiation frequencies (see Fig. 9).

Thus for a suitable choice of the value of the quasiparticle relaxation time τ_1 in real samples, the theory gives a quantitatively as well as qualitatively correct description of the descending part of the $l_E(\omega)/l_E(0)$ curve. As to the total experimental dependence of $l_E(\omega)/l_E(0)$, it differs fundamentally from the predictions of the theory in that it exhibits nonmonotonicity, which is due to mechanisms that were not taken into account in the existing theories.

To track the behavior of the ascending branch of of the $R_1(f)$ curve at high frequencies, we chose the longer sample Sn-2. Figure 10 shows the frequency dependence of the resistance R_1 and the maximum number N of ac PSCs in sample Sn-2.[84] We see that as the irradiation frequency is increased, the resistance of an ac PSC increases, this behavior of $R_1(f)$ persisting to frequencies comparable to the gap frequency $2\Delta/\hbar$, while N falls off with increasing frequency.[84] The behavior of the ascending branch, we believe, is due to nonlinear processes of relaxation of the populations of the electronlike and holelike branches of the quasiparticle energy spectrum under conditions of electromagnetic pumping at irradiation frequencies $\omega>\tau_Q^{-1}$. In this case the population imbalance of the branches of the quasiparticle spectrum due to the electromagnetic field does not have time to relax completely in a time ω^{-1}. As the frequency increases, this process becomes stronger, and an increase of $l_E(\omega)$ is observed as a result of spatial diffusion. It seems to us that the nonmonotonicity of the frequency dependence is a result of the existence of two mechanisms of relaxation of the charge imbalance, one of which leads to a decrease and the other to an increase of $l_E(\omega)$ as the irradiation frequency increases, the mechanism leading to the

growth of $l_E(\omega)$ being ''turned on'' for $\omega > \tau_Q^{-1}$ and becoming dominant as the irradiation frequency increases.

2.3. Temperature dependence of the resistance of a phase-slip center

Studying the temperature dependence of the resistance of a PSC is important for understanding the mechanisms of relaxation of the population imbalance of the branches of the quasiparticle spectrum in a narrow channel. In a number of studies of the properties of PSCs in whiskers and long, narrow films deposited on glass substrates, no temperature dependence of the resistance of a PSC (and, hence, of the penetration depth of the longitudinal electric field) was detected.[22–24] In Ref. 24 this fact led to the mistaken conclusion that the penetration depth of the longitudinal electric field in a superconductor is determined by the energy relaxation time τ_ε and not by the relaxation time of the charge imbalance, τ_Q. However, more-careful studies have shown that l_E does depend on temperature. In Ref. 85 the temperature dependence of l_E was investigated in long, thin, narrow tin films deposited on crystalline quartz substrates. It was found that at temperatures sufficiently far from T_c, the value of l_E is determined by collisions of electrons with impurities, as was predicted in Refs. 46 and 86. At temperatures close to T_c the situation is quite different, since here the characteristic times due to elastic relaxation, because of their strong temperature dependence $[(1-T/T_c)^{-1}]$, become larger, and elastic processes (scattering on phonons) begin to play the predominant role. In that case $l_E \propto (1-T/T_c)^{-1/4}$.

Measurements of l_E in thin and narrow films of tin and indium were also made in Ref. 44, but by a different method. At a certain place a notch was made in the film, so that its width at that place was decreased by approximately half. When a dc current exceeding the cirtical current was passed through the film, an electric field arose at the notch. The decay length of the field was determined by means of microprobes placed near the notch a short distance apart (~ 2 μm). In agreement with the theory, it was found that for $T \to T_c$ the length l_E decreases according to the law $l_E \propto \Delta^{-1/2} \propto (1-T/T_c)^{-1/4}$.

It was shown in Ref. 79 that near the critical temperature, thermal effects can obscure the temperature dependence of the resistance of the PSCs; this temperature dependence can nevertheless be extracted after allowing for the heating effect.

It should be noted that in certain theoretical models for the relaxation of the charge imbalance there is no temperature dependence of the PSC resistance. For example, it was shown in Ref. 87 that taking the scattering of quasiparticles on static inhomogeneities of the order parameter (structure fluctuations) into account leads to a temperature-independent penetration depth of the longitudinal electric field. However, in the overwhelming majority of experimental studies the temperature dependence of l_E has still been observed if the thermal effects were accurately taken into account.

For example, in Ref. 88 studies were made of the temperature dependence of the dynamic resistance $R_{d1}(P=0)$ of a PSC due to a dc current and of the resistance $R_1(f)$ of a PSC due to an electromagnetic field. Figure 11 shows the I–V characteristics of one of the samples at different temperatures.[88] It is seen that $R_1(f)$ decreases with decreasing temperature. Figure 12 shows the temperature dependence of l_E for several of the samples studied in Ref. 88. The numbers *2*, *3*, and *4* in this figure label the temperature dependence of the penetration depth of a longitudinal dc electric field into the superconductor in the absence of electromagnetic radiation, and the numbers *1*, *5*, *6*, and *7* label the temperature dependence of l_E under irradiation at powers $P > P_c$ and frequencies of 9.2, 4.3, 2.0, and 0.386 GHz, respectively. It is seen from the figure that $l_E \propto (1-T/T_c)^{-1/4}$ for both the dc and ac PSCs. This agrees with the results of Refs. 89–92.

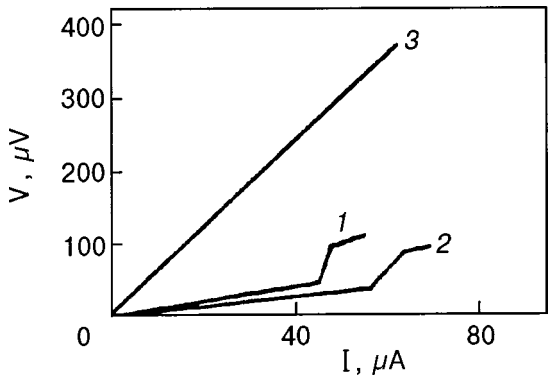

FIG. 11. Current–voltage characteristics of homogeneous film channel Sn-8 in an electromagnetic field with $f = 2.0$ GHz at $T = 3.782$ K (*1*), $T = 3.657$ K (*2*), and $T = T_c$ (*3*).

As we have said, an important role in the study of the temperature dependence of the resistance of the PSCs is played by overheating processes. The increase in the temperature of the film due to Joule heating of the PSCs is given by the relation[24]

$$\delta T = \frac{P}{(2\eta + l_E)\alpha'_{fs} w}, \tag{2.5}$$

where $\eta = (Kd/\alpha'_{fs})^{1/2}$ is the thermal length, K is the thermal conductivity of the metal, α'_{fs} is the coefficient of heat transfer from the film to the substrate, and w is the width of the film.

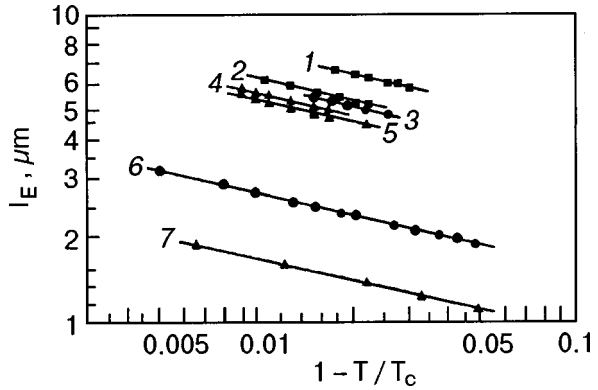

FIG. 12. Temperature dependence of the penetration depth of a longitudinal electric field into samples Sn-5 (▲), Sn-8 (●), and Sn-10 (■) in the absence of electromagnetic irradiation (*2,3,4*) and at various irradiation frequencies f [GHz]: 9.2 (*1*), 4.3 (*5*), 2.0 (*6*), and 0.386 (*7*) in the case $P > P_c$.

The thermal conductivity can be calculated from the resistivity of the sample using the Wiedemann–Franz law:

$$K=\frac{\pi^2 k_B T}{3e^2\rho}. \tag{2.6}$$

For tin films $K=0.05$–0.10 W/(cm·K), and the the coefficient of heat transfer from a tin film to a quartz substrate was calculated in Ref. 93 as 6 W/(cm·K). When a dc current flows through a PSC in the absence of electromagnetic field, a power $P\sim 10^{-9}$ W is released, so that the overheating of the film according to (2.5) will be of the order of 10^{-3} K.

It is much more complicated to estimate the overheating of the sample when both ac and dc currents are flowing through it simultaneously. The square of the amplitude of the ac critical current as a function of frequency has the form[94,95]

$$I_{c0}^2=\begin{cases} I_c^2(1+\sqrt{2}\omega\tau'), & \omega\tau'\ll 1 \\ 2I_c^2[1-(4\omega\tau')^{-2}], & \omega\tau'\gg 1. \end{cases} \tag{2.7}$$

Here $\tau'\approx 1.2\tau_\varepsilon/(1-T/T_c)^{1/2}$ is the relaxation time of the gap.

It follows from (2.7) that the maximum value of the amplitude I_{c0} of the ac critical current is equal to $\sqrt{2}I_c$. Here the power released at an ac PSC having resistance R_1 is given by

$$P_f=I_{\text{eff}}^2 R_1=I_c^2 R_1, \tag{2.8}$$

where $I_{\text{eff}}=I_{c0}/\sqrt{2}$ is the effective value of the current.

Since for tin films $P_f=I_c^2R_1\sim 10^{-9}$ W, the overheating of the film due to the Joule heat released at a PSC on passage of an ac current is not any bigger than the value obtained in the case of a dc current, i.e., it is of the order of a millikelvin. When a dc measuring current is passed through an ac PSC, a power $P'=I^2R_1$ is released. Since $I<I_c$ and $P'\ll P_f$, the overheating of the sample due to the passage of the dc current can be neglected in this case.

When a superconducting channel is irradiated by an rf electromagnetic field, the so-called Ohmic dissipation and relaxation dissipation occur.[95]

At high frequencies ($\omega\tau_\varepsilon>1$) the heating of the film due to Ohmic absorption can be estimated by the expression

$$\delta T_\Omega=\frac{I_c^2 R_1(3\omega/4\omega_\Delta)^2}{\alpha'_{fs} wl}, \tag{2.9}$$

where $\omega_\Delta=\pi\Delta^2/2\hbar k_B T$, and l is the length of the film.

For tin samples on quartz substrates the heating of the film due to Ohmic dissipation does not exceed a few tenths of a millikelvin, i.e., it is negligible. An estimate of the heating of the film due to relaxation absorption gives $\delta T_R/\delta T_\Omega<10^{-2}$, i.e., the contribution from relaxation dissipation is also negligible.

Thus in studying the temperature dependence of l_E, even high estimates of the overheating of tin films deposited on quartz substrates are so small that one can neglect thermal effects in determining the penetration depth of the longitudinal electric field into the superconductor.

The absence of overheating effects is also seen on the I–V characteristics (see Figs. 4, 8, and 11). The passage of a dc current of up to several tens of microamperes does not affect the resistance of an ac PSC (the extended linear parts of the I–V characteristics); this attests to the good thermal matching of the film and substrate, providing efficient heat removal from the sample into the helium bath.

3. INFLUENCE OF ELECTROMAGNETIC IRRADIATION ON THE RESISTIVE STATE OF A SUPERCONDUCTING CHANNEL BROUGHT ON BY THE PASSAGE OF A DIRECT CURRENT

3.1. Dynamic resistance of a superconducting channel

As was shown above, the dynamic resistance of a PSC is proportional to the penetration depth of the longitudinal electric field into the superconductor [see Eq. (1.20)] and is given by

$$R_{d1}=2l_E R_n/l=4[(D/\pi)(k_B T/\Delta)\tau_\varepsilon]^{1/2}R_n/l. \tag{3.1}$$

In view of (3.1), one might expect that suppression of the order parameter Δ by an electromagnetic field would increase the dynamic resistance of a PSC produced by the passage of a dc current, while stimulation of superconductivity would decrease it.[58,59] However, experimental studies of the effect of electromagnetic field on the resistive current state of a superconducting channel have shown that this is not the case.[77,88]

Figure 8 shows families of I–V characteristics for sample Sn-5 at different power levels of the irradiation at frequencies of 1.5 and 5.025 GHz. The length of sample Sn-5 is such that only one dc PSC, with a resistance of 2.25 Ω, can be accomodated in the absence of radiation. The lower frequency boundary for stimulation, f_{low}, calculated from the transcendental equation[60]

$$f_{\text{low}}^2=\Delta/[\tau_\varepsilon h\ln(8\Delta/hf_{\text{low}})], \tag{3.2}$$

is equal to 6 GHz. Therefore, increasing the irradiation power leads to a decrease of the critical current, i.e., suppression of superconductivity, at both 1.5 and 5.025 GHz. Let us first consider the case when the frequency of the external electromagnetic field is such that the resistance of a PSC caused by the passage of an ac current through the channel is smaller than the resistance of a PSC caused by the passage of a dc current, i.e., $R_1(f)<R_{d1}(P=0)$. Initially the dynamic resistance $R_{d1}(P)$ of a dc PSC is unaffected by small increases in the irradiation power, but, starting at a certain power level $P^*<P_c$ (see curves *2*, *3*, and *4* in Fig. 8a), in complete contradiction to the predictions of the theory, the dynamic resistance $R_{d1}(P)$ of the dc PSC begins to decrease smoothly.[77] It should be noted that as the irradiation power is increased, the state of a superconducting channel in which a dc PSC has formed becomes more stable against an increase in the dc current (the linear parts of the I–V characteristics, whose resistances are multiples of $R_{d1}(P)$, become longer). It is seen in Fig. 8a that as the irradiation power is increased, the I–V characteristics show the presence of other dc PSCs (indicated by arrows) in addition to the single dc PSC that existed at $P=0$. This is not surprising. If increasing the irradiation power decreases the dynamic resistance $R_{d1}(P)$ of the PSC, then its size $2l_E$ will also decrease as a consequence. Therefore, at a fixed channel length the maximum number of dc PSCs that can fit in the channel increases.

Curve *3* in Fig. 13 shows the dynamic resistance $R_{d1}(P)/R_{d1}(P=0)$ as a function of the irradiation power (at

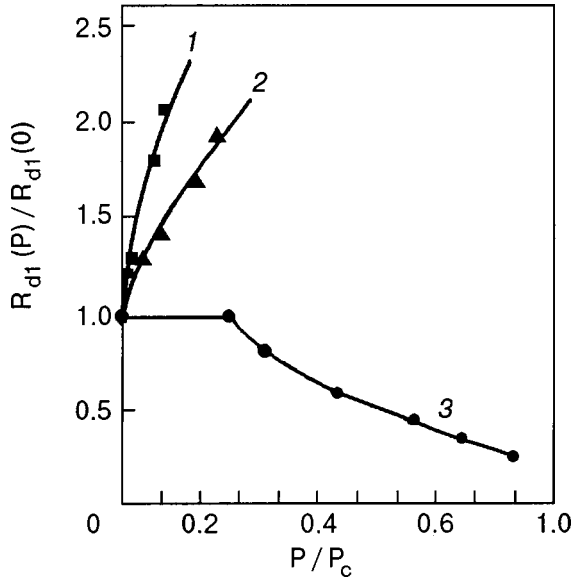

FIG. 13. Dynamic resistance of a phase-slip center caused by the passage of a dc current, $R_{d1}(P)/R_{d1}(P=0)$, versus the irradiation power: *1*,*2*) sample Sn-12: $f=23.39$ GHz (*1*) and $f=15.46$ GHz (*2*); *3*) sample Sn-6: $f=200$ MHz.

a frequency of 200 MHz) for one of the samples (Sn-6). It is seen that when the power of the electromagnetic field is increased from zero to the critical value P_c, the dynamic resistance of the current-induced PSC decreases by almost a factor of four.

At $P=P_c$ an ac PSC with a resistance R_1 equal to the dynamic resistance $R_{d1}(P)$ of a dc PSC at $P\geqslant P_c$ arises in the sample (see curve *6* in Fig. 14c).

At higher irradiation frequencies, when $R_1(f)\geqslant R_{d1}(f,P=0)$ (see Fig. 8b), the dynamic resistance of a dc PSC initially remains unchanged as the power increases, as in the previous case. Here one observes a decrease of its stability against dc current (the linear parts of the I–V characteristics, the resistances of which are multiples of $R_{d1}(P)$, become shorter). As the irradiation power is increased further, the existing dc PSC vanishes and a new dc PSC appears (indicated by an arrow in Fig. 8b), the stability of which against a rise in dc current increases with increasing power. Upon further increase in power the dynamic resistance of this PSC remains unchanged and, as in the case of low irradiation frequencies, when $R_1(f)<R_{d1}(f,P=0)$, is equal to the resistance R_1 of the PSC arising under the influence of an electromagnetic field at $P=P_c$ (see curves *7* and *8* in Fig. 8b). Thus on the basis of the experimental data presented above, one can state that irradiation by an electromagnetic field with a frequency below the boundary frequency for stimulation can either decrease the dynamic resistance (for $R_{d1}(P=0)>R_1$) or increase it (for $R_{d1}(P=0)<R_1$), and for $P\geqslant P_c$ the resistance $R_{d1}(P\geqslant P_c)$ of a dc PSC becomes equal to the resistance R_1 of an ac PSC. This behavior of the dynamic resistance of a dc PSC under the influence of electromagnetic radiation cannot be explained by suppression of the order parameter in the superconducting channel.

It is of considerable interest to study the transition of a superconducting channel from a state of stimulated superconductivity to a resistive current state.[88] Figure 14 shows

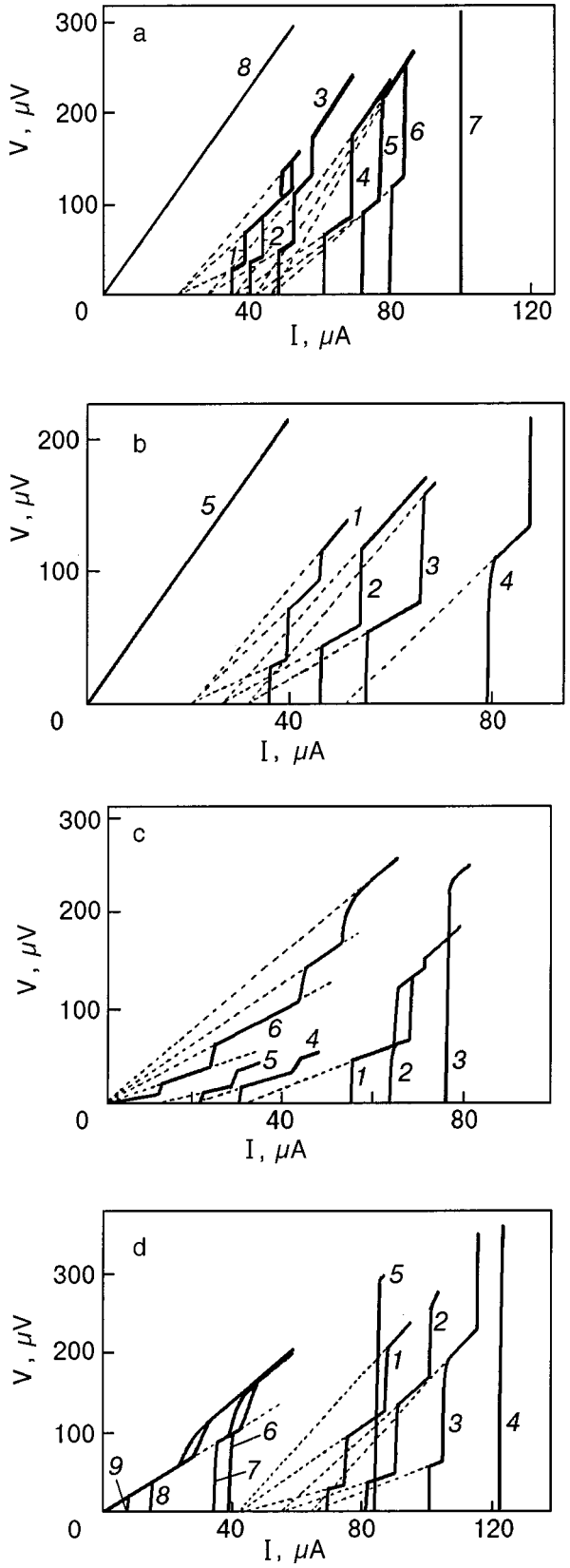

FIG. 14. Families of current–voltage characteristics of superconducting channels at various power levels of the irradiation. Sample Sn-12: $T=3.774$ K; $f=15.46$ GHz (a), $f=23.39$ GHz (b); $T=3.766$ K, $f=6.0$ GHz (c). Sample Sn-13: $T=3.762$ K, $f=14.16$ GHz (d).

families of I–V characteristics for samples Sn-12 and Sn-13 under irradiation at different power levels. For the first I–V characteristic (curve *1*) the irradiation power is zero, and the

other I–V characteristics are numbered in order of increasing power. The frequencies of the electromagnetic irradiation were above the lower boundary frequency for stimulation. Therefore, increasing the irradiation power leads to a rise in the critical current $I_c(P)$, i.e., to stimulation of superconductivity by the electromagnetic field. Here the resistance $R_{d1}(P)$ of a dc PSC initially remains unchanged as the irradiation power is increased (curve *2* in Fig. 14a; in Fig. 13 this is not visible on account of the scale). Then, starting at a certain power level P^*, the resistance $R_{d1}(P)$ of a dc PSC begins to increase smoothly with increasing P. It has been established experimentally[77] that there is a tendency for P^* to decrease with increasing irradiation frequency f. For example, $P^* \approx 0.25P_c$ for $f=200$ MHz (see curve *3* in Fig. 13), while for $f=15.46$ GHz one has $P^* \approx 0.01P_c$, where P^* is the power level above which the dynamic resistance of a dc PSC begins to deviate from $R_{d1}(P=0)$.

It should be noted that in the stimulated-superconductivity regime, as in the case of rather low irradiation frequencies, for which suppression of superconductivity is observed, as the irradiation power is increased, the state of the superconducting channel upon the formation of a dc PSC in it becomes more stable against an increase in the dc current; this is manifested on the I–V characteristics as a lengthening of the linear segments, the resistances of which are multiples of $R_{d1}(P)$ (see Fig. 14).

Upon further increase in the irradiation power in the stimulated-superconductivity regime one observes a shortening of the linear segments of the I–V characteristics (see curves *5* and *6* in Fig. 14a; curve *4* in Fig. 14b, and curve *3* in Fig. 14c) until they vanish completely and a breakoff from the state of stimulated superconductivity to the normal state occurs (see curve *7* in Fig. 14a and curves *4* and *5* in Fig. 14d). Then, as the irradiation power is increased further (the suppression of superconductivity has already set in, and the value of the dc current through the channel is much lower) the dc PSCs again appear (see curves *6–9* in Fig. 14d), and their stability against a rise of the dc current increases with increasing power of the electromagnetic field, just as it did in the case of superconductivity suppression at low irradiation frequencies.

It is important to emphasize that the dynamic resistance $R_{d1}(P)$ of a dc PSC at $P \geqslant P_c$, just as in the case of low irradiation frequencies, coincides precisely with the resistance R_1 of an ac PSC (see curves *6–9* in Fig. 14d), although the value of R_1 in this case is much larger than at low irradiation frequencies.

Curves *1* and *2* in Fig. 13 show the dynamic resistance $R_{d1}(P)/R_{d1}(P=0)$ of a dc PSC as a function of the irradiation power for sample Sn-12.[88] We see that in the regime of stimulated superconductivity, in the case when the dynamic resistance $R_{d1}(P=0)$ of a dc PSC is much less than the resistance R_1 of an ac PSC, the dynamic resistance $R_{d1}(P)$ increases with increasing irradiation power, and the rate of growth is higher for higher irradiation frequencies. This is clearly due to the following circumstance. As was shown above, with increasing irradiation power the dynamic resistance $R_{d1}(P)$ of a dc PSC tends toward the resistance R_1 of an ac PSC, and $R_1(f=23.39\ \text{GHz}) > R_1(f=15.46\ \text{GHz})$.

In the regime of stimulated superconductivity in the case when the dynamic resistance $R_{d1}(P=0)$ is much greater than the ac PSC resistance R_1 arising in the channel at an irradiation power $P=P_c$, one does not observe a decrease in $R_{d1}(P)$ with increasing irradiation power. However, when the power is increased further and superconductivity becomes suppressed, one observes a decrease in the dynamic resistance of a dc PSC, i.e., $R_{d1}(P)$ tends toward R_1, and at an irradiation power equal to or greater than the critical value one has $R_{d1}(P \geqslant P_c) = R_1$, as in the previous case (see Fig. 14c).

Thus the above results indicate that in the case of stimulation of superconductivity, as in the case of its suppression, starting at a certain power level $P^* < P_c$ the electromagnetic field plays a decisive role in the processes giving rise to the dc PSCs and, consequently, to a population imbalance between the branches of the quasiparticle energy spectrum. This conclusion was confirmed in Ref. 96, where a charge imbalance occurring under the influence of a relatively weak ($P < P_c$) microwave field was measured with a superconductor–insulator–normal metal (SIN) junction. The voltage across the SIN junction at zero bias is proportional to the charge imbalance. In the presence of the microwave field this voltage is the difference between the voltages of the autonomous and perturbed I–V characteristics at the point $I=0$, i.e., the detector response of the SIN junction to the microwave field. Measurements of the I–V characteristics and the differential resistance from the current through the SIN junction under irradiation by a microwave field at a frequency of 45 GHz revealed the presence of a charge imbalance.[96]

3.2. Time-averaged alternating supercurrent of a phase-slip center

As we mentioned at the beginning of this review, the time-averaged alternating supercurrent of a PSC, or the so-called cutoff current, is one of the main parameters characterizing the I–V characteristic of a channel.

In accordance with the above-described microscopic theory of the resistive current state,[1,51,53] the supercurrent exhibits Josephson oscillations in a PSC region with a length of the order of $x_1 \approx (\xi l_E)^{1/2}$. It was shown in Refs. 34, 35, and 57 that a PSC displays the properties of an SNS structure, where x_1 plays the role of a quasinormal region. It is also known that sinusoidal Josephson oscillations of the supercurrent can occur for superconducting microcontacts with dimensions much smaller than or comparable to the coherence length.[97,98] Since x_1 is manifestly greater than ξ, one would expect appreciable anharmonicity of the oscillations. The subharmonic current steps observed in Refs. 24 and 33 on the I–V characteristic of a channel irradiated by an electromagnetic field confirm this. Here the time-averaged supercurrent will be nonzero.

The cutoff current is determined by the intercepts on the current axis of the long segments of the I–V characteristic of the channel, the slopes of which are multiples of the dynamic resistance R_{d1} of a PSC (see Figs. 1, 14, and 15). The cutoff current on the I–V characteristic at zero voltage is just the time-averaged supercurrent $\overline{I_s}$ flowing through the nonequilibrium region in which the Josephson oscillations of the order parameter parameter arise.[24] We see from Figs. 1, 14, and 15 that by varying the critical current I_c and the dynamic

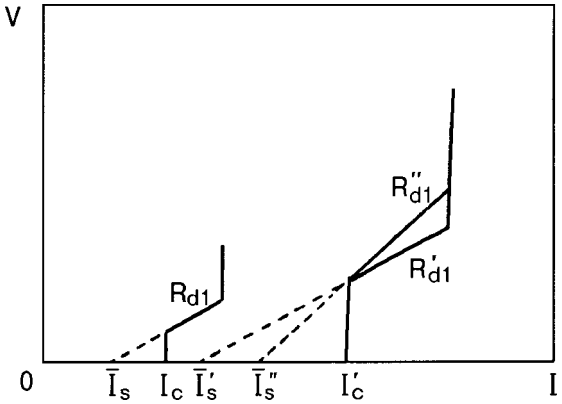

FIG. 15. Schematic current–voltage characteristics of a homogeneous superconducting channel.

resistance R_{d1} of a PSC, one can vary $\overline{I_s}$. Convenient parameters of the external influences for this purpose are the temperature and the frequency and power of the external electromagnetic radiation.

As we see in Fig. 8a and 14c, in the regime of suppression of superconductivity by electromagnetic radiation, in the case when the dynamic resistance $R_{d1}(P=0)$ of a dc PSC is larger than the resistance R_1 of a PSC produced by an electromagnetic field with $P \geqslant P_c$, the average supercurrent increases smoothly with increasing power. Here, as we have said, one observes a smooth decrease of the dynamic resistance. Curve *3* in Fig. 16 shows the reduced average supercurrent $\overline{I_s}(P)/\overline{I_s}(P=0)$ as a function of power for an irradiation frequency $f=200$ MHz.[99]

In the regime of stimulated superconductivity, in the case when the dynamic resistance $R_{d1}(P=0)$ is less than the resistance R_1 of an ac PSC, one observes an increase of the average supercurrent with increasing irradiation power (see

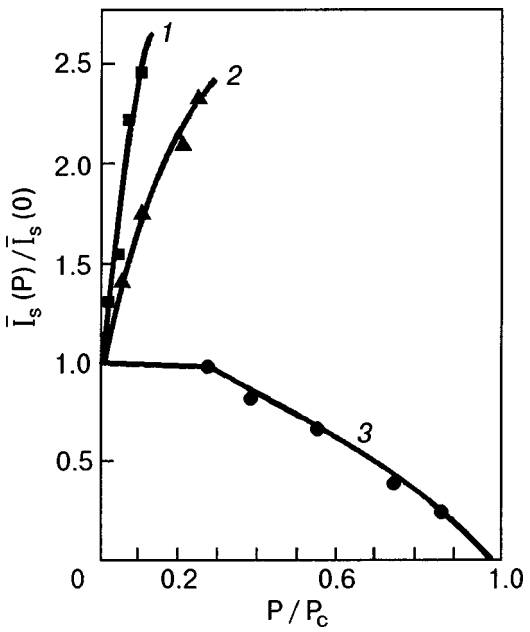

FIG. 16. Time-averaged supercurrent $\overline{I_s}(P)/\overline{I_s}(P=0)$ of a phase-slip center brought on by the passage of a dc current, as a function of the irradiation power: *1,2* — sample Sn-12, $f=23.39$ and 15.46 GHz, respectively; *3* — sample Sn-6, $f=200$ MHz.

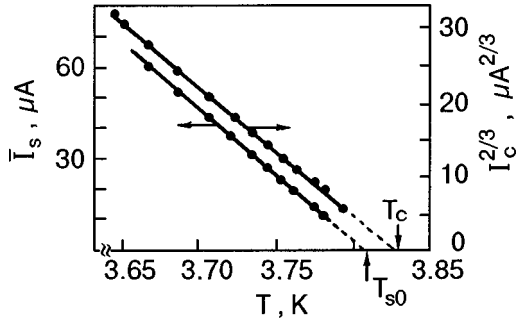

FIG. 17. Temperature dependence of the cutoff current $\overline{I_s}$ and the critical current $I_c^{2/3}$ for the tin film channel Sn-15.

Fig. 14a, 14b, 14d). It should be noted that the dynamic resistance $R_{d1}(P)$ also increases here. Curves *1* and *2* in Fig. 16 give $\overline{I_s}(P)/\overline{I_s}(P=0)$ as a function of the irradiation power in the stimulated superconductivity regime for two irradiation frequencies. We see that the rate of growth of the average supercurrent at an irradiation frequency of 23.39 GHz is higher than at $f=15.46$ GHz, i.e., the faster the dynamic resistance grows, the faster the average supercurrent of the PSC increases.

As the power is increased further, after suppression of superconductivity has set in, the average supercurrent also decreases, and this decrease in $\overline{I_s}(P)$ is faster for lower critical currents $I_c(P)$. Therefore, starting at some power level, the cutoff current of a dc PSC become equal to zero, while at the same time $I_c(P) \neq 0$ (see curves *6–9* in Fig. 14d), i.e., dc PSCs without a cutoff current appear.

It is important to note that the influence of the electromagnetic field on the value of the cutoff current, as on the dynamic resistance of a PSC, has a threshold character in both the stimulated- and suppressed-superconductivity regimes (see curve *3* in Fig. 16 and curve *2* in Fig. 14a; in Fig. 16 this is not visible at high frequencies on account of the scale),[99] as is characteristic for the influence of external radiation on an inhomogeneous superconductor.[100]

Figure 17 shows the $\overline{I_s}(T)$ and $I_c^{2/3}(T)$ curves of superconducting channel Sn-15. The domain of the function $\overline{I_s}(T)$ corresponds to the temperature region in which voltage jumps are observed due to the formation of dc PSCs.[99] At lower temperatures the I–V characteristics of the channel have a broken character, apparently because of overheating. If $\overline{I_s}(T)$ is approximated by a straight line, we obtain the temperature at which the cutoff current goes to zero: $T_{s0}=3.810\ \text{K}<T_c<3.830\ \text{K}$. Indeed, for $T>T_{s0}$ the I–V characteristics of the superconducting channels do not show evidence of the formation of dc PSCs, i.e., at the critical current there are no voltage jumps in the resistive region of the I–V characteristics.[99] An analogous picture is observed for whiskers. Figure 18 shows the temperature dependence of the cutoff current, critical current, and voltage jump $V_1(T)$ of the first dc PSC for an In–Pb whisker, as constructed from the family of I–V characteristics given in Ref. 101. For tin film channels one has $\Delta T=T_c-T_{s0}=20$–30 mK,[99] while for whiskers ΔT is several millikelvin, but the noncoincidence of T_c and T_{s0} is common property for them.

A similar situation has also been observed in the study of

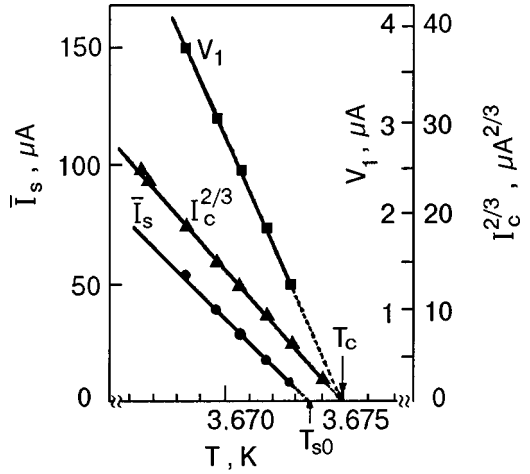

FIG. 18. Temperature dependence of the cutoff current $\bar{I}_s$, critical current $I_c^{2/3}$, and voltage jump V_1 of the first dc PSC of an In–Pb whisker.

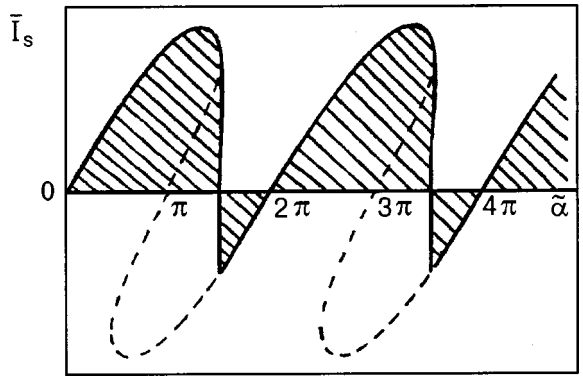

FIG. 20. Supercurrent–phase relation $\bar{I}_s(\tilde{\alpha})$ in a phase-slip center. At the points $\tilde{\alpha}_c$, $\tilde{\alpha}_c+2\pi$, ..., jumps occur to the branch corresponding to the minimum supercurrent.

superconducting channels of high-T_c superconductors (HTSCs). Figure 19 shows the temperature dependence of the cutoff current of the first, second, and third PSCs in a $YBa_2Cu_3O_{7-x}$ sample (HS-7).[76] In the resistive state this sample has a cutoff current. For the first and second dc PSCs the value of the cutoff current is the same ($\bar{I}_{s1}=\bar{I}_{s2}$), while for the third dc PSC $\bar{I}_{s3}>\bar{I}_{s1}=\bar{I}_{s2}$. This property is not exclusive to the HTSC sample. An analogous picture has been observed in a study of tin whiskers,[23] for example. When the $\bar{I}_{s1}(T)$, $\bar{I}_{s2}(T)$, and $\bar{I}_{s3}(T)$ curves are approximated by straight lines, we obtain the temperature at which the cutoff currents go to zero: $T_{s0}(88\ \mathrm{K})<T_c(93\ \mathrm{K})$. For ceramic samples $\Delta T=T_c-T_{s0}$ is much larger than for channel made of conventional superconductors. However, for ceramic samples the temperature region in which dc PSCs are observed is much larger than for conventional channels, but noncoincidence of T_c and T_{s0} is present in both cases.[76]

Several models have now been proposed in which the cutoff current has been estimated.[24,30,31,98,102] To explain the behavior of the average supercurrent of a dc PSC when the channel is irradiated by an electromagnetic field, we have used to model proposed in Ref. 98. As we have said, if the size x_1 of the nonequilibrium region of the PSC were smaller than the coherence length, the dependence of the supercurrent on the total phase shift $\tilde{\alpha}$ would be sinusoidal. In the real situation, when $x_1>\xi$, the phase dependence of the supercurrent is modified in such a way that $\bar{I}_s(\tilde{\alpha})$ is nonzero, and so a cutoff current appears. The greater the length x_1 of the nonequilibrium region, the larger the average supercurrent through the dc PSC[98] (see Fig. 20).

Thus in the framework of this model the value of the cutoff current depends on the amplitude of the supercurrent and the degree of anharmonicity of the Josephson oscillations, and the greater the length x_1 of the region where these oscillations occur, the higher the degree of anharmonicity.

It is seen in Fig. 15 that as the critical current increases ($I_c'>I_c$), so does the cutoff current ($\bar{I}_s'>\bar{I}_s$), but the dynamic resistance of the dc PSC remains unchanged ($R_{d1}'=R_{d1}$). Thus as the order parameter Δ and, with it, the amplitude of the superconducting current increase, so does the cutoff current,[23,103] provided that, in the process, the degree of anharmonicity of the Josephson oscillations, i.e., x_1 and, hence, R_{d1} either remain unchanged or change very slowly (as is observed for a superconducting channel on decreasing temperature). An increase in the average superconducting current ($\bar{I}_s''>\bar{I}_s'$) will also occur with increasing anharmonicity of the oscillations of the supercurrent, i.e., with increasing dynamic resistance ($R_{d1}''>R_{d1}'$), even if the amplitude of the supercurrent does not change in the process (the order parameter and, hence, the critical current remain constant) (see Fig. 15). Experimental studies of superconducting channels in a resistive current state have established that at fixed temperature ($T/T_c=\mathrm{const}$) for ''dirty'' samples the ratio $\bar{I}_s/I_c\approx 0.5$,[24] while for ''clean'' channels the ratio $\bar{I}_s/I_c$ reaches 0.8.[103] This behavior of the average supercurrent can be explained precisely by an increase in the anharmonicity of its Josephson oscillations. Indeed, with increasing mean free path the diffusion coefficient and, hence, the region of oscillations of the supercurrent $x_1=(\xi l_E)^{1/2}=\xi^{1/2}(D\tau_Q)^{1/4}$ also increase, leading to an increase in the cutoff current.

As the irradiation power is increased in the regime of stimulated superconductivity, the critical current of the channel and, hence, the amplitude of the supercurrent also increase. If the dynamic resistance $R_{d1}(P)$ and the region of

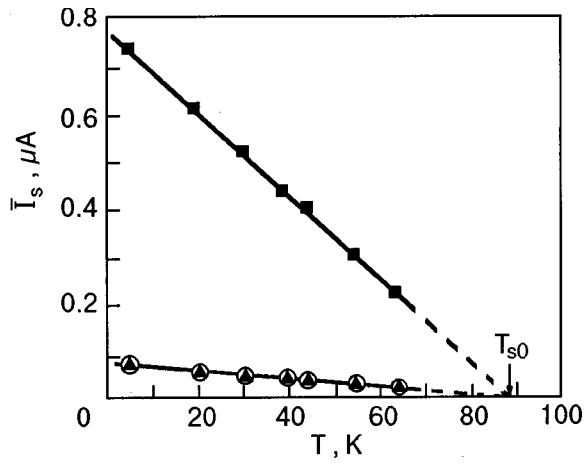

FIG. 19. Temperature dependence of the cutoff current $\bar{I}_s$ of the first (○), second (▲), and third (■) dc PSCs in sample HS-7.

supercurrent oscillations decrease in the process, then this leads to a decrease in the cutoff current. Therefore, for stimulation of superconductivity in the case when the dynamic resistance $R_{d1}(P=0)$ of a dc PSC is greater than the resistance R_1 of an ac PSC, $R_{d1}(P)$ and $\overline{I_s}$ remain unchanged (curve *2* in Fig. 14c). However, as the power increases further, when suppression of superconductivity sets in, the decrease of the cutoff current $\overline{I_s}$ occurs for two reasons: first, the amplitude of the supercurrent decreases, and, second, the resistance $R_{d1}(P)$ and, hence, the anharmonicity of the Josephson oscillations decrease.[99]

In the case when the dynamic resistance $R_{d1}(P=0)$ of a dc PSC is less than the resistance R_1 of an ac PSC, as the irradiation power increases in the regime of stimulated superconductivity the amplitude of the supercurrent and the dynamic resistance $R_{d1}(P)$ increase, and hence, so does the degree of anharmonicity of the oscillations of the supercurrent (Fig. 14a,b, and d). Therefore, the average supercurrent $\overline{I_s}$ also increases, and the larger the value of $R_{d1}(P)$ and, hence, of x_1, the larger the cutoff current (curves *1* and *2* in Fig. 16).[99]

As the irradiation power is increased in the regime in which the superconductivity is suppressed by an electromagnetic field, the value of the critical current and, hence, the amplitude of the supercurrent through a dc PSC decrease. Increasing the region of oscillations of the supercurrent $x_1 \sim R_{d1}(P)$ leads to growth of the cutoff current. Therefore, in the case when the dynamic resistance $R_{d1}(P)$ of a dc PSC is less than or of the order of the resistance R_1 of an ac PSC, the cutoff current is unchanged in the regime of suppressed superconductivity (see Fig. 8b).[99]

When $R_{d1}(P=0)>R_1$ both the oscillation region and the amplitude of the supercurrent decrease with increasing irradiation power. Therefore, the cutoff current also decreases (see Fig. 8a). At irradiation powers close to critical the average supercurrent of the dc PSCs becomes zero, while the critical current is nonzero. It can be assumed that at sufficiently high irradiation powers ($P \geqslant P_c$) the order parameter and supercurrent in the PSC executes harmonic oscillations with the frequency of the external electromagnetic field. Here averaging the supercurrent through the PSC over time gives a zero value of the cutoff current.[99]

As to the fact that the cutoff current in the temperature region $\Delta T = T_c - T_{s0}$ is equal to zero, here different situations, requiring further study, are possible. One possible is that as the temperature approaches T_c, the ratio x_1/ξ and the degree of anharmonicity of the Josephson oscillations of the supercurrent decrease, and at a certain temperature T_{s0} the cutoff current goes to zero, i.e., in the temperature interval ΔT there exist PSCs for which the Josephson oscillations of the supercurrent are practically harmonic. Indeed, for tin film samples the ratio $x_1/\xi \propto (1-T/T_c)^{1/8}$, and for $T \to T_c$ it goes to zero.[99] Granted, there remains an open question as to the fluctuations near T_c, which smear out the structure of the PSC.

4. CURRENTS FOR THE ONSET OF PHASE-SLIP CENTERS IN A SUPERCONDUCTING CHANNEL

At a dc current below the Ginzburg–Landau critical current I_c, the channel is in the superconducting state. At $I>I_c$ the first dc PSC, with a dynamic resistance R_{d1}, appears in the channel.[1,24,47] This resistive state of the channel is maintained in the current interval $\Delta I_1 = I_{c1} - I_c$, where I_{c1} is the current at which the second dc PSC arises in the channel. The resistive state of a channel with two dc PSCs is maintained in the current interval $\Delta I_2 = I_{c2} - I_{c1}$, where I_{c2} is the current at which a third dc PSC arises in the channel. As the dc current is increased further, more new dc PSCs form, until the whole channel has gone into the normal state.

The experimental dependence of the critical currents I_{ci} as a function of i ($i=1,2,3\ldots$) (see, e.g., Refs. 24 and 88) is qualitatively the same as predicted in Refs. 47 and 104. We note that the criticism of Ref. 47 brought in Ref. 105 was based on a misunderstanding in connection with the use of the asymptotic formula $I_{ci} = I_c[1+\exp(-l\sqrt{\Delta}/2i)]$. This formula is valid for describing I_{ci} only in extremely long channels ($l \gg 4il_E$). In the actual situation one must use the results of a numerical calculation, which are well approximated by the asymptotic expression:

$$I_{ci} = I_c\left[\frac{b}{a} + a^2\left(\frac{2il_E}{l}\right)\right] \approx I_c\left[0.841 + 2.075\left(\frac{2il_E}{l}\right)^2\right], \tag{4.1}$$

where

$$a = 3\int_{x_c}^{1} \frac{dx}{\sqrt{A(x)}} \frac{x^2 - x_c^2}{\sqrt{1-x^2}};$$

$$b = 3\int_{x_c}^{1} \frac{dx}{A^{3/2}(x)} B(x) \frac{x^2 - x_c^2}{\sqrt{1-x^2}};$$

$$A(x) = 3(x_c\sqrt{1-x_c^2} - x\sqrt{1-x^2}) + \arcsin x_c - \arcsin x;$$

$$B(x) = \frac{6}{5}x^5 - 2x_c^2x^3 + \frac{4}{5}x_c^5; \quad x_c = \left(\frac{2}{3}\right)^{1/2},$$

and, for simplicity, the cutoff current is assumed equal to zero. Formula (4.1) gives a value of I_{ci} which is several percent greater than that obtained in Ref. 104:

$$I_{ci} = I_c \frac{\cosh(l/2il_E) - \overline{I_s}/I_c}{\cosh(l/2il_E) - 1}. \tag{4.2}$$

It is known, however, that the current interval ΔI_i between voltage steps increases more rapidly with the number of the dc PSC in sequence than is predicted by the theories, i.e., the $(i+1)$-th PSC is formed by a current I_{ci} larger than the predicted current. The reason for this disagreement may be that the dc PSCs that have formed affect the remaining superconducting part of the channel, and this possibility was not taken into account in Refs. 47 and 104.

In an experimental study of the nonequilibrium states of tin whiskers with multipotential leads, it was shown[2] that dc PSCs separated by distances ($\sim 300\ \mu$m) much greater than the coherence length ξ and the penetration depth l_E of the longitudinal electric field into the superconductor interact with one another. This is manifested in the fact that a dc PSC arising at a current I_{ci} in one part of the channel can increase or depress the insertion current $I_{c(i+1)}$ of the next dc PSC, which is located in a different part of the channel at a much greater distance away than could be explained by diffusion

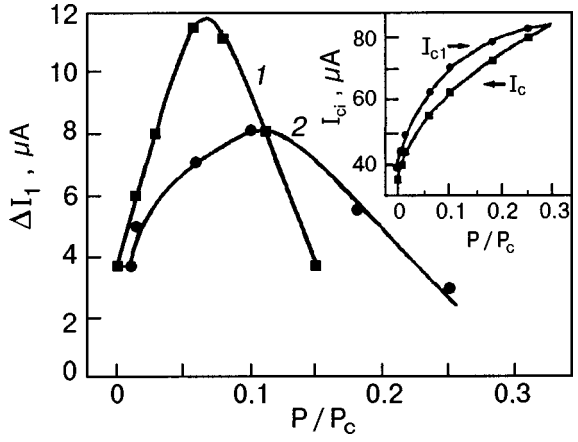

FIG. 21. The difference between the values of the currents at which the first and second voltage steps appear on the current–voltage characteristic of sample Sn-12, $\Delta I_1 = I_{c1} - I_c$, versus the power of the external electromagnetic field at frequencies $f = 23.39$ GHz (*1*) and 15.46 GHz (*2*), $T = 3.774$ K. The inset shows the critical currents I_{c1} and I_c of sample Sn-12 as functions of the power of the microwave field at $f = 15.46$ GHz.

of the quasiparticle current or by quasiparticle injection or extraction.[2] This implies that it is a long-range interaction.

As to the nature of the increase in the current I_{ci} for the onset of the next dc PSC, the most preferable hypothesis appears to be that proposed in Ref. 2 and confirmed in Ref. 106, viz., that the Josephson electromagnetic field of a dc PSC affects the superconducting properties of the channel.

4.1. Phase-slip centers caused by direct current. The influence of external irradiation

Let us consider the influence of external electromagnetic irradiation on the currents at which dc PSCs arise in the channel. Figure 21 shows the difference $\Delta I_1 = I_{c1} - I_c$ between the values of the currents at which the first and second voltage steps appear on the I–V characteristics of sample Sn-12 as a function of the power of the electromagnetic field for frequencies of 23.39 GHz (curve *1*) and 15.46 GHz (curve *2*).[106] At these irradiation frequencies stimulation of superconductivity is observed, i.e., the value of the critical current I_{ci} increases with increasing irradiation power (see the inset in Fig. 21). We see that as the irradiation power increases, $\Delta I_1(P/P_c)$ initially increases and then begins to decrease. This occurs because I_c and I_{c1} depend on the irradiation power in different ways: the critical current I_{c1} increases with increasing power more rapidly than does I_c, but then the increase in I_{c1} slows down, and at a certain power one has $I_{c1} = I_c$. Here the channel undergoes a transition from the superconducting to the normal state. It should be emphasized that as the irradiation frequency decreases, the maximum of $\Delta I_1(P/P_c)$ decreases in value and shifts to higher powers.[106]

The $\Delta I_1(P/P_c)$ curve (see Fig. 21) obtained in the regime of stimulated superconductivity is qualitatively similar to the temperature dependence $\Delta I_1(T)$ given in Ref. 2 (see Fig. 97 of that paper). It is seen from the figure that with decreasing temperature the $\Delta I_1(T)$ curve varies nonmonotonically, in fundamental disagreement with the predictions of the theories proposed in Refs. 47 and 104. It is possible that taking into account the interaction between dc PSCs, which was not done in those papers, will change the values of the critical currents I_{ci} of the superconducting channels. When a channel is subjected to an electromagnetic field at a frequency below the boundary frequency for stimulation,[59,60] the superconductivity is suppressed. In that case the critical currents I_c and I_{c1} decrease with increasing irradiation power, with the depression of I_{c1} occurring more slowly than that of I_c. Consequently, $\Delta I_1(P/P_c)$ increases, as in the previous case.[106]

The stabilizing of the resistive state, which is manifested in an increase in $\Delta I_1(P/P_c)$, decreases with increasing irradiation frequency. For tin film samples the increase of $\Delta I_1(P/P_c)$ under irradiation by an electromagnetic field starts at frequencies of ~ 100 MHz. Interestingly, the influence of an electromagnetic field on $\Delta I_1(P/P_c)$, like the influence on the dynamic resistance and the cutoff current of a dc PSC,[99] has a threshold in terms of the power of the microwave field.

Difficulties also arise in explaining the presence of a descending branch of $\Delta I_1(P/P_c)$, since even high-side estimates show that the overheating of the film in these experiments is negligibly small ($\sim 10^{-3}$ K; see Sec. 2.3). The absence of an overheating effect is also seen on the I–V characteristics (see Figs. 8 and 14). Therefore, the descending branch of $\Delta I_1(P/P_c)$ is not due to overheating of the sample but is a consequence of the inherent nature of the interaction of a dc PSC with an external electromagnetic field.

It can thus be stated that in the regime of stimulated superconductivity, as in the case of rather low irradiation frequencies, where suppression of superconductivity is observed, the state of a superconducting channel in which current-induced dc PSCs have formed becomes increasingly stable against a rise in the dc current as the irradiation power is increased. This is manifested in a lengthening of the linear parts of the I–V characteristics, with resistances that are multiples of R_{d1}. It should be noted that in the regime of stimulation of superconductivity by a microwave field, in certain cases tin channels, after the formation of the first current-induced dc PSC in them, withstood a dc current almost four times as large as in the case of zero irradiation power before the second dc PSC formed, i.e., the maximum $\Delta I_1(P)/\Delta I_1(P=0) \approx 4$. Here the value of I_c increased only by a factor of 1.5.[107] This indicates that the microwave field affects the currents I_c and I_{c1} differently.

Experimental studies[106] have confirmed the conjecture that the Josephson radiation from the dc PSC has a stabilizing influence on the resistive state of a channel. It is important to note that for tin whiskers the Josephson frequency of a dc PSC has a value $f_J \approx 500$ MHz,[2,33] which is much smaller than the lower frequency boundary for stimulation. However, even in this case a strong increase in ΔI_i with increasing i is observed. There is as yet no theoretical explanation for this effect.

4.2. Phase-slip centers caused by electromagnetic radiation

As was shown in Sec. 2, when a superconducting channel is acted on by an external rf electromagnetic field, ac PSCs arise in the channel, starting at a certain power level P_c. Figure 22 shows two families of I–V characteristics of

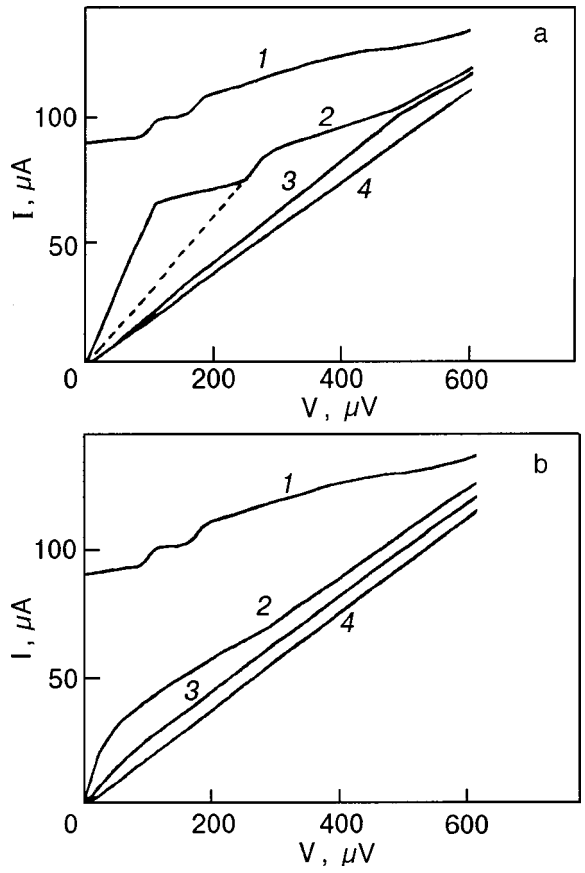

FIG. 22. Families of current–voltage characteristics of channel Sn-3 at various power levels of the external irradiation at $T=3.762$ K and $f=3.825$ GHz (a) and $f=0.075$ GHz (b). For the first I–V characteristic (curve *1*) the irradiation power is zero, and the rest of the curves are numbered in order of increasing power.

sample Sn-3.[107] It is seen that at a high irradiation frequency (3.825 GHz) the state of the channel in which an ac PSC has formed is more stable against a rise in the dc current (the initial parts of the I–V curves are extended). At a low irradiation frequency (75 MHz) the state of the channel in which an ac PSC has formed is extremely unstable with respect to the passage of a dc current: the I–V characteristics become nonlinear as the dc current increases.[107] It should be noted here that the resistance R_1 of an ac PSC at $f=3.825$ GHz is equal to 1.6 Ω, while at $f=75$ MHz one has $R_1=1.3$ Ω. Consequently, the Joule heating $I^2R_1(f)$ at an irradiation frequency of 3.825 GHz is even larger than at $f=75$ MHz. However, the ac PSC is more stable at the higher irradiation frequency than at the low frequency, as is convincingly seen on the initial parts of the I–V characteristics (see Fig. 22). Thus with increasing irradiation frequency the states of a superconducting channel in which ac PSCs have formed only become more stable against a rise in the dc current, and this takes place in the entire power interval in which the ac PSCs exist, i.e., one observes a preservation of the linearity of the initial segments of the I–V characteristics with increasing irradiation power at the given frequency.

One should also note the following circumstance. In Refs. 94 and 95 it was shown that with increasing irradiation frequency an increase of the critical power is observed; this behavior of P_c is observed up to frequencies $\omega' \approx (1-T/T_c)^{1/2}/1.2\tau_\varepsilon$ (here the frequency ω' is the inverse relaxation time of the gap), after which P_c remains practically unchanged as the irradiation frequency is increased further. Consequently, as the irradiation frequency increases, the value of the ac current giving rise to an ac PSC increases. However, as we have said, the states of the superconducting channel in which ac PSCs have formed become more, not less stable against the passage of dc current through them as the frequency of the ac current increases.

Thus it is clear from what we have said that the states of superconducting channels with PSCs become more stable against the passage of currents in the presence of an external electromagnetic field than in the absence of such a field. This effect is observed starting at irradiation frequencies of the order of the inverse relaxation time of the charge imbalance, $f_Q=(2\pi\tau_Q)^{-1}$ ($f_Q=100$ MHz for sample Sn-12). Consequently, this stimulation of superconductivity by an electromagnetic field cannot be explained, since that would require higher irradiation frequencies.

CONCLUSION

In summary, the onset and formation of phase-slip centers in an ac electromagnetic field are complex processes that remain largely unexplained. As the ongoing accumulation of experimental data continues, one can hope that adequate theoretical models will soon make their debut.

At present the resistive state of superconducting channels is represented as a set of individual noninteracting PSCs. To understand the process by which a channel of finite length is filled with PSCs and the interaction between PSCs will require further experimental and theoretical investigation. We hope that the present review will facilitate this.

We thank E. V. Bezuglyi, both for many years of scientific collaboration, in general, and for providing the asymptotic formulas (4.1) and for helpful discussions of the material presented in this review, in particular.

*E-mail: dmitriev@ilt.kharkov.ua

[1] B. I. Ivlev and N. B. Kopnin, Usp. Fiz. Nauk **142**, 435 (1984) [Sov. Phys. Usp. **27**, 206 (1984)].
[2] R. Tidecks, *Current-Induced Nonequilibrium Phenomena in Quasi-One-Dimensional Superconductors. Springer Tracts in Modern Physics, Vol. 142*, Springer-Verlag, Berlin/Heidelberg/New York (1990).
[3] I. M. Dmitrenko, Fiz. Nizk. Temp. **22**, 849 (1996) [Low Temp. Phys. **22**, 648 (1996)].
[4] J. A. Pals, K. Weiss, P. M. T. M. Attekum, R. E. Horstman, and J. Wolter, Phys. Rep. **86**, 323 (1982).
[5] I. L. Landau, JETP Lett. **11**, 293 (1970).
[6] A. B. Pippard, J. G. Shepherd, and D. A. Tindall, Proc. R. Soc. London, Ser. A **324**, 17 (1971).
[7] V. V. Shmidt, *Introduction to the Physics of Superconductors* [in Russian], Nauka, Moscow (1982).
[8] M. Tinkham and J. Clarke, Phys. Rev. Lett. **28**, 1366 (1972).
[9] S. N. Artemenko and A. F. Volkov, Usp. Fiz. Nauk **128**, 3 (1979) [Sov. Phys. Usp. **22**, 295 (1979)].
[10] V. P. Galaĭko, Zh. Éksp. Teor. Fiz. **66**, 379 (1974) [Sov. Phys. JETP **39**, 181 (1974)].
[11] P. G. de Gennes, *Superconductivity of Metals and Alloys* [Benjamin, New York (1966); Mir, Moscow (1968)].
[12] S. N. Artemenko and A. F. Volkov, JETP Lett. **21**, 313 (1975); **22**, 190 (1975).
[13] A. Schmid and G. Schon, J. Low Temp. Phys. **20**, 207 (1975).
[14] S. N. Artemenko, A. F. Volkov, and A. V. Zaitsev, J. Low Temp. Phys. **30**, 487 (1978).

[15] M. Tinkham, Phys. Rev. B **6**, 1747 (1972).
[16] J. Clarke and J. L. Paterson, J. Low Temp. Phys. **15**, 491 (1974).
[17] K. E. Gray (Ed.), *Nonequilibrium Superconductivity, Phonons and Kapitza Boundaries*, Plenum Press, New York (1981).
[18] M. Stuivinga, J. E. Mooij, and T. M. Klapwijk, J. Low Temp. Phys. **46**, 555 (1982).
[19] B. I. Ivlev, N. B. Kopnin, and C. J. Pethick, Zh. Éksp. Teor. Fiz. **79**, 1017 (1980) [Sov. Phys. JETP **52**, 516 (1980)].
[20] W. W. Webb, Bull. Am. Phys. Soc. **13**, 379 (1968).
[21] W. W. Webb and R. J. Warburton, Phys. Rev. Lett. **20**, 461 (1968).
[22] J. D. Meyer and G. V. Minnigerode, Phys. Lett. A **38**, 529 (1972).
[23] J. D. Meyer, Appl. Phys. **2**, 303 (1973).
[24] W. J. Skocpol, M. R. Beasley, and M. Tinkham, J. Low Temp. Phys. **16**, 145 (1974).
[25] G. E. Churilov, V. M. Dmitriev, and A. P. Beskorsyĭ, JETP Lett. **11**, 146 (1969).
[26] V. P. Galaĭko, V. M. Dmitriev, and G. E. Churilov, JETP Lett. **18**, 213 (1973).
[27] V. P. Galaiko, V. M. Dmitriev, E. V. Khristenko, and G. E. Churilov, Rev. Phys. Appl. **9**, 161 (1974).
[28] V. P. Galaĭko, Zh. Éksp. Teor. Fiz. **68**, 223 (1975) [Sov. Phys. JETP **41**, 108 (1975)].
[29] J. S. Langer and V. Ambegaokar, Phys. Rev. **164**, 498 (1967).
[30] T. J. Rieger, D. J. Scalapino, and J. E. Mercereau, Phys. Rev. Lett. **27**, 1787 (1971).
[31] T. J. Rieger, D. J. Scalapino, and J. E. Mercereau, Phys. Rev. B **6**, 1734 (1972).
[32] B. D. Josephson, Phys. Lett. **1**, 251 (1962).
[33] R. Tidecks and G. V. Minnigerode, Phys. Status Solidi A **52**, 421 (1979).
[34] G. E. Churilov, D. A. Dikin, V. M. Dmitriev, and V. N. Svetlov, Fiz. Nizk. Temp. **17**, 185 (1991) [Sov. J. Low Temp. Phys. **17**, 96 (1991)].
[35] G. E. Churilov, A. B. Agafonov, D. A. Dikin, and V. M. Dmitriev, Fiz. Nizk. Temp. **24**, 737 (1998) [Low Temp. Phys. **24**, 555 (1998)].
[36] T. M. Klapwijk and J. E. Mooij, Phys. Lett. A **57**, 97 (1976).
[37] T. M. Klapwijk, M. Supers, and J. E. Mooij, J. Low Temp. Phys. **27**, 801 (1977).
[38] M. Stuivinga, C. L. G. Ham, T. M. Klapwijk, and J. E. Mooij, J. Low Temp. Phys. **53**, 633 (1983).
[39] J. D. Meyer and R. Tidecks, Solid State Commun. **24**, 639 (1977).
[40] J. D. Meyer and R. Tidecks, Solid State Commun. **24**, 643 (1977).
[41] J. M. Aponte and M. Tinkham, J. Low Temp. Phys. **51**, 189 (1983).
[42] J. D. Meyer and R. Tidecks, Solid State Commun. **18**, 305 (1976).
[43] G. Slama and R. Tidecks, Solid State Commun. **44**, 425 (1982).
[44] G. J. Dolan and L. D. Jackel, Phys. Rev. Lett. **39**, 1628 (1977).
[45] V. P. Galaĭko, Zh. Éksp. Teor. Fiz. **71**, 273 (1976) [Sov. Phys. JETP **44**, 141 (1976)].
[46] V. P. Galaiko, J. Low Temp. Phys. **26**, 483 (1977).
[47] E. V. Bezuglyi, E. I. Bratus', and V. P. Galaĭko, Fiz. Nizk. Temp. **3**, 1010 (1977) [Sov. J. Low Temp. Phys. **3**, 491 (1977)].
[48] V. P. Galaĭko, Fiz. Nizk. Temp. **2**, 807 (1976) [Sov. J. Low Temp. Phys. **2**, 397 (1976)].
[49] V. P. Galaĭko, Zh. Éksp. Teor. Fiz. **61**, 382 (1971) [Sov. Phys. JETP **34**, 203 (1972)].
[50] V. P. Galaĭko, Zh. Éksp. Teor. Fiz. **64**, 1824 (1973) [Sov. Phys. JETP **37**, 922 (1973)].
[51] B. I. Ivlev, N. B. Kopnin, and L. A. Maslova, Zh. Éksp. Teor. Fiz. **78**, 1963 (1980) [Sov. Phys. JETP **51**, 986 (1980)].
[52] B. I. Ivlev, N. B. Kopnin, and L. A. Maslova, Fiz. Tverd. Tela (Leningrad) **22**, 252 (1980) [Sov. Phys. Solid State **22**, 149 (1980)].
[53] B. I. Ivlev and N. B. Kopnin, J. Low Temp. Phys. **44**, 453 (1981).
[54] B. I. Ivlev and N. B. Kopnin, JETP Lett. **28**, 592 (1978).
[55] L. Kramer and R. J. Watts-Tobin, Phys. Rev. Lett. **40**, 1041 (1978).
[56] R. J. Watts-Tobin, Y. Krahenbuhl, and L. Kramer, J. Low Temp. Phys. **42**, 459 (1981).
[57] G. A. Gogadze, V. M. Dmitriev, V. N. Svetlov, and G. E. Churilov, *Abstracts of the Twenty-Fourth All-Union Conference on Low-Temperature Physics* [in Russian], Tbilisi (1986), Part 1, p. 196.
[58] A. F. G. Wyatt, V. M. Dmitriev, W. S. Moore, and F. W. Sheard, Phys. Rev. Lett. **16**, 1166 (1966).
[59] V. M. Dmitriev and E. V. Khristenko, Fiz. Nizk. Temp. **4**, 821 (1978) [Sov. J. Low Temp. Phys. **4**, 387 (1978)].
[60] G. M. Eliashberg, JETP Lett. **11**, 114 (1970).
[61] A. G. Aronov, Zh. Éksp. Teor. Fiz. **70**, 1477 (1976) [Sov. Phys. JETP **43**, 770 (1976)].
[62] A. D. Smith, M. Tinkham, and W. J. Skocpol, Phys. Rev. B **22**, 4346 (1980).
[63] B. I. Ivlev, Zh. Éksp. Teor. Fiz. **72**, 1197 (1977) [Sov. Phys. JETP **45**, 626 (1977)].
[64] E. V. Ginzburg and B. Z. Spivak, Zh. Éksp. Teor. Fiz. **80**, 2013 (1980) [Sov. Phys. JETP **53**, 1047 (1980)].
[65] V. M. Dmitriev and E. V. Khristenko, JETP Lett. **29**, 697 (1979).
[66] Yu. I. Latyshev and F. Ya. Nad', JETP Lett. **26**, 354 (1977).
[67] Yu. I. Latyshev and F. Ya. Nad', J. Phys. (Paris) **39**, C 6-531 (1978).
[68] S. K. Tolpygo and V. A. Tulin, JETP Lett. **28**, 638 (1978).
[69] S. K. Tolpygo and V. A. Tulin, Zh. Éksp. Teor. Fiz. **78**, 2352 (1980) [Sov. Phys. JETP **51**, 1182 (1980)].
[70] P. J. M. Bentum, J. W. Gerritsen, and P. Wyder, Solid State Commun. **56**, 943 (1985).
[71] V. M. Dmitriev, I. V. Zolochevskii, V. P. Sklyarov, and E. V. Khristenko, Fiz. Nizk. Temp. **14**, 547 (1988) [Sov. J. Low Temp. Phys. **14**, 302 (1988)].
[72] P. J. M. Bentum, *Far Infrared Studies of Nonequilibrium Superconductivity* (Thesis), de Katholieke Universiteit te Nijmegen, Krips Repro, Meppel (1985).
[73] H. W. Ott, *Noise Reduction Techniques in Electronic Systems* (1st ed.) [Wiley, New York (1976); Mir, Moscow (1979)].
[74] A. van der Ziel, *Noise; Sources, Characterization, Measurement* [Prentice-Hall, Englewood Cliffs, N.J. (1970); Sov. Radio, Moscow (1973)].
[75] H. Nyquist, Phys. Rev. **32**, 110 (1928).
[76] V. M. Dmitriev, I. V. Zolochevskii, and E. V. Khristenko, Fiz. Nizk. Temp. **19**, 249 (1993) [Low Temp. Phys. **19**, 173 (1993)]; V. M. Dmitriev, I. V. Zolochevskii, and E. V. Khristenko, Physica C **235–240**, 1973 (1994).
[77] V. M. Dmitriev, I. V. Zolochevskii, and E. V. Khristenko, Fiz. Nizk. Temp. **12**, 643 (1986) [Sov. J. Low Temp. Phys. **12**, 365 (1986)].
[78] G. M. Éliashberg, Zh. Éksp. Teor. Fiz. **61**, 1254 (1971) [Sov. Phys. JETP **34**, 668 (1972)].
[79] A. M. Kadin, L. N. Smith, and W. J. Skocpol, J. Low Temp. Phys. **38**, 497 (1980).
[80] B. A. Mattoo and Y. Singh, Pramana. J. Phys. **19**, 483 (1982).
[81] I. O. Kulik, Fiz. Nizk. Temp. **5**, 1391 (1979) [Sov. J. Low Temp. Phys. **5**, 656 (1979)].
[82] N. M. Rudheimer, A. Lehoczky, and C. V. Briscoe, Phys. Rev. **154**, 414 (1967).
[83] V. M. Dmitriev, I. V. Zolochevskii, and E. V. Khristenko, Fiz. Nizk. Temp. **12**, 540 (1986) [Sov. J. Low Temp. Phys. **12**, 305 (1986)].
[84] V. M. Dmitriev, I. V. Zolochevskii, and E. V. Khristenko, Fiz. Nizk. Temp. **10**, 777 (1984) [Sov. J. Low Temp. Phys. **10**, 409 (1984)].
[85] V. M. Dmitriev and E. V. Khristenko, Fiz. Nizk. Temp. **3**, 1210 (1977) [Sov. J. Low Temp. Phys. **3**, 587 (1977)].
[86] V. P. Galaĭko, V. M. Dmitriev, and G. E. Churilov, Fiz. Nizk. Temp. **2**, 299 (1976) [Sov. J. Low Temp. Phys. **2**, 148 (1976)].
[87] G. A. Gogadze and I. O. Kulik, Fiz. Nizk. Temp. **6**, 1210 (1980) [Sov. J. Low Temp. Phys. **6**, 587 (1980)].
[88] V. M. Dmitriev, I. V. Zolochevskii, and E. V. Khristenko, Fiz. Nizk. Temp. **14**, 134 (1988) [Sov. J. Low Temp. Phys. **14**, 73 (1988)].
[89] M. L. Yu and J. E. Mercereau, Phys. Rev. Lett. **28**, 1117 (1972).
[90] M. L. Yu and J. E. Mercereau, Phys. Rev. B **12**, 4909 (1975).
[91] Yu. I. Latyshev and F. Ya. Nad', JETP Lett. **29**, 557 (1979).
[92] V. V. Ryazanov, L. A. Ermolaeva, and V. V. Schmidt, J. Low Temp. Phys. **45**, 507 (1981).
[93] J. D. N. Cheek, B. Nebral, and K. Martinon, J. Phys. (Paris) **18**, 557 (1973).
[94] J. A. Pals and J. J. Ramekers, Phys. Lett. A **87**, 186 (1982).
[95] E. V. Bezuglyi, V. M. Dmitriev, V. N. Svetlov, G. E. Churilov, and A. Yu. Azovskii, Fiz. Nizk. Temp. **13**, 906 (1987) [Sov. J. Low Temp. Phys. **13**, 517 (1987)].
[96] G. A. Ovsyannikov, S. V. Proklov, and I. L. Serpuchenko, Fiz. Tverd. Tela (Leningrad) **30**, 867 (1988) [Sov. Phys. Solid State **30**, 500 (1988)].
[97] K. K. Likharev and L. A. Yakobson, Zh. Tekh. Fiz. **46**, 1503 (1975) [Sov. Phys. Tech. Phys. **20**, 950 (1975)].
[98] I. O. Kulik, A. N. Omel'yanchuk, and V. A. Khlus, Fiz. Nizk. Temp. **6**, 988 (1980) [Sov. J. Low Temp. Phys. **6**, 480 (1980)].
[99] V. M. Dmitriev, I. V. Zolochevskii, and E. V. Khristenko, Fiz. Nizk. Temp. **19**, 764 (1993) [Low Temp. Phys. **19**, 545 (1993)].
[100] L. G. Aslamazov and A. I. Larkin, Zh. Éksp. Teor. Fiz. **74**, 2184 (1978) [Sov. Phys. JETP **47**, 1136 (1978)].
[101] R. Tidecks and T. Werner, J. Low Temp. Phys. **65**, 151 (1986).
[102] H. A. Notarys and J. E. Mercereau, Physica (Amsterdam) **55**, 424 (1971).
[103] R. Tidecks and J. D. Meyer, Z. Phys. B: Condens. Matter **32**, 363 (1979).
[104] M. Tinkham, J. Low Temp. Phys. **35**, 147 (1979).

[105] K. Yu. Arutyunov, N. P. Danilova, and A. A. Nikolaeva, Physica C **235–240**, 1967 (1994).
[106] V. M. Dmitriev, I. V. Zolochevskii, and E. V. Khristenko, Fiz. Nizk. Temp. **22**, 1371 (1996) [Low Temp. Phys. **22**, 1039 (1996)].
[107] V. M. Dmitriev, I. V. Zolochevskii, and E. V. Khristenko, J. Low Temp. Phys. **115**, 173 (1999).

Translated by Steve Torstveit

QUANTUM LIQUIDS AND QUANTUM CRYSTALS

Structure of the superfluid component and spectrum of elementary excitations in the quantum Bose liquid ^{4}He

É. A. Pashitskiĭ*

Institute of Physics, National Academy of Sciences of Ukraine, pr. Nauki 46, 03022 Kiev, Ukraine

S. I. Vil'chinskiĭ**

T. Shevchenko Kiev University, pr. Akad. Glushkova 6, 03022 Kiev, Ukraine

(Submitted December 20, 1999; revised July 17, 2000)
Fiz. Nizk. Temp. **27**, 253–267 (March 2001)

A self-consistent model is constructed for a superfluid Bose liquid in which the single-particle Bose–Einstein condensate (BEC) is suppressed on account of the strong interaction between bosons. The ratio of the density of the BEC to the total density of the Bose liquid is small, $n_0/n \ll 1$, in contrast to the Bogolyubov theory for a nearly ideal Bose gas, in which the small parameter is the ratio of the number of overcondensate excitations to the number of particles in the intense BEC, $(n-n_0)/n_0 \ll 1$. A closed system of nonlinear integral equations for the normal $\tilde{\Sigma}_{11}(\mathbf{p},\omega)$ and anomalous $\tilde{\Sigma}_{12}(\mathbf{p},\omega)$ self-energy parts is obtained in a renormalized perturbation theory constructed in the combined hydrodynamic (for $p \to 0$) and field (for $p \neq 0$) variables, the use of which ensures analyticity of the functions $\tilde{\Sigma}_{ij}(\mathbf{p},\varepsilon)$ for $p \to 0$ and $\varepsilon \to 0$ and a nonzero value of the superfluid order parameter $\tilde{\Sigma}_{12}(0,0) \neq 0$ at $T=0$. It is shown that the structure of the quasiparticle spectrum $E(p)$ and, in particular, the presence of a roton minimum are determined by the sign-varying and oscillatory behavior of the Fourier component of the pair interaction between bosons in the ''hard spheres'' model. An important role here is played by the renormalization (screening) of the pair interaction on account of many-particle (collective) effects, which are described by a polarization operator of the bosons on the ''mass shell'' and leads to enhancement of the effective attraction in certain regions of momentum space. It is shown that the superfluid component ρ_s at $T \to 0$ in this model is a superposition of the single-particle BEC and a pair coherent condensate, analogous to the condensate of Cooper pairs in superconductors. The structure of the superfluid state for $T \neq 0$ is also considered, with allowance for the appearance of a normal component ρ_n and a branch of second sound, the velocity of which goes to zero at the λ point. The applicability of the Landau superfluidity criterion is examined, and the question of the limiting permissible critical velocity of superfluid flow in the absence of quantum vortices is discussed. [DOI: 10.1063/1.1355516]

1. INTRODUCTION

The quantum structure of the superfluid state of liquid ^{4}He below the λ point (He II) remains in dispute (see, e.g., Refs. 1–3). As was pointed out in Ref. 4, there are a number of contradictions between underlying principles and conclusions of the microscopic theory of ^{4}He superfluidity[5–8] and the experimental data. In particular, according to recent results on the quantum evaporation of ^{4}He atoms,[9] the maximum density ρ_0 of the single-particle Bose–Einstein condensate (BEC) in by the Bose liquid ^{4}He, even at very low temperatures $T \ll T_\lambda$, does not exceed 10% of the total density ρ of liquid ^{4}He, whereas the density of the superfluid component $\rho_s \to \rho$ at $T \to 0$. This low density of the BEC is due to the strong interaction between the ^{4}He atoms and to the large energies of the quantum fluctuations (zero-point vibrations) as $T \to 0$ and of the thermodynamic (thermal) fluctuations for $T > 0$, and it indicates that this ''depleted'' single-particle BEC cannot by itself serve as the microscopic basis of the superfluid component ρ_s. Therefore, the quantum structure of the effective superfluid condensate in He II, with an ''excess'' density $\rho_s - \rho_0 \gg \rho_0$, requires deeper investigation.[10,11]

The model of a superfluid Bose liquid with pair condensation of bosons, analogous to the Cooper pairing of fermions (electrons) in superconductors, has been discussed for a number of years.[12] Two possibilities are considered in that model: the coexistence of a pair coherent condensate (PCC) with a BEC,[13–15] or the existence of an intense PCC in the complete absence of a BEC.[16–18] In the first case, problems with the stability of the ground state and with hybridization of the single-particle (gap) and collective (acoustical) branches of the spectrum of the Bose liquid can arise at low densities of the BEC.[17] In the model of a superfluid state with a ''Cooper'' PCC with no BEC ($\rho_0 = 0$) these problems

automatically disappear, since the phase of the PCC is arbitrary and can be chosen so as to ensure stability of the sound (hydrodynamic) branch of collective excitations. Here hybridization occurs only between those branches of the spectrum that correspond to the same parity of the number of particles taking part in the excitation (see Ref. 17).

However, in this case there arise difficulties in connection with the fact that the gap single-particle spectrum $\varepsilon(p)=\sqrt{\Delta^2+u^2p^2}$ violates the Hugenholtz–Pines theorem[19] and does not conform to the Reatto–Chester power-law asymptotic behavior[20] of the correlation function $\langle\hat{\psi}(\mathbf{r})\hat{\psi}(\mathbf{r}')\rangle\sim|\mathbf{r}-\mathbf{r}'|^{-2}$ but becomes exponential instead.[17] In addition, having a ''Cooper'' PCC of coupled boson pairs as the basis of the superfluid component in the absence of a BEC should lead to half-integer values of the circulation quantum $\kappa=\hbar/2m$ (where m is the mass of a ^{4}He atom), which have not been observed in experiments.[21–23]

Moreover, the finite gap $\Delta\neq 0$ in the quasiparticle spectrum for $p\to 0$ should give rise to exponential features in the temperature dependence of the heat capacity $C_p(T)$ and to first-order phase transitions in temperature and pressure, where the BEC vanishes and the PCC appears,[17] and those have not been observed experimentally, either.

On the other hand, numerous precision experiments in which the dynamic structure factor $S(\mathbf{p},\varepsilon)$ in liquid ^{4}He has been recovered from inelastic neutron scattering data[24–27] show that the elementary excitation spectrum $E(p)$ due to collective oscillations of the density of the ^{4}He Bose liquid depends very weakly on temperature up to the λ point ($T_\lambda\simeq 2.17$ K) at all momenta, including the phonon, maxon, and roton regions. This means that the critical velocity determined according to the Landau superfluidity criterion, $v_c=\min[E(p)/p]$, remains practically unchanged as T increases and does not go to zero as $T\to T_\lambda$. At the same time, we know that the destruction of superfluidity in macroscopic flows of He II is governed by processes of creation of extended Onsager–Feynman quantum vortices or of closed flux lines (loops, rings).[23] As a result of this, the observed value of the threshold velocity v_c^* for the destruction of nondissipative flow in He II can be two orders of magnitude smaller than the critical velocity $v_c\simeq[\Delta_r/p_r]\simeq 60$ m/s due to the roton gap $\Delta_r\simeq 8.6$ K at the point $p=p_r\simeq 1.9$ Å^{-1} in the quasiparticle spectrum $E(p)$.

However, under conditions such that the creation and motion of vortices (or vortex rings) is hindered, one can achieve much higher values of the threshold velocity. For example, maximum values $v_c^*\simeq 2$–3 m/s are observed[23] in ultrathin films and capillaries at $T<1$ K, and critical velocities $v_c^*\simeq 8$–10 m/s have been measured[28,29] in the passage of He II through thin obstacles via narrow openings several microns in diameter. Moreover, threshold velocities above 50 m/s have been obtained[30] in experiments on ion acceleration in He II at pressures $P\simeq 15$–20 bar.

In this paper we discuss problems pertaining to the microscopic quantum structure of the superfluid component ρ_s in He II and to the Landau superfluidity criterion, which determines the maximum permissible critical velocity in the absence of quantum vortices.

Our approach is based on the microscopic model proposed in Ref. 17 for the superfluidity of a Bose liquid with a suppressed BEC, the small parameter of the model being the ratio of the density of the BEC to the total density of the Bose liquid, $\rho_0/\rho_s\ll 1$, in contrast to the Bogolyubov theory[6] for a nearly ideal Bose gas, where the small parameter is the ratio of the number of overcondensate excitations to the number of particles in the intense BEC, $(n-n_0)/n_0\ll 1$.

In this model the superfluid state is described by a ''truncated'' system of Dyson–Belyaev equations for the normal $\tilde{\Sigma}_{11}(k,\omega)$ and anomalous $\tilde{\Sigma}_{12}(k,\omega)$ self-energy parts in a renormalized field-theoretic perturbation theory[10,11] constructed in combined variables,[31,32] which in the long-wavelength limit ($p\to 0$) reduce to the hydrodynamic variables of the macroscopic quantum (for $T=0$) or two-fluid (for $T\neq 0$) hydrodynamics, while in the short-wavelength region they correspond to the boson field operators of quasiparticle creation and annihilation.

The density of the superfluid component ρ_s here is determined by the quantity $\tilde{\Sigma}_{12}(0,0)$, which is a superposition of the ''depleted'' single-particle BEC and the intense ''Cooper'' PCC, with coincident phases (signs) of the corresponding order parameters. The pair interaction between bosons is chosen in the form of a regularized repulsive potential in the ''hard spheres'' model,[33,34] the Fourier component $V(p)$ of which is an oscillatory and sign-varying function of the momentum transfer p as a result of the ''excluded volume'' effect and the quantum diffraction of the particles on one another. The negative minima of $V(p)$ in certain regions of momentum space correspond to an effective attraction, which can be enhanced as a result of renormalization (screening) of the pair interaction on account of many-particle collective correlations.[17,18] It is shown that such an attraction can be sufficient for the formation of a PCC in momentum space (but not for the existence of coupled boson pairs in real space). Self-consistent iterative numerical calculations of the self-energy of the bosons, the pair order parameter, and the quasiparticle spectrum at $T=0$ permit finding the conditions under which the theoretical spectrum $E(p)$ is in good agreement with the experimentally measured spectrum of elementary excitations. Here it is shown that in the ''hard spheres'' model the roton minimum in the quasiparticle spectrum $E(p)$ in a Bose liquid with a suppressed BEC is uniquely related to the first negative minimum of the Fourier component of the renormalized potential (analogous to the minimum in the Bogolyubov spectrum[6] of a slightly nonideal dilute Bose gas[33,34]).

We also consider the structure of the superfluid state at $T\neq 0$ with allowance for the suppression of the normal component ρ_n and the branch of second sound, the velocity of which goes to zero at the λ point. We discuss the questions of the applicability of the Landau criterion of superfluidity and the value of the limiting permissible critical velocity of superfluid flow in the absence of quantum vortices.

2. GREEN'S FUNCTION AND THE EQUATIONS FOR THE SELF-ENERGY PARTS IN THE MODEL OF A BOSE LIQUID WITH A SUPPRESSED BEC

We start from the renormalized field-theortic perturbation theory[10,11] constructed in the combined variables[31,32]

$$\tilde{\Psi}(x)=\tilde{\Psi}_L(x)+\tilde{\Psi}_{\sinh}(x), \tag{1}$$

which in the long-wavelength region $|\mathbf{k}|<k_0$ (where k is some characteristic momentum) are just the hydrodynamic variables $\tilde{\Psi}_L(x)$ in the spirit of Landau quantum hydrodynamics,[5] and which in the short-wavelength region $|\mathbf{k}|>k_0$ coincide with the usual field operators $\tilde{\Psi}_{\rm sh}(x)$:

$$\tilde{\Psi}_L(x)=\sqrt{\langle\tilde{n}_L\rangle}\left[1+\frac{\tilde{n}_L-\langle\tilde{n}_L\rangle}{2\langle\tilde{n}_L\rangle}+i\tilde{\varphi}_L\right];$$

$$\tilde{\Psi}_{\rm sinh}=\psi_{\rm sinh}e^{-i\tilde{\varphi}_L};\quad \Psi_{\rm sinh}=\psi-\psi_L; \tag{2}$$

$$\psi_L(\mathbf{r})=\frac{1}{\sqrt{V}}\sum_{|\mathbf{k}|<k_0}a_{\mathbf{k}}e^{i\mathbf{kr}}=\sqrt{\langle\tilde{n}_L\rangle}e^{i\tilde{\varphi}_L}.$$

Here the approximate expression for the long-wavelength part $\tilde{\Psi}_L$ of the Bose field operator $\tilde{\Psi}$ includes only the first-order terms in the expansion in the slowly varying (hydrodynamic) phase $\tilde{\varphi}_L$ and in the small deviation of the density $\tilde{n}_L$ from its average value $\langle\tilde{n}_L\rangle$. In Refs. 31 and 32 it was assumed that at low T, owing to the rather weak interaction ($mk_0V(k_0)\ll 1$), almost all of the particles are found in the Bose condensate, and therefore the value of the momentum k_0 in Ref. 32 was chosen small enough so that the approximate equality $\langle\tilde{n}_L\rangle\simeq n_0$ would hold, where n_0 is the density of particles in the BEC. In a Bose liquid with a strong interaction, however, where the single-particle BEC is strongly suppressed ($n_0\ll n$), the quantity $\langle\tilde{n}_L\rangle$ should be normalized to the density of the superfluid component $n_s=\rho_s/m$.

On the basis of the field variables (1), (2) in the framework of the Green's function method[8] for $T\to 0$ one can construct the usual system of Dyson–Belyaev equations,[7] which allow one to express the normal $\tilde{G}_{11}$ and anomalous $\tilde{G}_{12}$ renormalized single-particle Green's functions of the bosons in terms of the corresponding self-energy parts $\tilde{\Sigma}_{11}$ and $\tilde{\Sigma}_{12}$:

$$\tilde{G}_{11}(\mathbf{p},\varepsilon)=\frac{G_0^{-1}(-\mathbf{p},-\varepsilon)-\tilde{\Sigma}_{11}(-\mathbf{p},-\varepsilon)}{Z(\mathbf{p},\varepsilon)}; \tag{3}$$

$$\tilde{G}_{12}(\mathbf{p},\varepsilon)=\tilde{\Sigma}_{12}(\mathbf{p},\varepsilon)/Z(\mathbf{p},\varepsilon). \tag{4}$$

Here

$$Z(\mathbf{p},\varepsilon)=[G_0^{-1}(-\mathbf{p},-\varepsilon)-\tilde{\Sigma}_{11}(-\mathbf{p},-\varepsilon)]\times[G_0^{-1}(\mathbf{p},\varepsilon)-\tilde{\Sigma}_{11}(\mathbf{p},\varepsilon)]-|\tilde{\Sigma}_{12}(\mathbf{p},\varepsilon)|^2; \tag{5}$$

$$G_0^{-1}(\mathbf{p},\varepsilon)=\left[\varepsilon-\frac{p^2}{2m}+\mu+i\delta\right];\quad \delta\to+0, \tag{6}$$

where μ is the chemical potential of the quasiparticles, which satisfies the Hugenholtz–Pines relation:[19]

$$\mu=\tilde{\Sigma}_{11}(0,0)-\tilde{\Sigma}_{12}(0,0). \tag{7}$$

The spectrum of all the elementary excitations with zero helicity, owing to the strong hybridization of the single-particle and collective branches in a Bose liquid with a finite BEC ($n_0\neq 0$) is determined by the poles of the single-particle Green's functions $\tilde{G}_{ik}(\mathbf{p},\varepsilon)$, i.e., by the zeros of the function $Z(\mathbf{p},\varepsilon)$:

$$E(\mathbf{p})=\left\{\left[\frac{p^2}{2m}+\tilde{\Sigma}_{11}^{s}(\mathbf{p},E(\mathbf{p}))-\mu\right]^2-\left|\tilde{\Sigma}_{12}(\mathbf{p},E(\mathbf{p}))\right|^2\right\}^{1/2}+\tilde{\Sigma}_{11}^{a}(\mathbf{p},E(\mathbf{p})), \tag{8}$$

where

$$\tilde{\Sigma}_{11}^{s,a}(\mathbf{p},\varepsilon)=\frac{1}{2}[\tilde{\Sigma}_{11}(\mathbf{p},\varepsilon)\pm\tilde{\Sigma}_{11}(-\mathbf{p},-\varepsilon)],$$

the plus sign corresponding to the symmetric part $\tilde{\Sigma}_{11}^{s}$, and the minus sign to the antisymmetric part $\tilde{\Sigma}_{11}^{a}$. We henceforth assume that $\tilde{\Sigma}_{11}$ is an even function of $\mathbf{p}$ and ε, so that $\tilde{\Sigma}_{11}^{a}=0$ and $\tilde{\Sigma}_{11}^{s}=\tilde{\Sigma}_{11}$.

Relation (7) gives an acoustic dispersion relation for the quasiparticles at $p\to 0$:

$$E(p\to 0)\simeq\tilde{c}|p|;\quad \tilde{c}=\sqrt{\tilde{\Sigma}_{12}(0,0)/\tilde{m}^*}, \tag{9}$$

where

$$\frac{1}{\tilde{m}^*}=\frac{1}{\tilde{B}}\left[\frac{1}{m}+2\frac{\partial\tilde{\Sigma}_{11}(0,0)}{\partial|\mathbf{p}|^2}-2\frac{\partial\tilde{\Sigma}_{12}(0,0)}{\partial|\mathbf{p}|^2}\right]; \tag{10}$$

$$\tilde{B}=\left[1-\frac{\partial\tilde{\Sigma}_{11}(0,0)}{\partial\varepsilon}\right]^2-\tilde{\Sigma}_{12}(0,0)\frac{\partial^2\tilde{\Sigma}_{11}(0,0)}{\partial\varepsilon^2}+\frac{1}{2}\frac{\partial^2}{\partial\varepsilon^2}|\tilde{\Sigma}_{12}(0,0)|^2. \tag{11}$$

For liquid ^{4}He the phase velocity $\tilde{c}$ should be equal to the velocity of first (hydrodynamic) sound, $c_1\simeq 236$ m/s, owing to hybridization of the single-particle and collective branches of the spectrum of elementary excitations. Here the long-wavelength asymptotic expression for the Green's functions has the form

$$\tilde{G}_{11}(\mathbf{p}\to 0,\varepsilon)=-\tilde{G}_{12}(\mathbf{p}\to 0,\varepsilon)=\frac{\tilde{\Sigma}_{12}(0,0)}{\tilde{B}[\varepsilon^2-c_1^2p^2+i\delta]}. \tag{12}$$

It should be emphasized that in the renormalized field theory the self-energy parts $\tilde{\Sigma}_{ij}$ are analytic functions of $\mathbf{p}$ and ε, so that in the limit $\mathbf{p}\to 0$ and $\varepsilon\to 0$ we have

$$\tilde{\Sigma}_{12}(0,0)\neq 0\quad\text{and}\quad\tilde{B}\neq 0,$$

in contrast to the renormalized perturbation theory,[7,8] in which, as was shown in Refs. 10 and 32, the functions $\Sigma_{ij}(\mathbf{p},\varepsilon)$ are nonanalytic at $\mathbf{p}\to 0$ and $\varepsilon\to 0$, and $\Sigma_{12}(0,0)=0$ and $B=0$. Here an additional procedure to resolve the indeterminacy of the type 0/0 is required in order to obtain the correct asymptotic expression:[35]

$$G_{11}(\mathbf{p}\to 0,\varepsilon)=-G_{12}(\mathbf{p}\to 0,\varepsilon)=\frac{n_0mc_1^2}{n[\varepsilon^2-c_1^2p^2+i\delta]};$$

$$c_1^2=\frac{n}{m}\frac{d\mu}{dn}, \tag{13}$$

where n is the total density of bosons, and n_0 is the density of particles in the BEC.

As was shown in Ref. 17, for a Bose liquid with a sufficiently strong interaction between particles, in which case

the BEC is strongly suppressed, one can to good accuracy keep only the first (lowest-order) term of the expansion in the small density of the BEC ($n_0 \ll n$). This approximation is in direct opposition to the Bogolyubov approximation[6] for a slightly nonideal Bose gas with an intense BEC, in which case $n_0 \simeq n$.

As a result, with an accuracy to terms of order $n_0/n \ll 1$, we obtain a truncated system of equations for $\tilde{\Sigma}_{ik}$ in a Bose liquid (Ref. 17):

$$\tilde{\Sigma}_{11}(\mathbf{p},\varepsilon) = n_0 \Lambda(\mathbf{p},\varepsilon)\tilde{V}(\mathbf{p},\varepsilon) + n_1 V(0) + \tilde{\Psi}_{11}(\mathbf{p},\varepsilon); \quad (14)$$

$$\tilde{\Sigma}_{12}(\mathbf{p},\varepsilon) = n_0 \Lambda(\mathbf{p},\varepsilon)\tilde{V}(\mathbf{p},\varepsilon) + \tilde{\Psi}_{12}(\mathbf{p},\varepsilon), \quad (15)$$

where

$$\tilde{\Psi}_{ij}(\mathbf{p},\varepsilon) = i\int \frac{d^3\mathbf{k}}{(2\pi)^3}\int \frac{d\omega}{2\pi}\tilde{G}_{ij}(\mathbf{k},\omega)\tilde{V} \times (\mathbf{p}-\mathbf{k},\varepsilon-\omega)\Gamma(\mathbf{p},\varepsilon,\mathbf{k},\omega), \quad (16)$$

$$\tilde{V}(\mathbf{p},\varepsilon) = V(\mathbf{p})[1 - V(\mathbf{p})\Pi(\mathbf{p},\varepsilon)]^{-1}. \quad (17)$$

Here $V(\mathbf{p})$ is the Fourier component of the bare potential of the pair interaction of the bosons; $\tilde{V}(\mathbf{p},\varepsilon)$ is the renormalized (screened) Fourier component of the retarded (nonlocal) interaction, the renormalization being due to many-particle collective effects; $\Pi(\mathbf{p},\varepsilon)$ is the boson polarization operator

$$\Pi(\mathbf{p},\varepsilon) = i\int \frac{d^3\mathbf{k}}{(2\pi)^3}\int \frac{d\omega}{2\pi}\Gamma(\mathbf{p},\varepsilon,\mathbf{k},\omega)\{\tilde{G}_{11}(\mathbf{k},\omega)\tilde{G}_{11} \times (\mathbf{k}+\mathbf{p},\varepsilon+\omega) + \tilde{G}_{12}(\mathbf{k},\omega)\tilde{G}_{12}(\mathbf{k}+\mathbf{p},\varepsilon+\omega)\}; \quad (18)$$

where $\Gamma(\mathbf{p},\varepsilon,\mathbf{k},\omega)$ is the vertex part (three-pole) describing many-particle correlations; $\Lambda(\mathbf{p},\varepsilon) = \Gamma(\mathbf{p},\varepsilon,0,0) = \Gamma(0,0,\mathbf{p},\varepsilon)$; and n_1 is the number of overcondensate particles ($n_1 \gg n_0$), which is determined from the condition of conservation of the total number of particles:

$$n = n_0 + n_1 = n_0 + i\int \frac{d^3\mathbf{k}}{(2\pi)^3}\int \frac{d\omega}{2\pi}\tilde{G}_{11}(\mathbf{k},\omega). \quad (19)$$

If one takes into account only the residues at the poles of the Green's function $\tilde{G}_{ij}(\mathbf{p},\varepsilon)$ and neglects the contribution of possible poles of the functions $\Gamma(\mathbf{p},\varepsilon,\mathbf{k},\omega)$ and $\tilde{V}(\mathbf{p},\varepsilon)$, then, with allowance for relations (3)–(6), (8), (14), and (17), equations (16) on the mass shell $\varepsilon = E(\mathbf{k})$ take the form (at $T=0$):

$$\tilde{\Psi}_{11}(\mathbf{p},E(\mathbf{p})) = \frac{1}{2}\int \frac{d^3\mathbf{k}}{(2\pi)^3}\Gamma(\mathbf{p},E(\mathbf{p});\mathbf{k},E(\mathbf{k}))\tilde{V} \times (\mathbf{p}-\mathbf{k},E(\mathbf{p})-E(\mathbf{k}))\left[\frac{A(\mathbf{k},E(\mathbf{k}))}{E(\mathbf{k})} - 1\right]; \quad (20)$$

$$\tilde{\Psi}_{12}(\mathbf{p},E(\mathbf{p})) = -\frac{1}{2}\int \frac{d^3\mathbf{k}}{(2\pi)^3}\Gamma(\mathbf{p},E(\mathbf{p});\mathbf{k},E(\mathbf{k}))\tilde{V} \times (\mathbf{p}-\mathbf{k},E(\mathbf{p})-E(\mathbf{k})) \times \frac{n_0\Lambda(\mathbf{k},E(\mathbf{k}))\tilde{V}(\mathbf{k},E(\mathbf{k})) + \tilde{\Psi}_{12}(\mathbf{k},E(\mathbf{k}))}{E(\mathbf{k})}, \quad (21)$$

where

$$A(\mathbf{p},E(\mathbf{p})) = n_0\Lambda(\mathbf{p},E(\mathbf{p}))\tilde{V}(\mathbf{p},E(\mathbf{p})) + n_1 V(0) + \tilde{\Psi}_{11}(\mathbf{p},E(\mathbf{p})) + \frac{p^2}{2m} - \mu. \quad (22)$$

Here the nonlinear equation (8) for finding the quasiparticle spectrum $E(\mathbf{p})$, according to Eqs. (14) and (15), becomes

$$E(\mathbf{p}) = \{A^2(\mathbf{p},E(\mathbf{p})) - [n_0\Lambda(\mathbf{p},E(\mathbf{p}))\tilde{V}(\mathbf{p},E(\mathbf{p})) + \tilde{\Psi}_{12}(\mathbf{p},E(\mathbf{p}))]^2\}^{1/2}, \quad (23)$$

and the total quasiparticle density in the Bose liquid is given by the relation

$$n = n_0 + \frac{1}{2}\int \frac{d^2\mathbf{k}}{(2\pi)^3}\left[\frac{A(\mathbf{k},E(\mathbf{k}))}{E(\mathbf{k})} - 1\right]. \quad (24)$$

The Hugenholtz–Pines relation (7), according to Eqs. (14) and (15), can be written in the form

$$\mu = n_1 V(0) + \tilde{\Psi}_{11}(0,0) - \tilde{\Psi}_{12}(0,0), \quad (25)$$

and, as a result, expression (22) reduces to the form

$$A(\mathbf{p},E(\mathbf{p})) = n_0\Lambda(\mathbf{p},E(\mathbf{p}))\tilde{V}(\mathbf{p},E(\mathbf{p})) + [\tilde{\Psi}_{11}(\mathbf{p},E(\mathbf{p})) - \tilde{\Psi}_{11}(0,0)] + \tilde{\Psi}_{12}(0,0) + \frac{p^2}{2m}. \quad (26)$$

It follows from Eqs. (23) and (26) that the quasiparticle spectrum, by virtue of the analyticity of the functions $\tilde{\Psi}_{ij}(\mathbf{p},\varepsilon)$ is acoustic for $p \to 0$, and its structure for $p \neq 0$ depends substantially on the character of the pair interaction of the bosons.

We also note that the expression for the sound velocity $\tilde{c}$, according to Eqs. (9) and (15), can be written in the form

$$\tilde{c} = \sqrt{\Lambda(0,0)\tilde{V}(0,0)\tilde{n}/\tilde{m}^*}; \qquad \tilde{n} = n_0 + \frac{\tilde{\Psi}_{12}(0,0)}{\Lambda(0,0)\tilde{V}(0,0)}, \quad (27)$$

which is analogous to the expression for the Bogolyubov velocity of sound for a slightly nonideal Bose gas, $c_B = \sqrt{V(0)n/m}$. The condition $\tilde{c} = c_1$, together with Eq. (13), imposes severe restrictions on the choice of the parameters for the model of the boson interaction (see below).

On the other hand, since for $T=0$ the density of the superfluid component ρ_s equals the total mass density of the Bose liquid $\rho = mn$, if it is assumed that $\tilde{n} = n$, when Eq. (20) is taken into account we obtain the relations

$$\rho_s = \rho_0 + \tilde{\rho}_s = m\frac{\tilde{\Sigma}_{12}(0,0)}{\Lambda(0,0)\tilde{V}(0,0)}; \quad (28)$$

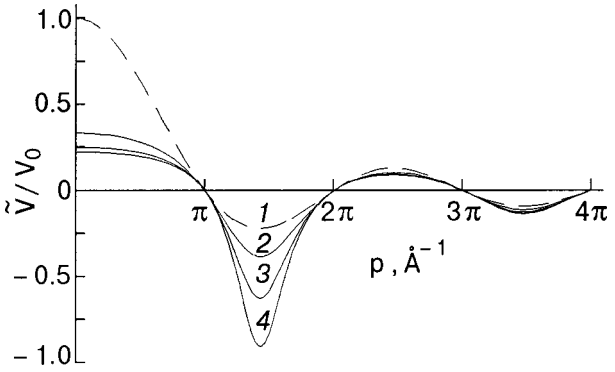

FIG. 1. Dependence of the ratio $\tilde{V}/V_0$ on p for different values of the dimensionless parameter $\alpha = V_0|\Pi|$: the dashed curve *1* shows the bare ''hard spheres'' potential for $\alpha = 0$; the solid curve *2* corresponds to a value $\alpha = 2$, curve *3* to $\alpha = 3$, and curve *4* to $\alpha = 3.5$.

$$\tilde{\rho}_s = mn_1 = m\frac{\tilde{\Psi}_{12}(0,0)}{\Lambda(0,0)\tilde{V}(0,0)}, \tag{29}$$

where $\rho_0 = mn_0$ is the density of the single-particle BEC, $\tilde{\rho}_s$ is the density of the ''Cooper'' PCC, and the density $n_1 = n - n_0$ is determined from relation (24) and, for ^{4}He at $T \to 0$, according to the experimental data,[9] should comprise not less than 90% of the total energy of ^{4}He atoms. Thus the superfluid component in this model is a superposition of the single-particle and pair coherent condensates, and relations (24) and (28) impose additional relations on the parameters of the microscopic theory of the superfluid Bose liquid.

3. INFLUENCE OF THE PAIR INTERACTION ON THE SPECTRUM OF ELEMENTARY EXCITATIONS IN A BOSE LIQUID WITH A SUPPRESSED BEC

As was shown in Refs. 33 and 34, in the case of a spherically symmetric (S-wave) scattering of the particles, a calculation of the Fourier component of the pair interaction potential between bosons in the ''hard spheres'' model in the ladder approximation gives a result in the form of a sign-varying and oscillatory function of the momentum transfer on account of the ''excluded volume'' effect, which can be regarded as a sort of analog of the Pauli exclusion principle in real space. Because of the mutual quantum diffraction of particles on an infinite potential jump $V(r) \to \infty$ as $r \to a$ (where a is the diameter of a hard sphere), the effective pair potential in momentum space has the form ($\hbar = 1$)

$$V(p) = V_0 j_0(pa); \quad j_0(x) = \frac{\sin x}{x}, \tag{30}$$

where V_0 is a positive constant that is determined in a self-consistent manner from a nonlinear integral equation for the single-particle Green's function at $p \to 0$ and depends on the dimensionless density na^3 of the Bose liquid (see Refs. 33 and 34), while $j_0(x)$ is the zero-order spherical Bessel function of the first kind.

The potential (30) is shown by the dashed curve in Fig. 1 and corresponds to repulsion, $V(p) > 0$, in those regions of momentum space in which $\sin(pa) > 0$ (in particular, for $pa < \pi$), or attractive, $V(p) < 0$, in those regions where $\sin(pa) < 0$ (e.g., $\pi < pa < 2\pi$). This oscillatory character of the interaction (30) is analogous to static Friedel oscillations of the screened Coulomb potential with period π/k_F in real space, which arise as a result of the scattering of electrons (fermions) on the filled (according to the Pauli principle) Fermi sphere of diameter $2k_F$, where k_F is the Fermi momentum of the electrons.

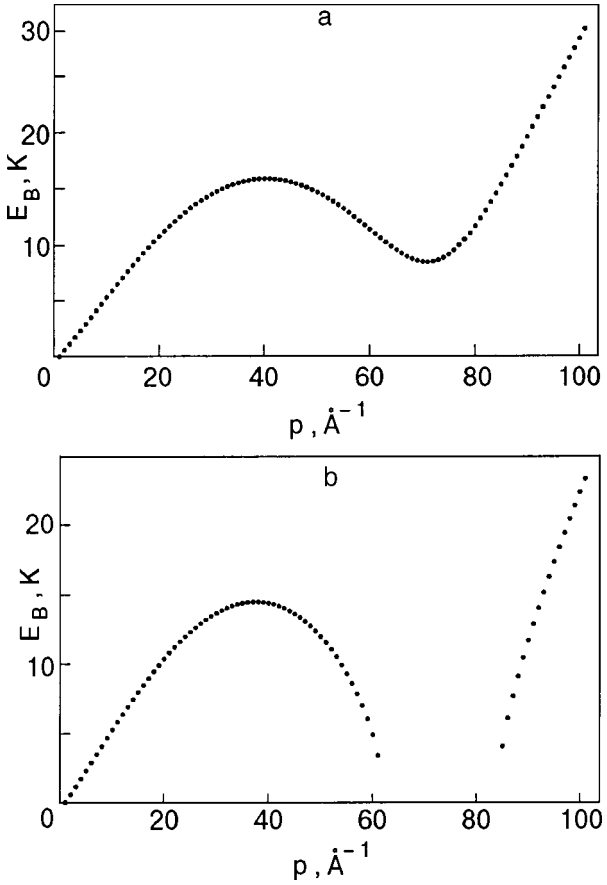

FIG. 2. a: Bogolyubov spectrum (31) for a dilute, nearly ideal Bose gas, obtained by substituting the potential (30) with an independent fitting of the two parameters $\alpha = 2.5$ and $V_0/a^3 = 169$ K at $a = 2.44$ Å. b: Instability of the Bogolyubov spectrum obtained by substituting potential (30) into the relation (31) for the typical ^{4}He parameters $n = 2.17 \times 10^{22}$ cm^{-2} and $a = 2.44$ Å. Here and in Figs. 3–5 the momentum p is expressed in terms of the number of divisions l of the integration interval; the number of a division i is related to the momentum as $p = 2\pi i/al$.

If potential (30) is substituted into the Bogolyubov spectrum for a dilute, nearly ideal Bose gas,[6]

$$E_B(p) = \left\{\frac{p^2}{2m}\left[\frac{p^2}{2m} + 2nV(p)\right]\right\}^{1/2}, \tag{31}$$

then by independently choosing the two parameters V_0 and a, one can achieve entirely satisfactory agreement of the spectrum $E_B(p)$ with the experimental spectrum of elementary excitations $E_{\exp}(p)$ observed by neutron scattering in liquid ^{4}He (Fig. 2a). However, the self-consistent solution obtained in Refs. 33 and 34 for $na^3 \simeq 0.23$ differs considerably from $E_{\exp}(p)$, and for the typical ^{4}He parameters $n = 2.17 \times 10^{22}$ cm^{-3} and $a = 2.44$ Å, for which $na^3 = 0.315$, the spectrum (31) with the potential (30) turns out to be unstable, since $E_B^2(p) < 0$ in a certain region of p (Fig. 2b), a circumstance which indicates that the Bogolyubov theory[6] is inapplicable for describing the Bose liquid.

Many-particle correlation effects in a Bose liquid lead to substantial renormalization (screening) of the pair interaction, which governs the normal and anomalous self-energy parts (14) and (15). When (17) and (30) are taken into account, the retarded screened interaction between bosons takes the form

$$\tilde{V}(\mathbf{p},\omega)=\frac{V_0\sin(pa)}{pa-V_0\Pi(\mathbf{p},\omega)\sin(pa)}, \tag{32}$$

where $\Pi(\mathbf{p},\omega)$ is the boson polarization operator (18), which is calculated in the Appendix with allowance for the pole parts of the Green's functions (3) and (4).

An important property of the renormalized potential (32) is that in those regions of the phase volume $\mathbf{p},\omega$ in which $\Pi(\mathbf{p},\omega)<0$, the screening causes a weakening of the repulsion for $\sin(pa)>0$ and an effective enhancement of the attraction for $\sin(pa)<0$.

It follows from (23) and (26) that the main influence on the quasiparticle spectrum $E(\mathbf{p})$ comes from the form of the interaction potential (32) on the ''mass shell,'' where $\omega=E(\mathbf{p})$. As to the vertices Λ and Γ, their comparatively weak dependence on $\mathbf{p}$ and ω can be neglected, assuming $\Lambda\simeq\Gamma\simeq\Lambda(0,0)=\text{const}$ and including the constant quantity $\Lambda(0,0)$ in the constant V_0, which will be treated below as a free adjustable parameter. The dependence of the functions $\tilde{\Psi}_{ij}(\mathbf{p},\varepsilon)$ on p, which is determined by the integral equations (16) with $\varepsilon=E(\mathbf{p})$, is also much weaker than the dependence of the potential $\tilde{V}(\mathbf{p},\omega)$, as will be seen below.

A key aspect of the behavior of the ''screened'' potential $\tilde{V}(\mathbf{p},\omega)$ is that the polarization operator $\Pi(\mathbf{p},E(p))$ on the ''mass shell'' remains negative for all $p>0$, provided that the quasiparticle spectrum $E(p)$ is stable against decay into pairs of quasiparticles,[36] i.e., if the following conditions hold for any $\mathbf{p}$ and $\mathbf{k}$:

$$\begin{aligned} &E(\mathbf{p})<E(\mathbf{k})+E(\mathbf{k}-\mathbf{p}),\\ &E(\mathbf{k})<E(\mathbf{p})+E(\mathbf{k}-\mathbf{p}). \end{aligned} \tag{33}$$

Indeed, it follows from the expressions (A5) and (A6) obtained in the Appendix for the integrands $I_{ij}(\mathbf{p},\mathbf{k},\omega)$ that under condition (33) for $\omega=E(\mathbf{p})$ the denominator in front of the curly brackets is always negative,

$$[E(\mathbf{k})-E(\mathbf{p})-E(\mathbf{k}-\mathbf{p})]<0,$$

whereas the denominator in the first term in curly brackets is always positive,

$$[E(\mathbf{k})-E(\mathbf{p})+E(\mathbf{k}-\mathbf{p})]>0,$$

and smaller than the positive denominator in the second term,

$$[E(\mathbf{k})+E(\mathbf{p})+E(\mathbf{k}-\mathbf{p})]>0.$$

Then, as numerical calculations have shown, the numerators of both terms remain positive (see Fig. 3) for any $\mathbf{p}$ and $\mathbf{k}$, and therefore the overall sign of the functions $I_{ij}(\mathbf{p},\mathbf{k},\omega)$ is negative, and so $\Pi(\mathbf{p},E(\mathbf{p}))<0$.

With allowance for the negative sign and the relatively weak momentum dependence of $\Pi(\mathbf{p},E(\mathbf{p}))$, we approximate the renormalized potential (32) for $\omega=E(\mathbf{p})$ by the simpler potential

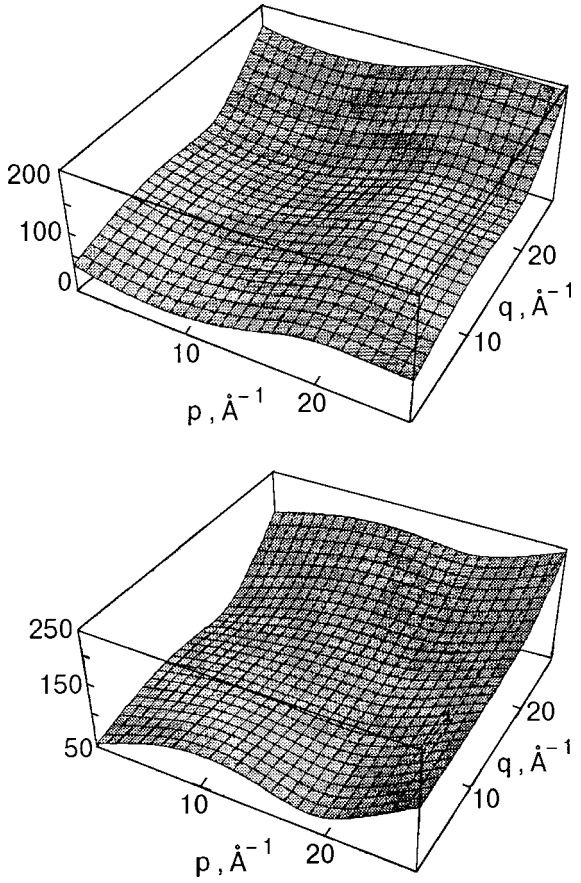

FIG. 3. Momentum dependence of the positive numerators (given in kelvins) of the two terms in the expression for the function $I_{11}(\mathbf{p},\mathbf{k},\omega)$ which appears in the definition of the polarization operator (see Appendix).

$$\tilde{V}(\mathbf{p})=\frac{V_0\sin(pa)}{pa-\alpha\sin(pa)}, \tag{34}$$

where $\alpha=V_0|\tilde{\Pi}|$ and $|\tilde{\Pi}|=\overline{|\Pi(\mathbf{p},E(\mathbf{p}))|}$ is the average value of the modulus of the polarization operator on the mass shell in the existence region of the spectrum $E(p)$. All of the numerical calculations reported below were done on the basis of the model potential (34) with α treated as a free adjustable parameter (together with V_0). Figure 1 shows curves of $\tilde{V}(p)$ for different values of the dimensionless parameter α.

As another adjustable parameter of the model we choose the effective mass m^* of the quasiparticles, which is related to the mass $\tilde{m}^*$, which according to (9) and (10) determines the sound velocity (9) in the limit $p\to 0$.

As a result, Eqs. (20) and (21) for the functions $\tilde{\Psi}_{ij}$ reduce to the simple form

$$\tilde{\Psi}_{11}(\mathbf{p})=\frac{1}{2}\int\frac{d^3\mathbf{k}}{(2\pi)^3}\tilde{V}(\mathbf{p}-\mathbf{k})\left[\frac{A_0(\mathbf{k})}{E(\mathbf{k})}-1\right], \tag{35}$$

$$\tilde{\Psi}_{12}(\mathbf{p})=-\frac{1}{2}\int\frac{d^3\mathbf{k}}{(2\pi)^3}\tilde{V}(\mathbf{p}-\mathbf{k})\frac{n_0\tilde{V}(\mathbf{k})+\Psi_{12}(\mathbf{k})}{E(\mathbf{k})}, \tag{36}$$

where

$$E(\mathbf{p})=\sqrt{A_0^2(\mathbf{p})-[n_0\tilde{V}(\mathbf{p})+\Psi_{12}(\mathbf{p})]^2}; \tag{37}$$

$$A_0(\mathbf{p}) = n_0\tilde{V}(\mathbf{p}) + [\tilde{\Psi}_{11}(\mathbf{p}) - \tilde{\Psi}_{11}(0)] + \tilde{\Psi}_{12}(0) + \frac{p^2}{2m^*}, \tag{38}$$

and the effective mass m^* is related to $\tilde{m}^*$ by the expression

$$\frac{1}{\tilde{m}^*} = \frac{1}{m^*} + p^2\frac{\partial^2\tilde{\Psi}_{11}(0)}{\partial|\mathbf{p}|^2}, \tag{39}$$

so that for $p\to 0$ we obtain from (37)

$$E(p\to 0) = p\sqrt{[n_0\tilde{V}(0) + \tilde{\Psi}_{12}(0)]/\tilde{m}^*}, \tag{40}$$

where $\tilde{V}(0) = V_0/(1+\alpha)$. The parameters V_0, α, and m^* are chosen so that the phase velocity $E(p\to 0)/p$ is equal to the hydrodynamic sound velocity $c_1 \simeq 236$ m/s in liquid ^{4}He. On the other hand, the choice of these parameters must ensure the best agreement of the spectrum $E(p)$ with the experimental spectrum $E_{\exp}(p)$ in ^{4}He (Refs. 24–27).

Figure 4 shows the momentum dependence of the functions $\tilde{\Psi}_{11}(p)$, $\tilde{\Psi}_{12}(p)$, and $A_0(p)$ obtained according to (35), (36), and (38), for a certain set of parameters V_0, α, m^*, and Fig. 5 shows the curve of the quasiparticle spectrum $E(p)$ calculated according to (37). We see that the nonmonotonic character of the spectrum $E(p)$ and, in particular, the presence of a ''roton'' minimum are governed by the momentum dependence of the functions $\tilde{\Psi}_{11}(p)$ and $A_0(p)$, which have deep minima because of the oscillations of the alternating potential $\tilde{V}(p)$ in the region $p < 2\pi/a$ (see Fig. 1). For the given choice of parameters the theoretical spectrum is in good agreement with the experimental spectrum of ^{4}He in terms of both the position and absolute values of the maxima and minima of $E(p)$. Here the density of the BEC calculated according to (24) is equal to 10% of the total density n, in agreement with the experimental data.[9]

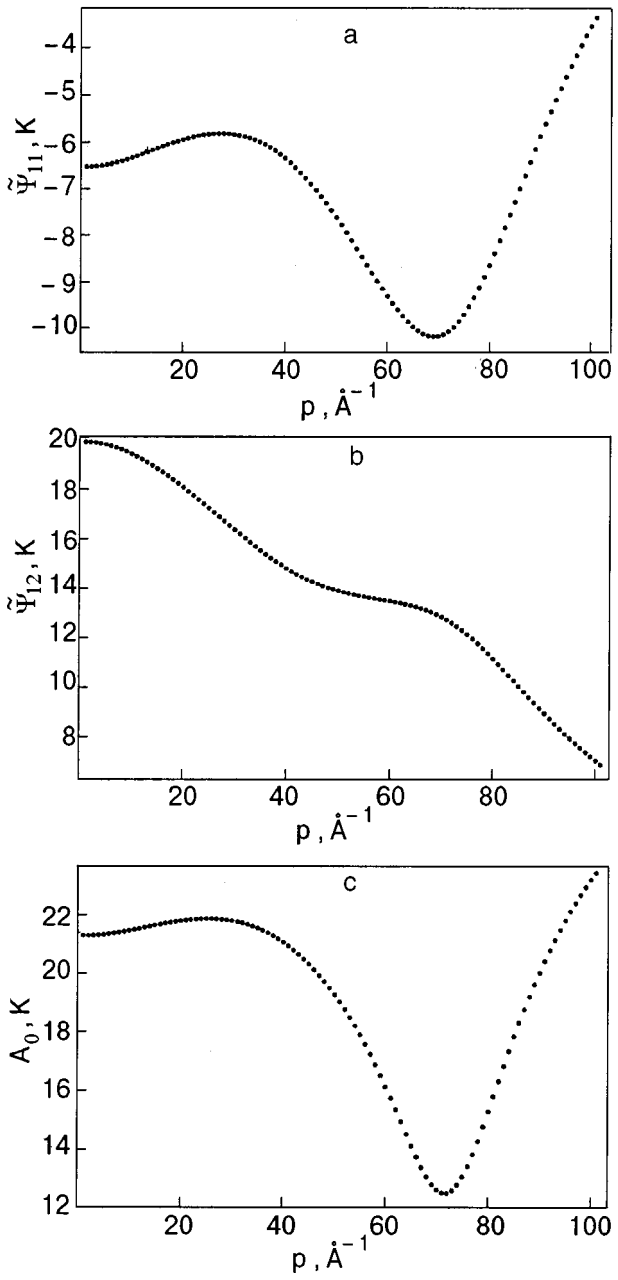

FIG. 4. Momentum dependence of the functions $\tilde{\Psi}_{11}(p)$ (a), $\tilde{\Psi}_{12}(p)$ (b), and $A_0(p)$ (c) obtained according to Eqs. (35), (36), and (38) for the following set of parameters: $n_0 = 10\%n$, $V_0/a^3 = 147$ K, $\alpha = 3.65$, $m/m^* = 0.00175$.

4. STRUCTURE OF THE SUPERFLUID STATE OF A BOSE LIQUID AT $T \neq 0$

Let us consider the superfluid state of a Bose liquid at $T \neq 0$, in which case a normal component $\rho_n(T)$ is present in addition to $\rho_s(T)$. As was shown in Refs. 31 and 32, for $T\to 0$ in the region of small $p \neq 0$ the expressions for the renormalized Green's functions $\tilde{G}_{ij}(p)$ constructed in the combined variables (1), (2) have the form

$$\tilde{G}_{11}(p) = -n_s g_{\varphi\varphi}(p) - ig_{\varphi\pi}(p) - \frac{1}{4\rho_s}g_{\pi\pi}(p) - \frac{n_s}{2}\Phi_{\varphi\varphi}(p)\ldots; \tag{41}$$

$$\tilde{G}_{12}(p) = n_s g_{\varphi\varphi}(p) - \frac{1}{4n_s}g_{\pi\pi}(p) - \frac{n_s}{2}\Phi_{\varphi\varphi}(p)\ldots; \tag{42}$$

where

$$\Phi_{\varphi\varphi}(p) = \int_{|q|<q_0}\frac{d^4q}{2\pi^4}g_{\varphi\varphi}(q)g_{\varphi\varphi}(p-q),$$

$$p = (\mathbf{k},\varepsilon), \quad q = (\mathbf{q},\omega), \tag{43}$$

and $g_{\mu\nu}(\mathbf{p})$ are the ''hydrodynamic'' Green's functions, which are associated with the long-wavelength fluctuations of the phase and density of the condensate ($\mu,\nu = \varphi,\pi$). The expressions for $g_{\varphi\varphi}(p)$, $g_{\varphi\pi}(p)$, and $g_{\pi\pi}(p)$ calculated in Ref. 11 for $T>0$ contain sums of two pole terms, corresponding to first and second sound, with velocities c_1 and c_2, in the Bose liquid with the normal and superfluid components:

$$g_{\mu\nu}(\mathbf{k},\varepsilon) = \frac{(a_{\mu\nu} - d_{\mu\nu}\rho_n/\rho)}{\varepsilon^2 - c_1^2k^2} + \frac{b_{\mu\nu}\rho_n/\rho}{\varepsilon^2 - c_2^2k^2},$$

$$\mu, \quad \nu = \varphi,\pi, \tag{44}$$

where $\rho = \rho_n + \rho_s$ is the total density of the liquid, and the coefficients $a_{\mu\nu}$, $d_{\mu\nu}$, and $b_{\mu\nu}$ are independent of T at low

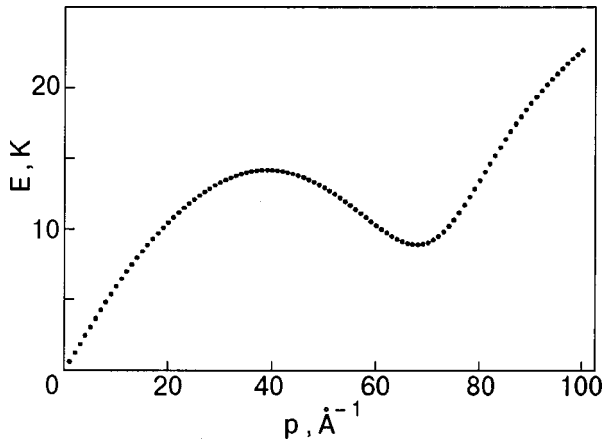

FIG. 5. Spectrum of elementary excitations $E(p)$ obtained according to Eq. (37), for the same set of parameters as in Fig. 4. The values $E_{\max}=14$ K and $E_{\min}=8.61$ K and also the hydrodynamic sound velocity $c_1=2.37\times10^4$ cm/s and total quasiparticle density $n=2.17\times10^{22}$ cm^{-3} in the Bose liquid agree with the experimental values.

temperatures. This result establishes a unique correspondence between the microscopic field theory of superfluidity[7,8] and the macroscopic two-fluid hydrodynamics.[36,37]

It follows from Eqs. (41), (42), and (44) that the pole parts of the renormalized Green's functions $\tilde{G}_{ij}$ can be represented in the form

$$\tilde{G}_{ij}(\mathbf{k},\varepsilon)=\frac{(A_{ij}-D_{ij}\rho_n/\rho)}{\varepsilon^2-c_1^2k^2}+\frac{B_{ij}\rho_n/\rho}{\varepsilon^2-c_2^2k^2},\quad i,\ j=1,2. \tag{45}$$

We henceforth assume that expression (45) is valid in the entire temperature interval $T<T_\lambda$.

It follows from Eq. (45) that for $T\to0$, where $\rho_n\to0$, the leading contribution to the integral over energy ε in (16) comes from the first-sound pole $\varepsilon=c_1k$ of the Green's functions. However, at higher temperatures $T>1$ K, where $\rho_n\sim\rho_s$, because of the strong inequality $c_1\gg c_2$ the main role comes to be played by the low-energy pole $\varepsilon=c_2k$, corresponding to second sound.

At finite temperatures ($T\neq0$), when the contributions of the first and second poles of the Green's functions (45) are taken into account, we obtain for the self-energy parts at $\Gamma=1$

$$\tilde{\Sigma}_{ij}(\mathbf{k},T)=-\frac{1}{2}\int\frac{d^3\mathbf{q}}{(2\pi)^3}\tilde{V}(\mathbf{k}-\mathbf{q})\left\{\left[A_{ij}-D_{ij}\frac{\rho_n(T)}{\rho}\right]\frac{1}{c_1q}\times\coth\left(\frac{c_1q}{2T}\right)+B_{ij}\,\frac{\rho_n(T)}{\rho}\,\frac{1}{c_2q}\coth\left(\frac{c_1q}{2T}\right)\right\}. \tag{46}$$

It should be emphasized that the long-wavelength approximation for the Green's functions (45) in this case are valid because of the divergence of the temperature factor $\coth(c_2q/2T)$ at $q\to0$ and the rather rapid decay of the interaction kernel as $q\to\infty$. Moreover, here the system of equations (46) does not need to be matched with the expression for the renormalized quasiparticle spectrum $E(k)$, as is ordinarily done in microscopic field theory for $T\to0$, since the substitution of the empirical spectra of the first and second sound (with the experimental values of the velocities c_1 and c_2) into the expressions for the Green's functions $\tilde{G}_{ij}(p)$ corresponds to automatically taking all the necessary renormalizations into account.

Using (46), one can determine the superfluid order parameter for $T\neq0$:

$$\tilde{\Sigma}_{12}(0,T)=\Psi_0(T)+\Psi_s(T)\frac{\rho_s(T)}{\rho}, \tag{47}$$

where

$$\Psi_0(T)=-\frac{1}{2}\int\frac{d^3\mathbf{q}}{(2\pi)^3}\tilde{V}(q)\left[\frac{A_{12}-D_{12}}{c_1q}\coth\left(\frac{c_1q}{2T}\right)+\frac{B_{12}}{c_2q}\coth\left(\frac{c_2q}{2T}\right)\right], \tag{48}$$

$$\Psi_s(T)=-\frac{1}{2}\int\frac{d^3\mathbf{q}}{(2\pi)^3}\tilde{V}(q)\left[\frac{D_{12}}{c_1q}\coth\left(\frac{c_1q}{2T}\right)-\frac{B_{12}}{c_2q}\coth\left(\frac{c_2q}{2T}\right)\right]. \tag{49}$$

On the other hand, assuming that for $T\neq0$ a relation analogous to (28) is maintained between $\rho_s(T)$ and $\tilde{\Sigma}_{12}(0,T)$, we obtain the following expression for the superfluid-component fraction in the Bose liquid:

$$\frac{\rho_s(T)}{\rho}=\frac{\Psi_0(T)}{\tilde{V}(0)n}\left[1-\frac{\Psi_s(T)}{\tilde{V}(0)n}\right]^{-1}. \tag{50}$$

The T-dependent density of the BEC, $\rho_0(T)=mn_0(T)$, according to (19) and (45), is given by the relation

$$\frac{\rho_0(T)}{\rho}=1-\frac{1}{2}\int\frac{d^3\mathbf{q}}{(2\pi)^3}\left\{\left[A_{11}-D_{11}\frac{\rho_n(T)}{\rho}\right]\frac{1}{c_1q}\coth\left(\frac{c_1q}{2T}\right)+B_{11}\frac{\rho_n(T)}{\rho}\,\frac{1}{c_2q}\coth\left(\frac{c_2q}{2T}\right)\right\}. \tag{51}$$

The velocity of first (hydrodynamic) sound is practically independent of T and in the given approximation can be determined as $c_1=[\tilde{V}(0)n/m^*]^{1/2}$, whereas the velocity of second sound c_2 is substantially T-dependent, varying from $c_2(0)=c_1/\sqrt{3}$ at $T=0$ to a value $c_2(T)\simeq20$ m/s in the region $T>1$ K, while for $T\to T_\lambda$ the velocity $c_2\to0$. Thus as the λ point is approached, owing to the strong inequality $c_1\gg c_2$, the main role begins to be played by the last terms in the integrands in (48) and (51), which are proportional to B_{12} and B_{11} and contain the temperature factor

$$f(q,T)=\frac{1}{c_2(T)q}\coth\left(\frac{c_2(T)q}{2T}\right)\simeq\frac{2T}{c_2^2(T)q^2},\quad c_2q<T, \tag{52}$$

which diverges quadratically as $q\to0$. Here the width of the singular peak increases rapidly with increasing T and decreasing c_2 (see Fig. 6).

As a result, with increasing T there is an increase in the contribution to the integral (48) from the repulsive part of the potential $\tilde{V}(q)>0$ in the long-wavelength region $q<\pi/a$ and a decrease in the function $\Psi_0(T)$, which plays the role of the superfluid order parameter and which is positive at

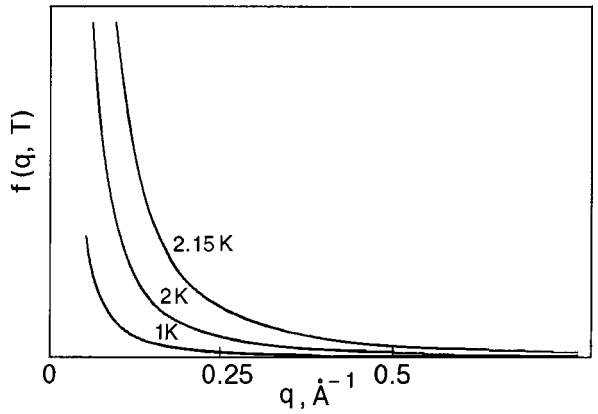

FIG. 6. Temperature factor $f(q,T)$ determined according to relation (52).

low $T<c_2q$ on account of the strong attraction $\tilde{V}(q)<0$ in the region $\pi/a<q<2\pi/a$ (see Fig. 1). At a certain critical temperature $T=T_c$ the function $\Psi_0(T)$ goes to zero and then becomes negative (for $T>T_c$), which corresponds to destruction of the superfluid state ($\rho_s=0$), i.e., T_c coincides with the λ point.

In a similar way, with increasing T the negative integral in (51) increases in magnitude while $\rho_0(T)$ decreases, until at a certain point $T=T_0$ the density of the BEC vanishes and formally becomes negative for $T>T_0$. The interaction parameters $\tilde{V}(q)$ and the coefficients B_{11} and B_{12} are chosen so that the temperatures T_c and T_0 coincide and equal T_λ. The results of numerical calculations done according to (50) with the parameters $A_{11}=6.24$ K, $D_{11}=2$ K, $B_{11}=0.00015$ K, $A_{12}=6.38$ K, $D_{12}=3.14$ K, and $B_{12}=0.0026$ K are presented in Fig. 7. Of course, these results, which correspond to the self-consistent field approximation, are inapplicable close to the λ point, where thermodynamic fluctuations play the governing role,[38] but the curves shown in Fig. 7 give a qualitatively correct description of the temperature dependence of the density of the superfluid component.

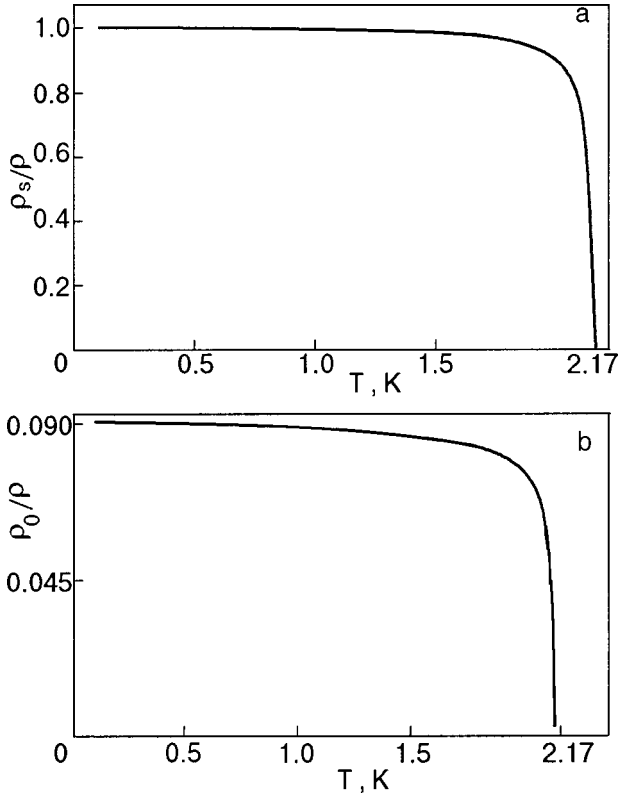

FIG. 7. Density of the superfluid component $\rho_s(T)/\rho$ calculated according to Eq. (50) (a), and the dependence of the BEC density $\rho_0(T)/\rho$ calculated according to Eq. (51) (b), for the following set of parameters: $A_{11}=6.24$ K, $D_{11}=2$ K, $B_{11}=0.00015$ K, $A_{12}=6.38$ K, $D_{12}=3.14$ K, $B_{12}=0.0026$ K.

5. SUPERFLUIDITY CRITERION AND THE LIMITING CRITICAL VELOCITIES

Let us conclude with a brief discussion of the applicability of the Landau criterion of superfluidity to He II and of the value of the limiting critical velocity in the absence of quantum vortices in a Bose liquid with coexisting BEC and PCC.

As we mentioned in the Introduction, the spectrum of elementary excitations $E_{\exp}(p)$ observed in neutron scattering experiments[24–27] leads to a value of the critical velocity, as determined by the roton minimum in accordance with the Landau criterion, that is much too high in comparison with the experimentally measured velocities at which the superfluid flow is destroyed. This is because of the creation of quantum vortices and vortex rings in He II,[23] but under conditions such that the creation and/or motion of vortices is hindered, the critical velocities increase sharply,[28,29] and at low temperatures $T_c<1$ K can reach values comparable to $v_c=\min[\varepsilon(p)/p]=60$ m/s.[30]

It should be emphasized that this situation is analogous to that observed in type-II superconductors, in which the critical current j_c is determined by the condition for the creation and pinning of Abrikosov quantum vortices at the surface of the superconductor or near various defects of the crystal lattice, whereas the true maximum value of j_c (the so-called depairing critical current, which corresponds to the decay of the Cooper pairs)[12] is much larger and is observed only in rather thin films and in wires whose thicknesses are much less than the London penetration depth of the magnetic field into the superconductor, in which case the creation of vortices is prevented.

In the Bose liquid ^{4}He at finite temperatures $T\neq 0$, in addition to the spectrum $E_{\exp}(p)$, which for $p\to 0$ corresponds to first (hydrodynamic) sound with a phase velocity c_1, in He II, owing to the appearance of a normal component ρ_n, there is also second sound, with a velocity $c_2\ll c_1$ in the region $T>1$ K. We know that[36,37] the second-sound branch, by virtue of the smallness of the thermal expansion of liquid ^{4}He, is actually nothing more than oscillations of the temperature (entropy) without any appreciable net mass transport of the substance of the normal ρ_n and superfluid ρ_s components, the oscillations of which occur in antiphase. Therefore, the excitations of second sound, with energy $\varepsilon_2(p)=c_2p$, cannot be observed in the standard neutron scattering experiments, unlike the case of first sound $\varepsilon_1(p)=c_1p$, which comprises in-phase oscillations of the densities ρ_s and ρ_n. At the same time, in a two-component Bose liquid the coexistence of two different types of acoustical Goldstone excitations is allowed; these are due, on the one hand, to the spontaneous breaking of the gauge symmetry deriving from the phase degeneracy of the coherent superfluid condensate ρ_s at $T\to 0$ and to the breaking of the con-

tinuous translational symmetry, i.e., the uniformity of the total density $\rho=\rho_n+\rho_s$ (first sound), and, on the other hand, to the spatially nonuniform deviations of the temperature from the uniform distribution as a result of oscillations of the density of the gas of normal excitations ρ_n (second sound). Nevertheless, the second-sound excitations transport energy and are therefore taken into account in the determination of the minimum critical velocity in in accordance with the initial concepts of the Landau superfluidity criterion,[5] which includes all types of excitations of the quantum liquid.

In connection with this one can assume that in the temperature region where $c_2(T)<v_c\simeq 60$ m/s, the limiting permissible critical velocity of a macroscopic superfluid flow in He II in the absence of quantum vortices (or in the case of their strong pinning) cannot exceed a value of the order of the second-sound velocity $c_2(T)$, which for $T\to T_\lambda$ goes to zero together with the density of the superfluid component $\rho_s(T)$. It is just such a situation that is typical for superconductors, in which the depairing critical current goes to zero at the critical point $T=T_c$ together with the energy gap Δ in the quasiparticle spectrum.

Finally, it should be noted that the coexistence of a weak BEC and an intense PCC preserves the integer nature of the circulation quantum of the superfluid velocity in the vortices, $\kappa=\hbar/m$, owing to the total mutual coherence of these condensates in the superfluid component ρ_s. Indeed, the rather strong effective attraction for the screened Fourier component of the singular ''hard spheres'' potential ensures the formation of a condensate of bound boson pairs with a positive sign of the pair order parameter $\tilde{\Psi}_{12}(0)$, the phase of which in this case coincides with the phase of the BEC.

6. CONCLUSIONS

In summary, the use of the renormalized field theory for describing the superfluid state of a Bose liquid with allowance for the low density of the single-particle BEC makes it possible to formulate a self-consistent model of superfluidity in which the superfluid component at $T\to 0$ is a coherent superposition of a weak BEC and an intense PCC, the latter arising on account of the effective attraction between bosons in momentum space, and to obtain in the framework of the ''hard spheres'' model an explicit expression for the quasiparticle spectrum which agrees with the experimental spectrum of elementary excitations in ^{4}He. The use of empirical data on the frequencies of first and second sound for $T\neq 0$ makes it possible to describe the superfluid state in a comparatively simple and self-consistent way all the way up to the point of the λ transition, and also to obtain the condition that the critical velocity v_c in macroscopic flows of He II in the absence of quantum vortices are limited by the velocity of second sound $c_2(T)$.

In closing, we express our sincere gratitude to P. I. Fomin for many helpful discussions.

APPENDIX

The polarization operator (13) can be written in the following form without allowance for the vertex part Γ with the of expressions (3)–(6):

$$\Pi(\mathbf{p},\omega)=\int\frac{d^3\mathbf{k}}{(2\pi)^3}[I_{11}(\mathbf{p},\mathbf{k},\omega)+I_{12}(\mathbf{p},\mathbf{k},\omega)], \tag{A1}$$

where

$$I_{ij}(\mathbf{p},\mathbf{k},\omega)=i\oint\frac{dz}{2\pi}\tilde{G}_{ij}(\mathbf{k},z)\tilde{G}_{ij}(\mathbf{k}-\mathbf{p},z-\omega). \tag{A2}$$

We assume that the Green's functions $\tilde{G}_{ij}$ have only one pole inside the integration contours:

$$\tilde{G}_{11}(\mathbf{k},\varepsilon)=\frac{\varepsilon+(k^2/2m)-\mu+\tilde{\Sigma}_{11}(-\mathbf{k},-\varepsilon)}{\varepsilon^2-E^2(\mathbf{k})+i\delta}; \tag{A3}$$

$$\tilde{G}_{12}(\mathbf{k},\varepsilon)=\frac{\tilde{\Sigma}_{12}(\mathbf{k},\varepsilon)}{\varepsilon^2-E^2(\mathbf{k})+i\delta};\quad \delta\to 0. \tag{A4}$$

Evaluating the integrals (A.2) with allowance for the poles at the points $\varepsilon=E(\mathbf{k})$ and $\varepsilon=E(\mathbf{k}-\mathbf{p})+\omega$ in the complex Z plane, we obtain

$$\begin{aligned}I_{11}(\mathbf{p},\mathbf{k},\omega)=\frac{1}{2[E(\mathbf{k})-E(\mathbf{k}-\mathbf{p})-\omega]}\Bigg\{&\left[E(\mathbf{k})+\frac{k^2}{2m}-\mu+\tilde{\Sigma}_{11}(-\mathbf{k},-E(\mathbf{k}))\right]\\&\times\frac{[E(\mathbf{k})-\omega+[(\mathbf{k}-\mathbf{p})^2/2m]-\mu+\tilde{\Sigma}_{11}(-\mathbf{k}+\mathbf{p},-E(\mathbf{k})+\omega)]}{E(\mathbf{k})[E(\mathbf{k})+E(\mathbf{k}-\mathbf{p})-\omega]}\\&-\frac{[E(\mathbf{k}-\mathbf{p})+\omega+(k^2/2m)-\mu+\tilde{\Sigma}_{11}(-\mathbf{k},-E(\mathbf{k}-\mathbf{p})-\omega]}{E(\mathbf{k}-\mathbf{p})[E(\mathbf{k})+E(\mathbf{k}+\mathbf{p})+\omega]}\\&\times\left[E(\mathbf{k}-\mathbf{p})+\frac{(\mathbf{k}-\mathbf{p})^2}{2m}-\mu+\tilde{\Sigma}_{11}(-\mathbf{k}+\mathbf{p},-E(\mathbf{k}-\mathbf{p}))\right]\Bigg\},\end{aligned} \tag{A5}$$

$$I_{12}(\mathbf{p},\mathbf{k},\omega)=\frac{1}{2[E(\mathbf{k})-E(\mathbf{k}-\mathbf{p})-\omega]}\left\{\frac{\tilde{\Sigma}_{12}(\mathbf{k},E(\mathbf{k}))\tilde{\Sigma}_{12}(\mathbf{k}-\mathbf{p},E(\mathbf{k})-\omega)}{E(\mathbf{k})[E(\mathbf{k})+E(\mathbf{k}-\mathbf{p})-\omega]}-\frac{\tilde{\Sigma}_{12}(\mathbf{k},E(\mathbf{k}-\mathbf{p})+\omega)\tilde{\Sigma}_{12}(\mathbf{k}-\mathbf{p},E(\mathbf{k}-\mathbf{p}))}{E(\mathbf{k}-\mathbf{p})[E(\mathbf{k})+E(\mathbf{k}-\mathbf{p})+\omega]}\right\}. \tag{A6}$$

In the static limit ($\omega\to 0$, $p\to 0$) expression (A.5) reduces to

$$I_{11}(0,\mathbf{k},0)=-\frac{1}{4}\left\{\frac{1}{E^2(\mathbf{k})}\left[E(\mathbf{k})+\frac{k^2}{2m}-\mu+\tilde{\Sigma}_{11}(\mathbf{k},E(\mathbf{k}))\right]^2+\left[\frac{2}{E(\mathbf{k})}\left(1+\frac{\partial\tilde{\Sigma}_{11}(k)}{\partial\varepsilon}\right)-\frac{k}{mE(k)}\,\frac{1}{\partial E(k)/\partial k}\right]\times\left[E(\mathbf{k})+\frac{k^2}{2m}-\mu+\tilde{\Sigma}_{11}(\mathbf{k},E(\mathbf{k}))\right]\right\}. \quad \text{(A7)}$$

It follows that in a significant region of momentum space the function $I_{11}(0,\mathbf{k},0)<0$. A similar result is obtained for the function in (A.6) at $\mathbf{p}=0$ and $\omega=0$, i.e., $I_{12}(0,\mathbf{k},0)<0$, so that the static polarization operator $\Pi(0,0)$ is a negative quantity, which corresponds to a weakening of the ''screened'' repulsion for $p\to 0$.

It is also seen from (A.5) and (A.6) that on the mass shell $\omega=E(\mathbf{p})$ the integrals I_{11} and I_{12} remain negative over a wide region of momentum space owing to the negative sign of the common denominator, $[E(\mathbf{k})-E(\mathbf{k}-\mathbf{p})-E(\mathbf{p})]<0$. The positive sign of the denominator $[E(\mathbf{k})+E(\mathbf{k}-\mathbf{p})-E(\mathbf{p})]>0$ is related to the fact that the quasiparticle spectrum $E(p)$ is nondecaying.

Thus the polarization operator on the mass shell $\varepsilon=E(\mathbf{p})$ is negative throughout the region $p<2\pi/a$, which leads to enhancement of the attraction in the region $\pi/a<p<2\pi/a$, where $\sin(pa)<0$.

*E-mail: pashitsk@iop.kiev.ua
**E-mail: sivil@phys.univ.kiev.ua

[1] S. Putterman, P. H. Roberts, C. A. Jones, and A. Larraza, in *Extitations in Two-Dimensional and Three-Dimensional Quantum Fluids*, edited by A. F. G. Wyatt and H. J. Lauter, New York (1991).
[2] B. Fak, L. P. Regnault, and J. Bossy, J. Low Temp. Phys. **89**, 345 (1992).
[3] H. R. Glyde, J. Low Temp. Phys. **93**, 861 (1993).
[4] É. A. Pashitskiĭ, Fiz. Nizk. Temp. **25**, 115 (1999) [Low Temp. Phys. **25**, 81 (1999)].
[5] L. D. Landau, Zh. Éksp. Teor. Fiz. **11**, 592 (1941) [Sov. Phys. JETP **17**, 91 (1947)].
[6] N. N. Bogolyubov, Izv. Akad. Nauk SSSR, Ser. Fiz. **11**, 77 (1947); Physica (Amsterdam) **9**, 23 (1947).
[7] S. T. Belyaev, Zh. Éksp. Teor. Fiz. **34**, 417, 433 (1958) [Sov. Phys. JETP **7**, 289, 299 (1958)].
[8] A. A. Abrikosov, L. P. Gor'kov, and I. E. Dzyaloshinskiĭ, *Metods of Quantum Field Theory in Statistical Physics* [Prentice-Hall, Englewood Cliffs, N.J.; Dover, New York (1963); Fizmatgiz, Moscow (1962)].
[9] A. F. G. Wyatt, Nature (London) **391**, No. 6662, 56 (1998).
[10] Yu. A. Nepomnyashchiĭ and A. A. Nepomnyashchiĭ, Zh. Éksp. Teor. Fiz. **75**, 976 (1978) [Sov. Phys. JETP **48**, 493 (1978)].
[11] Yu. A. Nepomnyashchiĭ, Zh. Éksp. Teor. Fiz. **85**, 1244 (1983) [Sov. Phys. JETP **58**, 722 (1983)]; Zh. Éksp. Teor. Fiz. **89**, 511 (1985) [Sov. Phys. JETP **62**, 289 (1985)].
[12] J. R. Schrieffer, *Theory of Superconductivity* [Benjamin, New York (1964); Nauka, Moscow (1970)].
[13] W. A. B. Evans and Y. Imry, Nuovo Cimento **63**, 155 (1969).
[14] A. Coniglio and F. Manchini, Nuovo Cimento **63**, 227 (1969).
[15] R. Hasting and T. W. Halley, Phys. Rev. B **12**, 267 (1975).
[16] P. S. Kondratenko, Teor. Mat. Fiz. **22**, 228 (1975).
[17] Yu. A. Nepomnyashchiĭ and É. A. Pashitskiĭ, Zh. Éksp. Teor. Fiz. **98**, 178 (1990) [Sov. Phys. JETP **71**, 98 (1990)].
[18] S. I. Vil'chinsky, É. A. Pashitsky, and P. I. Fomin, Fiz. Nizk. Temp. **23**, 1267 (1997) [Low Temp. Phys. **23**, 951 (1997)].
[19] N. Hugenholtz and D. Pines, Phys. Rev. **116**, 489 (1959).
[20] L. Reatto and C. V. Chester, Phys. Rev. **155**, 88 (1967).
[21] G. W. Rayfield and F. Reif, Phys. Rev. Lett. **11**, 305 (1963).
[22] S. C. Whitmore and W. Zimmermann, Phys. Rev. **166**, 181 (1968).
[23] S. J. Putterman, *Superfluid Hydrodynamics* [North-Holland, New York (1974); Mir, Moscow (1968)].
[24] H. R. Glyde and E. C. Svensson, in *Neutron Scattering*, edited by D. L. Price and K. Skold, *Methods of Experimental Physics*, Vol. 23 Part B, Academic Press, New York (1987), p. 303.
[25] E. F. Tabbot, H. R. Glyde, W. G. Stirling, and E. C. Svensson, Phys. Rev. B **38**, 11229 (1988).
[26] H. R. Glyde and W. G. Stirling, Phys. Rev. B **42**, 4224 (1990).
[27] K. H. Andersen, W. G. Stirling, R. Scherm, A. Stanault, B. Fak, H. Godfrin, and A. J. Dianoux, J. Phys.: Condens. Matter **6**, 821 (1994).
[28] G. B. Gess, *Low Temperature Physics LPT-13*, New York, Plenum (1974), p. 302.
[29] J. R. Hulin, D. D'Humieres, B. Perrin, and A. Lichaber, Phys. Rev. A **9**, 885 (1974).
[30] G. Rayfield, Phys. Rev. Lett. **20**, 1467 (1968).
[31] V. N. Popov, *Continuous Integrals in Quantum Field Theory and Statistical Physics*, Nauka, Moscow (1973).
[32] V. N. Popov and A. V. Serednyakov, Zh. Éksp. Teor. Fiz. **77**, 377 (1979) [Sov. Phys. JETP **50**, 193 (1979)].
[33] K. A. Bruckner and K. Sawada, Phys. Rev. **106**, 1117,1128 (1957).
[34] K. A. Bruckner, *Theory of Nuclear Matter*, Mir, Moscow (1964).
[35] J. Gavoret and P. Nozières, Ann. Phys. (Paris) **28**, 349 (1964).
[36] I. M. Khalatnikov, *Theory of Superconductivity* [in Russian], Nauka, Moscow (1971).
[37] B. N. Esel'son, V. H. Grigor'ev, V. G. Ivantsov, É. Ya. Rudavskiĭ, D. G. Sanikidze, and I. A. Serbin, *Solutions of Quantum Liquids* ^{3}He–^{4}He [in Russian], Nauka, Moscow (1973).
[38] A. Z. Patashinskii and V. L. Pokrovskii, *Fluctuation Theory of Phase Transitions* [Pergamon Press, Oxford (1979); Nauka, Moscow (1975)].

Translated by Steve Torstveit

Precessing states with ''zero'' magnetization in the superfluid *A* phase of liquid ^{3}He

N. G. Suramlishvili*

É. Andronikashvili Institute of Physics, Academy of Sciences of Georgia, ul. Tamarashvili 6, 380077 Tbilisi, Georgia

(Submitted July 31, 2000; revised October 24, 2000)
Fiz. Nizk. Temp. **27**, 268–274 (March 2001)

The regimes of coherent precession of ''zero'' magnetization in a transverse rf field in the superfluid *A* phase of liquid ^{3}He are investigated with dissipative processes taken into account.
 [DOI: 10.1063/1.1355517]

1. The coherent precession of the magnetization in superfluid ^{3}He is a time-dependent ordered state with broken symmetry. The stability of the precessing states is maintained mainly by the spin stiffness of the order parameter of the ordered phases of liquid ^{3}He and the spin–orbit interaction. The magnetic dynamics in this case reduces to collective excitations of the magnetization and the spin part of the order parameter of the triplet condensate. Here in superfluid ^{3}He the existence of long-lived coherent precessing states in which the magnitude of the magnetization $|\mathbf{M}|$ is substantially different from its equilibrium value $M_0=\chi H_0$ (χ is the magnetic susceptibility of superfluid ^{3}He, and H_0 is the strength of the external static magnetic field). In Refs. 1–3 it was predicted theoretically that long-lived precessing states with half ($M=M_0/2$) or double ($M=2M_0$) magnetization can exist in a high magnetic field. The theoretical predictions as to the precessing states with half magnetization have been confirmed experimentally[4,5] in the case of ^{3}He–*B*. In addition, the authors of Refs. 4 and 5 also observed an unexpected precessing mode with ''zero'' magnetization ($M \ll M_0$). The possibility of stabilization of this mode had been previously pointed out in Ref. 6.

The coherent spin dynamics of the states with the equilibrium magnetization ($M=M_0$) and of the states with half and double magnetization correspond to the so-called ''resonant'' regimes of precession of the magnetic moment. The stability of these precessing states is due to the presence of local minima of the dipole–dipole interaction energy averaged over the fast motions. In the formation of steadily precessing states with ''zero'' magnetization, however, an important contribution is made by the balance between magnetic relaxation processes and the effect of the transverse radio-frequency (rf) magnetic field. It follows from Refs. 4–7, in particular, that such processes determine the residual value of the magnetic moment for the state with ''zero'' magnetization in ^{3}He–*B*. It is naturally of interest to elucidate the role of these processes in the *A* phase of superfluid ^{3}He. That is the subject of this paper.

2. In the calculations that follow it will be convenient to use the dimensionless variable

$$\mathbf{S}=\frac{\mathbf{M}}{M_0}. \tag{1}$$

The equation describing the nondissipative spin dynamics of the superfluid phases of liquid ^{3}He are written with the aid of the Leggett Hamiltonian in the form

$$H_L=\frac{\mathbf{S}^2}{2}-S_Z+U_D. \tag{2}$$

The order parameter that determines the characteristic features of the superfluid phases of ^{3}He in this Hamiltonian is represented with the use of the dipole–dipole interaction potential U_D. For the superfluid *A* phase of liquid ^{3}He

$$U_D=-\frac{1}{2}\left(\frac{\Omega_A}{\omega_0}\right)^2(\hat{\mathbf{d}}\cdot\hat{\mathbf{l}})^2, \tag{3}$$

where Ω_A is the longitudinal NMR frequency, g is the gyromagnetic ratio for the ^{3}He nuclei, the vector $\hat{\mathbf{l}}$ specifies the axis of the orbital anisotropy, and $\hat{\mathbf{d}}$ is the order parameter in spin space ($\hat{\mathbf{d}}^2=1$) of the superfluid *A* phase of ^{3}He.

Using the notation

$$\hat{\mathbf{l}}=l_Z\hat{\mathbf{z}}+\sqrt{1-l_Z^2}\hat{\mathbf{x}}, \quad \hat{\mathbf{d}}=\vec{\mathbf{R}}\ (\alpha,\beta,\gamma)\cdot\hat{\mathbf{x}}, \tag{4}$$

where the orthogonal matrix $\vec{\mathbf{R}}$ is parametrized by the Euler angles α, β, and γ, we obtain for the dipole–dipole interaction potential

$$U_D=\varepsilon f(s_Z,l_Z,\alpha,\gamma)=\varepsilon\sum_{k,l} f_{kl}(s_Z,l_Z)\exp[i(k\alpha+l\gamma)], \tag{5}$$

where $\varepsilon\propto(\Omega_A/\omega_0)^2$, and $s_Z=\cos\beta$. The nonzero coefficients f_{kl} are given by the expressions [we have set $\varepsilon=(1/8)(\Omega_A/\omega_0)^2$ below]

$$\begin{aligned}
f_{00}&=-[1+l_Z^2+(1-3l_Z^2)s_Z^2],\\
f_{10}&=f_{-10}=2s_Zl_Z\sqrt{1-s_Z^2}\sqrt{1-l_Z^2},\\
f_{20}&=f_{-20}=\frac{1}{2}(1-s_Z^2)(1-l_Z^2),\\
f_{02}&=f_{0-2}=\frac{1}{2}(1-s_Z^2)(1-3l_Z^2),\\
f_{22}&=f_{-2-2}=-\frac{1}{4}(1-l_Z^2)(1+s_Z)^2,\\
f_{2-2}&=f_{-22}=-\frac{1}{4}(1-l_Z^2)(1-s_Z)^2,
\end{aligned} \tag{6}$$

$$f_{12}=f_{-1-2}=l_Z(1+s_Z)\sqrt{1-s_Z^2}\sqrt{1-l_Z^2},$$

$$f_{1-2}=f_{-12}=-l_Z(1-s_Z)\sqrt{1-s_Z^2}\sqrt{1-l_Z^2}.$$

3. In the discharge approximation the relaxation processes are described with the help of the dissipative function

$$F_{\rm dis}=\frac{1}{2}\kappa\left[\frac{S^2}{S^2-S_Z^2}\left(\dot S^2+\dot S_Z^2-2\dot S_Z\dot S\frac{S_Z}{S}\right)+(S^2-S_Z^2)(\dot\alpha+1)^2\right], \tag{7}$$

where κ is a phenomenological parameter.[8]

Compensation of the dissipation is achieved by applying to the system an external transverse rf field $\mathbf{H}_\perp$, with projections $H_\perp\cos$ and $H_\perp\sin\varphi$ along the $\hat{\mathbf{x}}$ and $\hat{\mathbf{y}}$ axes, respectively. The interaction energy of the magnetic moment of the system with this field is described by the expression

$$F_\perp=-\sqrt{S^2-S_Z^2}\,h_\perp\cos\theta, \tag{8}$$

where $h_\perp=H_\perp/H_0$, and $\theta=\alpha-\varphi$ is the angle between the transverse component of the magnetization and the transverse rf field.

In the case of a high magnetic field ($\varepsilon\ll1$) we choose (S_Z,α) and (S,γ) as the two pairs of canonically conjugate variables. By the standard procedure we construct for these variables the following equations of motion from expressions (2), (7), and (8):

$$\dot S_Z=-\varepsilon\left(\frac{\partial f}{\partial\alpha}\right)+\varepsilon^2\kappa(S^2-S_Z^2)\left(\frac{\partial f}{\partial S_Z}\right)^2-\sqrt{S^2-S_Z^2}\,h_\perp\sin\theta, \tag{9}$$

$$\dot S=-\varepsilon\frac{\partial f}{\partial\gamma}, \tag{10}$$

$$\dot\alpha=-1+\varepsilon\frac{\partial f}{\partial S_Z}-\varepsilon\kappa\frac{S^2}{S^2-S_Z^2}\left(\frac{\partial f}{\partial\alpha}-\frac{S_Z}{S}\frac{\partial f}{\partial\gamma}\right)+\frac{S}{\sqrt{S^2-S_Z^2}}h_\perp\cos\theta, \tag{11}$$

$$\dot\gamma=S+\varepsilon\frac{\partial f}{\partial S}-\varepsilon\kappa\frac{S^2}{S^2-S_Z^2}\left(\frac{\partial f}{\partial\gamma}-\frac{S_Z}{S}\frac{\partial f}{\partial\alpha}\right)-\frac{S}{\sqrt{S^2-S_Z^2}}h_\perp\cos\theta. \tag{12}$$

The right-hand sides of these equations contain terms of order 1, ε, and ε^2. This allows us to analyze equations (9)–(12) by the method[8,9] of separation of motions occurring at substantial different velocities, introducing the new variables $\overline{S}$, $\overline{S_Z}$, $\overline{\alpha}$, and $\overline{\gamma}$, the variations of which will be determined by the spin-system dynamics averaged over the fast variables. We see from system (9), (10) that in the general case the angles α and γ are rapidly varying quantities, and the moments S_Z and S are slowly varying.

It is not hard to see that the coefficient f_{00} in (6) is the dipole–dipole interaction potential averaged over the fast variables α and γ. The profile of the coefficient f_{00} is presented in Fig. 1. It follows from the figure that the nonresonant equilibrium state corresponds to the spin–orbit configurations

$$l_Z=0,\quad s_Z=\pm1, \tag{13}$$

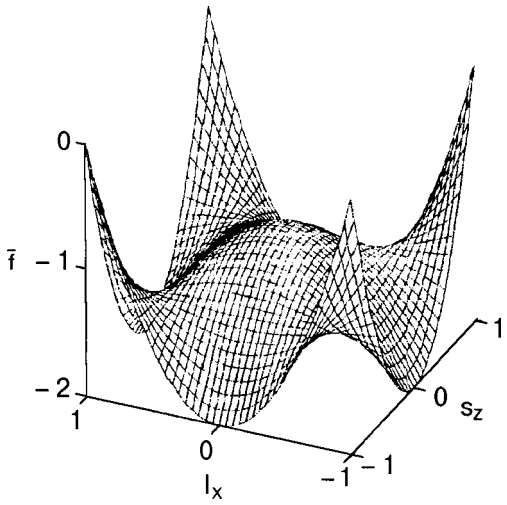

FIG. 1. Profile of the averaged dipole–dipole interaction potential $\overline{f}$ in the case when $\sqrt{\varepsilon}\ll\overline{S}\ll1/2$ [the coefficient f_{00} from Eq. (6)].

$$l_Z=\pm1,\quad s_Z=0. \tag{14}$$

4. The procedure of averaging over the fast variables leads to equations describing the relaxation of $\overline{S}$ and $s_Z=\overline{S}/\overline{S_Z}$. These equations have the form

$$\dot{\overline{S}}=-\frac{2\varepsilon^2\kappa}{1-s_Z^2}\left[\frac{4}{\overline{S}}f_{02}^2+\frac{8}{\overline{S}-1}(1-s_Z)f_{22}^2+\frac{1}{\overline{S}-1/2}(5-4s_Z)f_{12}^2+\frac{8}{\overline{S}+1}(1+s_Z)f_{2-2}^2+\frac{1}{\overline{S}+1/2}(5+4s_Z)f_{1-2}^2\right], \tag{15}$$

$$\dot s_Z=\frac{1}{\overline{S}}\left\{\frac{2\varepsilon^2\kappa}{1-s_Z^2}\left[f_{10}^2+f_{20}^2+\frac{4s_Z}{\overline{S}}f_{02}^2-\frac{8}{\overline{S}-1}(1-s_Z)^2f_{22}^2-\frac{1-2s_Z}{2(\overline{S}-1/2)}(5-4s_Z)f_{12}^2+\frac{8}{\overline{S}+1}(1+s_Z)^2f_{2-2}^2+\frac{1+2s_Z}{2(\overline{S}+1/2)}(5+4s_Z)f_{1-2}^2\right]+\varepsilon^2\kappa(1-s_Z^2)\sum_{kl}\left(\frac{\partial f_{kl}}{\partial s_Z}\right)^2\right\}-\sqrt{1-s_Z^2}\,h_\perp\sin\theta. \tag{16}$$

In addition to the usual resonance, which corresponds to $\overline{S}=1$, Eqs. (15) and (16) for $f_{02},f_{12}\neq0$ also contain terms describing resonant regimes of precession with $\overline{S}=0$ and $\overline{S}=1/2$.

We begin our study of relaxation processes with the case when there is no transverse rf field ($h_\perp=0$). It is easy to see that for $l_Z=0$ (the so-called Leggett orbital configuration) only those term corresponding to the resonances $\overline{S}=0$ and $\overline{S}=1$ remain in Eqs. (15) and (16). Then when the magnetization is oriented along the magnetic field ($s_Z=1$) we arrive at the result obtained previously,[8] according to which the magnetization $\overline{S}$ relaxes to the equilibrium value $\overline{S}=1$ by a square-root law:

$$\overline{S}=1\pm\sqrt{(S_0-1)^2-16\varepsilon^2\kappa(t-t_0)}. \tag{17}$$

Here $\overline{S_0}$ is the value of the magnetization at the initial time $t=t_0$; the upper sign on the right-hand side of expression (17) corresponds to the case $\overline{S_0}>1$ and the lower sign to the case $\overline{S_0}<1$.

Let us now consider the case when the magnetization is oriented antiparallel to the magnetic field ($s_Z=-1$). Solving Eqs. (15) and (16) with the initial conditions $t=t_0$, $\overline{S}=\overline{S_0}$, we find that $\overline{S}$ relaxes to the value $\overline{S}=0$ by a square-root law:

$$\overline{S}=-1+\sqrt{(\overline{S_0}+1)^2-16\varepsilon^2\kappa(t-t_0)}. \tag{18}$$

When $l_Z=\pm 1$, the relaxation equations contain terms corresponding to the resonance $\overline{S}=0$:

$$\dot{\overline{S}}=-\frac{8\varepsilon^2\kappa}{\overline{S}}(1-s_Z^2), \tag{19}$$

$$\dot{s}_Z^2=-\frac{8\varepsilon^2\kappa}{\overline{S}}s_Z(1-s_Z^2)\left(\frac{1}{\overline{S}}+3s_Z\right). \tag{20}$$

According to (14), the minimum value of the dipole energy corresponds to the value $s_Z=0$. In this case s_Z remains constant, and the magnetization $\overline{S}$ relaxes toward $\overline{S}=0$ according to the law

$$\overline{S}=\sqrt{S_0^2-16\varepsilon^2\kappa(t-t_0)}. \tag{21}$$

5. From the results obtained in the previous Section it is seen that the magnetization can relax toward the value $\overline{S}=0$. As it approaches a value of zero, the order of the terms appearing in the right-hand sides of equations (9)–(12) will depend on $\overline{S}$ as well as on the parameter ε. If

$$\sqrt{\varepsilon}\ll\overline{S}\ll\frac{1}{2}, \tag{22}$$

then the the usual nonresonant regime of precession of the magnetization will be realized, and the averaging is done over the fast variables α and γ. If, on the other hand, $\overline{S}\sim\sqrt{\varepsilon}$, then the angle variable γ varies slowly, and the averaging is done over the single remaining fast variable α.

Let us first consider the case when $\overline{S}$ satisfies conditions (22). Following Ref. 7, we obtain from Eqs. (11) and (12)

$$\frac{\overline{\omega}-1}{\varepsilon}\overline{S}+\frac{h_\perp}{\varepsilon}\frac{s_Z\overline{S}}{\sqrt{1-s_Z^2}}\cos\theta+\frac{\partial\overline{f}}{\partial s_Z}=0, \tag{23}$$

$$\frac{\overline{S}-\omega_\gamma}{\varepsilon}\overline{S}-\frac{h_\perp}{\varepsilon}\frac{\overline{S}}{\sqrt{1-s_Z^2}}\cos\theta-s_Z\frac{\partial\overline{f}}{\partial s_Z}=0. \tag{24}$$

Here $\overline{\omega}=-\dot{\overline{\alpha}}$, $\omega_\gamma=\dot{\overline{\gamma}}$, and $\overline{f}=f_{00}$. In the actual experiments[4,5] done on ^{3}He-B the parameter $(\overline{\omega}-1)/\varepsilon$ varied from 0 to 10, and the parameter $h_\perp/\varepsilon$ varied from 1 to 10. We assume that similar conditions can also be realized in the case of ^{3}He–A. Equation (23) is the condition of minimum free energy of the system, which is the sum of the dipole and spectroscopic parts and the energy of interaction with the transverse rf field. From the condition $\overline{S}\ll 1/2$ it follows that the main contribution to the free energy of the system is the dipole–dipole interaction energy, while the spectral energy and the energy of interaction with the rf field are small perturbations and to a first approximation can be neglected.

The averaged dipole–dipole potential $\overline{f}$ has four degenerate minimum values, the spin–orbit configurations of which are given by expressions (13) and (14). In the next approximation the angle θ is determined from Eq. (23) and the frequency ω_γ from Eq. (24). The values of $\overline{S}$ and s_Z are found from the relaxation equations describing the evolution of the spin system to the second approximation in the small parameter ε. These equations are obtained from system (15), (16) and under conditions (22) have the form

$$\dot{\overline{S}}=-\frac{4\varepsilon^2\kappa}{1-s_Z^2}\left[\frac{2}{\overline{S}}f_{02}^2-4(1-s_Z)f_{22}^2-(5-4s_Z)f_{12}^2+4(1+s_Z)f_{2-2}^2+(5+4s_Z)f_{1-2}^2\right], \tag{25}$$

$$\dot{s}_Z=\frac{1}{\overline{S}}\left\{\frac{2\varepsilon^2\kappa}{1-s_Z^2}\left[\frac{4s_Z}{\overline{S}}f_{02}^2+f_{10}^2+4f_{20}^2+8(1-s_Z)^2f_{22}^2+(1-2s_Z)(5-4s_Z)f_{12}^2+8(1+s_Z)^2f_{2-2}^2+(1+2s_Z)(5+4s_Z)f_{1-2}^2\right]+\varepsilon^2\kappa(1-s_Z^2)\sum_{kl}\left(\frac{\partial f_{kl}}{\partial s_Z}\right)^2\right\}-h_\perp\sqrt{1-s_Z^2}\sin\theta. \tag{26}$$

Let us consider the neighborhood of the states (13) and (14). For $l_Z=0$ the system of equations (25), (26), according to expressions (6), becomes

$$\dot{\overline{S}}=-\varepsilon^2\kappa\left(\frac{1-s_Z^2}{\overline{S}}-3s_Z-2s_Z^3\right), \tag{27}$$

$$\dot{s}_Z=\frac{\varepsilon^2\kappa}{\overline{S}}(1-s_Z^2)\left(\frac{s_Z}{\overline{S}}+4+11s_Z^2\right)-h_\perp\sqrt{1-s_Z^2}\sin\theta. \tag{28}$$

In the case $s_Z=-1+\beta^2/2$, where $\beta\ll 1$, we obtain the following equations for $\overline{S}$ and β from the system (27), (28):

$$\dot{\overline{S}}=-\varepsilon^2\kappa\left(\frac{2\beta^2}{\overline{S}}+5\right), \tag{29}$$

$$\dot{\beta}=\frac{2\varepsilon^2\kappa}{\overline{S}^2}\beta-h_\perp\sin\theta. \tag{30}$$

This system of equations does not have stationary solutions, since the right-hand side of (29) is always negative.

In the case $s_Z=1-\beta^2/2$ equations (27) and (28) become

$$\dot{\overline{S}}=-\varepsilon^2\kappa\left(\frac{\beta^2}{\overline{S}}-5\right), \tag{31}$$

$$\dot{\beta}=-\frac{\varepsilon^2\kappa}{\overline{S}^2}\beta+h_\perp\sin\theta. \tag{32}$$

In the stationary state $\dot{\overline{S}}=\dot{\beta}=0$. For it we obtain

$$\bar{S}_0=\frac{\beta^2}{5},\quad \beta_0=\left(\frac{25\varepsilon^2\kappa}{h_\perp\sin\theta}\right)^{1/3}. \tag{33}$$

Since the stationary value $\bar{S}_0$ must satisfy condition (22), the transverse rf field must satisfy the condition $h_\perp \ll \sqrt{5}\kappa\varepsilon^{5/4}/\sin\theta$.

Let us now consider the problem of the behavior of a small perturbation against the background of the stationary state characterized by the parameters (33). After localization of the system (31), (32), we obtain the following equations for the perturbed quantities δS and $\delta\beta$:

$$\left(\frac{\partial}{\partial t}-\frac{\beta_0^2}{\bar{S}_0^2}\varepsilon^2\kappa\right)\delta S+2\varepsilon^2\kappa\frac{\beta_0}{\bar{S}_0}\delta\beta=0,$$
$$2\varepsilon^2\kappa\frac{\beta_0}{S_0^3}\delta S-\left(\frac{\partial}{\partial t}+\frac{1}{S_0^2}\varepsilon^2\kappa\right)\delta\beta=0. \tag{34}$$

We seek a solution of this system in the form $\delta S_0\exp(i\omega t)$, $\delta\beta_0\exp(i\omega t)$. The dispersion relation obtained has the following solutions:

$$\omega\approx i\frac{5\varepsilon^2\kappa}{2S_0^2}\beta_0^2,\quad \omega\approx i\frac{\varepsilon^2\kappa}{S_0^2}. \tag{35}$$

Consequently, the perturbations are aperiodically damped with decrements of $5\varepsilon^2\kappa\beta_0^2/\bar{S}_0^2$ and $\varepsilon^2\kappa/\bar{S}_0^2$. This means that the stationary state with parameters (33) is stable.

For the case $l_Z=\pm1$, we obtain the following equations from (25) and (26):

$$\dot{\bar{S}}=-\frac{8\varepsilon^2\kappa}{\bar{S}}(1-s_Z^2), \tag{36}$$

$$\dot{s}_Z=\frac{8\varepsilon^2\kappa}{S^2}s_Z(1-s_Z^2)-h_\perp\sqrt{1-s_Z^2}\sin\theta. \tag{37}$$

This system does not have stationary solutions. It follows from Eq. (36) that for any values of s_Z the modulus of the magnetization $\bar{S}$ decreases with time and tends toward a value $\bar{S}\sim\sqrt{\varepsilon}$.

6. In the case when $\bar{S}\sim\sqrt{\varepsilon}$, it follows from (12) that $\dot{\bar{\gamma}}\sim\sqrt{\varepsilon}$. Still, this rate is greater than the rates of change of $\bar{S}$ and $\bar{S}_Z$. However, $\bar{S}$ and $\bar{S}_Z$ appear in the dipole–dipole interaction potential in the form of the ratio $\bar{S}_Z/\bar{S}$. Furthermore, $\dot{s}_Z=\dot{\bar{S}}_Z-s_Z\dot{\bar{S}}$. It follows that $\dot{s}_Z\sim\sqrt{\varepsilon}$. Thus the rates of change of γ and s_Z are quantities of the same order. Therefore, only one fast variable, α, remains in the dipole–dipole interaction potential. In this situation we write the dipole–dipole interaction potential in the form of a Fourier series expansion:

$$f=\sum_{k=-2}^{2}f_k(\bar{S},\bar{S}_Z,l_Z,\bar{\gamma})e^{ik\bar{\alpha}} \tag{38}$$

and we write out only those expansion coefficients which are necessary for further analysis:

$$f_0=\bar{f}=-[1+l_Z^2+(1-3l_Z^2)s_Z^2-(1-3l_Z^2)(1-s_Z^2)\cos2\gamma], \tag{39}$$

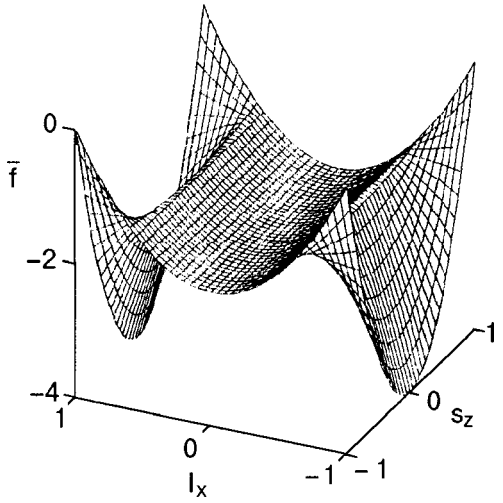

FIG. 2. Profile of the averaged dipole–dipole interaction potential $\bar{f}$ in the case when $\bar{S}\sim\sqrt{\varepsilon}$ (Eq. (39) after minimization with respect to the variable γ).

$$f_1=f_{-1}^*=-2l_Z^2\sqrt{1-l_Z^2}\sqrt{1-s_Z^2}[s_Z^2+\cos2\gamma-is_Z\sin2\gamma], \tag{40}$$

$$f_2=f_{-2}^*=-\frac{1}{2}(1-l_Z^2)[1-s_Z^2-(1+s_Z^2)\cos2\gamma-is_Z\sin2\gamma]. \tag{41}$$

It is easy to see that f_0 is the dipole–dipole potential averaged over the fast variable $\bar{\alpha}$, and its minimization determines the spin–orbit configuration of the equilibrium precessing states. The profile of f_0 after minimization with respect to the variable $\bar{\gamma}$ is shown in Fig. 2. It follows from an analysis of f_0 that for $|l_Z|\leqslant1/\sqrt{3}$ the stationary value $\gamma_{st}=\pi/2$. In this case the spin system has a family of degenerate minima with the spin–orbit configurations

$$l_Z=0,\quad |s_Z|\leqslant1. \tag{42}$$

If, on the contrary, $|l_Z|>1/\sqrt{3}$, then $\gamma_{st}=0$, and the minimum values of the dipole energy correspond to the states

$$l_Z=\pm1,\quad s_Z=0. \tag{43}$$

In the the case under discussion the system of equations for $\bar{S}$ and s_Z have the form

$$\dot{\bar{S}}=\frac{2\varepsilon^2\kappa}{1-s_Z^2}\sum_{k>0}\left[\frac{1}{k}\mathrm{Im}\left(\frac{\partial^2 f_k}{\partial\bar{\gamma}^2}\frac{\partial f_k^*}{\partial\bar{\gamma}}\right)+s_Z\,\mathrm{Re}\left(\frac{\partial^2 f_k}{\partial\bar{\gamma}^2}f_k^*\right)\right.$$
$$\left.+k\,\mathrm{Im}\left(\frac{\partial f_k}{\partial\bar{\gamma}}f_k^*\right)-s_Z\left|\frac{\partial f_k}{\partial\bar{\gamma}}\right|^2\right], \tag{44}$$

$$\dot{s}_Z=\frac{2\varepsilon^2\kappa}{1-s_Z^2}\frac{1}{\overline{S}}\sum_{k>0}\left\{\left[(1+s_Z^2)\left|\frac{\partial f_k}{\partial\overline{\gamma}}\right|^2+k^2|f_k|^2\right.\right.$$
$$+s_Z k\,\mathrm{Im}\left(\frac{\partial f_k}{\partial\overline{\gamma}}f_k^*\right)-\frac{s_Z}{k}\mathrm{Im}\left(\frac{\partial^2 f_k}{\partial\overline{\gamma}^2}\frac{\partial f_k^*}{\partial\overline{\gamma}}\right)$$
$$\left.\left.-s_Z^2\,\mathrm{Re}\left(\frac{\partial^2 f_k}{\partial\overline{\gamma}^2}f_k^*\right)\right]\right\}+\frac{2\varepsilon^2\kappa}{\overline{S}}(1-s_Z^2)\left[\frac{1}{2}\left(\frac{\partial f_0}{\partial s_Z}\right)^2\right.$$
$$\left.+\sum_{k>0}\left|\frac{\partial f_k}{\partial s_Z}\right|^2\right]-\sqrt{1-s_Z^2}h_\perp\sin\theta, \tag{45}$$

It follows from these equations that the value of the magnetization $\overline{S}$ relaxes much more slowly than value of the projection of the magnetic moment on the direction of the external static magnetic field, i.e., $\dot{\overline{S}}/\dot{s}_Z\sim\sqrt{\varepsilon}\ll 1$. Therefore, we may rightly consider the change of s_Z against the background of a frozen value of $\overline{S}$.

Since $\gamma_{\mathrm{st}}=\pi/2$ at $l_Z=0$, we find from Eq. (45) that

$$\dot{s}_Z=\frac{4\varepsilon^2\kappa}{\overline{S}(1-s_Z^2)}[s_Z^4-s_Z^3+s_Z^2+4]-h_\perp\sqrt{1-s_Z^2}\sin\theta. \tag{46}$$

In the limiting case $s_Z\approx -1$ the temporal behavior of β is determined by the equation

$$\dot{\beta}=\frac{28\varepsilon^2\kappa}{\overline{S}\beta^3}-h_\perp\sin\theta, \tag{47}$$

i.e., the stationary value β_0 is described by the expression

$$\beta_0=\left(\frac{28\varepsilon^2\kappa}{\overline{S}h_\perp\sin\theta}\right)^{1/3}, \tag{48}$$

and small perturbations against the background of the stationary state (48) decay with a decrement $84\varepsilon^2\kappa/\overline{S}\beta_0^4$.

For $s_Z\approx 1$ the temporal behavior of β is determined by the equation

$$\dot{\beta}=\frac{20\varepsilon^2\kappa}{\overline{S}\beta^3}-h_\perp\sin\theta, \tag{49}$$

so that the stationary value of β_0 has the form

$$\beta_0=\left(\frac{20\varepsilon^2\kappa}{\overline{S}h_\perp\sin\theta}\right)^{1/3}, \tag{50}$$

and small perturbations against the background of the stationary state (50) grow with an increment $60\varepsilon^2\kappa/\overline{S}\beta_0^4$.

Thus the precessing states with $l_Z=0$, $s_Z\approx -1$ are stable, and those with $s_Z\approx 1$ are unstable.

For the case $l_Z=\pm 1$ we obtain from (45), with allowance for the fact that $\gamma_{\mathrm{st}}=0$,

$$\dot{s}_Z=\frac{32\varepsilon^2\kappa}{\overline{S}}s_Z(1-s_Z^2)-h_\perp\sqrt{1-s_Z^2}\sin\theta. \tag{51}$$

From this equation we obtain the following expression for the stationary value s_Z^0:

$$s_0^Z=\pm\left(\frac{h_\perp\overline{S}\sin\theta}{32\varepsilon^2\kappa}\right)^{1/2}. \tag{52}$$

Consequently, against a background of positive stationary values $s_Z^0>0$ small perturbations grow with an increment of $64\varepsilon^2\kappa s_Z^0/\overline{S}$, while against a background of negative values $s_Z^0<0$ they decay with a decrement of $64\varepsilon^2\kappa s_Z^0/\overline{S}$. Thus the states with $s_Z^0>0$ are unstable, while those with $s_Z^0<0$ are stable.

7. It follows from the above analysis of the spin dynamics in ^{3}He–*A* that with allowance for the relaxation processes and the interaction with the transverse rf field, coherently precessing states both with half and with ''zero'' magnetization are realized for arbitrary values of l_Z. Depending on the order of magnitude of the modulus of the magnetic moment, the precession of the magnetization will take place in the usual nonresonant regime with two fast angle variables or in a regime characterized by the presence of only one fast angle variable.

In the nonresonant regime the value of the magnetization is determined from the balance of magnetic relaxation and the effect of the transverse rf field. Here stabilization of the state is possible in the neighborhood of the point $l_Z=0$, $s_Z=1$.

In the other case the magnetization $S\sim\sqrt{\varepsilon}$, and the balance of the magnetic relaxation and the effect of the rf field leads to a spin–orbit configuration of equilibrium precessing states. For $l_Z=0$ stabilization of the state is effected in the neighborhood of the value $s_Z=-1$. In the case $l_Z=\pm 1$ the equilibrium states are stabilized at negative values of s_Z.

The author is deeply grateful to G. A. Kharadze for steady interest, guidance, and numerous discussions.

This study was supported in part by Grant No. 2.16 of the Academy of Sciences of Georgia.

*E-mail: nugzars@iph.hepi.edu.ge; nugzars@hotmail.com

[1] G. Kharadze and G. Vachnadze, JETP Lett. **56**, 458 (1992).
[2] A. D. Gongadze, G. E. Gurgenishvili, and G. A. Kharadze, Zh. Éksp. Teor. Fiz. **78**, 615 (1980) [Sov. Phys. JETP **51**, 310 (1980)].
[3] G. Kharadze and G. Vachnadze, Zh. Éksp. Teor. Fiz. **106**, 479 (1994) [JETP **79**, 262 (1994)].
[4] V. V. Dmitriev, L. V. Kosarev, M. Krusius, D. V. Ponarin, V. M. H. Ruutu, and G. E. Volovik, Phys. Rev. Lett. **78**, 86 (1997).
[5] V. B. Eltsov, V. V. Dmitriev, H. Krusius, J. J. Ruohio, and G. E. Volovik, J. Low Temp. Phys. **113**, 645 (1998).
[6] É. B. Sonin, Zh. Eksp. Teor. Fiz. **94**(9), 100 (1988) [Sov. Phys. JETP **67**, 1791 (1988)].
[7] G. Kharadze and N. Suramlishvili (to be published).
[8] I. A. Fomin, Zh. Éksp. Teor. Fiz. **77**, 279 (1979) [Sov. Phys. JETP **50**, 144 (1979)].
[9] N. N. Moiseev, *Asymptotic Methods of Nonlinear Mechanics* [in Russian], Nauka, Moscow (1981).

Translated by Steve Torstveit

SUPERCONDUCTIVITY, INCLUDING HIGH-TEMPERATURE SUPERCONDUCTIVITY

Anisotropy of the vortex creep in a $YBa_2Cu_3O_{7-x}$ single crystal with unidirectional twin boundaries

A. V. Bondarenko,* M. G. Revyakina, A. A. Prodan, M. A. Obolenskiĭ, and R. V. Vovk

V. N. Karazin Kharhov National University, pl. Svobody 4, 61077 Kharkov, Ukraine

T. R. Arouri

Physics Department of Bir-Zeit University, P.O. Box 15, Bir-Zeit, West Bank, Israel
(Submitted September 25, 2000; revised November 15, 2000)
Fiz. Nizk. Temp. **27**, 275–293 (March 2001)

Vortex creep in a single crystal containing unidirectional twin boundaries (TBs) is investigated at temperatures of 82–87 K in a special experimental geometry: $\mathbf{J}\|ab$, $\mathbf{J}\|$TB, $\mathbf{H}\perp\mathbf{J}$, with $\alpha\equiv\angle\mathbf{H},ab$ as a variable parameter. It is shown that in low magnetic fields the TBs alter the configuration of the structure of the flux lines at angles of misorientation θ between the magnetic field vector **H** and the planes of the TBs of up to 70°: at angles $\theta<70°$ a part of the flux line is trapped by the planes of the TBs. It is shown that a TB is an efficient pinning center for the motion of the vortices perpendicular to the plane of the TB, and therefore in low magnetic fields at angles $\theta<70°$ a directed motion of the vortices along the planes of the TBs occurs. The angle dependence of the activation energy for a plastic mechanism of flux creep is determined, and it is found to agree with the theoretical estimates made. For an orientation of the vector **H** close to the ab plane of the crystal, the maximum of the angle dependence of the measured ''critical'' current $J_{cE}(\alpha)$ observed for the the $\mathbf{H}\|ab$ orientation of the field vector in low magnetic fields gives way to a minimum at higher magnetic fields; this is explained by a change from single-vortex creep to collective creep as the magnetic field is increased.
 [DOI: 10.1063/1.1355518]

INTRODUCTION

High-T_c superconductors have an anisotropic layered structure. As a result, the characteristic scales of the Abrikosov vortices, which are characterized by a coherence length ξ and a penetration depth λ, and the vortex lattice, which is characterized by the intervortex distance a_0, are also anisotropic. This leads to anisotropy of the magnetic flux pinning, which is ordinarily characterized by the angle dependence of the measured ''critical'' current $J_m(\alpha)$, where α is the angle between the magnetic field vector **H** and the ab plane of the crystal. Analysis of published data shows that the angle dependence of the current J_m depends on the direction of motion of the magnetic flux, on the density of defects in the sample, and on the strength of the external magnetic field. For example, studies of the magnetization of YBaCuO single crystals in a relatively low magnetic field at not very small angles α have shown[1] that for motion of vortices off the ab plane, J_m does not depend on the angle α, while for motion along the ab plane, J_m decreases with angle α as $J_m(\alpha)\approx J_m(\mathbf{H}\|\mathbf{c})\sin\alpha$.

Numerous experimental studies[2–4] of high-T_c superconductors attests to a nonmonotonic field dependence of the current J_m, which is called the ''fishtail effect.'' The position of the minimum of $J_m(H)$, which, according to the existing ideas, can correspond to a phase transition of the vortex lattice[5] or a transition between different regimes of creep of the vortex lattice,[3,6] and also the position of the maximum, which corresponds to a transition from an elastic to a plastic mechanism of creep,[7] depends on the orientation of the magnetic field vector.[4] Therefore, the magnitude of the magnetic field may govern the appearance of additional features on the angle dependence of the current J_m owing to a transition between different creep regimes or phase states of the vortex system.

Still another reason for the anisotropic pinning is the intrinsic pinning that arises when the magnetic field is oriented close to the ab plane, $\alpha\leqslant\varepsilon$, and which is manifested as a sharp increase in J_m with decreasing angle α.[8] This type of pinning takes place in layered superconductors and is due to modulation of the order parameter along the **c** axis. It is assumed that when the vector **H** is oriented parallel to the ab plane, the flux lines are situated between the CuO superconducting layers so as to minimize the core energy.[9] Here the flux lines are found in the field of a periodic potential, the maxima of which correspond to the positions of the cores of the flux lines in the CuO planes. It is assumed that in a magnetic field tilted at angles $\alpha\leqslant\varepsilon$ the flux lines have a stepped structure. The flux lines now lie partly between the CuO planes, as before, and partly parallel to the **c** axis. If the pinning of the vortex segments localized between CuO planes is large, then in a tilted magnetic field the magnetic flux creep will be mainly governed by the thermally activated motion of the segments oriented along the **c** axis. Ex-

perimental studies of tilted $YBa_2Cu_3O_{7-x}$ films[10] indeed show evidence of the motion of these segments along the ab plane.

In the high-T_c superconductor YBaCuO twin boundaries are another source of anisotropic pinning. In a magnetic field $\mathbf{H}\|\mathbf{c}$ the anisotropy is manifested as preferential motion of the magnetic flux along the planes of the TBs rather than along the direction of the Lorentz force.[11] This effect indicates that TBs form channels of easy motion of the magnetic flux along the plane of the TBs, while the motion of the flux perpendicular to the TB plane is suppressed. Indeed, a comparison of the current–voltage (I–V) characteristics of YBaCuO single crystals containing unidirectional TB planes has shown that at a temperature of 84 K and in a magnetic field of 15 kOe oriented along the **c** axis, the value of the current J_m in the motion of vortices in the direction perpendicular to the TB plane is approximately seven times as large as in their motion along the TB plane.[12]

In a magnetic field tilted with respect to the TB planes the anisotropy is manifested as a nonmonotonic angle dependence of the current $J_m(\theta)$, where θ is the angle between the field vector **H** and the TB plane. When the magnetic field is oriented close to the ab plane and the field vector is rotated out of the plane of the TB, this anisotropy is manifested as a maximum on the $J_m(\theta)$ curve.[13] When the magnetic field is oriented close to the **c** axis, on the other hand, the minimum on the $J_m(\theta)$ curve observed at a low level of energy dissipation gives way to a maximum at a high level of energy dissipation.[14] The influence of the TBs on the magnetic flux pinning in tilted magnetic fields is due to the circumstance that at angles θ less than a certain critical angle θ_{cr} a part of the vortex line is trapped by the TB plane.[15] Theoretical studies[15,16] have shown that the value of the critical angle depends on the orientation of the magnetic field relative to the crystallographic axes of the single crystal.

Despite the large number of experimental papers devoted to the study of pinning and the dynamics of the magnetic flux in $YBa_2Cu_3O_{7-x}$ single crystals, a number of questions on this topic remain open. For example, we have not found any published experimental research on the anisotropy of the plastic creep due to the motion of dislocations of the vortex lattice. Similarly, there has been no discussion of the influence of twin boundaries on the magnetic flux pinning and dynamics when the field vector is oriented close to the ab plane. Under certain conditions, this influence can be quite substantial, since if a stepped structure of the flux lines is realized, the parts of the vortex segments oriented parallel to the **c** axis will be trapped by the TB planes. There is also a lack of agreement as to the region of angles θ within which the TBs affect the flux pinning. For example, in Ref. 14 it was reported that when the vector **H** is rotated away from the **c** axis, the TBs play a role in the magnetic flux pinning for $\theta \leqslant 15°$, while in Ref. 17 it was concluded that their influence is felt all the way to $\theta = 50°$. These and certain other aspects of the magnetic flux pinning and dynamics in YBaCuO single crystals will be the subject of this paper.

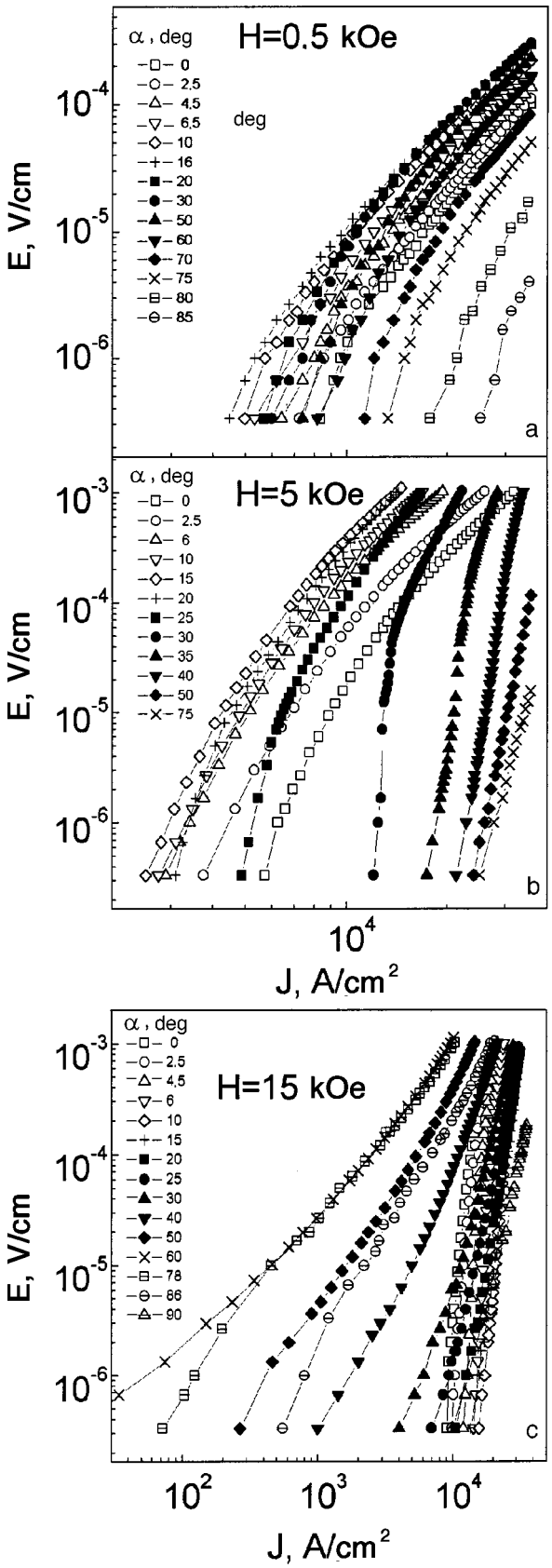

FIG. 1. Current–voltage (I–V) characteristics at $T = 84$ K in magnetic fields of 0.5 (a), 5 (b), and 15 kOe (c) for different angles α, indicated in the figures.

EXPERIMENTAL RESULTS

We present the results of resistive studies of the anisotropy of the magnetic flux creep in a $YBa_2Cu_3O_{7-x}$ single crystal containing unidirectional twin boundaries. The sample had a critical temperature $T_c = 92$ K and a superconducting transition width of 0.3 K. The transport current was

passed along the ab plane of the crystal, and the current density vector **J** was nearly parallel to the plane of the TBs, specifically, $\angle$**J**,TB$<7°$. The magnetic field vector **H** was rotate out of the ab plane toward the **c** axis, and the vector **H** was always perpendicular to the vector **J**. The stability of the temperature during the measurements was of the order of 0.03 K, and the stability of the magnetic field was not worse than 0.05%. Measurements on the sample in the normal state showed that its overheating at the highest level of energy dissipation, 10^{-4} W, did not exceed 0.05 K. The error in determining the angle α was 0.1°.

The I–V characteristics measured at $T=84$ K in magnetic fields of 0.5, 5, and 15 kOe are shown in Fig. 1. At 0.5 kOe the electric field increases with increasing angle α in the regions of angles $\alpha<20°$, and then it decreases as α is increased further to the orientation **H**$\|$**c**. We also note that in a magnetic field parallel to the **c** axis and, hence, to the TB plane, the electric field is zero in the investigated interval of current densities. For this orientation of the field, parts of the vortices are trapped by the TB planes, and the Lorentz force is oriented perpendicular to the TB plane. Thus the TB planes are efficient pinning centers for the motion of the vortices in the direction perpendicular to them; this agrees with the previous studies[11,12] of the anisotropy of the pinning by the TB planes for a field orientation **H**$\|$**c**. A similar behavior of the $E(J)$ curves is observed at $H=5$ kOe. The $E(J)$ curves are shifted first to lower currents with increasing angle α for $\alpha<20°$ and then to larger currents as α is increased further to the field orientation **H**$\|$**c**.

Completely different behavior of $E(J)$ is observed for $H=15$ kOe. As α increases, the $E(J)$ curves shift to larger transport currents in the region of angles $\alpha<20°$, to smaller currents in the angular interval $20°<\alpha<70°$, and then again to larger currents at angles $\alpha>75°$. The change of the pinning force with angle α is most clearly seen in Fig. 2a, which shows the curves of the ''critical'' $J_{cE}(\alpha)$ curves measured at an electric field $E=10^{-6}$ V/cm on the sample.

Another difference between the I–V characteristics in Fig. 1 is that at $H=0.5$ kOe the log–log plots of $E(J)$ have a negative curvature at all angles α. In magnetic fields of 5 and 15 kOe, in contrast, the negative curvature observed when the magnetic field vector **H** is oriented close to the ab plane changes to positive curvature when **H** is oriented close to the **c** axis. The negative curvature indicates that when the I–V characteristics are described by a dependence of the form $E\propto\exp[-(U/k_BT)(J_c/J)^{\mu}]$, the exponent $\mu>0$. Positive curvature corresponds to $\mu<0$. The angle dependence of μ obtained when the I–V characteristics are described by an exponential dependence is shown in Fig. 2b. The shaded parts correspond to regions of angles in which the experimental $E(J)$ curves cannot be described by an exponential function with a constant value of the exponent μ. In this interval of angles, as is seen in Fig. 1b, the negative curvature of the I–V characteristics, which is observed at high transport current densities, becomes positive at low current densities.

As we see in Fig. 2b, the variation of μ with angle α depends on the magnitude of the magnetic field. In a magnetic field of 0.5 kOe the exponent is independent of α ($\mu=1/2$) over a wide range of angles ($2.5°\leqslant\alpha\leqslant75°$), and only

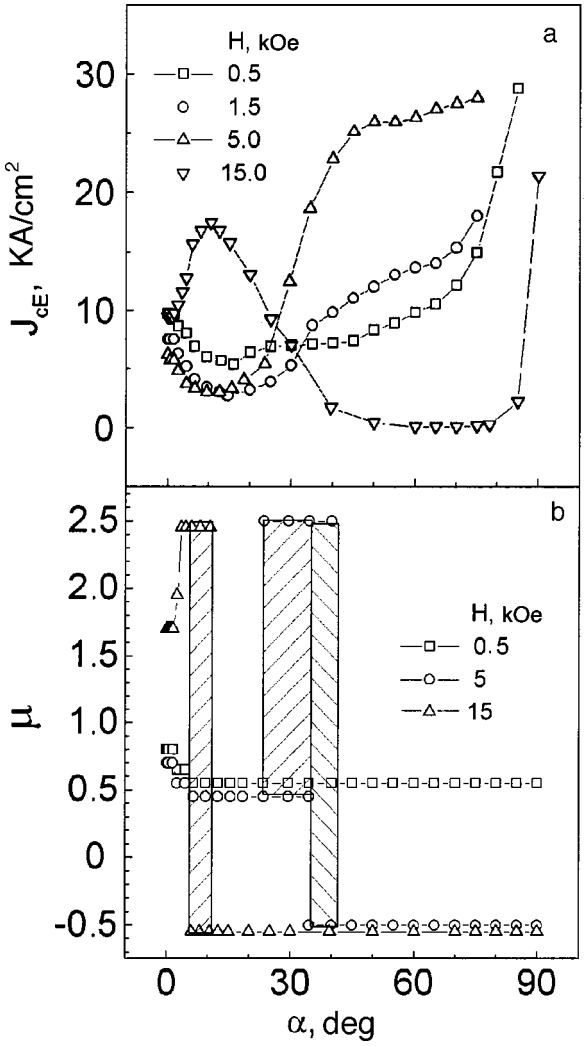

FIG. 2. Angle dependence of the ''critical'' current J_{cE} determined from the level of the voltage drop across the sample, $E=10^{-6}$ V/cm (a), and the exponent μ obtained when the I–V characteristic is described by an exponential dependence of the form $E\propto\exp[-(U/kT)(J_c/J)^{\mu}]$.

for $\alpha<2°$ does one observe a slight increase in the exponent ($\mu=0.8$). At $H=5$ kOe the exponent μ takes on values of 3/4, 1/2, 5/2, and $-1/2$ as α increases, and for $H=15$ kOe it takes on values of 7/4, 5/2, and $-1/2$. A comparison of $\mu(\alpha)$ and $J_{cE}(\alpha)$ shows that only in certain cases is there a correlation between the value of μ and the angle dependence of the current J_{cE}. For example, the value $\mu=5/2$ always corresponds to a rapid increase in the current J_{cE}. However, the same value $\mu=1/2$ corresponds to a decrease of J_{cE} with increasing α in the range $\alpha\leqslant20°$ and to an increase in J_{cE} with α for $\alpha>20°$. Also, the same value $\mu=-1/2$ corresponds to an increase of the current J_{cE} with increasing α in a magnetic field of 5 kOe, while at 15 kOe the angle dependence of the current is nonmonotonic. The value of the exponent μ characterizes the current dependence of the activation energy of magnetic flux creep, and its increase or decrease may be evidence of a change in the creep regime. Thus the angle dependence of the current J_{cE} in a given creep regime depends on both the region of angle α under study and on the magnitude of the external magnetic field. To elucidate the cause of this behavior will require a more detailed analysis of the experimental data.

CREEP WHEN THE MAGNETIC FIELD ORIENTATION IS CLOSE TO THE *ab* PLANE

Low magnetic fields

Let us examine the results of measurements made in magnetic fields $H \leqslant 5$ kOe at a field orientation close to the ab plane, specifically, at angles $\alpha \leqslant 15°$.

As we see in Fig. 2a, in this interval for $H \leqslant 5$ kOe the current J_{cE} increases with decreasing α, in agreement with many experimental results.[8,14,17] Figure 3 shows the I–V characteristics measured in this region of angles at a temperature of 82 K in semilogarithmic scale ($\log E - J^{-1/2}$). At angles α less than a certain critical angle α_L the electric field does not depend on α. The critical angle α_L decreases with increasing magnetic field: $\alpha_L \approx 1.5°$ in a magnetic field of 0.5 kOe, and 0.5° at 1.5 and 5 kOe. This behavior can be explained in terms of the existing ideas about intrinsic pinning. It is assumed that for α less than the trapping angle α_L the flux lines are localized between the CuO superconducting planes to minimize the core energy. Therefore, the pinning of the magnetic flux in the angle region $\alpha < \alpha_L$ does not depend on the orientation of the field vector **H**.

The trapping angle is given by the relation $\alpha_L \cong 2\nu H_{c1}^c / H$ (Ref. 18), where $\nu \cong l_c / l_{ab}$ is the demagnetizing factor, H_{c1}^c is the lower critical field, and l_c and l_{ab} are the dimensions of the sample along the **c** axis and in the ab plane, respectively. The demagnetizing factor of our sample was approximately equal to 0.05, and the value of H_{c1}^c at 82 K $\leqslant T \leqslant$ 85 K lay in the interval 100–200 Oe, respectively; hence, at a magnetic field of 500 Oe the trapping angle is estimated to be 1–2°. The experimental value $\alpha_L(500\ \text{Oe}) \cong 1.5°$ agrees with the theory, as does the experimentally observed decrease of α_L with increasing magnetic field.

As we see from the inset in Fig. 3c, for a field orientation $\mathbf{H} \| ab$ the $E(J)$ curves plotted in the coordinates $\log E - J^{-0.8}$ are close to being straight lines. This means that the experimental data can be described by an exponential dependence of the form

$$E = E_0 \exp\{-(U_0/k_B T)[(J_c/J)^{\mu} - 1]\}, \qquad (1)$$

where $\mu = 0.8$, E_0 is a constant, U_0 is the activation energy, which is independent of J, k_B is Boltzmann's constant, and J_c is the critical current for depinning. It is also obvious that the slope of the $E(J)$ curves is independent of the magnetic field and that the electric field increases linearly with H. These two relationships indicate that the product $U_0 J_c^{0.8}$ and the velocity of the magnetic flux $v = E/B$, where B is the magnetic induction, are independent of the magnetic field, and, from the standpoint of the collective pinning theory,[6] presuppose single-vortex creep (i.e., noninteracting vortices). Indeed, in the collective pinning theory it is predicted that for this creep regime both the critical current and the pinning potential and, accordingly, the velocity of the vortices also are independent of the magnitude of the magnetic field. The value of the exponent 0.8 is close to the value $\mu = 1$ predicted for single-vortex creep in a magnetic field $\mathbf{H} \| ab$ in the motion of vortices along the **c** axis. Thus the results obtained constitute experimental evidence that single-vortex creep is realized in low magnetic fields.

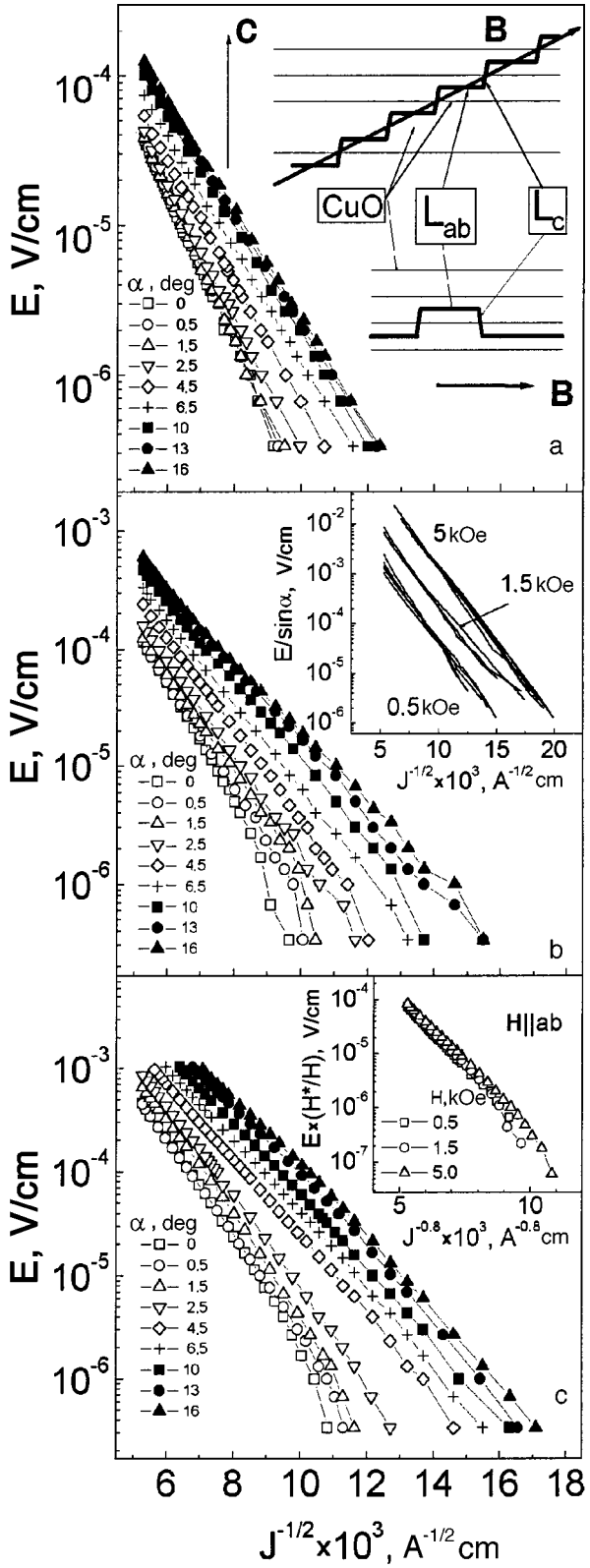

FIG. 3. I–V characteristics at $T = 84$ K and $H = 0.5$ (a), 1.5 (b), and 5 kOe (c) in the angle interval $0° \leqslant \alpha \leqslant 16°$. The upper inset in Fig. 3a shows the stepped structure of the flux line that is realized for $\alpha < \varepsilon$, and the lower inset shows the half-loop formed in the creep of the vortex lattice for the field orientation $\mathbf{H} \| ab$ (Ref. 6). The inset in Fig. 3b shows the angular scaling of the I–V characteristics measured at $T = 82$ K in different magnetic fields. The inset in Fig. 3c shows the I–V characteristic at $T = 82$ K and $\alpha = 0°$, normalized to the value of the magnetic field ($E \times (H^*/H)$), where $H^* = 1$ kOe).

At angles in the region $\alpha_L < \alpha \leqslant 15°$ the $E(J)$ curves in the coordinates $\log E - J^{-1/2}$ are close the being straight lines. Consequently, when the I–V characteristics are described by relation (8), the exponent is $\mu = 1/2$. It is seen in the inset in Fig. 3b that the slope of the $E(J)$ curves is almost independent of α and of the magnetic field. The latter circumstance means that the product $U_0 J_c^{1/2}$ is independent of the value of the magnetic field and, as we have said, is evidence that single-vortex creep is realized. The data presented in the inset of Fig. 3b also show that in the angle interval $2.5° \leqslant \alpha \leqslant 15°$ the electric field increases as $\sin\alpha$. Such an angle dependence is natural if the flux lines have a stepped structure (see the inset in Fig. 3a), if it is assumed that the pinning of the vortex segments l_{ab} localized between CuO planes is large and that the electric field on the sample arises as a result of the motion of the vortex segments l_c oriented along the **c** axis. Indeed, the electric field in such a creep is given by the expression $E = B_c v_{ab} \propto \sin\alpha$, where the component of the magnetic induction along the **c** axis is $B_c = B\sin\alpha$, while v_{ab} is the velocity of the segments along the ab plane, which in the case of single-vortex creep is independent of the magnitude of the magnetic field.

High magnetic fields

Let us first mention that in a magnetic field of 15 kOe and at $\alpha \leqslant 15°$ the current J_{cE} increases with increasing angle α, in contrast to its monotonic decrease in magnetic fields $H \leqslant 5$ kOe (see Fig. 2). The exponent μ in a field of 15 kOe takes values of 1.75–2.5, which are substantially greater than the values of μ obtained in magnetic fields $H \leqslant 5$ kOe (0.5–0.8). Furthermore, the slope of the $E(J)$ curves increases linearly with increasing α (Fig. 4a). This means that when the I–V characteristics are described by relation (1), the product $U_0 J_c^{\mu}$ increases with increasing α. From the standpoint of the collective pinning theory the value of the exponent $\mu = 1.75$–2.5 and the increase of $U_0 J_c^{\mu}$ and of the current J_{cE} with increasing angle α may be evidence of flux-bundle creep. Let us analyze this possibility. We first consider the evolution of the I–V characteristics with increasing magnetic field.

Figure 4b shows I–V characteristics measured in magnetic fields up to 15 kOe at $T = 85$ K and $\alpha = 0$. We see that up to 7 kOe the I–V curves are described satisfactorily by relation (1) with $\mu = 0.8$ and that the electric field increases almost linearly with increasing magnetic field, i.e., one observes the regularities characteristic of single-vortex creep. As the magnetic field is increased further, the electric field decreases rapidly in the regions of small transport currents $J < J_b$. Here the value of the crossover current J_b and the slope of the I–V characteristic for $J < J_b$ increase with increasing magnetic field (see Fig. 4b). The slope angle γ of the $E(J)$ curves plotted in the coordinates $\log E - J^{-7/4}$ increases continuously with increasing magnetic field and is satisfactorily described by the power law $\gamma \propto H^{1.9}$.

The growth of the current J_b and slope angle γ with increasing magnetic field is characteristic of a transition from single-vortex to flux-bundle creep. Indeed, according to the collective pinning theory, the correlation length L_c along the direction of the magnetic induction increases with decreasing current as $L_c = \xi(\varepsilon/\varepsilon_\alpha)(J_0/J_c)^{1/2}(J_c/J)^{5/7}$, where $\varepsilon_\alpha = (\varepsilon^2\cos^2\alpha + \sin^2\alpha)^{1/2}$, $J_0 = (4/3\sqrt{3})(c\varepsilon_0/\xi\Phi_0)$ is the depairing current, J_c is the critical current in a magnetic field $\mathbf{H} \| \mathbf{c}$ in the case of single-vortex creep (it is independent of the magnitude of the magnetic field and of the angle α), and ε is the anisotropy parameter, which for YBaCuO superconductors varies from 1/8 to 1/6. If the current density becomes smaller than a certain characteristic value J_b, at which the correlation length becomes greater than $\varepsilon a_0 \varepsilon_\alpha^{-1/2}$, then the vortex lattice separates into domains. Within each of these domains the flux lines are pinned collectively, while the domains themselves move independently of one another. According to the collective pinning theory, the I–V characteristics at currents $J < J_b$ are also described by the exponential dependence (1), but the critical current J_c in that relation

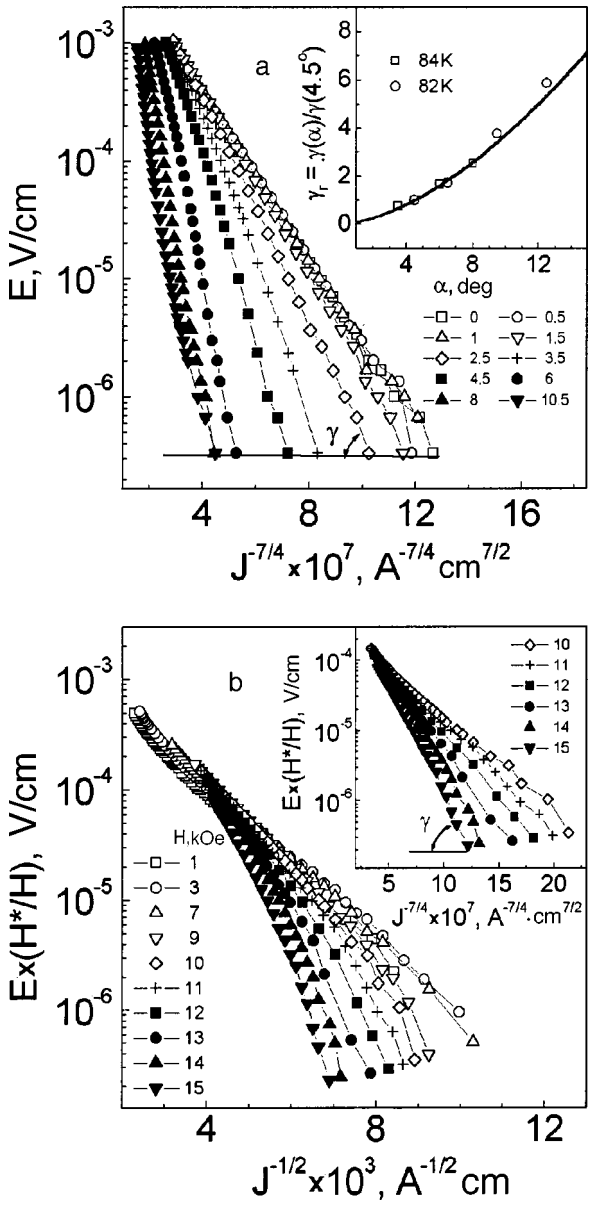

FIG. 4. I–V curve for $H = 15$ kOe and $T = 84$ K in the angle interval $0° \leqslant \alpha \leqslant 10.5°$ in the coordinates $E - J^{-7/4}$. The inset shows a plot of $\gamma_r(\alpha) \equiv \gamma(\alpha)/\gamma(4.5°)$ at $T = 84$ and 82 K (a). The I–V characteristics normalized to the value of the magnetic field ($E \times H^*/H$, where $H^* = 1$ kOe) at $T = 84$ K and $\alpha = 0°$ in various magnetic fields. The inset shows the change in the slope angle γ of the I–V characteristic plotted in the coordinates $E - J^{-7/4}$ as the value of the magnetic field is changed (b).

must be replaced by the crossover current J_b. The value of the exponent μ and the field dependence of the crossover current $J_b(B)$ and activation energy $U_0(B)$ are determined by the direction of the magnetic induction vector. For a field orientation $\mathbf{H}\perp\mathbf{c}$ and with an orientation of the Lorentz force $\mathbf{F}_L\|\mathbf{c}$ the exponent $\mu=2$, and the crossover current and activation energy have the of the form[6]

$$J_b(B)\cong(3\sqrt{3}\pi/4)(\xi/c_0)(c_0/a_0)^2J_0\propto B \tag{2a}$$

and

$$U_0(B)\cong\varepsilon_0 c_0, \tag{2b}$$

where c_0 is the period of the crystal lattice along the **c** axis, $\varepsilon_0=(\Phi_0/4\pi\lambda_c)^2$, λ_c is the penetration depth for the field orientation $\mathbf{H}\|\mathbf{c}$, and Φ_0 is the magnetic flux quantum. At angles $\alpha>\varepsilon$ the exponent $\mu=2.5$, and the crossover current and activation energy are given by the relations[6]

$$J_b(\alpha,B)\cong J_c(\sqrt{\varepsilon_\alpha}L_c^c/\varepsilon a_0)^{7/5}\propto(\varepsilon_\alpha B)^{0.7} \tag{2c}$$

and

$$U_0(\alpha,B)\cong U_{sv}^c(\varepsilon a_0/\sqrt{\varepsilon_\alpha}L_c)^{1/5}\propto(\varepsilon_\alpha B)^{-0.1}, \tag{2d}$$

where U_{sv}^c is the activation energy corresponding to single-vortex creep in a magnetic field $\mathbf{H}\|\mathbf{c}$, which is independent of the magnitude and orientation of the magnetic field.

In a magnetic field $\mathbf{H}\perp\mathbf{c}$ and with the Lorentz force oriented perpendicular to the ab plane, the magnetic flux creep occurs as a result of the formation of rectangular half-loops,[6] which are shown in the lower inset of Fig. 3a. Since the vortex segments l_{ab} and l_c are mutually orthogonal, it is assumed that they do not interact with each other and therefore move independently of each other.[19] The electric field arising in thermally activated creep can be written as

$$E=E_1\exp(-U_1/k_BT)+E_{12}\times\exp(-U_1/k_BT)\exp(-U_2/k_BT), \tag{3a}$$

where the first term corresponds to the motion of the vortex segments l_{ab} along the **c** axis, and the second term to motion of the vortex segments l_c along the ab plane. In this relation U_1 is the activation energy of a half-loop, which is given by expression (2b); U_2 is the activation energy of the vortex segments l_c in their motion along the ab plane, and E_1 and E_{12} are constants whose values depend on the specific microscopic model, and the factor $\exp(-U_1/kT)$ in the second term determines the density of the vortex segments l_c.

Since the electric field for $\mathbf{H}\perp\mathbf{c}$ is given by relation (3a), the question arises: which subsystem of vortex segments (oriented along the ab plane or along the **c** axis) experiences crossover from single-vortex creep to flux-bundle creep? It follows from Eqs. (2a) and (2d) that for a vortex subsystem oriented parallel to the ab plane the crossover current $J_b\propto B$ and the I–V slope angle $\gamma\propto U_0J_b^2\propto B^2$, while for the vortex subsystem oriented along the **c** axis $J_b\propto B^{0.7}$ and $\gamma\propto U_0J_b^{2.5}\propto B^{1.65}$. Thus the collective pinning theory predicts approximately the same field dependence of the crossover current and slope angle γ for both vortex subsystems. It is therefore impossible to answer the above question on the basis of measurements of the I–V characteristics in different magnetic fields, but it is possible to answer it by measuring the I–V characteristics for different angles α.

Indeed, if the stepped structure of the flux lines shown in the upper inset of Fig. 3a is realized in magnetic fields tilted at angles $\alpha_L<\alpha<\varepsilon$, then in the creep of such a vortex line the electric field can be written in the form

$$E=E_1\exp(-U_1/k_BT)+E_{12}\exp(-U_1/k_BT)\times\exp(-U_2/kT)+E_2\exp(-U_2/k_BT), \tag{3b}$$

where the third term corresponds to motion of the steps along the ab plane. In this expression the contribution of the first term is independent of α, since the magnetic induction along the ab plane does not change in the case of a stepped structure of the vortex lines. The contributions of the second and third terms, however, are very sensitive to a change in the angle α, since the magnetic induction component along the **c** axis, B_c, increases as $\sin\alpha$. Therefore, according to the collective pinning theory, the crossover current of the vortex subsystem oriented along the **c** axis should increase as $(\sin\alpha)^{0.7}$, and the slope angle of the $E(J)$ curves in currents $J<J_b$ should go as $\gamma(\alpha)\propto U_0J_b^{5/2}\propto(\sin\alpha)^{1.65}$. The inset in Fig. 4a shows the angle dependence of the reduced slope angle $\gamma_r(\alpha)\equiv\gamma(\alpha)/\gamma(4.5°)$, where γ is the slope angle of the $E(J)$ curves shown in Fig. 4a, and the function $F(\alpha)=(\sin\alpha/\sin 4.5°)^{1.65}$. The fact that the experimental data are found to agree with the theoretical dependence argues in favor of a transition from single-vortex creep to flux-bundle creep in the vortex subsystem oriented along the **c** axis. The agreement between $\gamma_r(\alpha)$ and $F(\alpha)$ also suggests that the contribution of the first term in (2a) and (2b) is small compared to the contribution of the other terms.

CREEP AT ANGLES $\alpha>\varepsilon$

Low magnetic fields

Let us now turn to a discussion of the experimental data obtained at angles $\alpha>\varepsilon$, where the intrinsic pinning does not affect the configurational structure of the flux lines and thus does not influence the dynamics of the magnetic flux. In this region of angles the vortex system can be described in an anisotropic superconductor model, and we shall take this approach to the interpretation of the experimental results. As we see in Fig. 1a, in this region of angles and in low magnetic fields the $E(J)$ curves are continuously shifted to higher transport currents with increasing α. This behavior is substantially different from the behavior of the I–V curves measured in the motion of the vortices along the planes of the TBs (in the experimental geometry with $\mathbf{J}\|ab$, $\mathbf{J}\perp$TB, $\mathbf{H}\perp\mathbf{J}$, and variable parameter α), i.e., in the direction of easy motion of the magnetic flux. In the latter case the electric field for $\alpha>\varepsilon$ increases with the angle α as ε_α (Ref. 20). When the transport current is flowing in the ab plane of an anisotropic superconductor, the electric field generated by the motion of the vortices with velocity v is given by the relation $E=\varepsilon_\alpha vB$, where the factor $\varepsilon_\alpha=\eta(\alpha)/\eta_c$ appears because of the anisotropy of the viscous drag coefficient $\eta(\alpha)=\eta_c\varepsilon_\alpha$, where η_c is the drag coefficient for the field orientation $\mathbf{H}\|\mathbf{c}$. Thus in the motion of vortices along the planes of the twins, the velocity of the vortices is independent of the magnetic field direction. However, the decrease of the electric field observed in this experimental geometry is evidence of a substantial decrease in the velocity of the vor-

tices with increasing α. This decrease may be due to the influence of the TBs, which, as we have said, are efficient pinning centers for the motion of vortices perpendicular to the TB plane. Let us analyze this possibility in more detail.

It is assumed that in a magnetic field tilted at angles $\theta \equiv \angle \mathbf{H}$,TB less than the critical angle θ_{cr}, the flux lines have the configurational structure presented in the inset in Fig. 5a.[16,21] It is seen that part of the vortex line (segment L_{tr}) is trapped by the plane of the TB, and that near the TB the vortex segment L_h is oriented at the critical angle θ_{cr} to the plane of the TB, while far from the TB the vortex line is oriented along the magnetic induction vector **B**. If the pinning force on the vortex segments L_{tr} in their motion off the TB plane is large (and the absence of creep in the case of the magnetic field orientation $\mathbf{H} \| \mathbf{c}$ is evidence in favor of such an assumption), then the motion of the vortex lines along the ab plane will be suppressed. However, the vortices can move along the **c** axis under the influence of the Lorentz force component $F_c = F_L \cos\alpha$. Indeed, the pinning force on the vortex segments L_{tr} in their motion along the **c** axis, i.e., parallel to themselves, is equal to zero. In this case the magnetic flux pinning is governed by the interaction of point defects with the vortex segments lying off the TB plane. In the motion of vortices along the **c** axis the ratio J_c/J in Eq. (1) must be replaced by $J_c/J_\parallel$, where $J_\parallel \cong J[\gamma \sin\theta_{cr} + (1-\gamma)\cos\alpha]$, $\gamma \equiv 2L_h/(d-2L_h)$ is a coefficient giving the fraction of the vortex comprised by segments L_h ($L_h \cong (\varepsilon a_0/2\sqrt{\pi})\ln(a_0/\xi)$; Ref. 16), and d is the distance between TB planes. In a magnetic field of 500 Oe the intervortex distance $a_0 \cong 200$ nm, the coherence length $\xi(82\text{K}) \cong 5$ nm, and $L_h \cong 20$ nm, and we obtain $\gamma \cong 0.1$ for the crystal under study, which had an average distance between TBs of 500 nm. Thus if $\gamma = 0.1$ and $\theta_{cr} = 70°$ and single-vortex creep is realized, the $E(J)$ curves measured at different angles α and plotted in the coordinates $E(J)/\varepsilon_\alpha$ as functions of $J_\parallel$ should all lie on a universal curve. This is confirmed in Fig. 5a, which shows the $E(J)$ curves measured at angles in the interval $20° \leqslant \alpha < 90°$. The observed scaling of the I–V characteristics leads to three conclusions. First, in low magnetic fields the TBs deform the vortex lines for $\alpha \geqslant 20°$, i.e., $\theta_{cr} = 70°$. Second, for $\theta < \theta_{cr}$ the configurational structure of the vortex lines proposed in Refs. 16 and 21 is realized. Third, since the pinning of the vortex segments L_{tr} trapped by the TBs is large for their motion off the TB plane and equal to zero for their motion along the TB planes, in magnetic fields tilted at $\theta < \theta_{cr}$ a directed motion of the vortices along the TB planes occurs under the influence of the Lorentz force component F_c along the **c** axis.

The slope angle of the $E(J)$ curves increases with increasing temperature (see Fig. 5a). This indicates that when the experimental data are described by the exponential dependence (1) the product $U_0 J_c^{1/2}$ increases with decreasing temperature. The value of J_c can be determined in the Bardeen–Stephen model, as was proposed in Ref. 22. Assuming that the differential electrical resistivity $\rho_d \equiv dE/dJ$ at $J = J_c$ is equal to the viscous drag of the magnetic flux flow in the Bardeen–Stephen model, $\rho_{BS} = \rho_N B/B_{c2}(\alpha)$,[23] we determine the value of J_c by extrapolating the ratio ρ_d/ρ_{BS} to unity. Here ρ_N is the resistivity of the sample in the normal state, and $B_{c2}(\alpha) = \Phi_0/(4\pi\xi^2\varepsilon_\alpha)$ is the magnetic induction at the upper critical field. The curves of $\rho_d(J_\parallel)/\rho_{BS}$ are plotted in the inset of Fig. 5b, and their extrapolation to unity gives $J_c = 4.5\times10^4$, 3×10^4, and 2×10^4 A/cm^2, respectively, at $T = 82$, 84, and 85 K. If the experimental data are interpolated according to Eq. (1) with these values of the critical current substituted in, we obtain $U_0/k_BT = 1.3$, 1.2, and 1.1, respectively, at $T = 82$, 84, and 85 K. These values agree with the result $U_0/kB = 140$–160 K obtained[24] in the collective pinning theory from measurements of the relaxation of the magnetization over a wide temperature range ($3\text{ K} < T < 80$ K).

As the magnetic field and angle α are increased, as can be seen in Fig. 5b and 5c, in the region of low transport currents one observes a deviation from the universal curve. At currents $J < J_b$ the electric field decreases rapidly with decreasing J, and the crossover current J_b and slope of the $E(J)$ curves increase with increasing magnetic field and angle α. These trends agree with the predictions of the collective pinning theory for a transition from single-vortex to flux-bundle creep. Indeed, according to relations (3a) and (3b), with increasing magnetic field and angle α the crossover current increases quite rapidly and the activation energy decreases slowly. The transition from single-vortex creep to flux-bundle creep as the magnetic field is increased is discussed in detail in Ref. 22. The experimental data presented in the present paper, however, indicate that this transition also occurs with increasing angle α at a constant value of the magnetic field.

In addition, we note that the scaling of the I–V characteristic in the coordinates $E/(H\varepsilon_\alpha) - J^{-1/2}$ observed at high transport current densities and in magnetic fields at least up to 2.5 kOe attests to the fact that at $T = 84$ K the motion of the magnetic flux along the ab plane is suppressed, and directed motion of the magnetic flux along the TB planes takes place. However, as the temperature is increased ($T = 86.7$ K) the ratio E/H at high transport currents increases with increasing magnetic field for $H \geqslant 0.9$ kOe (Fig. 6). The most probable cause of the breakdown of the field scaling of the I–V characteristic at high current densities is a decrease in the pinning force on the vortex segments L_{tr} at high temperatures. Because of this, the length L_{tr} of the trapped segments and, accordingly, their contribution to the pinning force at relatively low fields are rather large, so that the creep along the ab plane is suppressed, and directed motion of the magnetic flux along the TB planes takes place. As the magnetic field is increased, however, the length of the trapped segments decreases, $L_{tr} \propto a_0 \propto H^{-1/2}$ (Ref. 16), and their contribution to the pinning force also decreases. This leads to depinning of the vortex segments from the TB planes and, hence, to additional creep of the magnetic flux along the ab plane, and that increases the electric field.

High magnetic fields

Let us now turn to an analysis of the experimental data obtained in magnetic fields of 5 and 15 kOe. At $H = 5$ kOe and $\alpha > 15°$ the $E(J)$ curves are shifted to higher transport currents with increasing α. In addition, at angles in the interval $20° \leqslant \alpha \leqslant 30°$ the slope of the I–V characteristics increases rapidly. The increase in slope and the shift of the curves to higher transport currents can be explained in the

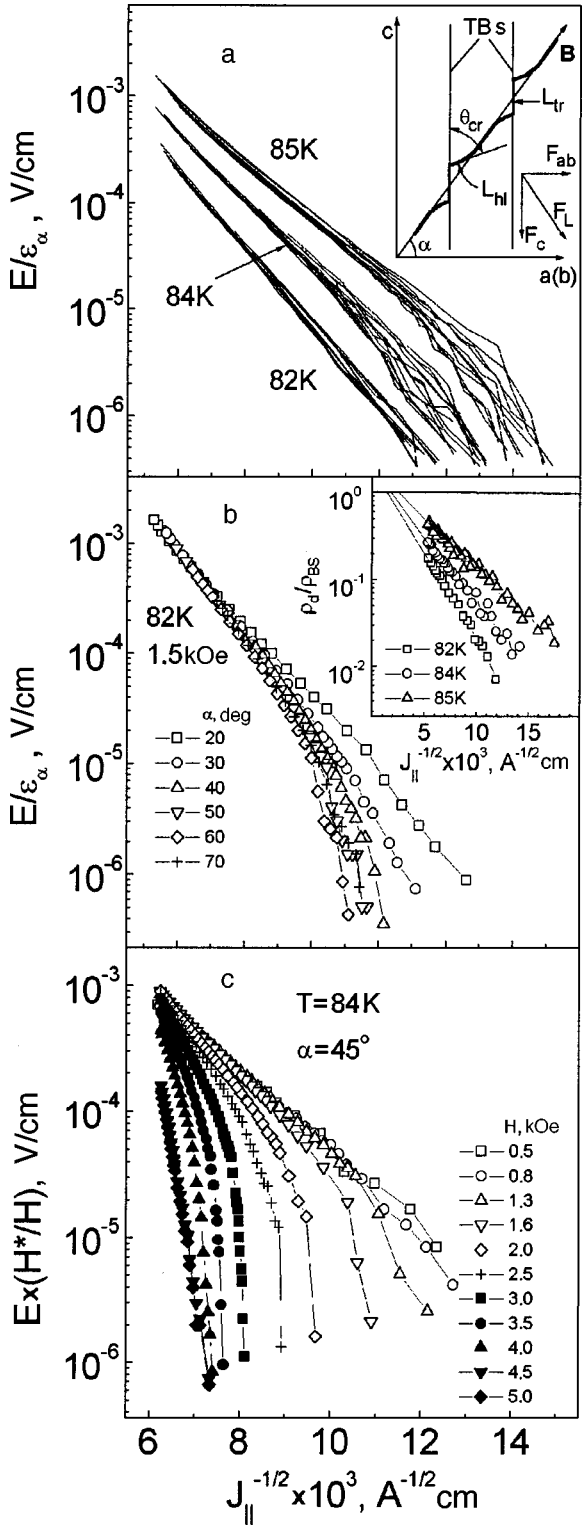

FIG. 5. Angular scaling of the I–V characteristics in a field of 0.5 kOe in the angle interval $20° \leqslant \alpha \leqslant 85°$. The inset shows the configurational structure of the flux line in a magnetic field tilted with respect to the planes of the twin boundaries (a). Angular scaling of the I–V characteristic in a field of 1.5 kOe in the angle interval $20° \leqslant \alpha \leqslant 70°$. The inset shows the current dependence of the differential electrical resistivity normalized to the value of the viscous drag of the flux flow in the Bardeen–Stephen model (b). The I–V characteristics normalized to the value of the magnetic field ($E \times (H^*/H)$, where $H^* = 1$ kOe), at $T = 84$ K and $\alpha = 45°$ for various magnetic fields (c).

framework of the collective pinning theory by a transition from single-vortex creep to flux-bundle creep. Indeed, ac-

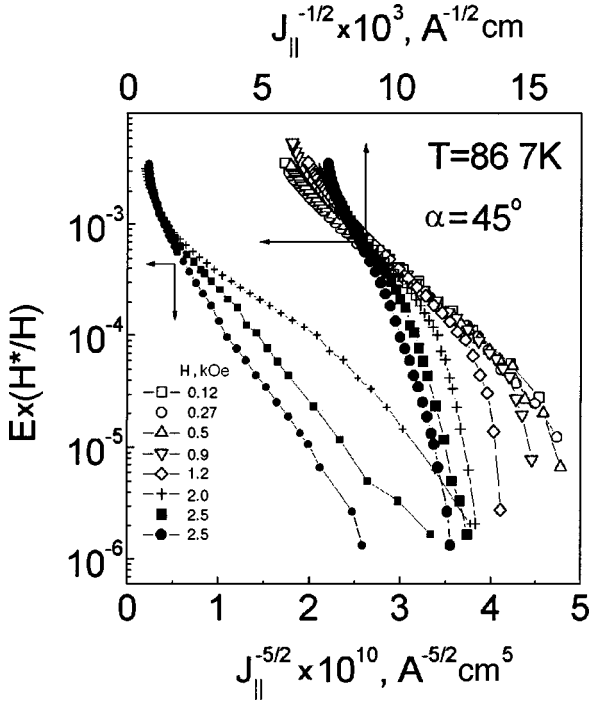

FIG. 6. I–V characteristics at $T = 86.7$ K and $\alpha = 45°$ in various magnetic fields, normalized to the value of the magnetic field and plotted in the coordinates $E-J^{-5/2}$ and $E-J^{-1/2}$.

cording to relations (2c) and (2d), the crossover current $J_b \propto \varepsilon_\alpha^{0.7}$ and the slope of the I–V characteristic at currents $J < J_b$, viz., $\gamma \propto J_b^{2.5} U_0 \propto \varepsilon_\alpha^{1.65}$, increase with increasing α. However, quantitative estimates have shown that they increase faster than they should according to relations (2c) and (2d). This is apparently due to the circumstance that it is in this region of angles that the pinning of the vortices on TBs begins to play a role, and Eqs. (3a) and (3b) were obtained on the assumption of pinning at point defects. The contribution of the pinning on twins leads to additional growth of the critical current J_c and, hence, of the crossover current J_b and slope of the I–V characteristic. We note in addition that the idea that flux-bundle creep is realized in the angle region $25° \leqslant \alpha \leqslant 40°$ is also indicated by the increased value of the exponent obtained, $\mu \cong 5/2$, which is the value predicted for the creep of small flux bundles.

In a magnetic field of 5 kOe at angle $\alpha \geqslant \alpha_{cr}(5\text{ kOe}) \cong 30°$ the positive curvature exhibited by the I–V characteristics in the coordinates log$E$–log$J$ at large values of the transport current gives way to negative curvature at low values of the transport current (see Fig. 1b). As the angle α is increased further ($\alpha > 40°$) the negative curvature is observed throughout the entire interval of transport currents studied, and the slope of the I–V characteristic decreases with increasing α. In a magnetic field of 15 kOe the transition from negative curvature to positive occurs at smaller angles (for $\alpha \geqslant \alpha_{cr}(15\text{ kOe}) \cong 10°$), and the slope of the I–V characteristic for $\alpha > \alpha_{cr}$ also decreases with increasing α. In the region of negative curvature, the $E(J)$ curves measured in magnetic fields $H = 5$ and 15 kOe are close to being straight lines if they are plotted in the coordinates log(E/J) $-J^{1/2}$ (Fig. 7). This means that the experimental data are well

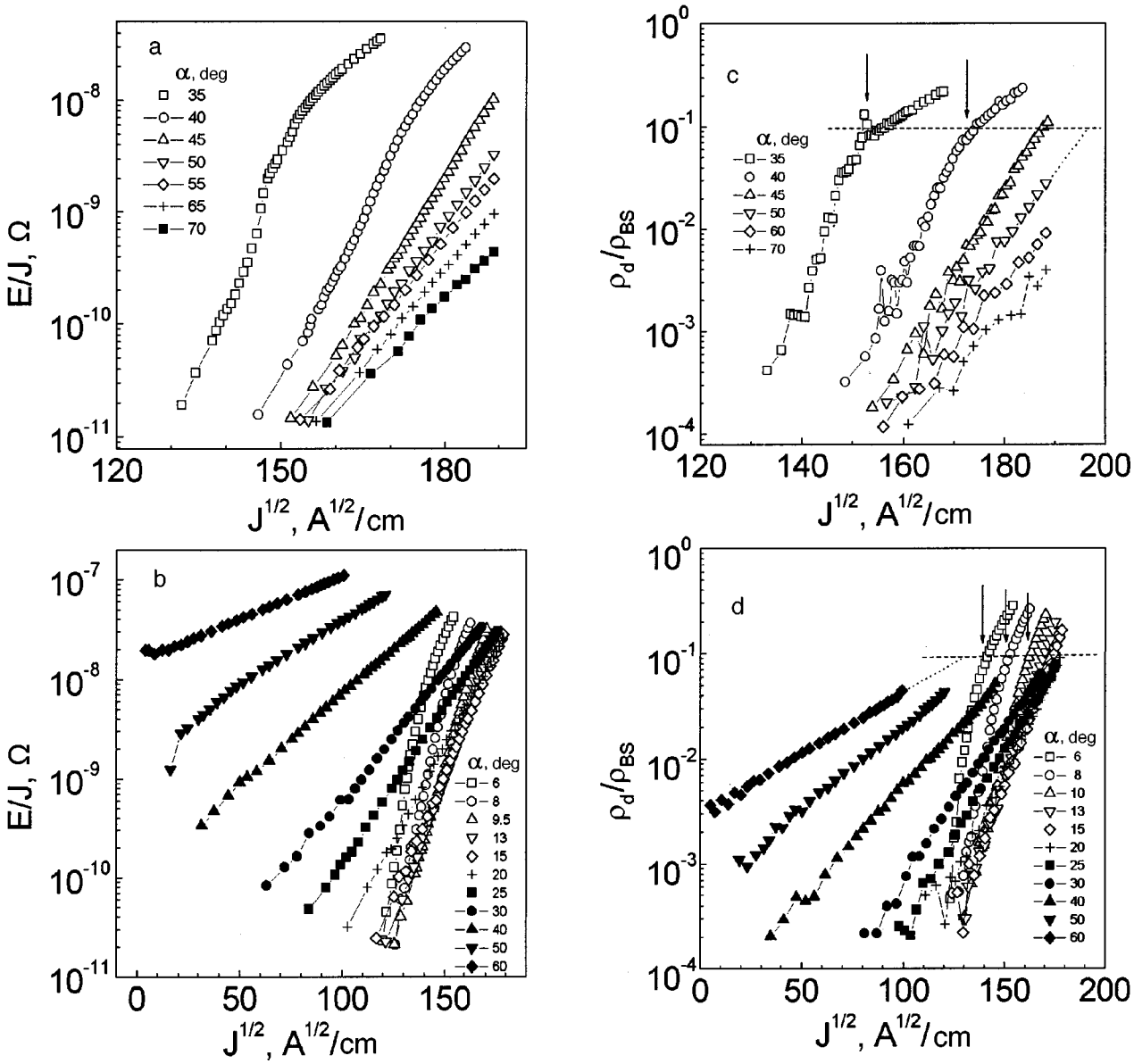

FIG. 7. I–V characteristics (in the coordinates $\log E/J$–$J^{1/2}$) at $T=84$ K for different angles α and $H=5$ (a) and 15 kOe (b). The current dependence of the differential electrical resistivity for the I–V characteristics normalized to the value of the viscous drag of the flux flow in the Bardeen–Stephen model, at different angles α (c,d).

described by the relation predicted for the creep of dislocations of the vortex lattice:[7,25]

$$E(J)=\rho_0 J\exp\{(-U_0/k_BT)[1-(J/J_{\rm pl})^{1/2}]\}, \qquad (4)$$

where ρ_0 is a constant and $J_{\rm pl}$ is the critical current corresponding to motion of the dislocations of the vortex lattice. For this creep mechanism the activation energy in a magnetic field $\mathbf{H}\|\mathbf{c}$ is given by the relation $U_0\approx\varepsilon\varepsilon_0 a_0\propto H^{-1/2}$ (Ref. 26), where $\varepsilon_0=(\Phi_0/4\pi\lambda)^2$, with λ being the penetration depth for the field orientation $\mathbf{H}\|\mathbf{c}$. Previous measurements[27,28] in this same single crystal at $\alpha=45°$ have shown that the energy $U_{\rm pl}$ determined in the region of temperature and magnetic field in which the I–V characteristics are described by Eq. (3), does in fact decrease with increasing magnetic field, a circumstance that also argues in favor of creep of dislocations of the vortex lattice. Thus the results obtained show that the collective (elastic) creep that takes place at small angles α become plastic creep at large angles α.

The angle dependence of the energy U_0 when the I–V characteristics are described by relation (4) can be found from the experimental curves of $E(J)$ if the critical current $J_{\rm pl}$ is known. For an elastic mechanism of creep the vortex lattice moves coherently, i.e., all of the vortices make approximately the same contribution to the energy dissipation. In this case, as we have said, the critical current can be determined by extrapolation of the ratio ρ_d/ρ_{BS} to unity. For a plastic mechanism of creep involving the motion of dislocations of the vortex lattice, the main contribution to the energy dissipation comes from only some of the flux lines, and the fraction that these comprise is dependent on the density of dislocations of the vortex lattice. For example, if the dislocations are inserted into every tenth vortex row, then

only one-tenth of the vortex lines contribute to the energy dissipation in plastic creep. It is in fact at values of the differential resistivity $\rho_d \approx 0.1\rho_{BS}$ that one observes a sharp decrease of the slope of the $\rho_d(J)$ curves (Fig. 7c and 7d). We therefore assume that the value of the transport current at which we have $\rho_d/\rho_{BS} \cong 0.1$ corresponds to the critical current $J_{\rm pl}$ in the case of a plastic mechanism of creep. The relatively weak growth of the differential resistivity that is actually observed at transport currents $J > J_{\rm pl}$ is probably due to the onset of coherent creep of the vortex lattice. This scenario agrees with the theoretical studies of depinning of an anisotropic charge-density wave,[29] which was a prototype for the depinning of the vortex lattice in the field of a random potential. It was shown that as the transport current was increased, incoherent (2D) creep preceded the coherent (3D) creep. By extrapolating the ratio ρ_d/ρ_{BS} to 0.1, as is shown in Fig. 7c and 7d, we obtain the dependence $J_{\rm pl}(\alpha)$ shown in Fig. 8a. By substituting the values obtained for $J_{\rm pl}$ into Eq. (4) and interpolating the experimental $E(J)$ curves by these formulas, we arrive at the $U_0(\alpha)$ curve shown in Fig. 8b. We see that the activation energy U_0 decreases with increasing angle α.

The theoretical angle dependence of the activation energy during plastic creep can be obtained as follows: assume that a dislocation is oriented along one of the principal vectors of the vortex lattice, $\mathbf{b}_1$ or $\mathbf{b}_2$ (the lower inset in Fig. 8c). Then the activation energy is minimum for the motion of dislocations along $\mathbf{b}_1$ or $\mathbf{b}_2$, since the motion in the other directions gives rise to additional structural defects of the vortex lattice and therefore requires greater energies.[30] We consider the translation of the vortex segment L_0 by the minimum intervortex distance b_1 or b_2 (see the inset in Fig. 8b). The energy of such an oblique-angled half-loop can be written in the form $U_0(\alpha,\beta) = 2U_{\rm el} + A$, where $U_{\rm el} = \varepsilon_\beta \varepsilon_0 L_\beta$ is the elastic energy of the vortex segment L_β making an angle β with the ab plane,[31] A is the work necessary for moving the vortex segment L_0 by an intervortex distance b_1 or b_2, and $\varepsilon_\beta = (\varepsilon^2\cos^2\beta + \sin^2\beta)^{1/2}$. A displacement of the vortex segment L_0 by the minimum intervortex distance is stable if $A \approx 2U_{\rm el}$ and, hence, $U_0 \approx 4U_{\rm el}$. If the plane of the dislocation is oriented along the vector $\mathbf{b}_1$ and it moves along this direction, then the length of the segment $L_\beta = a_0/[(\varepsilon_\alpha)^{1/2}\sin(\alpha+\beta)]$. Minimizing the elastic energy $U_{\rm el}(\alpha,\beta) = \varepsilon_\beta \varepsilon_0 a_0/[(\varepsilon_a)^{1/2}\sin(\alpha+\beta)]$ yields the relation $\tan\alpha \tan\beta = \varepsilon^2$ between the angles α and β and the energy $U_{\rm el}(\alpha) = \varepsilon\varepsilon_0 a_0 \varepsilon_1^{-1/2}$. Thus the angle dependence of the activation energy in plastic creep has the form

$$U_0(\alpha) = 4\varepsilon\varepsilon_0 a_0 \varepsilon_\alpha^{-1/2} = U_0^c/\varepsilon_\alpha^{1/2}, \tag{5}$$

where $U_0^c = 4\varepsilon\varepsilon_0 a_0$ is the activation energy for the field orientation $\mathbf{H} \| \mathbf{c}$. This energy is equal, to within a factor of 4, with the value $\varepsilon\varepsilon_0 a_0$ obtained previously[26] for the activation energy of the the plastic creep mechanism.

If the plane of the dislocation is oriented along the vector $\mathbf{b}_2$ and the dislocation moves along this direction, then the length of the segment $L_\beta = (a_0/2)\{[3\varepsilon_\alpha/\sin^2(\alpha+\beta)]^2 + 1/\varepsilon_\alpha\}^{-1/2}$. In this case the energy $U_{\rm el}(\alpha,\beta)$ is minimum if the segment L_β lies in the plane forming an angle $\varphi = \arctan(\varepsilon^2/\tan\alpha)$ with the ab plane of the crystal, and $\beta = \arcsin\{\sin\varphi/[1+\sin^2(\alpha+\varphi)/3\varepsilon_\alpha^2]^{1/2}\}$. Here the minimum energy $U_{\rm el}(\alpha)$ is determined by the same relation as for the motion of a dislocation along the vector $\mathbf{b}_1$, i.e., the activa-

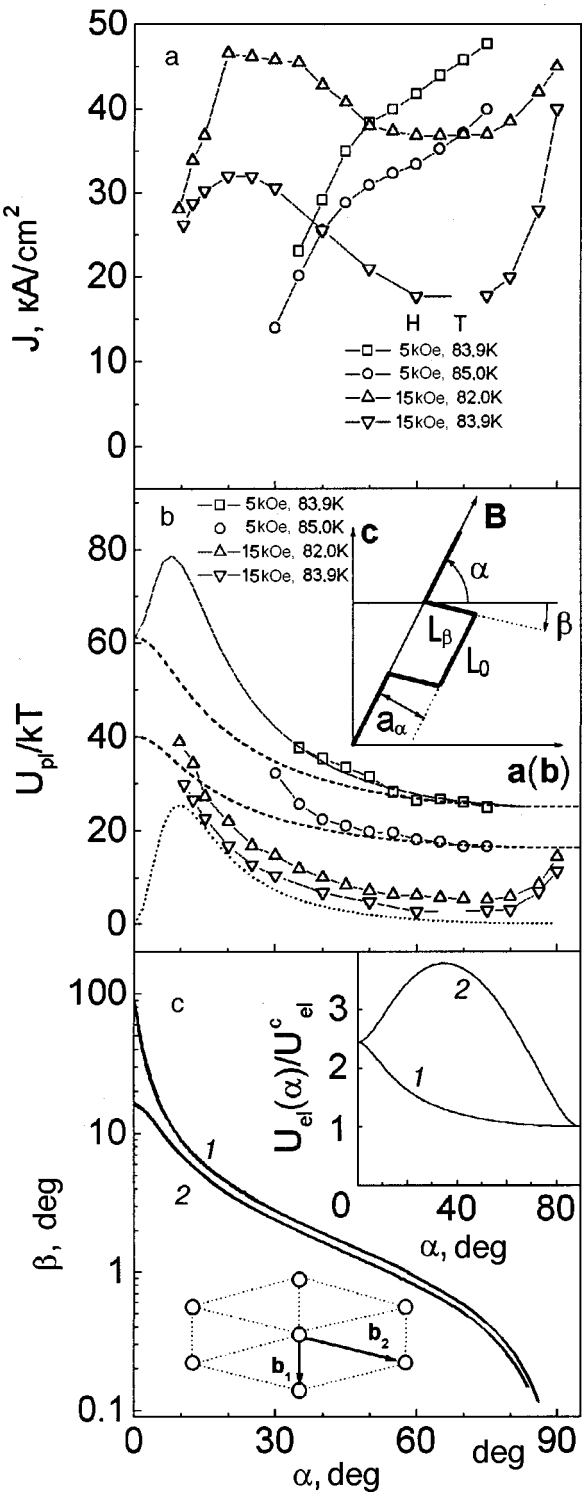

FIG. 8. Angle dependence of the critical current corresponding to a plastic mechanism of magnetic flux motion in the framework of the Bardeen–Stephen model (a), and the activation energy for the plastic mechanism of creep. The dashed curve shows $U_{\rm pl}$ determined by relation (5) on the assumption that $U_{\rm pl}(\mathbf{H}\|\mathbf{c}) = U_{\rm pl}(75°)$, the dotted curve shows $U_{\rm int}$, and the solid curve shows the dependence determined by relation (6). The inset shows a half-loop in a tilted magnetic field (b). The angle β formed by the vortex segment L_β with the ab plane versus the orientation of the magnetic field for motion of the vortices along the vector $\mathbf{b}_1$ (*1*) and along the vector $\mathbf{b}_2$ (*2*). The inset shows a plot of $U_{\rm pl}(\alpha)/U_{\rm pl}(\mathbf{H}\|\mathbf{c})$ for a rectangular (*3*) and an oblique-angle (*4*) shape of the half-loop (the inset in Fig. 8b) (c).

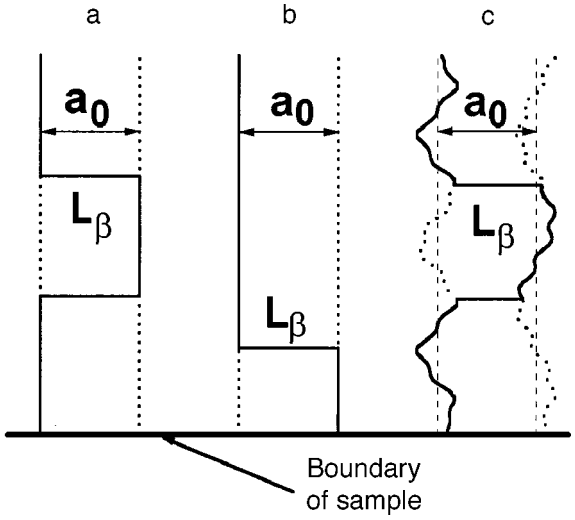

FIG. 9. Schematic illustration of the half-loop formed in a magnetic field $\mathbf{H}\|\mathbf{c}$ in the case of a plastic creep mechanism in the bulk of the crystal (a) and near its surface (b) in the absence of randomly located pinning centers, and of a half-loop formed in the bulk of the crystal in the presence of randomly located pinning centers (c).

tion energy of the creep is also given by expression (5).

The upper inset in Fig. 8c shows the angle dependence of the reduced energy normalized to its value at $\alpha=\pi/2$, $U_0(\alpha)/U_0(\alpha=\pi/2)=\varepsilon_\alpha^{-1/2}$. In the angle interval $0<\alpha<\pi/2$ this energy is always less than the energy $U_0^r(\alpha)/U_0^r(\alpha=\pi/2)=\varepsilon_\alpha^{1/2}\varepsilon_\beta/\varepsilon$ obtained[28] for a dislocation moving along the vector $\mathbf{b}_1$ on the assumption that the half-loop in the inset of Fig. 5 has a rectangular shape, i.e., if $\alpha+\beta=\pi/2$. The cause of this difference is as follows. The energy $U_{\rm el}$ is determined by the product $\varepsilon_\beta L_\beta$, in which the length of the segment L_β is minimum, in the case of a rectangular shape of the half-loop, when the angle β increases linearly with decreasing angle α. On the other hand, the linear tension of the flux line is minimum if it is oriented parallel to the ab plane (for $\beta=0$) and increases with increasing angle β as ε_β. The competition between these two factors leads to the change of β with α shown in Fig. 9c. We see that for $\alpha>30°$ the angle β is not more than 3°, i.e., the segment L_β is nearly parallel to the ab plane, and that when the dislocation moves along the vector $\mathbf{b}_2$ the angle β is always less than 16°.

For $\mathbf{H}\|\mathbf{c}$ relation (5) gives an energy $4\varepsilon\varepsilon_0 a_0$. Assuming $\lambda(0)\cong 140$ nm, $\lambda(T)=\lambda(0)/[1-(T/T_c)^2]^{1/2}$, and $\varepsilon=1/6$, we find the values of the activation energy for $\mathbf{H}\|\mathbf{c}$ (left-hand column of Table I). The right-hand column gives the experimental values of the activation energy obtained for an orientation of the magnetic field close to the **c** axis, $\alpha=75°$. We see that for $H=5$ kOe and $T=84$ K the experimental value of the activation energy is approximately twice the theoretical value. This difference becomes even greater with increasing magnetic field and temperature. There are at least three factors that decrease the activation energy in the case of a plastic mechanism of creep which were ignored in the derivation of Eq. (5). One of these is the presence of the boundaries of the sample. For a plastic creep mechanism the elastic energy necessary for the formation of a step near the surface of the sample is one-half as large as the elastic energy necessary for the formation of a half-loop in the bulk of the crystal. This is because, as can be seen in Fig. 9a and 9b, in the formation of step near the boundary of an object only a single vortex segment L_β arises, whereas the formation of a half-loop in the bulk of the sample requires two vortex segments L_β. Therefore the activation energy for plastic creep near the surface of the sample is one-half as large as the value in the bulk of the sample. A second factor that decreases the activation energy is the presence of point pinning centers, the fluctuations of the density of which lead to curvature of the vortex lines. Therefore, along the vortex line there can appear segments for which the length of the vortex segments L_β is shorter than their length in the absence of point pinning centers. This situation is illustrated schematically in Fig. 9c. The experimental studies of $YBa_2Cu_3O_{7-x}$ single crystals indeed provide evidence that the introduction of additional pinning centers leads to a decrease in the activation energy for a plastic creep mechanism.[32] The third factor decreasing the activation energy is the thermal motion of the vortices. It was shown in Refs. 7 and 28 that as the melting point of the vortex lattice is approached, the activation energy decreases considerably more rapidly with increasing magnetic field and temperature than the dependence given by expression (5). When all three of these mechanisms leading to a decrease in the activation energy are taken into account, the difference between the experimental and theoretical estimates seems completely reasonable.

Assuming that U_0^c is equal to the values in the right-hand column of Table I, we obtain from (5) the angle dependence of the activation energy shown by the dashed curves in Fig. 8b. We see that the activation energy $U_0(\alpha)$ (according to the experimental data) increases with decreasing angle α somewhat faster than the energy calculated according to Eq. (5). One reason for this difference may be that in deriving relation (5) we did not take into account the interaction of the vortex segments L_β with the neighboring vortices. In the magnetic field orientation $\mathbf{H}\|\mathbf{c}$ the vortex segments L_β are orthogonal to the neighboring vortices, and they therefore do not interact with the vortex lattice.[19] For any other magnetic field orientation, however, the projection of the vortex segment L_β on the magnetic induction vector, $L_\beta^B=a_0\varepsilon_\alpha^{1/2}/\tan(\alpha+\beta)$, is nonzero, and therefore it interacts with the neighboring vortices. The energy of this interaction is given by $U_{\rm int}\approx\varepsilon\varepsilon_0(u/a_0)^2L$ (Ref. 6), where L is the effective length of the deformable segments. In the linear approximation the deformation u is proportional to L_β^B. Therefore, the value of the deformation can be written as $u=ka_0\varepsilon_\alpha^{1/2}/\tan(\alpha+\beta)$, where the coefficient k can depend on the magnitude of the magnetic field, and in an anisotropic superconductor it can also depend on the orientation of the field.

TABLE I. Activation energy of plastic creep for various T and H.

		$4\varepsilon\varepsilon_0 a_0/k_B T$	$U_0(75°)/k_B T$
H, kOe	T, K	$\mathbf{H}\|\mathbf{c}$	**H** close to the **c** axis
5	83.9	63	25
5	85	42	16
15	82	32	6
15	83.9	27	3.3

Assuming, however, that $k=1/5$ and $L=\lambda$ and that the angle dependence of the energy $U_{\rm int}$ is mainly determined by the value of the projection L_β^B, we obtain a dependence $U_{\rm int}(\alpha)=\varepsilon\varepsilon_0\lambda[\varepsilon_\alpha^{1/2}/2\tan(\alpha+\beta)]^2$, which is shown by the dotted curve in Fig. 8b. The angle dependence

$$U_{\rm pl}(\alpha)=4U_{\rm el}(\alpha)+U_{\rm int}(\alpha)$$
$$=4\varepsilon\varepsilon_0[a_0\varepsilon_\alpha^{-1/2}+k^2\lambda\varepsilon_\alpha/4\tan^2(\alpha+\beta)] \qquad (6)$$

is shown by the solid curves in Fig. 8b. We see that the experimental dependence is well described by relation (6).

DISCUSSION OF THE RESULTS

In a magnetic field of 500 Oe at $\alpha\cong 20°$ the current J_{cE} is increasing. The I–V characteristic is a universal curve when plotted in the coordinates $E(J)/\varepsilon_\alpha - J_\parallel$ on the assumption that for $\theta<70°$ the twin boundaries alter the configurational structure of the flux lines (see the inset in Fig. 5a), and the vortex segments L_h are oriented at an angle $\theta\cong 70°$ to the planes of the TBs. These feature attest to the fact that $\theta=70°$ corresponds to the critical value. An expression for the critical angle is given in Ref. 16:

$$\theta_{\rm cr}\cong[2\alpha_p/\varepsilon^2\ln(a_0/\xi)]^{1/2}, \qquad (7)$$

where the dimensionless parameter $\alpha_p=U_p/\varepsilon_0$, U_p is the pinning potential at the TB, and $\varepsilon_0=(\Phi_0/4\pi\lambda_{ab})^2$. Starting from the value $\theta_{\rm cr}\cong 1.22$ rad and assuming that $\xi(84\ {\rm K})=5$ nm, we obtain $\alpha_p=0.055$. This value is approximately 2–3 time greater than the values $\alpha_p\cong 0.026$ and $\alpha\cong 0.017$, respectively, obtained at low temperatures in experiments involving decoration of the vortex structure[33] and in magnetooptical studies,[34] and also the value $\alpha_p\cong 0.023$ obtained in resistive studies of the anisotropy of the magnetic flux creep near the melting temperature of the vortex lattice.[16] This increase in value is possibly due to the different conditions of heat treatment of the single crystals in the oxygen flow and, accordingly, different oxygen content in the bulk of the crystals and at the twin boundaries. This conjecture requires additional experimental investigation, however.

At angles $\theta\leqslant 70°$ in magnetic fields of 1.5 and 5 kOe one observes a rapid growth of the current J_{cE} (see Fig. 2a), which apparently is also due to the onset of pinning at the TBs. This assumption is justified because, according to (7), the critical angle depends weakly (logarithmically) on the magnetic field. At $H=15$ kOe the current J_{cE} increases with angle α only at $\alpha\geqslant 75°$, i.e., $\theta_{\rm cr}\cong 15°$. Thus relation (7) does not describe the sharp decrease in the critical angle for $H=15$ kOe. The cause of this decrease in $\theta_{\rm cr}$ is probably due to the influence of thermal fluctuations. They substantially decrease the value of the critical angle near the melting temperature T_M, which in a magnetic field of 15 kOe in the $\mathbf{H}\|\mathbf{c}$ orientation is approximately 86 K. The value of the critical angle with allowance for the thermal depinning is given by the expression $\theta_{\rm cr}(T\cong T_M)\approx\alpha_p^{3/2}\varepsilon_0 a_0/(2k_BT)$.[16] If one uses the value $\alpha_p=0.055$, this relation gives a value $\theta_{\rm cr}(T\cong T_M)\cong 26°$, which agrees satisfactorily with the value $\theta_{\rm cr}(15\ {\rm kOe})\cong 15°$ obtained from the experimental data presented above, and also with the values $\theta_{\rm cr}\cong 15$–$20°$ observed previously in resistive measurements at $H=15$ kOe and at temperatures above[35] and below[14] the melting temperature of the vortex lattice.

The scaling of the I–V characteristics in the coordinates $E(J)/\varepsilon_a - J_\parallel$ at $H=0.5$ kOe is experimental evidence of the directed motion of vortices parallel to the TB plane in magnetic fields tilted with respect to the TB plane. This directed motion presupposes that the pinning of the vortex segments $L_{\rm tr}$ in their motion perpendicular to the TB plane is greater than the pinning force on the vortex segments localized off the TB plane; such an assumption is justified. Indeed, the value of J_{cE} for the crystal studied here exceeds 34 kA/cm^2 at $T=82$ and 83.9 K and $H=0.5$ kOe for the the field vector orientation $\mathbf{H}\|\mathbf{c}$. For the motion of the vortices along the TB planes, on the other hand, for $T=83$ K, $\mathbf{H}\|\mathbf{c}$, and 0.1 kOe $\leqslant H\leqslant 15$ kOe, one has $J_{cE}\approx 2.7$ kA/cm^2 (Ref. 20). It should be noted that for $H=0.1$ kOe the intervortex distance is equal to the average distance between twins in the crystals under study, each flux line is localized at a TB, and J_{cE} is governed by the pinning of these vortices. In a magnetic field of 15 kOe the intervortex distance is approximately 12 times the distance between twins, so that the overwhelming majority of the flux lines are localized off the planes of the TBs. Therefore, in high magnetic fields J_{cE} is mainly determined by the pinning of vortices lying off the TB planes by point defects. Thus the pinning force on vortices localized at the TBs in their motion perpendicular to the TB plane is more than 12 times as large as both the pinning force on vortices located in the bulk of the crystal and the pinning force on vortices trapped by twins in their motion parallel to the TB plane. We also note that the conclusion that directed motion of the magnetic flux occurs along the TB planes and, hence, along the **c** axis of the crystal agrees with the experimental observations[11] of directed motion of the magnetic flux in a magnetic field $\mathbf{H}\|\mathbf{c}$, where the vortices were probably moving along the TB planes parallel to the ab plane of the crystal and not along the direction of the Lorentz force.

The strong anisotropy of the pinning of vortices localized at the TBs in their motion perpendicular to and parallel to the TB planes is due to different physical mechanisms of formation of the pinning force in the two cases. The pinning by an ideal (defect-free) twin-boundary plane in the parallel motion of the vortices is equal to zero, and the pinning depends mainly on the interaction of the vortices with point defects. In the motion of the vortices in the direction perpendicular to the TB plane, however, the pinning force is mainly due to the suppression of the order parameter at the TB and is given by the relation[36]

$$J_c^{TB}\approx\alpha_p J_0. \qquad (8)$$

At $T=84$ K the depairing current $J_0\approx 2\times 10^7$ A/cm^2, and, according to relation (8), $J_c^{TB}=10^6$ A/cm^2. Therefore, the fact that the critical current in magnetic fields $H\leqslant 5$ kOe exceeds 3.4×10^4 A/cm^2 is completely reasonable. We also note that in a magnetic field of 15 kOe in the field orientation $\mathbf{H}\|\mathbf{c}$ the critical current for depinning is approximately equal to 40 kA/cm^2 and is a factor of three greater than the value $J_c=13$ kA/cm^2 at angles $\theta<\theta_{\rm cr}$, where the value of J_c is determined by the interaction with point defects. Therefore, assuming additivity of the pinning forces and taking into

account that in a magnetic field of 15 kOe only every twelfth vortex line is localized at a TB, we obtain a critical current $J_c = 5 \times 10^5$ A/cm^2 for the vortices trapped by the TB planes. This value is in satisfactory agreement with the calculated value 10^6 A/cm^2 determined from relation (8).

In a magnetic field of 15 kOe in the field orientation $\mathbf{H} \| \mathbf{c}$ the activation energy increases substantially, $U_0/k_BT \cong 14$, in comparison with its value $U_0/k_BT \cong 3.4$ obtained for an angle $\alpha = 75°$ (see Fig. 8b). This increase is possibly due to the influence of the twins. Indeed, the thermal motion of the vortices trapped by the TB planes is suppressed on account of the two-dimensional nature of these vortices,[15] and therefore the activation energy for the creep of trapped vortices should be larger than the activation energy of the vortices localized off the TB planes. Since in the experimental geometry the creep is mainly governed by the depinning from the TB planes, the latter should lead to an increase in the activation energy determined from the experimental data.

In the experimental geometry under study the twins should also have a substantial influence on the pinning and dynamics of the magnetic flux in the case when the magnetic field vector is oriented close to the ab plane. This is because a stepped structure of the flux lines is realized in the region of angles $\alpha < \varepsilon$, so that part of a flux line is oriented parallel to the **c** axis and, accordingly, parallel to the TB planes. As we have said, the evolution of the I–V characteristics with changes in the magnetic field and angle α in this region of angles indicates that the magnetic flux creep is mainly governed by vortex segments oriented along the **c** axis, which move perpendicular to the TB planes. The theory of the collective pinning predicts that if single-vortex creep is realized, then the critical current and activation energy for these vortex subsystems coincide with the critical current J_c^c and activation energy U_c^c measured in the orientation $\mathbf{H} \| \mathbf{c}$. Therefore the I–V characteristics in the region of angles $\alpha < \varepsilon$ when plotted in the coordinates $E(J) - \sin\alpha$ should coincide with the plots of $E(J)$ obtained for $\mathbf{H} \| \mathbf{c}$. Thus angular scaling is in fact observed in the experimental geometry with $\mathbf{J} \| ab$, $\mathbf{J} \perp$ TB, $\mathbf{H} \perp \mathbf{J}$, and α as a variable parameter,[20] in which the vortices move along the TB planes, i.e., the pinning is governed solely by the interaction with point defects. In the experimental geometry under study, however, the vortices and vortex segments oriented along the **c** axis move in the direction perpendicular to the plane of the TB and, as we have mentioned above, the critical angle in this case is mainly determined by the suppression of the order parameter at the TBs. The experimental data obtained in this study show that the critical current for $\mathbf{H} \| \mathbf{c}$ is substantially larger than for the orientation of the vortex subsystem along the **c** axis. This can be explained by the fact that the coherence length L_c^c along the magnetic field direction for $\mathbf{H} \| \mathbf{c}$ is substantially larger than the correlation length $L_c \cong c_0$ of the vortex subsystem oriented along the **c** axis, where c_0 is the crystal lattice parameter along the **c** axis.

The difference of the angle dependences of the currents J_{cE} measured in different magnetic fields (see Fig. 2) can be explained as follows. When the magnetic field vector is oriented close to the ab plane, $\alpha < \varepsilon$, the flux lines have a stepped structure (see the upper inset in Fig. 3a). Analysis of the I–V characteristics shown in Figs. 3 and 4 indicates that the vortex segments L_{ab} are pinned on account of the strong intrinsic pinning due to the layered structure of the superconductor, and the energy dissipation occurs on account of the thermally activated motion of the vortex segments L_c oriented along the **c** axis of the crystal. As α and H are increased, the number of vortex segments L_c and, accordingly, the magnetic induction B_c along the **c** axis also increase. Therefore, for the creep of noninteracting vortex segments L_c (which, as we see in Fig. 4b, is realized for $H \leqslant 7$ kOe), when the velocity v of the vortices is independent of B_c and α, the electric field increases with increasing H and α: $E = B_c v = Bv \sin\alpha$. This leads to a decrease in the current J_{cE} with increasing α and increasing magnetic field strength. As the magnetic field is increased further, $H > 7$ kOe, a transition occurs from single-vortex creep to flux-bundle creep. The crossover current J_b corresponding to the transition to collective creep increases with increasing B (see Fig. 4b) and α (see Fig. 4a), $J_b \propto B_c^{0.7} \propto (B \sin\alpha)^{0.7}$, which leads to an increase of J_{cE} with the field H and angle α.

The experimental data obtained attest to the fact that for θ less than the critical value $\theta_{cr} \cong 70°$, i.e., for $\alpha \geqslant 20°$, the twin boundaries alter the configurational structure of the flux lines, as is shown in the inset in Fig. 5a. It turns out that the pinning force on the vortex segments L_{tr} trapped by the TB planes is large for the motion of the segments perpendicular to the TB plane. Therefore, directed motion of the magnetic flux along the TB planes occurs under the influence of the Lorentz force component F_c directed along the **c** axis. Because the value of the force F_c decreases with increasing α, at a constant transport current density the velocity of the motion of the magnetic flux and, accordingly, the electric field $E = Bv$ decrease, and the current J_{cE} increases.

With increasing H and α in the region of low transport currents one observes a rapid decrease in the voltage with decreasing transport current (see Fig. 5b and 5c and Fig. 6). This behavior can be explained in the framework of the collective pinning theory as a transition from single-vortex creep to flux-bundle creep at transport currents less than the crossover current J_b. Indeed, according to relation (2c), the crossover current increases with increasing magnetic field and angle α, $J_b \propto (\varepsilon_\alpha B)^{0.7}$, while the activation energy for creep at $J < J_b$ increases rapidly with decreasing current density and increasing crossover current, $U_b(\alpha, B, J) \propto (J_b/J)^{5/2} \propto (\varepsilon_\alpha B)^{7/4} J^{-5/2}$. As a result, as H and α increase, one observes a rapid decrease of the voltage at a constant current density, and that in turn leads to an increase in J_{cE}.

Analysis of the I–V characteristics measured[22] for the crystal under study in various magnetic fields at $\alpha = 45°$ showed that for $H \geqslant 5$ kOe the activation energy of collective creep becomes larger than that of plastic creep involving the motion of dislocations of the vortex lattice. This is due to the difference in the field dependence of the activation energy: it increases with increasing magnetic field in the case of collective creep, while in the case of plastic creep it decreases. Therefore the collective creep realized in low magnetic fields gives way to plastic creep in high fields. The experimental data obtained in the present study show that an analogous crossover also takes place with increasing angle α. Indeed, the results shown in Fig. 4a and 4b attest to the fact that the activation energy of collective creep increases with the angle

α, in agreement with the collective pinning theory. The activation energy for plastic creep, on the contrary, decreases with increasing angle α (see Fig. 9b), which agrees with the theoretical estimates made here. Therefore, the transition from collective creep at small α to plastic creep at large α appears completely plausible.

The difference of the angle dependence of J_{cE} for plastic creep observed in measurements at fields of 5 and 15 kOe is due to the presence of twin boundaries. At $H=5$ kOe the twins affect the configurational structure and pinning of the vortices for $\alpha \geqslant 20°$, which leads to growth of the critical current for depinning with increasing α, since the length of the vortex segments $L_{\rm tr}$ trapped by the TB planes increases continuously with increasing α. Despite the decrease in the activation energy with increasing α, the growth of the critical current for depinning turns out to be dominant, since the measured current J_{cE} increases with increasing angle α. For $H=15$ kOe, because of thermal depinning, the influence of the twins is felt only for $\alpha \geqslant 75°$. Therefore, the activation energy and critical current for depinning, respectively, and the measured current J_{cE} decrease with increasing angle α up to 75°. For $\alpha \geqslant 75°$ the presence of the twins comes into play, so that the activation energy, critical current for depinning, and measured current J_{cE} increase with increasing angle α.

CONCLUSIONS

1. The experimental data presented here attest to the fact that twin boundaries influence the configurational structure and pinning of vortices at misorientation angles θ between the magnetic field vector and the planes of the TBs of up to 70°. We have shown that at angles $\theta < 70°$ the configurational structure of the flux lines proposed in Refs. 16 and 21 is realized, so that a part of each flux line is pinned by TB planes. Because of the strong pinning of the trapped segments with respect to their motion perpendicular to the plane of the TB, the motion of the flux lines along the ab plane is suppressed, and only motion parallel to the TB plane can occur; this leads to motion of the magnetic flux along the **c** axis of the crystal. As the magnetic field is increased, i.e., as the melting point of the vortex lattice is approached, a thermal depinning of the trapped vortex segments occurs, sharply decreasing the region of angles $\theta \leqslant 15°$ in which the TBs influence the configurational structure and pinning of the flux lines.

2. We have shown that the activation energy for a plastic mechanism of creep increases as the magnetic field vector is rotated away from the **c** axis toward the ab plane, in agreement with the theoretical estimates made; in the case of pinning at point defects, the critical current corresponding to the motion of dislocations of the vortex lattice decreases with increasing deviation of the field vector from the ab plane. In the region of angles for which pinning on TBs plays a substantial role, the critical current increases as the field vector is rotated away from the ab plane toward the **c** axis.

3. In the region of angles $\alpha < \varepsilon$, in which an important role is played by intrinsic pinning, increasing the magnetic field leads to crossover from single-vortex creep to flux-bundle creep. The experimental data obtained show that this transition takes place in the vortex subsystem oriented along the **c** axis of the crystal. A consequence of this crossover is a change of the angle dependence of the critical current J_{cE} and a change of the usual maximum on the $J_{cE}(\alpha)$ curve (observed in the field orientation $\mathbf{H} \| ab$ in low magnetic fields) to a minimum at high magnetic fields.

*E-mail: Aleksandr.V.Bondarenko@univer.kharkov.ua

[1] E. M. Gyorgy, R. B. van Dover, K. A. Jackson, L. F. Schneemeyer, and J. V. Waszczak, Appl. Phys. Lett. **55**, 283 (1989). See also the interpretation of the experimental results on p. 1165 of Ref. 6 below.
[2] M. Daeumling, J. M. Seutjens, and D. C. Larbalestier, Nature (London) **346**, 332 (1990); V. V. Moschalkov, A. A. Zhukov, I. V. Gladyshev, S. N. Gordeev, G. T. Karapetrov, V. D. Kusnetsov, V. V. Metlushko, V. A. Murashov, V. I. Voronkova, and V. K. Janovskii, J. Magn. Magn. Mater. **90&91**, 611 (1990).
[3] L. Krusin-Elbaum, L. Civale, V. M. Vinokur, and F. Holtzberg, Phys. Lett. **69**, 2280 (1992).
[4] L. Klein, E. R. Yacoby, Y. Yeshurun, A. Erb, G. Muller-Vogt, V. Breit, and H. Wuhl, Phys. Rev. B **49**, 4403 (1994).
[5] B. Khaikovich, E. Zeldov, D. Majer, T. W. Li, P. H. Kes, and M. Konczykowski, Phys. Rev. Lett. **76**, 2555 (1996); D. Giller, A. Shaulov, R. Prozorov, Y. Abulafia, L. Burlachkov, Y. Yeshurun, E. Zeldov, V. M. Vinokur, J. L. Peng, and R. L. Greene, Phys. Rev. Lett. **79**, 2542 (1997); D. Giller, A. Shaulov, Y. Yeshurun, and J. Giapintzakis, Phys. Rev. B **60**, 106 (1999).
[6] G. Blatter, M. V. Feigel'man, V. B. Geshkenbein, A. I. Larkin, and V. M. Vinokur, Rev. Mod. Phys. **66**, 1125 (1994).
[7] Y. Abulafia, A. Shaulov, Y. Wolfus, R. Prozorov, L. Burlachkov, Y. Yeshurun, D. Majer, E. Zeldov, H. Wuhl, V. B. Geshkenbein, and V. M. Vinokur, Phys. Rev. Lett. **77**, 1596 (1996).
[8] Y. Iye, T. Terashima, and Y. Bando, Physica C **177**, 393 (1991); A. Walkenhorst, C. Tome-Rosa, C. Stolzel, G. Jakob, M. Schmitt, and H. Adrian, Physica C **177**, 165 (1991); Y. Iye, A. Fukushima, T. Tamegai, T. Terashima, and Y. Bando, Physica C **185–189**, 297 (1991).
[9] M. Tachiki and S. Takahashi, Solid State Commun. **70**, 291 (1989).
[10] P. Bergus, E. Di Bartolomeo, G. A. Wagner, and J. E. Evetts, Phys. Rev. Lett. **79**, 2332 (1997).
[11] C. Duran, P. L. Gammel, R. Wolfe, V. J. Fratello, D. J. Bishop, J. P. Rice, and D. M. Ginsberg, Nature (London) **357**, 474 (1992); A. I. Belyaeva, S. V. Vojtsenya, V. P. Yurijev, M. A. Obolenskii, and A. V. Bondarenko, Solid State Commun. **85**, 427 (1993).
[12] M. A. Obolenskiĭ, A. V. Bondarenko, V. I. Beletskiĭ, R. V. Vovk, A. A. Prodan, M. Él'-Siidavi, D. Niarkhos, M. Pissas, G. Kallias, and A. G. Sivakov, Funktsional'nye Materialy **2**, 403 (1995).
[13] M. A. Obolenskii, A. V. Bondarenko, M. G. Revyakina, and V. A. Shklovskij, Supercond., Phys. Chem. Technol. **7**, 43 (1994); M. A. Obolenskii, A. V. Bondarenko, V. A. Shklovskij, and M. G. Revyakina, Fiz. Nizk. Temp. **22**, 892 (1996) [Low Temp. Phys. **22**, 683 (1996)].
[14] V. F. Solovjov, V. M. Pan, and H. C. Freyhardt, Phys. Rev. B **50**, 13724 (1994); V. M. Pan, V. F. Solovjov, and H. C. Freyhardt, Physica C **279**, 18 (1997).
[15] G. Blatter, J. Rhyner, and V. M. Vinokur, Phys. Rev. B **43**, 7826 (1991).
[16] W. K. Kwok, J. A. Frendrich, V. M. Vinokur, A. E. Koshelev, and G. W. Grabtree, Phys. Rev. Lett. **76**, 4596 (1996).
[17] R. Hiergeist and R. Hergt, Phys. Rev. B **55**, 3258 (1997).
[18] B. I. Ivlev, Yu. N. Ovchinnikov, and V. L. Pokrovsky, Mod. Phys. Lett. B **5**, 73 (1991); S. S. Maslov and V. L. Pokrovsky, Europhys. Lett. **14**, 591 (1991).
[19] P. H. Kes, J. Aarts, V. M. Vinokur, and C. J. van der Beek, Phys. Rev. B **64**, 1063 (1990); S. Theodorakis, Phys. Rev. B **42**, 10172 (1990); L. N. Bulaevskii, L. N. Ledvij, and V. G. Kogan, Phys. Rev. B **46**, 366 (1992).
[20] A. V. Bondarenko, A. A. Prodan, M. A. Obolenskii (to be published).
[21] E. B. Sonin, Phys. Rev. B **48**, 10287 (1993).
[22] M. A. Obolenskii, R. V. Vovk, A. V. Bondarenko, and A. A. Prodan, Functional Materials **4**, 4 (1997); A. V. Bondarenko, A. A. Prodan, M. A. Obolenskii, R. V. Vovk, M. Pissas, D. Niarchos, G. Kallias, and T. R. Arouri, Physica C **317–318**, 655 (1999).
[23] J. Bardeen and M. J. Stephen, Phys. Rev. A **140**, 1179 (1965).
[24] J. R. Thompson, Y. R. Sun, L. Civale, A. P. Malozemoff, M. W. McElfresh, A. D. Marwick, and F. Holtzberg, Phys. Rev. B **47**, 14440 (1993).

[25] J. P. Hirth and J. Lothe, *Theory of Dislocations*, Wiley, New York (1982).
[26] V. Geshkenbein, A. Larkin, M. Feigel'man, and V. Vinokur, Physica C **162–164**, 239 (1989).
[27] M. A. Obolenskii, A. V. Bondarenko, V. A. Shklovskij, R. V. Vovk, and A. A. Prodan, Fiz. Nizk. Temp. **24**, 71 (1998) [Low Temp. Phys. **24**, 53 (1998)].
[28] A. V. Bondarenko, V. A. Shklovskij, M. A. Obolenskii, R. V. Vovk, A. A. Prodan, M. Pissas, D. Niarchos, and G. Kallias, Phys. Rev. B **58**, 2445 (1998).
[29] V. M. Vinokur and T. Nattermann, Phys. Rev. Lett. **79**, 3471 (1997).
[30] S. Scheidl and V. M. Vinokur, Phys. Rev. B **56**, 8522 (1997).
[31] R. A. Klemm and J. R. Clem, Phys. Rev. B **21**, 1868 (1980); A. V. Balatskii, L. I. Burlachkov, and L. P. Gor'kov, Zh. Éksp. Teor. Fiz. **90**, 1478 (1986) [Sov. Phys. JETP **63**, 866 (1986)].
[32] A. V. Bondarenko, Yu. T. Petrusenko, F. Dworszhak, A. A. Prodan, V. Borisenko, and U. Dedek (to be published).
[33] L. Ya. Vinnikov, I. V. Grigor'eva, L. A. Gurevich, and A. E. Koshelev, Supercond., Phys. Chem. Technol. **3**, 1121 (1990).
[34] L. A. Dorosinskii, V. I. Nikitenko, A. A. Polyanskii, and V. K. Vlasko-Vlasov, Physica C **246**, 283 (1995).
[35] S. Flesher, W. K. Kwok, U. Welp, V. M. Vinokur, M. K. Smith, J. Downey, and G. W. Grabtree, Phys. Rev. B **47**, 14448 (1993).
[36] D. R. Nelson and V. M. Vinokur, Phys. Rev. B **48**, 13060 (1993).

Translated by Steve Torstveit

ELECTRONIC PROPERTIES OF METALS AND ALLOYS

Optical functions of the Drude model: transformation of the spectra over wide ranges of parameters

A. I. Galuza* and A. B. Beznosov

B. Verkin Institute for Low Temperature Physics and Engineering, National Academy of Sciences of Ukraine, pr. Lenina 47, 61164 Kharkov, Ukraine

(Submitted August 29, 2000; revised October 18, 2000)
Fiz. Nizk. Temp. **27**, 294–308 (March 2001)

The spectral features of the optical functions of the Drude model are investigated over wide ranges of parameters — the plasma frequency ω_p of the current carriers, their transport relaxation frequency g, and the dielectric constant ε_∞ due to high-energy electronic transitions in the system. The conditions are determined for: a) the square-root frequency dependence of the modulus and phase of the reflection; b) linearity of the phase $\theta = 2\omega/\omega_p\sqrt{\varepsilon_\infty} + \theta_0$; c) the existence of a plasma reflection edge. Approximate relations are obtained which permit simplifying the analysis of optical reflection and electron characteristic energy loss data both in ''good'' metals and in materials with a strong temperature dependence of the electrical conductivity (semiconductors, doped and nonstoichiometric oxides, granular metal films, and amorphous alloys). The parameters of the systems of conduction electrons in Al and U_2Zn_{17} are determined.
 [DOI: 10.1063/1.1355519]

With the intense development of microelectronics in the final quarter of the twentieth century, the problem of controlling the electrical conductivity of matter over a wide range of temperatures has become increasingly urgent. The extensive use of semiconductors, including magnetic ones, and the discovery of high-T_c superconductors has raised the level of interest in the study of the electronic systems of these materials by optical methods.

The interpretation of the results of optical measurements of conducting objects is most often done using the so-called Drude model, which, despite its outward simplicity, requires an attentive approach to the analysis of individual spectral intervals. In general, the search for the optimal interpretation of the data of optical studies is complicated by the fact that the number of parameters is not small (there are three in the expanded model: the plasma frequency ω_p of the current carriers, their transport relaxation frequency g, and the dielectric constant ε_∞ due to the polarization of the atomic cores) and by the large number of optical functions used (the real $\varepsilon_1(\omega)$ and imaginary $\varepsilon_2(\omega)$ components of the dielectric function, the modulus $r(\omega)$ and phase $\theta(\omega)$ of the optical reflection, the optical conductivity $\sigma(\omega)$, the energy loss function $L(\omega)$, etc.), which have different sensitivities to the individual parameters of the Drude model and their combinations. This is especially noticeable when comparing the results obtained by different authors using different techniques over wide ranges of parameters, primarily of g and ω_p (metal–insulator transitions in crystals[1,2] and amorphous materials,[1,3] systems exhibiting the giant magnetoresistance effect,[3–7] etc.).

Large changes of the electrical conductivity of a substance may be a consequence of qualitative changes in the conduction mechanism, which are radically reflected both in temperature and field effects and in the spectral behavior of the optical functions.[3,8] Knowledge of the corresponding features deriving from the Drude mechanism of conduction can make it easier to correctly separate out the different contributions to the optical characteristics. Because of the need for such an analysis, in this paper we address the problem of determining the basic regularities of the spectral behavior of the optical functions of the Drude model and their transformation upon changes in the parameters of the model over wide ranges of values.

DRUDE MODEL

In 1900 Drude published two papers[9] on the electronic theory of metals in a free-electron model approximation, laying a foundation for explaining the optical properties of metals and other conducting materials (those papers are discussed in detail in the monograph by Lorentz[10]). In the one-hundred years since that time the electronic theory has been developed, become quantum,[11] and been supplemented with the concepts of numerous quasiparticles. Nevertheless, the purely classical Drude model is still being used successfully to explain many new results.[12]

Since the beginning of the widespread study of the physical properties of semiconductors, the Drude model has become an important tool, often the main tool, for studying their low-frequency optical absorption due to the current carriers.[13–15] Here the complex interaction of the set of itinerant electrons with the atomic cores can often be taken into account simply by introducing an effective mass m^* and the sign of the carrier charge. It is appropos to note that in his theory[16] Drude also proposed the existence of two types of carriers with additive contributions to the absorption, in a

sense foreseeing the discovery of semiconductors and importance of his model for studying them.

The next peak in the demand for the Drude model came with the discovery of high-T_c superconductors (HTSCs), for which some form or other of the Drude model is employed in the majority of papers to interpret the results of optical studies in the infrared. For example, in Ref. 17 three Drude parameters were determined for YBaCuO by fitting the reflection curve in the interval 1 eV$<E<$1.9 eV, and in Refs. 18 and 19 this interval was extended to 3 eV and then, in Ref. 20, to 5.6 eV (in Refs. 19 and 20 the anisotropy of the optical characteristics was studied). Because of the low concentration of carriers, the infrared spectra of HTSCs can display phonon peaks, and the visible spectra have strong bands of interband transitions. In such cases an adequate description of the observed spectra is most often achieved by supplementing the Drude model with Lorentzian oscillators,[21–24] although in some papers modifications of the Drude model with an increased number of parameters are employed;[25–27] the Drude model for a normal metal is organically related[28] to the Mattis–Bardeen model[29] of a superconductor. There is no denying the productivity of the Drude model in studies of promising new conducting materials, in particular, of structures with metallic layers of nanometer thickness, manganites,[3,4,6,7] and systems with correlated electrons.[30]

The expressions obtained in the framework of the Drude model for the real part of the dynamic dielectric function $\varepsilon_1(\omega)$ and the dynamic conductivity $\sigma(\omega)$ are known as the Drude–Zener formulas,[11] the Drude–Lorentz[1)] formulas,[12] and the Kramers–Kronig relations:[15]

$$\sigma(\omega)=\frac{Ne^2}{m^*}\frac{g}{\omega^2+g^2}=\frac{g^2}{\omega^2+g^2}\sigma_0,$$
$$\varepsilon_1(\omega)=\varepsilon_\infty-\frac{4\pi Ne^2}{m^*}\frac{1}{\omega^2+g^2}=\varepsilon_\infty-\frac{4\pi g}{\omega^2+g^2}\sigma_0, \tag{1}$$

where N and e are the concentration and charge of the current carriers, σ_0 is the static conductivity, and the plasma frequency is given by the relation $\omega_p^2=4\pi Ne^2/m^*\varepsilon_\infty$. From now on we will drop the explicit indication of the frequency dependence of the optical functions in those cases where it is obvious.

Relations (1) allow one to express in terms of the Drude model parameters ε_∞, g, and σ_0 (or ε_∞, g, and ω_p) the frequency dependence of the optical constants n and k ($\varepsilon_1=n^2-k^2$, $4\pi\sigma/\omega=\varepsilon_2=2nk$) and of all the other optical functions. For $\omega<\omega_p$ the optical transparency of conductors is negligible, and so one most often studies experimentally the energy coefficient of reflection $R=|\hat{r}|^2=r^2$ ($\hat{r}=re^{-i\theta}$ is the complex amplitude of the reflection coefficient, and θ is the change in phase of the light wave on reflection),[11,13,14] and the characteristic electron energy loss in their passage through thin slices of a substance,[32,33] and the photoelectron spectra.[34] The electron energy loss function is related to the dynamic dielectric function of the system by the relation $L=\varepsilon_2/(\varepsilon_1^2+\varepsilon_2^2)$. It can also be measured by purely optical methods, by exciting plasma oscillations of the electrons by the p component of the polarization of an electromagnetic wave in the case of oblique incidence of the latter on the reflecting surface of a thin metal film.[35]

The expressions for n and k (and, even more so, those for R, r, and θ) obtained from (1) are rather awkward and are amenable to analytical study only after substantial simplifications, usually involving the approximation of low (or high) frequencies in comparison with the values of g or ω_p. In the present study, the use of numerical methods for finding criteria of applicability of these simplifications in the region of intermediate frequencies and also for studying L, R, and θ directly at values of the ratio $w=g/\omega_p$ in the interval 0–10 has made it possible to obtain a number of approximate relations between the parameters of the Drude model and the characteristic features of these functions, in particular, for the upper boundary of the region of the square-root frequency dependence of the modulus and phase of reflection (the Hagen–Rubens region[36]), for the region of phase linearity observed at low frequencies,[2)] for refining the concept of the plasma reflection edge, and for determining the characteristics of the reflection minimum that is formed (for $\varepsilon_\infty>1$) beyond the plasma edge.

MAIN SPECTRAL INTERVALS

Figure 1a, b, and c shows the spectra of the reflection coefficient R and its phase θ, calculated at $\varepsilon_\infty=4/3$, 4, and 20, respectively, and for $w=g/\omega_p=0.001$ (solid curves), $w=0.1$ (dashed curves), and $w=1$ (dotted curves); the curves in Fig. 1a (for $w\leqslant 0.1$) are typical for ordinary metals, those in part b for HTSC materials, and those in part c for semiconductors. The chosen horizontal scale makes it possible to represent all frequencies from 0 to ∞ by substantially compressing the region $(\sim 3\omega_p,\infty)$, which is relatively uninformative for the Drude model.

Usually in the Drude model one singles out three or four characteristic parts of the spectrum, ignoring the question of the boundaries between them: $\omega\ll g$, $g\ll\omega\ll\omega_p$, $\omega\sim\omega_p$, and $\omega>\omega_p$ (Refs. 11–14 and 36). In the present paper we consider in the given case ($\varepsilon_\infty>1$) five characteristic spectral regions, the boundaries between which will be determined below: 1) the Hagen–Rubens region, 2) the region of linearity of the phase, 3) the neighborhood of the plasma reflection edge, 4) the neighborhood of the reflection minimum, 5) frequencies substantially higher than the frequency of the reflection minimum.

The frequency dependence of $1-r$ and θ in the Hagen–Rubens region is the same. On the whole, the reflection decreases monotonically from $R(0)=1$ to a minimum value $R_{\min}=R(\omega_{\min})$ for $\varepsilon_\infty>1$, then increases to $R(\infty)$, while θ increases monotonically from $\theta(0)=0$ to a maximum $\theta_{\max}$ (at small g this is most likely a plateau), after which it falls off to $\theta(\infty)=0$. If the relaxation frequency is not too high (up to $w\sim 0.01$–0.1), the width $\Delta\omega_{\min}$ of the reflection minimum, determined at the level $R=2R_{\min}$, is approximately equal to g, while the width of the phase plateau $\Delta\omega_\theta$, which we find as the difference of the frequencies of the maximum rates of rise and fall, increases without bound as $\varepsilon_\infty\to 1$ and decreases to zero as $\varepsilon_\infty\to\infty$, assuming the value $\Delta\omega_\theta=\omega_p$ at $\varepsilon_\infty=4/3$.

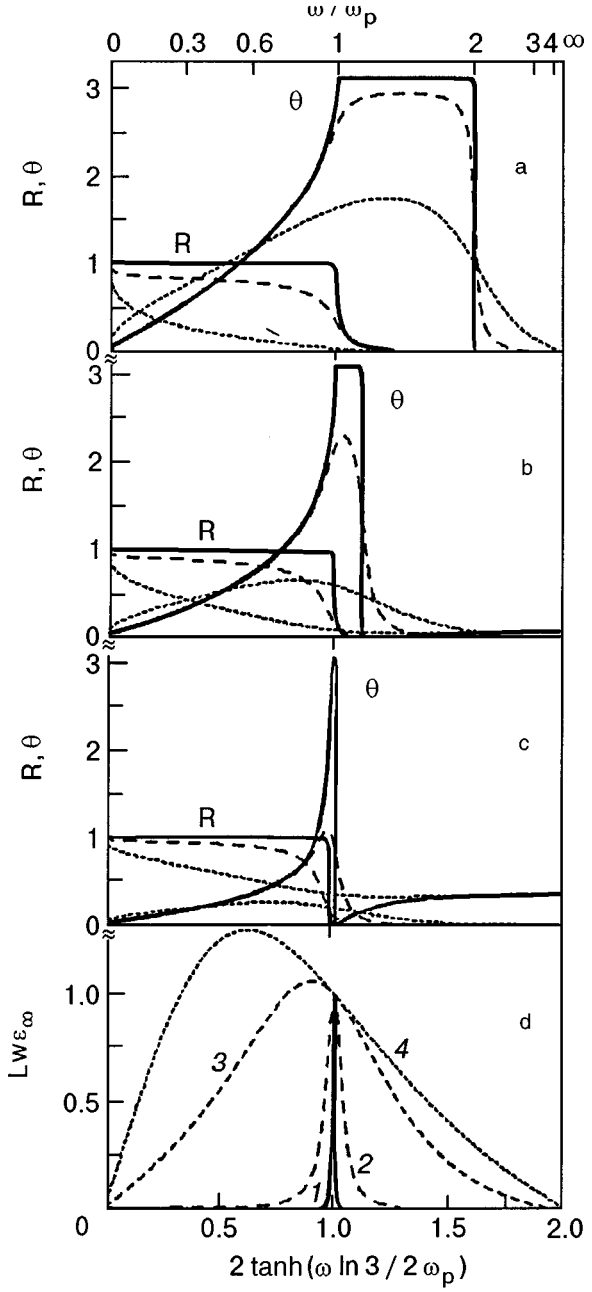

FIG. 1. Spectral dependence of the reflection coefficient R and phase θ for various ω: 0.001 (solid curves), 0.1 (dashed curves), 1 (dotted curves) and $\varepsilon_\infty = 4/3$ (a), 4 (b), 20 (c), and the values of $Lw\varepsilon_\infty$ for different values of w: 0.01 (*1*), 0.1 (*2*), 1 (*3*), 2 (*4*) (d).

For $g \ll \omega_p$ the Drude model gives the following asymptotic expressions for the different characteristics of the optical functions near and above the plasma frequency:

$$\Delta\omega_\theta \simeq \omega_p[\sqrt{\varepsilon_\infty/(\varepsilon_\infty-1)}-1], \quad \theta_{\max} \simeq \pi; \tag{2a}$$

$$\omega_L \simeq \omega_b \simeq \omega_\varepsilon \simeq \omega_p, \quad L_{\max} \simeq \omega_p/g\varepsilon_\infty, \quad \Delta\omega_L \simeq \Delta\omega_{\min} \simeq g, \tag{2b}$$

$$R_{\min} \simeq \frac{g^2(\varepsilon_\infty-1)^3}{16\omega_p^2\varepsilon_\infty}, \quad \omega_{\min} \simeq \omega_p\sqrt{\varepsilon_\infty/(\varepsilon_\infty-1)}, \tag{2c}$$

$$R(\infty) \simeq \frac{(\varepsilon_\infty^{1/2}-1)^2}{(\varepsilon_\infty^{1/2}+1)^2}. \tag{2d}$$

Here ω_b is the frequency of the maximum rate of rise of the reflection (i.e., the inflection point of $R(\omega)$: $d^2R/d\omega^2=0$, $d^3R/d\omega^3>0$ for $\omega=\omega_b$), which is natural to call the plasma edge or threshold of reflection, ω_ε is the frequency at which the dielectric function goes to zero, ω_L, $L_{\max}$, and $\Delta\omega_L$ are the position of the maximum of the loss function, its value there, and the width of the L peak at half maximum, respectively.

SCATTERING OF THE CURRENT CARRIERS

The region of the square-root frequency dependence of the reflection (the Hagen–Rubens region) is governed by the scattering of current carriers upon the breaking of the translational symmetry of the system. This part of the spectrum begins at $\omega=0$ and extends (within certain error limits) to a certain boundary frequency ω_{H-R}. For $\omega\to 0$ this dependence is also inherent to the inverse optical constants $n^{-1} \simeq k^{-1} \simeq (\omega/2\pi\sigma)^{1/2}$, the absorptivity $A \simeq 1-R \simeq (2\omega/\pi\sigma)^{1/2}$ (Ref. 11), the amplitude coefficient of reflection $r \simeq 1-(\omega/2\pi\sigma)^{1/2}$, and the phase $\theta \simeq (\omega/2\pi\sigma)^{1/2}$; these last two satisfy relations of the type

$$r(\omega)+\theta(\omega) \simeq 1, \quad \omega < \omega_{H-R}. \tag{3}$$

We note that in the expressions given here one can take for the conductivity its value in the static limit σ_0, since for $\omega\to 0$ we have $\sigma \simeq \sigma_0(1-\omega^2/g^2)$, and in the Hagen–Rubens region $\omega^2/g^2 \ll 1$. Our detailed analysis will be limited to the complex reflection, since R is a directly measurable optical function (and over a wide spectral region it is often the only one), and its phase θ is of interest, in particular, in connection with the problem of the high-frequency extrapolation of R in determining the optical functions of conductors by the Kramers–Kronig method.

Analysis of the spectral dependence $\hat{r}(\omega)$ for different metals, calculated from the known experimental values of their optical constants,[37] has shown that at the low-frequency boundary of the data used, $\omega \approx 0.05$–0.10 eV, the Hagen–Rubens region has not yet been reached, and the spectral dependence of θ exhibits a rather extended (0.1 eV$<\omega<$1 eV) linear region with one or two kinks, which will be discussed below.

Upper boundary of the Hagen–Rubens region

The upper boundary ω_{H-R} of the Hagen–Rubens region is naturally defined as the frequency at which the relative deviation δ of the curve of $1-r(\omega)$ from the square-root dependence $(\omega/2\pi\sigma_0)^{1/2}$ reaches a certain specified value (in this paper we take $\delta=0.01$). This boundary will obviously depend on g, and it is clear that the boundary frequencies will be different for the other functions mentioned which have analogous spectral behavior for $\omega\to 0$. We shall consider these frequencies in parallel for r and θ, denoting them for arbitrary values of g as ω_r and ω_θ, respectively (see Fig. 2a). An analysis shows that the boundary frequency for the phase ω_θ is directly proportional to the values of g and δ up to values of the deviation $\sim 10\%$ or more, with a coefficient of proportionality $p_\theta(w,\varepsilon_\infty)$:

$$\omega_\theta = p_\theta(w,\varepsilon_\infty) g\,\delta, \tag{4a}$$

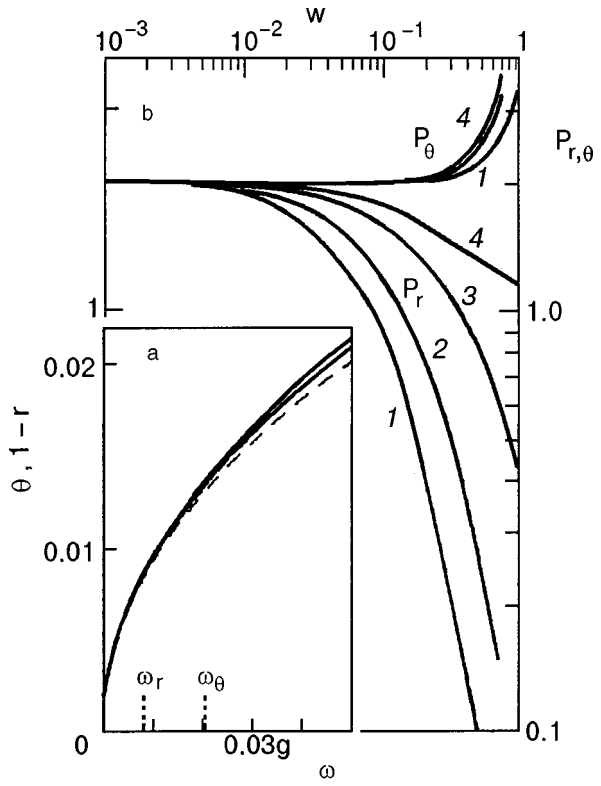

FIG. 2. Spectra of the quantities $(w/2\pi\sigma)^{1/2}$ (middle curve), $1-r$ (dashed curve), and θ (upper curve) in the Hagen–Rubens region for $w=0.17$ and $\varepsilon_\infty=2$ (ω_r and ω_θ are the boundaries of this region for r and θ at a tolerance level $\delta=1\%$) (a); the dependence on w and ε_∞ of the coefficients P_r and P_θ that determine the values of ω_r and ω_θ in Eqs. (4a) and (4b) (the P_r and P_θ are numbered from *1* to *4* for $\varepsilon_\infty=4/3$, 4, 20, and 56, respectively) (b).

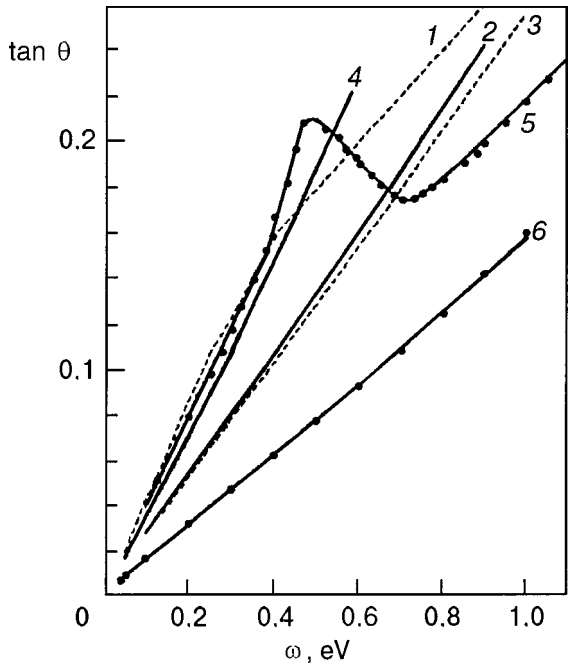

FIG. 3. Regions of nearly linear dispersion of the phase of reflection for the metals: Ni (*1*), Ag (*2*), Au (*3*), W (*4*), Pt (*5*), and Al (*6*) (the phases θ are calculated from the data of Ref. 37 for the optical constants).

whereas the dependence of ω_r on δ remains substantially nonlinear even at very small dimensions ($\delta\sim10^{-4}$), i.e.,

$$\omega_r=p_r(\delta,\varepsilon_\infty,w)g\delta. \tag{4b}$$

Furthermore, p_r is much more sensitive than p_θ to changes in ε_∞ and $w=g/\omega_p$. This is clearly seen on the p_r and p_θ curves obtained for $\varepsilon_\infty=4/3$, 4, 20, and 56 (curves *1–4* in Fig. 2b, respectively); all of the functions were calculated for values of the deviations of r and θ from the square-root behavior at the 1% level. In general the upper boundary of the Hagen–Rubens region for r is always lower than for θ (for $w\sim1$ it is an order of magnitude or more lower), but for values $w\leqslant0.01$ and $\delta=0.01$ the coefficients p_θ and p_r are practically equal and have a value ~2, i.e., in this case, independently of ε_∞, we have

$$\omega_r=\omega_\theta=\omega_{H-R}=0.02g(w\leqslant0{,}1,\ \delta=0.01). \tag{4c}$$

Let us use relation (4c) as the general definition of the upper boundary of the Hagen–Rubens region for the complex reflection coefficient. It is valid, first, for various metals, in which for 0.001 eV$<g<$0.3 eV the plasma frequency ω_p varies from ~3 eV (Cs) to ~15 eV (Al) and, accordingly, w does not exceed 0.1. However, it can also be valid in semiconductors and in oxide superconducting materials. The use of Eq. (4c) in these cases leads to estimates of the absolute value of ω_r and ω_θ (at the adopted level of deviation $\delta=0.01$) which are equal in order of magnitude to 10^{-3} eV; this is the region of millimeter waves, which are more pertinent to radiophysics than to optics. At the same time, for poor metals and other conducting materials with $w>1$ the Hagen–Rubens region extends to the near-IR and even to the visible, but here the relation $\omega_r=\omega_\theta$ no longer holds.

REGION OF PHASE LINEARITY

Frequency dependence of the phase of the reflection in the form of straight (sometimes broken) lines is often observed on the experimental curves for metals in the optical region of the spectrum (Fig. 3) and can be explained completely in the framework of the Drude model: a dependence close to linear also exists at the transition from a convex shape of the θ curve for $\omega\to0$ to a convex shape near ω_p (see Fig. 1). One is interested in the extent of this segment and the presence of kinks. We define the lower ω_{L1} and upper ω_{L2} boundaries of this region of linearity like we did for the Hagen–Rubens region, as the frequencies at which the deviation of the phase from its rectilinear approximation reaches 1%. For all the metals considered the linear-phase region is contained inside the region

$$k^2(\omega)/n^2(\omega)\gg1, \tag{5}$$

and the use of this inequality together with the Drude–Zener formulas (1) gives a correct expression for the slope of the linear segment of the phase. A more detailed analysis under the condition $g^2\ll\omega^2\ll\omega_p^2$ yields the initial ordinate θ_0 of the desired straight line:

$$\theta=2\omega/\omega_p\sqrt{\varepsilon_\infty}+\theta_0. \tag{6}$$

The constant θ_0 determined by the Drude parameters is positive and smaller in size (of the order of 10^{-3} rad) than the error limits for the experimental determination of the phase; at the same time, it is extremely sensitive to the low-

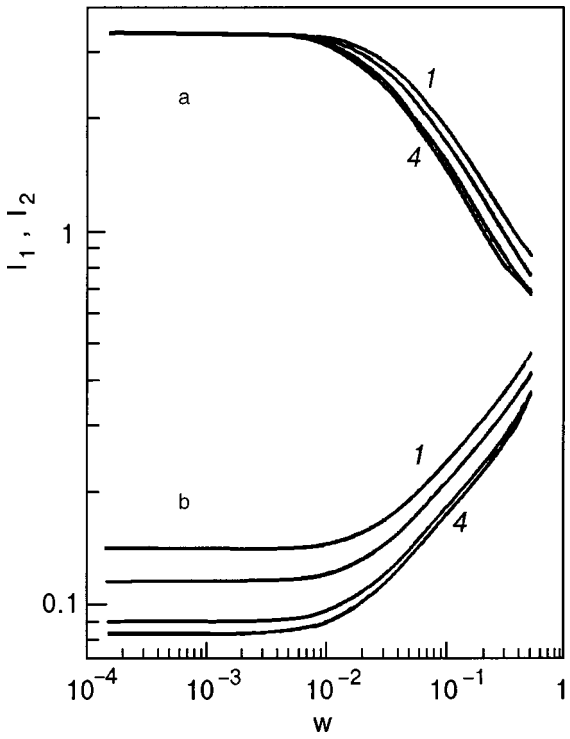

FIG. 4. Dependence on w of the coefficients l_1 (a) and l_2 (b) that determine the boundaries of the linear-phase region (7); curves *1–4* are correspond to the values $\varepsilon_\infty = 1$, 4/3, 4, and 20, respectively.

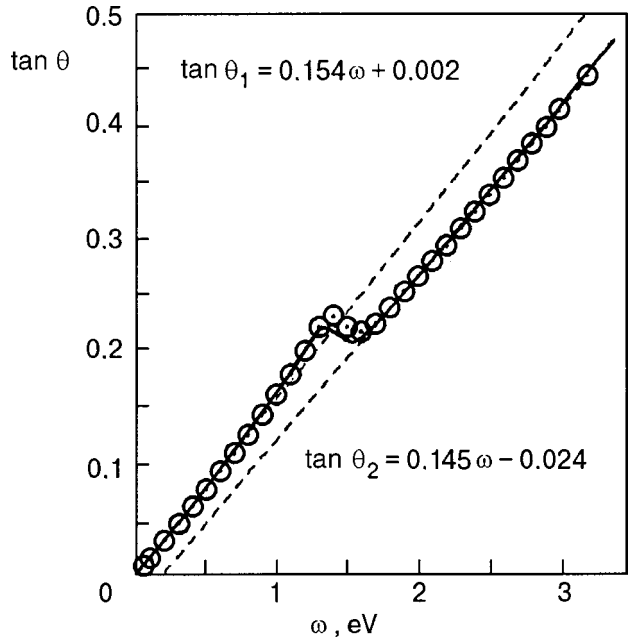

FIG. 5. Influence of interband transitions on the spectral behavior of the phase of reflection for aluminum: the experimental values of the phase (○), a linear approximation of the latter (– – –), a model including a Lorentzian oscillator and a correction for the effective mass after the interband transition (———).

frequency absorption bands, so that an experimental value $\theta_0 > \sim 10^{-2}$ (or $\theta_0 < 0$) can be indicative of the presence of such bands.

The real region of practically linear dispersion of the phase is quite wide (even for $\delta \sim 1\%$). Analysis shows that for values of w up to ~ 0.01 (i.e., for the majority of metals) ω_{L1} is directly proportional to the collision frequency a, while ω_{L2} is proportional to the plasma frequency (see Fig. 4):

$$\omega_{L1} \simeq l_1 g, \quad l_1 = \text{const} = 3.40, \quad \omega_{L2} \simeq l_2 \omega_p, \qquad l_2 = l_2(\varepsilon_\infty) \simeq (\varepsilon_\infty + 0.68)/12.5\varepsilon_\infty. \tag{7}$$

As w is increased from ~ 0.01 to ~ 0.1 the linear-phase region decreases in size by almost a factor of three, while the coefficient of its slope changes insignificantly.

Expression (6) can be useful, in particular, in a Kramers–Kronig analysis of the reflection spectra of metals, where it allows one to obtain reference values of the phase for calculating the coefficients of a high-frequency extrapolation of R; here one uses the known values of the conductivity and electron density.

In the spectral region $0.05\ \text{eV} < \omega < 0.5\ \text{eV}$ the fan of $\theta(\omega)$ curves in Fig. 3 can be divided up according to the number of valence electrons and the values of the plasma frequencies into three mutually nonintersecting narrow pencils. The spread of the values of the phase in each of the pencils relative to its axis does not exceed ~ 0.01 rad (i.e., it is of the order of the error in the determination of the phase in the Kramers–Kronig method), making it possible to use those values directly in the absence of conductivity data for the object under study. In a still narrower frequency interval ($\sim 0.05\ \text{eV} < \omega < \sim 0.1\ \text{eV}$) the following approximation relation holds to an accuracy of 0.01 rad for any metal with $g \leqslant 0.01$:

$$\theta[\text{rad}] \sim 0.30\omega[\text{eV}], \quad \sim 0.05\ \text{eV} < \omega < \sim 0.1\ \text{eV}. \tag{8}$$

We also note that in the linear-phase region the reflection decreases with frequency by a parabolic law, and the steepness of the fall increases with increasing g; for sufficiently small g the reflection can be considered constant: $r \simeq 1 - w/\sqrt{\varepsilon_\infty}$, $R \simeq 1 - 2w/\sqrt{\varepsilon_\infty}$. At the point ω_w determined by the condition $R''(\omega_w) = 0$, the difference between $(1-R)\sqrt{\varepsilon_\infty}/2$ and w does not exceed 0.01% for $w \leqslant 0.01$ and amounts to $\sim 1\%$ for $w = 0.1$.

THE ROLE OF THE OSCILLATORY CONTRIBUTION: DISPERSION OF THE PHASE OF THE REFLECTION FOR ALUMINUM

In real crystals the linear-phase region also narrows when local bands of interband transitions are superposed on the continuous absorption of free carriers; these local bands can distort the spectral dependence of the phase as shown in Fig. 3. The behavior of the phase for aluminum, the metal studied in the greatest detail in the optical region, is typical in this regard. For aluminum, with its high plasma frequency ($\omega_p \sim 15$ eV), condition (5) holds up to $\sim 0.97\omega_p$ (Ref. 37), whereas the linear trend of the phase is interrupted at $\sim 1\ \text{eV} \leqslant \omega \leqslant \sim 2$ eV, i.e., in the region of the intense band of interband absorption with a maximum near 1.5 eV[38,39] (see Fig. 5); a much weaker band near 0.5 eV, which is manifested as a slight kink of $\theta(\omega)$ at this point, can be observed on the scale of the figure.

The value of N/m^* (the ratio of the concentration of valence electrons N to the electron effective mass m^*) calculated from the slope κ of the linear part of the $\theta(\omega)$ curve

for aluminum is 12.5×10^{22} cm^{-3}, which agrees with the value $N=18.1\times10^{22}$ cm^{-3} determined by other methods when the known data on m^* are used (values ranging from 1.15 to 1.5 are given in Ref. 40). The value $2/\omega_p\sqrt{\varepsilon_\infty}=\kappa$ gives $\kappa_1\simeq0.154$ on the segment before the kink on the experimental $\theta(\omega)$ curve, and $\kappa_2\approx0.145$ after the kink (Fig. 5). The difference in the values of κ before and after the interband absorption band can be attributed to a difference in the effective masses in the $3s$ and $3p$ conduction bands of aluminum, at the transition between which a correction should be made to the slope coefficient of the straight line describing the dispersion of the phase. The values obtained for κ_1 and κ_2 give a ratio of the masses for the first and second straight lines of $m_1^*/m_2^*\approx1.13$, so that in units of the free electron mass one has $m_1^*\approx1.45$ and $m_2^*\approx1.28$ if a value $N=18.1\times10^{22}$ cm^{-3} is taken.

Analysis of the other curves in Fig. 3 confirms the conclusion reached for Al: local disruptions of the linear trend of $\theta(\omega)$ in the linear-phase region of metals are due to quantum transitions of electrons between subbands within the conduction band. Here weak transitions lead only to kinks in $\theta(\omega)$ without breaking the monotonic increase of the phase with frequency, while stronger absorption can give rise to a region of anomalous decrease (the extent of which is approximately equal to the half-width of the absorption band), which is especially large in Pt. Modeling the optical absorption band of aluminum by a Lorentzian oscillator of strength $A=4\pi ne^2/m^*\simeq22$ eV^2 with a frequency $\omega_0\simeq1.53$ eV and a damping $g\simeq0.37$ eV gives good agreement with experiment (Fig. 5) when the correction for the non-Lorentzian shape of the interband transitions is taken into account (the latter makes it necessary to use a different effective mass after the transition).

PLASMA REFLECTION EDGE

Let us now discuss the three remaining spectral regions of the five listed above. In region 5 the reflection is described by formula (2d), which contains only one Drude model parameter, ε_∞, and this is all the information that can be extracted in this case. The phase of the reflection at the intersection of regions 3 and 4 is characterized by formulas (2a), which contain ω_p and ε_∞, and these can also be used to find the Drude model parameters. Usually in region 3 — in the neighborhood of the frequency of the plasma oscillations of the current carriers — one studies the shape of the reflection[13,14] and characteristic energy loss[32,41] curves, which are well described in the Drude model, especially at small (semiconductors with $\omega_p\sim g$ and $\varepsilon_\infty\sim5$–30) or else large (metals, $\varepsilon_\infty\sim1$) concentrations of carriers. For them expressions (2b) and (2c) were obtained above, which describe the quantities under discussion here in the limit of an ideal metal (i.e., for $w=g/\omega_p\to0$), the maximum of the loss function L (2b) and the minimum of the reflection R (2c), and also the position of the plasma edge ω_b and the frequency ω_ε at which the dielectric function goes to zero (2b).

Frequency derivatives of the reflection

For the frequencies ω_b and ω_ε expressions (2b) hold to an error of less than 1% all the way to values $w\sim0.15$, and on further increase of g both frequencies rapidly decrease;

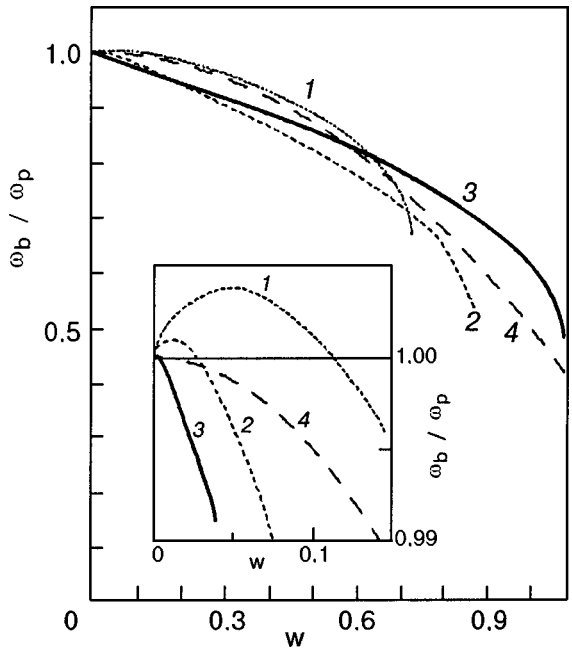

FIG. 6. Dependence on w of the frequency position of the plasma reflection edge ω_b. Curves *1–3* correspond to the values $\varepsilon_\infty=1$, 4, and 25, respectively, and curve *4* is the approximation $\omega_b/\omega_p=1-(w^2/2)$.

this, by the way, is what limits the similarity of their dependence on w. The ratio $\omega_\varepsilon(w)/\omega_p$ approaches unity as $\omega\to0$ and, independently of the values of ω_p and ε_∞, it decreases monotonically to 0 as $w\to1$, describing a regular circle:

$$\omega_\varepsilon(w)/\omega_p=(1-w^2)^{1/2},\quad 0\leqslant w\leqslant1. \tag{9}$$

The position of the frequency ω_b (its ratio to ω_p is shown in Fig. 6 for the values $\varepsilon_\infty=1$, 4, and 25) depends on w in a more complicated way which, moreover, is different for different ε_∞ and coincides with the plasma frequency only for $g=0$. With increasing g the value of ω_b/ω_p (see the inset in Fig. 6) initially increases, passes through a small maximum (the height and position of which are inversely proportional to the value of ε_∞), and then decreases monotonically and loses meaning at $w=w_{\rm lim}$ (the inflection point vanishes because of a transformation of the reflection line shape). In general the relation between ω_b/ω_p and w depends weakly on ε_∞ and is approximated to an accuracy of $\sim5\%$ by the quadratic dependence

$$\omega_b/\omega_p\simeq1-w^2/2,\quad 0<w<\sim0.7. \tag{10a}$$

In turn, the dependence of $w_{\rm lim}$ on ε_∞ shown in Fig. 7 is nontrivial: in the ''good'' metal region ($\varepsilon_\infty\sim1$) $w_{\rm lim}$ falls from $\simeq0.734$ at $\varepsilon_\infty=1$ to a minimum value $\simeq0.724$ near $\varepsilon_\infty=1.25$, and then it increases monotonically as ε_∞ is increased further. Starting at $\varepsilon_\infty\sim2$–3 and above, $w_{\rm lim}(\varepsilon_\infty)$ satisfactorily obeys the logarithmic law (see Fig. 7):

$$w_{\rm lim}(\varepsilon_\infty)\simeq0.108\ln\varepsilon_\infty+0.734. \tag{10b}$$

We note that at $w=w_{\rm lim}$ a spectral region of linear behavior of $R(\omega)$ appears, the extent of which can reach $2\omega_p/3$ or more (at the $\pm1\%$ level), and extrapolation of R to zero (at the point $\omega=\omega^*$) yields the plasma frequency (to an accuracy $\sim1\%$ for $\varepsilon_\infty<\sim4$) as

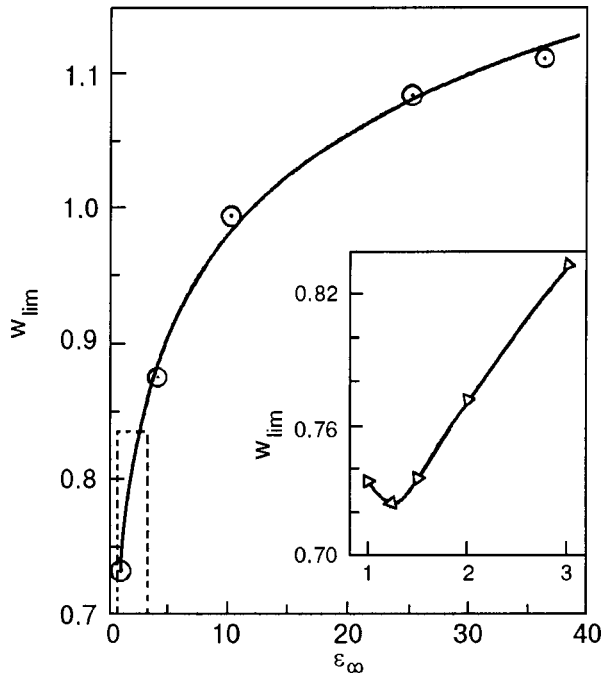

FIG. 7. Dependence on ε_∞ of the limiting value $w_{\lim}$ for the existence of the plasma reflection edge.

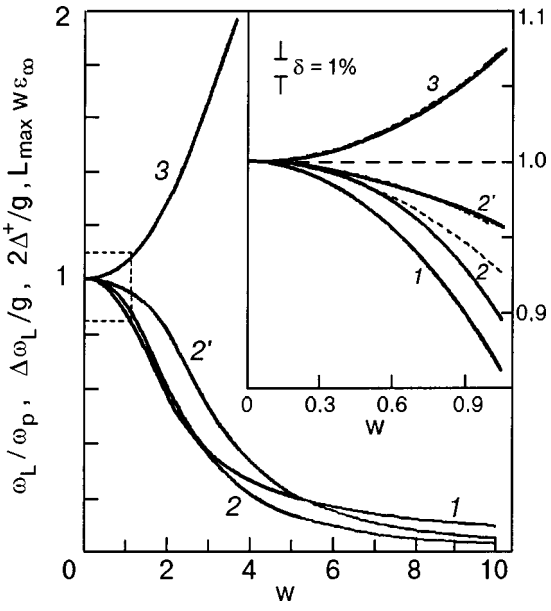

FIG. 8. Dependence on w of the loss function parameters ω_L, $\Delta\omega_L$, $2\Delta^+$, and $L_{\max}$ (curves *1*, *2*, *2′*, *3*, respectively) for the interval $0.1 \leqslant w \leqslant 10$; the ratios of these quantities to their values from Eq. (2b). The solid curves are calculated by the Drude formulas, the dashed curves show an approximation according to (11a).

$$\omega_p \simeq 0.9\omega^*. \tag{10c}$$

For practical use it is more convenient to make use of a fact observed in an analysis of the spectral dependence of the second derivative $d^2R/d\omega^2$, viz., that the frequency ω_{d2R} of its maximum is close to the plasma frequency:

$$\omega_p \simeq \omega_{d2R}; \quad \delta_{\max} \sim 5\%, \quad 0 < w < \sim 0.7. \tag{10d}$$

Thus, by using expressions (10a), (10c), and (10d), one can determine the parameters ω_p and g with an acceptable maximum error of $\sim 5\%$ from measurements of the reflection near the plasma reflection edge.

Energy loss function

For the energy loss function $L(\omega)$ the difference between the frequency ω_L of the maximum and ω_p is not more than one percent at values below $w \sim 0.3$ (and it does not exceed 13% for $w \sim 1$). The half-width and especially the maximum value of L are even less dependent on w: for them formulas (2b) hold to an accuracy of one percent below $w \sim 0.4$, and even at $w = 1$ the deviation is less than 11% for $\Delta\omega_L$ and 7% for $L_{\max}$. Thus formulas (2b) describe the parameters of the loss function to high accuracy for ''good'' metals (for which $w \sim 0.01$; Ref. 11), while for processing the spectra of certain alloys and other ''poor'' metals and of semiconductors they can only be used to make preliminary estimates. In such cases a substantial (by orders of magnitude) improvement in the accuracy can be achieved by taking the dependence of ω_L, $\Delta\omega_L$, and $L_{\max}$ on w into account even in a simple parabolic approximation of the form

$$F(w) = F(0)(1 + w^2/a), \tag{11}$$

where a has values of -8, -24, and 15 for ω_L, $\Delta\omega_L$, and $L_{\max}$, respectively; they hold to an accuracy of $\sim 0.1\%$ (Fig. 8) in the case of ω_L and $L_{\max}$ for w in the range from 0 to 1 and above, but only to $w \sim 0.3$ for $\Delta\omega_L$. This last circumstance is due to the fact that as w increases, the plasma peak shifts toward zero frequency, which limits the broadening of its low-frequency wing, and the peak becomes asymmetric as a result (the width $\Delta\omega_L$ is treated as the sum of a low-frequency part Δ^- and a high-frequency part $\Delta^+ > \Delta^-$ at half maximum). Here it turns out that for $2\Delta^+(w)$ an expression of the form (11) with $a \simeq -24$ holds to an accuracy of 0.1% to a value $w \sim 1$, i.e., an accuracy no worse than for ω_L and $L_{\max}$. As a result, we obtain a system of equations relating the Drude parameters and the shape of the experimental $L(\omega)$ curve to a rather high accuracy (of the order of 0.1% for $w \leqslant 1$):

$$\omega_L(w) \cong \omega_p(1 - w^2/8),$$

$$L_{\max}(w) \cong (1 + w^2/15)/w\varepsilon_\infty, \tag{11a}$$

$$2\Delta^+(w) \cong g(1 - w^2/24), \quad 0 < w < 1.$$

The first and last of Eqs. (11a) contain only ω_p and g as unknowns, so that one can eliminate g and solve the remaining equations numerically.

For $w > 1$ the accuracy of the simple formulas (11a) becomes lower, although it remains better than 1% up to $w \sim 1.5$. As we see in Fig. 1, in contrast to the R and θ curves, whose shapes become smeared for $w \sim 1$ (especially in the case $\varepsilon_\infty > 2$), the $L(\omega)$ peak remains well delineated. Because of this, one can extract information from it even above $w = 1$, although there it, too, suffers broadening, a red shift, and an increasing asymmetry. A technique for obtaining the parameters of the electronic system of conductors from the data of measurements of ω_L, $L_{\max}$, and Δ^+ for $w > 1$ is described in Appendix I (see also Fig. 9).

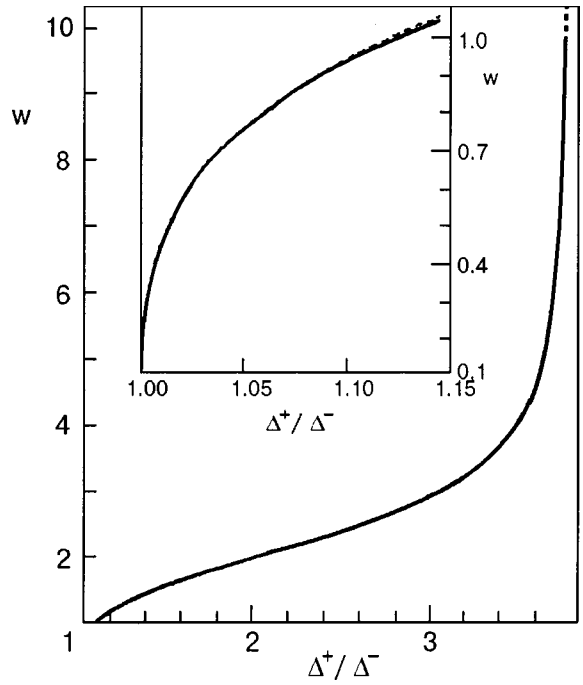

FIG. 9. Interrelationship between the asymmetry parameter Δ^+/Δ^- of the peak of the characteristic loss function $L(\omega)$ and the quantity $w=g/\omega_p$ (solid curves) and its approximation by expressions (AI.2) (the dashed curve, which is practically coincident with the solid curves on the scale of the figure).

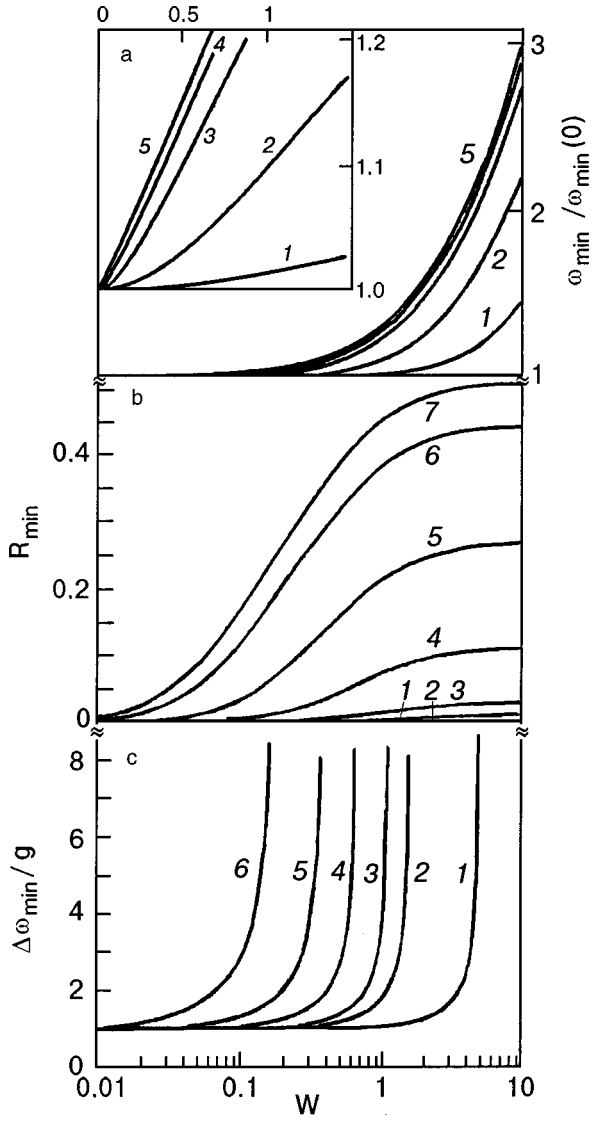

FIG. 10. Dependence on w of the characteristics of the minimum of R above the plasma edge: the spectral position ω_{min} for $\varepsilon_\infty=1.05$, 1.5, 4, 10, 36 (curves *1–5*, respectively) (a); the minimum value R_{min} for different ε_∞: 1.05 (*1*), 1.5 (*2*), 2 (*3*), 4 (*4*), 10 (*5*), 25 (*6*), and 36 (*7*) (b); the widths of the minimum $\Delta\omega_{min}$ at a level of $2R_{min}$ for various ε_∞: 1.05 (*1*), 1.5 (*2*), 2 (*3*), 4 (*4*), 10 (*5*), 36 (*6*) (c).

Reflection minimum

For determining the parameters of the Drude model it is of primary interest to use the characteristics of the reflection minimum above the plasma edge, w_{min}, R_{min}, and $\Delta\omega_{min}$, since they are relatively amenable to measurement. However, it turns out that they remain equal (within limits of $\sim 1\%$) to the values from expressions (2c) and (2b) only to $w\sim 0.01$, above which the value of g depends substantially on both w and ε_∞; this complicates the problem considerably and lowers the accuracy of the calculations in comparison with analysis of the loss peak. From Fig. 10, which shows the behavior of the ratios $\omega_{min}/\omega_{min}(0)$ and $\Delta\omega_{min}/g$ and of the minimum reflection R_{min} with increasing w for values of ε_∞ from 1.05 to 36, we see that all of these entities increase both with w and with ε_∞: R_{min} tends to a value R_∞, while ω_{min} and $\Delta\omega_{min}$ increase without bound ($\Delta\omega_{min}(w)$ has vertical asymptotes at $w=W(\varepsilon_\infty)$. In contrast to the loss function, the shape of the $R(\omega)$ curve even at $w\sim 1$ has become too smeared to permit experimental processing (see also Fig. 1), so that it makes sense to restrict the analysis of the latter to values below $w=1$. For metals, HTSCs, and other conductors with ε_∞ below ~ 4 the dependence on ε_∞ can be eliminated almost entirely by constructing the curves of $\Delta\omega_{min}/g$ and $R_{min}(w)/R_\infty$ as functions of $w(\varepsilon_\infty-1)^{1/2}$, and of $\omega_{min}(w)/\omega_{min}(0)$ (with greater error) as a function of $w[(\varepsilon_\infty-1)/(\varepsilon_\infty+1)]^{1/2}$ (Fig. 11a and 11b and Fig. 12, respectively).

The shape of the reflection minimum even at small values of g has a strong asymmetry (see Fig. 1), from an analysis of which one can obtain additional information about the Drude parameters and use this information in calculating them. For example, it has been found that over a wide interval of values of ε_∞ (from 1 to ~ 4) the product $w(\varepsilon_\infty-1)^{1/2}$ is uniquely determined by the ratio of the high-frequency component Δ^+_{min} of the width of the reflection minimum to the low-frequency component Δ^-_{min} (Fig. 11c). Moreover, the observed dependence can be expressed analytically (with an average error of $<4\%$) as

$$w(\varepsilon_\infty-1)^{1/2}\simeq 1.17[(x-1)/(x+0.1)]^{4/3},$$
$$x=\Delta^+_{min}/\Delta^-_{min}\ \ (1.1<x<30). \tag{12}$$

A technique for determining the Drude model parameters from reflection measurements with the use of relations (12), (10a), and (AII.1)–(AII.3) is set forth in Appendix II.

The behavior of the low-frequency component of the width of the reflection minimum with increasing g merits a separate analysis. This behavior is shown in Fig. 13 in the form of curves of $y=2\Delta^-_{min}/g$ versus w for values $\varepsilon_\infty=1.05$, 1.5, 2, 4, 10, and 36 (curves *1–6*, respectively). All

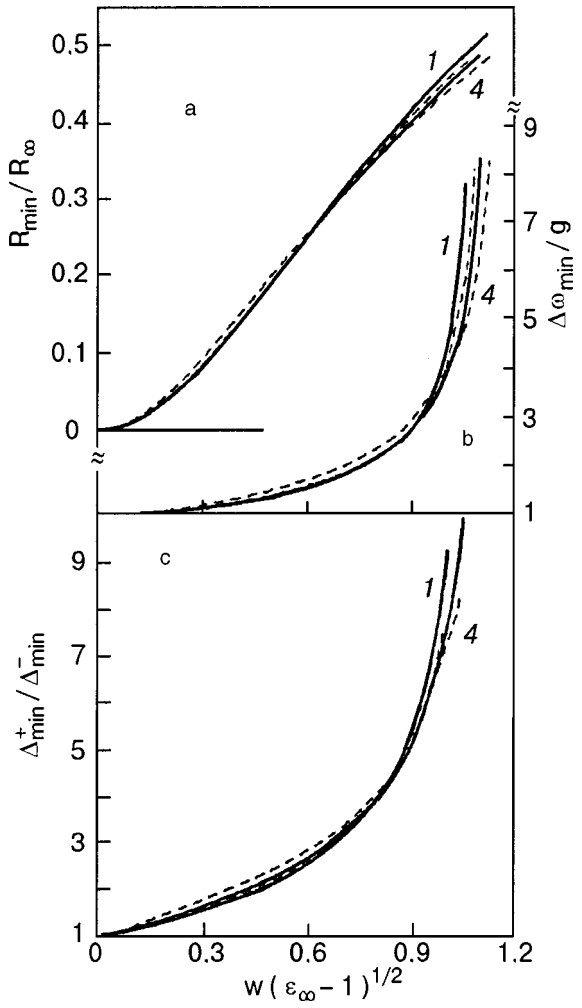

FIG. 11. Dependence on $w(\varepsilon_\infty-1)^{1/2}$ of those characteristics of the reflection minimum for which the choice of horizontal scale contains all the influence of ε_∞ beyond that given by expressions (2): R_{min}/R_∞ (a), $\Delta\omega_{min}/g$ (b); the asymmetry parameter $\Delta^+_{min}/\Delta^-_{min}$ (c). Curves *1–4* correspond to the values $\varepsilon_\infty=1.05$, 1.5, 2, and 4.

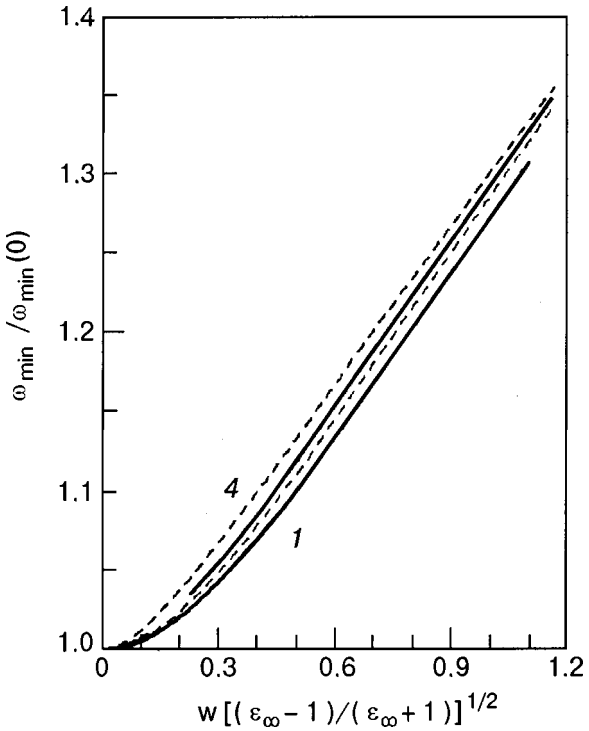

FIG. 12. Dependence on $w[(\varepsilon_\infty-1)/(\varepsilon_\infty+1)]^{1/2}$ of the spectral position of the reflection minimum with respect to $\omega_{min}(0)$. Curves *1–4* correspond to the values $\varepsilon_\infty=1.05$, 1.5, 2, and 4.

of the curves execute some kind of oscillations about $y=1$: emerging from a common point $y(0)=1$, they dip to a minimum of the same depth ($\simeq 0.85$) and then pass through a maximum (with an amplitude proportional to ε_∞) and again dip below $y=1$, nearly merging at a single point at a level $y\simeq 0.90$ near $w=5$; the positions of the two extrema are inversely proportional to ε_∞. It is remarkable that over wide intervals of values of ε_∞ (from 1 to ~ 4) and w (from 0 to ~ 7) the value of $2\Delta^-_{min}/g$ differs from 1 by not more than 15–20%, so that the following relation holds to the same accuracy:

$$g\simeq 2\Delta^-_{min} \qquad (13)$$

$$(\varepsilon_\infty<\sim 4; \quad g<\sim 7\omega_p).$$

In the case of normal metals ($\varepsilon_\infty<\sim 1.5$ and $g<\sim 0.1\omega_p$) the error in the above expression is an order of magnitude lower, so that the accuracy of determining g from Eq. (13) is limited mainly by the error of measurement of the reflection spectrum.

Thus it is more efficient to use relation (13) for determining g than relation (2b), since (13) holds over a wider range of variation of both w and the values of R_{min}: relations (2b) and (2c) have meaning under two restrictions on R_{min}, viz., $R_{min}<0.5$ and $R_{min}<R_\infty/2$, while relation (13) has only the weaker restriction $R_{min}<0.5$.

It should be noted that in a considerable number of real conductors the frequencies of rather intense interband transitions lie near ω_p and cause substantial dispersion $\varepsilon_\infty(\omega)$ in

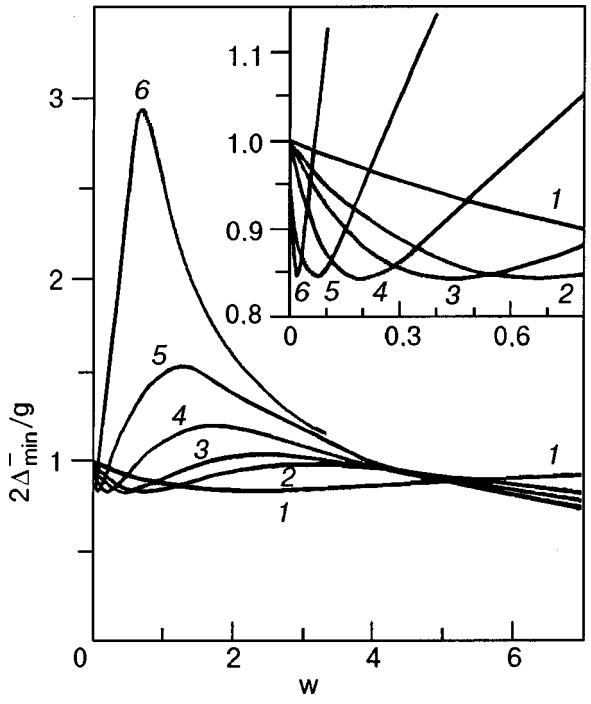

FIG. 13. Dependence on w of the low-frequency component Δ^-_{min} of the width of the reflection minimum. Curves *1–6* correspond to the values $\varepsilon_\infty=1.05$, 1.5, 2, 4, 10, and 36.

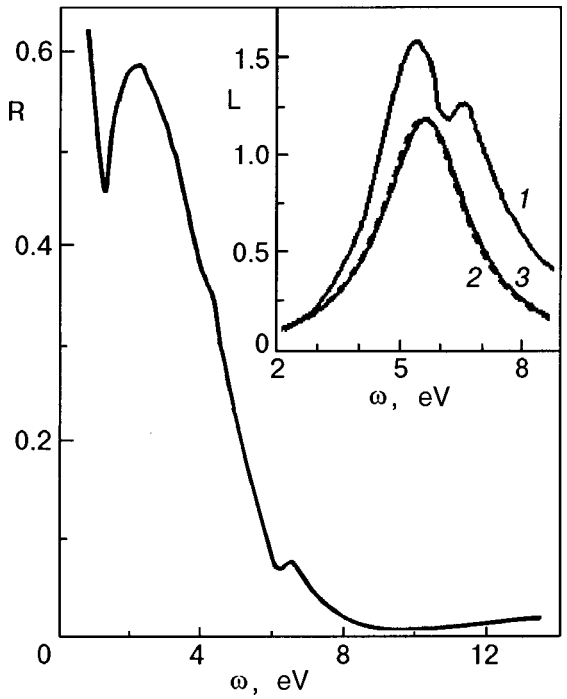

FIG. 14. Spectra of the reflection R and the loss function L (inset) of a U_2Zn_{17} film. Curve *1* is obtained by the Kramers–Kronig method, while curves *2* and *3* (curve *2* is the dashed curve, which is nearly coincident with the solid curve on the scale of the figure) were calculated from the Drude parameters determined from Eqs. (12), (13), and (10c) and Eqs. (12), (13), and (10d), respectively.

the region of the plasma reflection edge (this is shown for Ag in Ref. 42), as a result of which the use of formulas (9)–(13) is inefficient, since it requires introducing awkward corrections.

REFLECTION AND THE ENERGY LOSS FUNCTION OF U_2Zn_{17}

The reflection spectrum measured on a thin ($\sim$230 Å) film of U_2Zn_{17} in the interval 0.5–13 eV[43] was processed by the Kramers–Kronig method with the use of Eq. (6), Eqs. (11a), (13), and (10c), and Eqs. (11a), (13), and (10d) (Fig. 14) and yielded the following values of the Drude model parameters: $g=2.6$ eV, $\omega_p=5.7$ eV, and $\varepsilon_\infty=1.9$.

The loss function peaks calculated in different ways (inset in Fig. 14) are on the whole close in position and shape except for the additional maximum on curve *1*, which is due to interband transitions. Thus we have successfully eliminated the influence of the oscillatory contribution in finding the parameters of the system of itinerant electrons. This result, in view of the complexity of the electronic structure of the heavy-fermion antiferromagnet U_2Zn_{17}, attests to the efficiency of the technique developed in this paper for determining the Drude model parameters even for compounds of this type.

DOMAIN OF APPLICABILITY OF THE DRUDE MODEL

The Drude model, which is based on the assumption of free charge carriers, is applicable to conducting systems in which the current carriers are electrons belonging to broad bands of the *s* and *p* types, for which the concepts of a pseudopotential[44,45] and, accordingly, nearly free electrons are valid. This automatically rules out transition and noble metals[45] and their alloys and compounds, including those of the semiconductor type,[44] if the current carriers in the latter are *d* or *f* electrons (holes). Even for *s* and *p* systems, however, the three-parameter Drude model is, generally speaking, an extremely idealized scheme. The point is that each of the model parameters is fundamentally dependent on frequency. Some of the reasons for this are: ω_p varies with increasing excitation energy of the electrons on account of the nonparabolicity of the conduction bands, g varies because of the ''Cherenkov'' generation of quasiparticles (phonons, etc.[46]), and ε_∞ varies near the resonance frequencies of interband transitions. All of these factors can, in principle, be taken into account by introducing additional parameters, but that greatly complicates the use of the model in general form. One of the main provisions at the present time is to eliminate the ''constant background'' (i.e., the known spectral behavior) in analysis of the optical properties of conducting materials, making it possible to observe and study the mechanisms causing the changes in their electronic characteristics.

When using the Drude model parameters one should take into account the presence of limitations on the maximum values of w for metallic conductivity[47] and for conductivity via the fundamental and impurity bands of semiconductors.[3] According to Ref. 47, the change in the character of the conductivity (metallic to semiconductor) occurs when the room-temperature resistivity $\rho_{300\,\mathrm{K}}$ of the system exceeds a certain characteristic value ρ_c for the given class of system, where ρ_c lies in the range 100–200 $\mu\Omega\cdot$cm, i.e., for $\rho_c=150$ $\mu\Omega\cdot$cm and $\omega_p=5$ eV the temperature coefficient of the resistance for a system with $w>0.1\varepsilon_\infty$ will be negative. An estimate of the minimum conductivity $\sigma_{\min}$ of three-dimensional conductors gives 200 $\Omega^{-1}\mathrm{cm}^{-1}$ and for conductivity in purity zone is 12 $\Omega^{-1}\,\mathrm{cm}^{-1}$ (Ref. 3), which for $\omega_p=1$ eV gives maximum permissible values of $w_{\max}\approx 0.7\varepsilon_\infty$ and $w_{\max}\approx 10\varepsilon_\infty$, respectively. However, even before the system loses conductivity at absolute zero it is possible for a radical change to occur in the spectral dependence of the optical functions in the low-frequency region.[3,8]

CONCLUSIONS

The results of an analysis of the spectra of the optical functions of the Drude model over wide intervals of parameters ($0.001\leqslant W\leqslant 10$, $1\leqslant\varepsilon_\infty\leqslant 36$) have made it possible to determine the conditions for observing a number of the characteristic features of their behavior. In particular:

a) the square-root frequency dependence of the modulus and phase of the reflection holds in an interval $0\leqslant\omega\leqslant 0.02g$ for $w\leqslant 0.1$ with a tolerance of $\delta=0.01$;

b) the linear frequency dependence of the phase in the form $\theta=2\omega/\omega_p\sqrt{\varepsilon_\infty}+\theta_0$ in the region $g<\omega<\omega_p$ for $w\leqslant 0.01$ and $\delta=0.01$ is restricted to the interval $3.4g\leqslant\omega\leqslant 0.1\omega_p$;

c) the concept of the plasma reflection edge as the frequency of the maximum rate of rise of $R(\omega)$ is correct only for values of w not exceeding a certain value $w_{\lim}(\varepsilon_\infty)$.

The relations obtained (both for $\omega<\omega_p$ and for the region of plasma frequencies and the reflection minimum) de-

scribing the overall picture of the transformation of the characteristic features of the spectra upon changes in the Drude model parameters are useful in the Kramers–Kronig method and simplify the analysis of the experimental data for optical reflection and electron characteristic energy loss both in ''good'' metals and in materials with a strong temperature dependence of the electrical conductivity (semiconductors, doped and nonstoichiometric oxides, granular metallic films, and amorphous alloys).

The values obtained for the parameters of the electronic systems of Al and U_2Zn_{17} in comparison with the published data indicate the possibilities of the scheme proposed in this paper for analysis of the spectra of the optical functions (for Al the ratio of the concentration of the valence electrons to the effective mass, expressed in units of the free electron mass, is $N/m^*=12.5\times10^{22}$ cm^{-3}, the frequency of the first band of strong interband transitions is $\omega_0=1.53$ eV, the oscillator strength is 22 eV^2, and the half-width of the band is $g=0.37$ eV; for U_2Zn_{17} the plasma freqency is $\omega_p=5.7$ eV, and $\varepsilon_\infty=1.9$).

The authors are grateful to V. V. Eremenko and N. F. Kharchnko for their interest in and support of this study, and to A. A. Galuza for assistance in carrying it out.

This study was supported in part by the grants ISF No. U9L000 and ISF/UA No. U9L200.

APPENDIX I

Technique for calculating the Drude model parameters from experimental values of the parameters of the energy loss function

Below $w\sim10$ (to an accuracy of $\sim1\%$) the parameters ω_L, $2\Delta^+$, and $L_{\max}$ of the function $L(\omega)$ can be approximated by the polynomials

$$P_n^\alpha(w)=\sum A_i w^i, \quad i=0,1,\ldots,n(\alpha);$$

$$\alpha=\omega,L,\Delta; \quad n(\omega)=5, \quad n(L)=4, \quad n(\Delta)=6.$$

In this case relations (11) become

$$\omega_L(w)\cong\omega_p P_n^\omega(w), \quad L_m(w)\cong(w\varepsilon_\infty)^{-1}P_n^L(w),$$
$$2\Delta^+(w)\cong gP_n^\Delta(w), \tag{AI.1}$$

where the coefficients A_i for $1.5<w<10$ have the following values:

1.616, -0.8532, 0.2158, -0.02857, 1.908×10^{-3}, -5.072×10^{-5} for ω_L;

0.8920, 0.04210, 0.1013, -0.01007, 0.000368 for $L_{\max}$;

0.418945, 1.10685, -0.77719, 0.209238, -0.0280498, 1.86974×10^{-3}, -4.94383×10^{-5} for $2\Delta^+$.

A substantial simplification of the solution of the system of equations (11)–(A1.1) can be achieved by the following method. Consider the process of deformation (which will be characterized by the ratio Δ^+/Δ^-) of the function $L(w)$ with increasing w. The plot of $w(\Delta^+/\Delta^-)$ in Fig. 9 shows that the domain of Δ^+/Δ^- values is strictly bounded by the values $(\Delta^+/\Delta^-)_{\min}=1$ and $(\Delta^+/\Delta^-)_{\max}\simeq3.7322$, and the function itself is single-valued and admits the following approximation to an average error $\delta_{\rm av}$ of the order of 1% or less (the dashed curves in Fig. 9):

$$w(\Delta^+/\Delta^-)\simeq\begin{cases}A_1(x-1)^{1/3}+\sum_{i=2}^{6}A_i x^{i-2}, & 0,1<w<1, \quad \delta_{\rm av}\sim1\%;\\ \dfrac{B_1}{(3.7322-x)^{1/4}}+\sum_{i=2}^{6}B_i x^{i-2}, & 1<w<10, \quad \delta_{\rm av}\sim0.3\%.\end{cases} \tag{AII.2}$$

Here $A_i=2.01713$, -1408.5, 5213.5, -7231.7, 4455.5, -1028.8, and $B_i=2.8756$, -6.0338, 7.9701, -4.4584, 1.1500, and -0.1102, and $x=\Delta^+/\Delta^-$. Expression (AI.2) can be used to obtain the value of w immediately from the measured Δ^+/Δ^-, and substituting the value found into relation (11a) for $w<1.5$ or into (AI.1) for $w>1.5$ allows one to find the Drude parameters by a simple calculation. This solves the problem of determining the optical functions of conductors from the experimental values of $L(w)$ without the use of the Kramers–Kronig relations.

APPENDIX II

Technique for calculating the Drude model parameters from experimental values of the parameters of the plasma reflection minimum

By approximating the curves shown in Figs. 11 and 12 we obtain a system of equations for determining the Drude parameters ω_p, ε_∞, and g from the experimental values of $\omega_{\min}$, $R_{\min}$, and $\Delta\omega_{\min}$:

$$\Delta\omega_{\min}/g\simeq1+\tan^2 x, \quad x=w(\varepsilon_\infty-1)^{1/2},$$

$$w=g/\omega_p, \tag{AII.1}$$

$$R_{\min}/R_\infty\simeq\sum_{i=0}^{3}A_i x^i, \quad x=w(\varepsilon_\infty-1)^{1/2}, \tag{AII.2}$$

$$\omega_{\min}/\omega_p[\varepsilon_\infty/(\varepsilon_\infty-1)]^{1/2}\simeq\sum_{i=0}^{3}B_i x^i,$$
$$x=w[(\varepsilon_\infty-1)/(\varepsilon_\infty+1)]^{1/2}. \tag{AII.3}$$

Here $A_0=-0.02$, $A_1=0.0727$, $a_2=0.861$, $A_3=-0.488$, $B_0=1$, $B_1=0.09$, $B_2=0.39$, and $B_3=-0.18$.

Combining relations (12) and (10a) with equations (AII.1)–(AII.3) and solving the resulting system of overdetermined equations by the least-squares method will considerably improve the accuracy of determination of the Drude parameters from reflection measurements.

*E-mail: galuza@ilt.kharkov.ua

[1)] In the Russian-language literature the letter ''t'' is often omitted from the last name of H. A. Lorentz,[12,14,15,31] which leads to a certain confusion beetween this Nobel laureate from Holland and his Danish contemporary L. Lorenz, particularly in view of their overlapping scientific interests, as reflected in the Lorenz–Lorentz formula.[31]

[2)] The authors do not know of any cases where the linear dispersion of the phase in the Drude model has been studied by other investigators.

[1] N. F. Mott, *Metal–Insulator Transitions* [Taylor & Francis, London (1974); Nauka, Moscow (1979)].
[2] E. V. Kuz'min and S. G. Ovchinnikov, in *Physics of Magnetic Materials* [in Russian], Nauka, Novosibirsk (1983).
[3] N. F. Mott and E. A. Davis, *Electronic Processes in Non-Crystalline Materials* [Clarendon Press, Oxford (1971); Vol. 1, Mir, Moscow (1982)].
[4] É. L. Nagaev, *Physics of Magnetic Semiconductors* [in Russian], Nauka, Moscow (1979).
[5] N. F. Mott and E. A. Davis, *Electronic Processes in Non-Crystalline Materials* [Clarendon Press, Oxford (1971); Vol. 2, Mir, Moscow (1982)].
[6] É. L. Nagaev, Usp. Fiz. Nauk **166**, 833 (1996).
[7] V. M. Loktev and Yu. G. Pogorelov, Fiz. Nizk. Temp. **26**, 231 (2000) [Low Temp. Phys. **26**, 171 (2000)].
[8] Z. Simsa, Phys. Status Solidi B **96**, 581 (1979).
[9] P. Drude, Ann. Phys. (Leipzig) **1**, 566 (1900); **3**, 369 (1900).
[10] H. A. Lorentz, *The Theory of Electrons and Its Applications to the Phenomena of Light and Radiant Heat* [2nd ed., Dover, New York (1952); ONTI, Leningrad–Moscow (1934)].
[11] A. V. Sokolov, *Optical Properties of Metals* [in Russian], Fizmatgiz, Moscow (1961).
[12] P. Grosse, *Free Electrons in Solids*, Mir, Moscow (1982).
[13] T. S. Moss, *Optical Properties of Semi-Conductors* [Butterworths, London (1959); Izd. Inostr. Lit., Moscow (1961)].
[14] T. S. Moss, G. J. Burrell, and B. Ellis, *Semiconductor Opto-Electronics* [Butterworths, London (1973); Mir, Moscow (1976)].
[15] H. Y. Fan, *Photon–Electron Interaction: Crystals Without Fields* [Springer-Verlag, Berlin (1967); Mir, Moscow (1969)].
[16] P. Drude, Phys. Z. **1**, 161 (1900).
[17] Z. Schlesinger, R. T. Collins, D. L. Kaiser, and F. Holtzberg, Phys. Rev. Lett. **59**, 1958 (1987).
[18] I. Bozovic, D. Kirillov, A. Kapitulnik, K. Char, M. R. Hahn, M. R. Beasley, T. H. Geballe, Y. H. Kim, and A. J. Heeger, Phys. Rev. Lett. **59**, 2219 (1987).
[19] M. P. Petrov, A. I. Grachev, M. V. Krasin'kova, A. A. Nechitaĭlov, V. V. Poborchiĭ, S. I. Shagin, and S. V. Miridonov, JETP Lett. **50**, 29 (1989).
[20] I. Bozovic, K. Char, J. B. Yoo, A. Kapitulnik, M. R. Beasley, T. H. Geballe, Z. Z. Wang, S. Hagen, N. P. Ong, D. E. Aspnes, and M. K. Kelly, Phys. Rev. B **38**, 5077 (1987).
[21] J. Petzelt, S. Kamba, S. Pacesova, J. Sramek, O. Smrckova, and D. Sikorova, Phys. Status Solidi B **146**, 743 (1988).
[22] B. Coch, H. P. Geserich, and Th. Wolf, Solid State Commun. **71**, 495 (1989).
[23] A. I. Golovashkin, K. V. Kraĭskaya, and A. L. Shelekhov, Fiz. Tverd. Tela (Leningrad) **32**,175 (1990) [Sov. Phys. Solid State **32**, 98 (1990)].
[24] I. Ya. Fugol', V. N. Svishchev, and M. Yu. Libin, Fiz. Nizk. Temp. **24**, 195 (1998) [Low Temp. Phys. **24**, 145 (1998)].
[25] P. Wachter, B. Bucher, and R. Pittini, Phys. Rev. B **49**, 13164 (1994).
[26] Joseph Orenstein, G. A. Thomas, C. G. Rapkine, C. G. Bethea, B. F. Levine, R. J. Cava, E. A. Rietman, and D. W. Johnson, Jr., Phys. Rev. B **36**, 729 (1987).
[27] H. Nakano, and M. Imada, Technical Report of ISSP, Ser. A, N 3467 (1999).
[28] G. A. Thomas, H. K. Ng, A. J. Millis, R. N. Bhatt, R. J. Cava, E. A. Rietman, D. W. Johnson Jr., G. P. Espinosa, and J. M. Vandenberg, Phys. Rev. B **36**, 846 (1987).
[29] D. C. Mattis and J. Bardeen, Phys. Rev. **111**, 412 (1958).
[30] P. Kostic, Y. Okada, N. C. Collins, Z. Schlesinger, J. W. Reiner, L. Klein, A. Kapitulnik, T. H. Geballe, and M. R. Beasley, Phys. Rev. Lett. **81**, 2498 (1998).
[31] *Physics Encyclopedia* [in Russian], Sov. Éntsiklopediya, Moscow (1990), Vol. 2, p. 611.
[32] E. A. Bakulin and O. V. Konstantinov, in *Materials of the VI Winter School on the Physics of Semiconductors* [in Russian], Leningrad (1975), p. 51.
[33] P. Keil, Z. Phys. **214**, 251 (1968).
[34] W. E. Spicer, in *Optical Properties of Solids*, edited by F. Abeles, North-Holland Publishing Company, Amsterdam–London, 756 (1972).
[35] A. J. McAlister and E. A. Stern, Phys. Rev. **132**, 1599 (1963).
[36] J. M. Ziman, *Principles of the Theory of Solids* [Cambridge University Press (1964); Mir, Moscow (1974)].
[37] E. D. Palik (Ed.), *Handbook of Optical Constants of Solids*, Academic Press, New York (1985).
[38] L. G. Schulz, J. Opt. Soc. Am. **44**, 357 (1954).
[39] I. N. Shklyarevskiĭ and R. G. Yarovaya, Opt. Spektrosk. **16**, 85 (1964).
[40] H. Ehrenreich, H. R. Philipp, and B. Segall, Phys. Rev. **132**, 1918 (1963).
[41] H. Philipp and H. Ehrenreich, in *Optical Properties of Semiconductors*, Mir, Leningrad (1970), p. 103.
[42] V. K. Miloslavskiĭ and R. G. Yarovaya, Opt. Spektrosk. **21**, 708 (1966).
[43] A. I. Galuza, A. B. Beznosov, and V. V. Eremenko, *Abstracts of the IX All-Union Conference VUV-91* [in Russian], Tomsk (1991), p. 104.
[44] W. A. Harrison, *Electronic Structure and the Properties of Solids: The Physics of the Chemical Bond* [Freeman, San Francisco (1980); Dover, New York (1989); Mir, Moscow (1983)].
[45] V. Heine, M. L. Cohen, and D. Weaire, Solid State Physics, Vol. 24, edited by H. Ehrenreich, F. Seitz, and D. Turnbull (Academic Press, New York (1970) [Russian trans.] *Theory of the Pseudopotential* (Mir, Moscow, 1973).
[46] M. M. Noskov, *Optical and Magnetooptical Properties of Metals* [in Russian], UNTs AN SSSR, Sverdlovsk (1983).
[47] J. H. Mooij, Phys. Status Solidi A **17**, 521 (1973).

Translated by Steve Torstveit

QUANTUM EFFECTS IN SEMICONDUCTORS AND DIELECTRICS

Hydrodynamic fluctuations in a gas of quasiparticles

V. F. Aleksin†

Kharkov Physicotechnical Institute National Science Center, ul. Akademicheskaya 1, 61108 Kharkov, Ukraine

V. D. Khodusov*

V. N. Karazin Kharkov National University, pl. Svobody 4, 61077 Kharkov, Ukraine
(Submitted February 10, 2000; revised November 8, 2000)
Fiz. Nizk. Temp. **27**, 309–315 (March 2001)

The hydrodynamic fluctuations in a slightly nonideal gas of Bose quasiparticles with nonconservation of quasiparticle number are considered. The fluctuation dissipation theorem is used to find the spectral densities of the correlations of the fluctuations for the basic quantities characterizing the quasiparticle gas, which are expressed in terms of the kinetic coefficients. In the existence region of secondary waves in the gas of quasiparticles these spectral densities have a Lorentzian shape. For certain pure single crystals of cubic symmetry the temperature dependence of the resonant spectral density of energy fluctuations of the phonon gas are given, from which one can determine the temperature interval in which second sound waves exist. For NaF this interval agrees with the temperature region in which second sound is observed in experiment. [DOI: 10.1063/1.1355520]

INTRODUCTION

The fluctuations in a gas of Bose quasiparticles can be studied by different approaches: microscopic, based on the use of Green's functions,[1–5] and macroscopic, using the gasdynamic equations of the quasiparticles and the fluctuation dissipation theorem (FDT). The macroscopic approach was first proposed in Refs. 6 and 7 for studying the fluctuations in liquids, and in Ref. 8 it was applied to the study of fluctuations in the gas of quasiparticles in quantum liquids. In Refs. 1–5 the fluctuations in a phonon gas in insulators was considered with the use of Green's functions and the Hamiltonian for a single phonon branch of oscillations. The expressions obtained for the spectral densities of the correlation functions of the fluctuations were rather awkward and hard to analyze in the different limiting cases, in particular, in the hydrodynamic or gasdynamic limits. The hydrodynamic limit is of greatest interest for studying the fluctuations because of the presence of a resonant effect in the existence region of second sound waves. It would be natural and quite a bit simpler to investigate fluctuations in this region on the basis of the equations of phonon hydrodynamics.

In the review by Akhiezer *et al.*[9] the gasdynamics of quasiparticles is considered without taking fluctuations into account. Quasiparticle gasdynamics differs substantially from the particle gasdynamics, which is described by the Navier–Stokes equation,[10] in that the number of quasiparticles is not conserved in interaction processes. In addition, in the equations of quasiparticle gasdynamics an external friction force enters in due to the interaction of the quasiparticles with the external medium (umklapp processes, impurity scattering, etc.). Under certain conditions these equations describe weakly damped secondary waves of the second-sound type, which, in essence, are temperature or entropy waves, and the existence of coupled waves is possible, with the participation of the secondary waves. All of these differences affect the behavior of the fluctuations in a quasiparticle gas.

In this paper we investigate the hydrodynamic fluctuations in a gas of Bose quasiparticles (phonons, magnons, plasmons, etc.). We use the method proposed in Refs. 6 and 7 for studying hydrodynamic fluctuations in liquids; the method is based on the introduction of external random sources into the dissipative flows and the use of the FDT.[11–13]

Results are obtained for the spectral dependence of the hydrodynamic fluctuations, which are expressed in terms of the kinetic coefficients for a gas of quasiparticles and which, for some of them, have a Lorentzian shape in the existence region of the secondary waves; in particular, the spectral densities of the the square of the temperature and of the energy density of the quasiparticle fluctuations. Such behavior of the spectral densities can be made manifest by studying the evolution of thermal pulses and light scattering in the quasiparticle gas, where satellite peaks due to the secondary waves arise. The observation of these peaks in light scattering experiments in different quasiparticle gases can serve as evidence of the existence of secondary waves.

In phonon gasdynamics in the region of low temperatures the second-sound waves in solids have been observed experimentally in a study of the evolution of thermal pulses in pure single crystals of ^{4}He,[14] NaF,[15,16] and sapphire.[17] The reduced isotropic crystal model proposed in Ref. 9 has made it possible to determine the numerical values of the kinetic coefficients of phonon gasdynamics of specific crystals and to calculate the values of the spectral energies of the corre-

lations of fluctuations for specific crystals, in contrast to the qualitative values of the spectral density obtained in the microscopic approach in the gasdynamic limit with the use of Green's functions and a Hamiltonian with a single-phonon branch of oscillations. We conclude by presenting the temperature dependence of the resonant spectral density of energy fluctuations for some pure single crystals belonging to the cubic group, making it possible to establish the temperature region (window) in which second sound exists and to determine which of the crystals has the highest spectral density. For NaF crystals this temperature region is found to agree with that in which second sound has been observed experimentally.[15,16]

GASDYNAMIC FLUCTUATIONS IN A GAS OF QUASIPARTICLES WITH A NONCONSERVED NUMBER OF QUASIPARTICLES

For describing fluctuations in quasiparticle gasdynamics we shall start from the quasiparticle transport equations,[9] introducing external sources into them as is done in the theory of hydrodynamic fluctuations.[6,7]

The system of linear equations of gasdynamics with external sources $\mathbf{y}$ and y_4 for the quasiparticle drift velocity $\mathbf{u}$ and the relative temperature $\theta=(T-T_0)/T_0$ in the case when the number of quasiparticles is not conserved in their interaction has the form

$$\begin{aligned}&\tilde{\rho}_{ij}\dot{u}_j+S_0T_0\frac{\partial\theta}{\partial x_i}-\tilde{\eta}_{ijlm}\frac{\partial^2u_l}{\partial x_m\partial x_j}+r_{ij}u_j=y_i;\\&C_0\dot{\theta}+S_0\,\mathrm{div}\,\mathbf{u}-\tilde{\kappa}_{ij}\frac{\partial^2\theta}{\partial x_i\partial x_j}=y_4,\end{aligned}\tag{1}$$

where T_0 is the equilibrium temperature, $\tilde{\rho}_{ij}$ is a tensor having dimensions of mass density and characterizing the inertia of the quasiparticles, C_0 and S_0 are the equilibrium densities of the heat capacity and entropy, $\tilde{\eta}_{ijlm}$ and $\tilde{\kappa}_{ij}$ are the viscosity and hydrodynamic thermal conductivity tensors, respectively, and r_{ij} is the symmetric tensor of the external friction in the gas of quasiparticles. The values of these quantities in the kinetic theory of quasiparticles are presented in Ref. 9.

The general solution of system (1) is represented in the form of a sum of two solutions: a regular solution, which is the solution of the corresponding homogeneous system of equations with the boundary conditions, and an irregular solution, which is the solution of the inhomogeneous system of equations and which consists of linear functionals with respect to the external sources $\mathbf{y}$ and y_4.

In studying the fluctuations we shall consider an infinite spatially homogeneous medium and will assume that the external sources are random. In that case the regular solutions will be zero, and the irregular solutions will be random quantities, the mean values of which are equal to zero. The fluctuations of these quantities will be determined by the following space–time correlation functions:

$$\langle\theta(\mathbf{x}_1,t_1)\theta(\mathbf{x}_2,t_2)\rangle;\ \langle\theta_1(\mathbf{x}_1,t_1)u_i(\mathbf{x}_2,t_2)\rangle;$$

$$\langle u_i(\mathbf{x}_1,t_1)u_j(\mathbf{x}_2,t_2)\rangle,$$

which will depend on the differences $\mathbf{x}_2-\mathbf{x}_1=\mathbf{x}$ and $t_2-t_1=t$. These correction fluctuations will also be determined by the linear functionals of the correlation functions of the random sources $\mathbf{y}$ and y_4, which are found with the help of the FDT.[12]

Let us introduce the spectral energies of the correlation functions defined by the following Fourier transformations for the space–time functions $A(\mathbf{x},t)$:

$$A(\mathbf{x},t)=\int A(\mathbf{k},\omega)\exp(i(\mathbf{kx}-\omega t))d\mathbf{k}d\omega.\tag{2}$$

For the correlation function of two random functions $A(\mathbf{x}_1,t_1)$ and $B(\mathbf{x}_2,t_2)$ we have

$$\langle A(\mathbf{x}_1,t_1),B(\mathbf{x}_2,t_2)\rangle=\int\langle AB\rangle_{\mathbf{k}\omega}\exp(i(\mathbf{kx}-\omega t))d\mathbf{k}d\omega,\tag{3}$$

where $\langle AB\rangle_{\mathbf{k}\omega}$ is the spectral density of the correlation function. If the Fourier components of A and B are known, then their correlation functions are related to the spectral density by the relation

$$\langle A(\mathbf{k},\omega),B(\mathbf{k}',\omega')\rangle=\langle AB\rangle_{\mathbf{k},\omega}\delta(\mathbf{k}+\mathbf{k}')\delta(\omega+\omega').\tag{4}$$

After using the FDT we obtain the following expressions for the spectral densities of the correlation functions of the random quantities $\mathbf{y}$ and y_4:

$$\begin{aligned}&\langle y_4,y_i\rangle_{\mathbf{k},\omega}=0;\quad\langle y_4^2\rangle_{\mathbf{k},\omega}=c(\omega)\frac{k^2\tilde{\kappa}}{T_0};\\&\langle y_i,y_j\rangle_{\mathbf{k},\omega}=c(\omega)(r_{ij}+k^2\tilde{\eta}_{ij}),\end{aligned}\tag{5}$$

where $c(\omega)=\hbar\omega/(2\pi)^4\coth(\hbar\omega/2T_0)$, and $\tilde{\kappa}$ and $\tilde{\eta}_{ij}$ denote the contractions of the tensors $\tilde{\kappa}_{ij}$ and $\tilde{\eta}_{ijlm}$ with the unit vector $\mathbf{n}=\mathbf{k}/k$ in the form $\tilde{\kappa}=\tilde{\kappa}_{ij}n_in_j$; $\tilde{\eta}_{ij}=\tilde{\eta}_{iljm}n_in_m$. In an isotropic medium $\tilde{\eta}_{ij}=(\tilde{\xi}+(4/3)\tilde{\eta})n_in_j+\tilde{\eta}(\delta_{ij}-n_in_j)$, and $\tilde{\eta}$ and $\tilde{\xi}$ are the first and second viscosity coefficients, respectively.

Applying the Fourier transformation (2) to the system (1), we obtain a system of linear algebraic equations for the Fourier components $\mathbf{u}_{\mathbf{k},\omega}$ and $\theta_{\mathbf{k},\omega}$:

$$\begin{aligned}&a_{lj}u_j-STk_l\theta=iy_l;\\&(\omega C+ik^2\tilde{\kappa})\theta-S(\mathbf{k},\mathbf{u})=iy_4,\end{aligned}\tag{6}$$

with the symmetric tensor a_{lj}:

$$a_{lj}=\omega\tilde{\rho}_{lj}+i(r_{lj}+k^2\tilde{\eta}_{lj}).\tag{7}$$

From here on we have dropped the subscript zero on the equilibrium quantities and the indices of the Fourier components.

On the real ω axis in the case of dissipative systems the tensor a_{lj} is nondegenerate ($\mathrm{Det}\|a_{ij}\|\neq0$) and has an inverse a_{lj}^{-1}, and therefore the solution of the system of equations (6) can be written in the form

$$\theta=\frac{i}{D}(y_4+Ska_j^{-1}y_j);\quad u_j=STk\theta a_j^{-1}+ia_{jl}^{-1}y_l,\tag{8}$$

where D is the determinant of system (8):

$$D=(\omega C+i\tilde{\kappa}k^2)-k^2S^2Ta^{-1},\tag{9}$$

and $a_i^{-1}=a_{ij}^{-1}n_j$ and $a^{-1}=a_{ij}^{-1}n_in_j$ are the contractions of the tensor a_{ij}^{-1}.

Using expression (8), we find the spectral densities of the correlation functions of the fluctuations of the fields θ and $\mathbf{u}$:

$$\langle\theta^2\rangle_{\mathbf{k},\omega}=-\frac{c(\omega)}{T}\,\mathrm{Im}\left\{\frac{1}{D}\right\};$$

$$\langle u_j\theta\rangle_{\mathbf{k},\omega}=-c(\omega)kS\,\mathrm{Im}\left\{\frac{a_i^{-1}}{D}\right\}; \tag{10}$$

$$\langle u_iu_j\rangle_{\mathbf{k},\omega}=-c(\omega)\mathrm{Im}\left\{\frac{a_i^{-1}a_j^{-1}}{D}S^2Tk^2+a_{ij}^{-1}\right\}.$$

In the derivation of these expressions we have used the relation

$$r_{ij}+k^2\tilde{\eta}_{ij}=\frac{1}{2i}(a_{ij}-a_{ij}^*).$$

The spectral density of the energy of the fluctuations is given by the expression

$$\langle\delta U\rangle_{\mathbf{k},\omega}=\frac{CT}{2}\langle\theta^2\rangle_{\mathbf{k},\omega}+\frac{\tilde{\rho}_{ij}}{2}\langle u_iu_j\rangle_{\mathbf{k},\omega}. \tag{11}$$

We note that the entropy fluctuation $\delta S=S-S_0$ is related to the fluctuation of θ as $\delta S=C\theta$ (Ref. 9), and the spectral density of the entropy correlation function obeys the relation $\langle(\delta S)^2\rangle_{\mathbf{k},\omega}=C^2\langle\theta^2\rangle_{\mathbf{k},\omega}$.

At low viscosities, when $r_{ij}+k^2\tilde{\eta}_{ij}\ll\omega\tilde{\rho}_{ij}$, the tensor a_{ij}^{-1} is given approximately by

$$a_{ij}^{-1}\approx\frac{1}{\omega}\tilde{\rho}_{ij}^{-1}-\frac{i}{\omega^2}\tilde{\rho}_{il}^{-1}(r_{lm}+k^2\tilde{\eta}_{lm})\tilde{\rho}_{mj}^{-1}. \tag{12}$$

In this case the determinant D in Eq. (9) can be written in the form

$$D=\frac{a^{-1}C}{\tilde{\rho}^{-1}}(\omega^2-\Omega^2+2i\omega\Gamma_\parallel), \tag{13}$$

where $\Omega=kW_\parallel$; $W_\parallel=[(TS/C)\tilde{\rho}^{-1}]^{1/2}$;

$$\Gamma_\parallel=\frac{1}{2\tilde{\rho}^{-1}}[\tilde{\rho}_j^{-1}(r_{ij}+k^2\tilde{\eta}_{il})\tilde{\rho}_l^{-1}]+\frac{k^2}{2C}\tilde{\kappa}; \tag{14}$$

$\tilde{\rho}_j^{-1}$ and $\tilde{\rho}^{-1}$ are the contractions of the tensor ρ_{ij}^{-1}, i.e., $\tilde{\rho}_j^{-1}=\tilde{\rho}_{jl}^{-1}n_l$, $\tilde{\rho}^{-1}=\tilde{\rho}_{ij}^{-1}n_in_j$. Under certain conditions, viz., in the so-called existence window of the secondary waves, the quantities Ω, $W_\parallel$, and $\Gamma_\parallel$, respectively, determine the frequency, velocity, and damping coefficient of secondary waves.[9] In this case the spectral densities have a Lorentzian form:

$$\langle\theta^2\rangle_{\mathbf{k},\omega}=\frac{c(\omega)}{T}\,\frac{\omega}{C}\,\frac{2\omega\Gamma_\parallel}{(\omega^2-\Omega^2)^2+4\omega^2\Gamma_\parallel^2};$$

$$\langle u_i\theta\rangle_{\mathbf{k},\omega}=\frac{TSk\tilde{\rho}_i^{-1}}{\omega}\langle\theta^2\rangle_{\mathbf{k},\omega}; \tag{15}$$

$$\langle u_iu_j\rangle_{\mathbf{k},\omega}=CT\,\frac{\Omega^2}{\omega^2}\,\frac{\tilde{\rho}_i^{-1}\tilde{\rho}_j^{-1}}{\tilde{\rho}^{-1}}\langle\theta^2\rangle_{\mathbf{k},\omega};$$

$$\langle\delta U\rangle_{\mathbf{k},\omega}=\frac{CT}{2}\langle\theta^2\rangle_{\mathbf{k},\omega}\left(1+\frac{\Omega^2}{\omega^2}\right).$$

In an ideal medium, when the aforementioned kinetic coefficients go to zero ($\Gamma_\parallel\to0$), it follows from (15) that in the frequency region $\omega=\pm\Omega$ the spectral densities have a δ-functionlike character:

$$\langle\theta^2\rangle_{\mathbf{k},\omega}=\frac{\pi c(\omega)}{2CT}(\delta(\omega-\Omega)+\delta(\omega+\Omega)).$$

Let us consider another limiting case, that when $\omega\tilde{\rho}_{ij}\ll r_{ij}+k^2\tilde{\eta}_{ij}$ and the external friction r plays a governing role. The tensor a_{ij}^{-1} in this case has the following form in the linear approximation in the parameter $\omega\tilde{\rho}/r$:

$$a_{ij}^{-1}=-ir_{ij}^{-1}+\omega r_{im}^{-1}\tilde{\rho}_{ml}r_{lj}^{-1}. \tag{16}$$

The tensor r_{ij}^{-1} is related to the static thermal conductivity tensor κ_{ij} by the relation $\kappa_{ij}=TS^2r_{ij}^{-1}$ (Ref. 9), and therefore

$$a_{ij}^{-1}=-\frac{i}{TS^2}\left(\kappa_{ij}+\frac{i\omega}{TS^2}\kappa_{im}\tilde{\rho}_{ml}\kappa_{mj}\right). \tag{17}$$

One can show that the second term in (17) is small if $(kl_\kappa)^2\ll1$, where $l_\kappa=CW_\parallel\kappa$ is the mean free path of the quasiparticles with respect to the external friction. Then the determinant D has the form

$$D=C\omega+ik^2(\kappa+\tilde{\kappa}), \tag{18}$$

and the spectral densities of the correlation functions are as follows:

$$\langle\theta^2\rangle_{\mathbf{k},\omega}=\frac{c(\omega)}{T}\,\frac{k^2(\kappa+\tilde{\kappa})}{(C\omega)^2+k^4(\kappa+\tilde{\kappa})^2};$$

$$\langle u_i\theta\rangle_{\mathbf{k},\omega}=\frac{c(\omega)k\omega}{TS}\,\frac{C\kappa_i}{(C\omega)^2+k^4(\kappa+\tilde{\kappa})^2}; \tag{19}$$

$$\langle u_iu_j\rangle_{\mathbf{k},\omega}=\frac{c(\omega)}{TS^2}\left\{\kappa_{ij}-\frac{k^4\kappa_i\kappa_j(\kappa+\tilde{\kappa})}{(C\omega)^2+k^4(\kappa+\tilde{\kappa})^2}\right\},$$

where $\kappa=\kappa_{ij}n_in_j$; $\kappa_i=\kappa_{ij}n_j$. We note that in this case $\langle\theta^2\rangle_{\mathbf{k},\omega}$ is equal to the spectral density of the correlation function of the temperature in an elastic anisotropic medium with allowance for the thermal conductivity of the phonon gas $\kappa_{ij}+\tilde{\kappa}_{ij}$.

SPECTRAL DENSITY OF THE CORRELATION FUNCTION OF THE HYDRODYNAMIC FLUCTUATIONS IN AN ISOTROPIC MEDIUM

Let us investigate the basic properties of the hydrodynamic fluctuations in quasiparticle gasdynamics for the particular example of an isotropic medium. In an isotropic medium the tensor a_{ij} can be written in the form

$$a_{ij}=a_1n_in_j+a_2(\delta_{ij}-n_in_j), \tag{20}$$

and the inverse tensor a_{ij}^{-1} can be obtained without any approximations:

$$a_{ij}^{-1}=a_1^{-1}n_in_j+a_2^{-1}(\delta_{ij}-n_in_j),$$

where $a_1=\omega\tilde{\rho}+ir+ik^2(\tilde{\xi}+\frac{4}{3}\tilde{\eta})$, $a_2=\omega\tilde{\rho}+ir+ik^2\tilde{\eta}$. The determinant D in (9) in this case will be equal to $(C\tilde{\rho}/a_1)\Delta$, where

$$\Delta=\left[\left(\omega+ik^2\frac{\tilde{\kappa}}{C}\right)\left(\omega+i\frac{r}{\tilde{\rho}}+i\frac{k^2}{\tilde{\rho}}\left(\tilde{\xi}+\frac{4}{3}\tilde{\eta}\right)\right)-\Omega^2\right]. \quad (21)$$

We introduce the following notation for the characteristics of the dissipative processes: the frequency $\nu_r=r/\tilde{\rho}$, which governs the relaxation of the quasiparticle drift velocity **u** as a result of the external friction, and the diffusion times for the energy ($\tau_{\tilde{\kappa}}$) and momentum ($\tau_{\tilde{\eta}}$ and $\tilde{\tau}$) of the quasiparticles owing to their interaction:[9]

$$\tau_{\tilde{\kappa}}=\frac{\tilde{\kappa}}{CW_\parallel^2}; \quad \tau_{\tilde{\eta}}=\frac{\tilde{\eta}}{\tilde{\rho}}W_\parallel^2\}; \quad \tilde{\tau}=\frac{(\xi^2+\frac{4}{3}\tilde{\eta})}{\tilde{\rho}W_\parallel^2}. \quad (22)$$

In an isotropic medium it is natural to introduce the longitudinal $y_\parallel$, $u_\parallel$ and transverse $y_\perp$, $u_\perp$ components of the vectors **y** and **u** with respect to the direction of the vector **k**. The spectral densities of the correlation functions of the random quantities $y_\parallel$ and $y_\perp$ are

$$\langle y_\parallel^2\rangle_{\mathbf{k},\omega}=c(\omega)\tilde{\rho}(\nu_r+\Omega^2\tilde{\tau});$$
$$\langle y_{i\perp}y_{j\perp}\rangle_{\mathbf{k},\omega}=c(\omega)\tilde{\rho}(\nu_r+\Omega^2\tau_{\tilde{\eta}})(\delta_{ij}-n_in_j). \quad (23)$$

The longitudinal and transverse components $y_\parallel$ and $y_\perp$ are uncorrelated, i.e., $\langle y_\parallel y_{\perp i}\rangle_{\mathbf{k},\omega}=0$.

For θ, $u_\parallel$, and $u_\perp$ we find

$$\langle\theta^2\rangle_{\mathbf{k},\omega}=-\frac{c(\omega)}{CT}\mathrm{Im}\left\{\frac{\omega+i(\nu+\nu')}{\Delta}\right\};$$
$$\langle u_\parallel^2\rangle_{\mathbf{k},\omega}=-\frac{c(\tilde{\omega})}{\tilde{\rho}}\mathrm{Im}\left\{\frac{\omega+i(\nu-\nu')}{\Delta}\right\}; \quad (24)$$
$$\langle u_{i\perp}u_{j\perp}\rangle_{\mathbf{k},\omega}=-\frac{c(\omega)}{\rho}(\delta_{ij}-n_in_j)\mathrm{Im}\left\{\frac{1}{\omega+i\nu_r+i\Omega^2\tau_{\tilde{\eta}}}\right\};$$
$$\langle u_\parallel\theta\rangle_{\mathbf{k},\omega}=-\frac{Skc(\omega)}{C\tilde{\rho}}\mathrm{Im}\left\{\frac{1}{\Delta}\right\};$$
$$\langle u_{i\perp}u_\parallel\rangle_{\mathbf{k},\omega}=0; \quad \langle u_{i\perp}\theta\rangle_{\mathbf{k},\omega}=0,$$

where $\Delta=(\omega+i\nu)^2-(\Omega^2-\nu'^2)$;

$$\nu=\frac{1}{2}(\nu_r+\Omega^2(\tilde{\tau}+\tilde{\tau}_\kappa)); \quad \nu'=\frac{1}{2}(\nu_r+\Omega^2(\tilde{\tau}-\tilde{\tau}_\kappa)). \quad (25)$$

The energy density is given by $\delta U=\delta U_\parallel+\delta U_\perp$, where $\delta U_\parallel=1/2(CT\theta^2+\tilde{\rho}u_\parallel^2)$, and $\delta U_\perp=(1/2)\tilde{\rho}u_\perp^2$. The spectral density of the energy of fluctuations has the form

$$\langle\delta U_\parallel\rangle_{\mathbf{k},\omega}=-c(\omega)\mathrm{Im}\left\{\frac{\omega+i\nu}{\Delta}\right\};$$
$$\langle\delta U_\perp\rangle_{\mathbf{k},\omega}=-c(\omega)\mathrm{Im}\left\{\frac{1}{\omega+i\nu_r+i\Omega^2\tau_{\tilde{\eta}}}\right\}. \quad (26)$$

In the existence region of the secondary waves, which is determined by the condition $\min(1/\tau_{\tilde{\kappa}};1/\tilde{\tau})\gg\Omega\gg\nu_r$, the spectral density $\langle\delta U_\parallel\rangle_{\mathbf{k},\omega}$ has a Lorentzian shape, and there is no spectral density $\langle\delta U_\perp\rangle_{\mathbf{k},\omega}$.

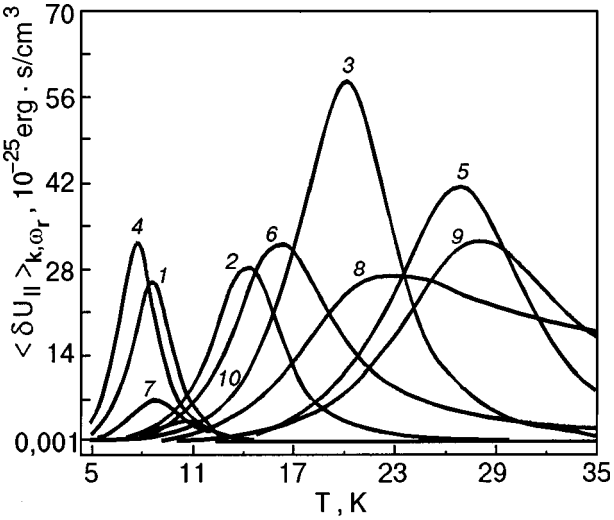

FIG. 1. Temperature dependence of the resonant spectral density of fluctuations of the phonon energy $\langle\delta U_\parallel\rangle_{\mathbf{k},\omega}$ for various crystals: NaCl (*1*), NaF (*2*), LiF (*3*), KCl (*4*), MgO (*5*), GaAs (*6*), InSb (*7*), YIG (*8*), Si (*9*), Ge (*10*).

CONCLUSION

In Ref. 9 in the reduced isotropic crystal model the values of the kinetic coefficients of the phonon gasdynamics were calculated in the low-temperature region for the following pure single crystals belonging to the cubic system: NaCl, NaF, LiF, KCl, MgO, GaAs, InSb, YIG, Si, and Ge. Let us use the handbook data[18] for these crystals to calculate the phonon heat capacity C, entropy S, density $\tilde{\rho}$, and the second-sound velocity $W_\parallel$. If the dimensions of the crystals are of the order of 1 cm (it is in NaF crystals of such dimensions that the second sound has been observed experimentally), then the wave vector of the second sound $k=2\pi$ cm^{-1}. Substituting these values into Eq. (26), we obtain the spectral density of the fluctuations of the phonon energy as a function of temperature and frequency. As an example, let us give the values of these quantities for NaF: density $\rho=2.801$ g/cm^3; $\nu_t=5.64\times10^5$ cm/s; $\nu_l=3.31\times10^5$ cm/s; phonon density $\tilde{\rho}=7.06\times10^{-11}T^4$ g/cm^3; $\tilde{n}=0.203T^{-1}$ g/(cm·s); $C=3S=24.3T^3$ erg/cm^{3}K; $W_\parallel=1.96\times10^5$ cm/s; $\tilde{\kappa}=7.19\times10^{12}T^{-2}$ erg/(cm·s·K); $\nu_r=4.3\times10^{15}T^{-3}\exp\times(-220/T)[1+10^{-3}T^2\exp(-12/T)]$ s^{-1}, and $\Omega=1.23\times10^6$ s^{-1}.

In an isotropic medium the spectral densities (26) of the energy of the fluctuations in a gas of quasiparticles have their maximum value at the frequency $\omega_r=\Omega[1+\tilde{\tau}_{\tilde{\kappa}}(\nu_r+\Omega^2\tilde{\tau})]^{1/2}$, which is the frequency of the second-sound wave with allowance for the dissipative corrections. Figure 1 shows the temperature dependence of the resonant spectral densities of the energy fluctuations at a frequency $\omega=\omega_r$ for certain crystals of the cubic system, each of which has a Lorentzian shape and indeed determines a temperature existence window for second sound. Let us check this out for the particular example of NaF (curve *2* in Fig. 1). We see that the existence region of second sound lies in the interval 9–16 K. This coincides with the temperature interval in which second sound has been observed experimentally.[15,16] Indeed, from the form of the frequency dependence of the spectral density of the energy fluctuations for NaF at temperatures of

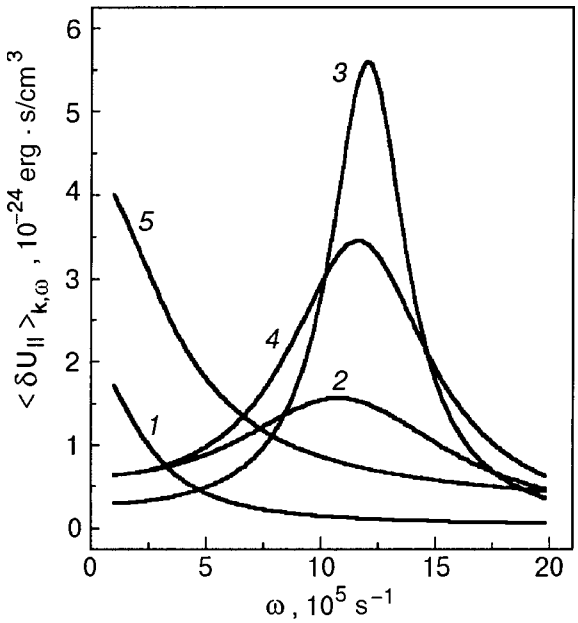

FIG. 2. Spectral density of fluctuations of the phonon energy $\langle \delta U_{\parallel} \rangle_{\mathbf{k},\omega}$ for NaF as a function of frequency in the neighborhood of the second-sound frequencies for different temperatures T [K]: 6 (*1*), 10 (*2*), 13.3 (*3*), 15 (*4*), 18 (*5*).

6, 10, 13.33, 15, and 18 K it follows that they have a Lorentzian shape in the vicinity of the second-sound frequency for the temperatures 10, 13.33, and 15 K (see Fig. 2). For NaF the curve of the resonant spectral density of the phonon energy has a maximum at a temperature of 13.33 K. This coincidence of the temperature regions in which second sound exists for NaF serves to confirm that the reduced isotropic crystal model proposed in Ref. 9 is the closest to real crystals.

It follows from an analysis of the curves in Fig. 1 that the highest value of the resonant spectral density of fluctuations of the phonon energy is for LiF crystals, and the lowest is for Ge.

Knowing the spectral densities of the correlation functions of the fluctuations, one can find the space and time correlation functions of the fluctuations.

This study was supported by the STCU (Project No. 1499).

†Deceased
*E-mail: khodusov@pem.kharkov.ua

[1] P. C. Kwok, P. C. Martin, and P. B. Miller, Solid State Commun. **3**, 181 (1965).
[2] P. C. Kwok and P. C. Martin, Phys. Rev. **142**, 495 (1966).
[3] A. Griffin, Rev. Mod. Phys. **40**, 167 (1968).
[4] R. K. Wehner and R. Klein, Physica **62**, 161 (1972).
[5] R. A. Cowley, Adv. Phys. **12**, 421 (1963).
[6] L. D. Landau and E. M. Lifshitz, Zh. Eksp. Teor. Fiz. **32**, 618 (1957) [Sov. Phys. JETP **5**, 511 (1957)].
[7] L. D. Landau and E. M. Lifshitz, *Electrodynamics of Continuous Media* [Pergamon Press, Oxford (1960); Gostekhizdat, Moscow (1957)].
[8] I. M. Khalatnikov, *Theory of Superfluidity* [in Russian], Nauka, Moscow (1971).
[9] A. I. Akhiezer, V. F. Aleksin, and V. D. Khodusov, Fiz. Nizk. Temp. **20**, 1199 (1994) [Low Temp. Phys. **20**, 939 (1994)]; Fiz. Nizk. Temp. **21**, 3 (1995) [Low Temp. Phys. **21**, 1 (1995)].
[10] L. D. Landau and E. M. Lifshitz, *Fluid Mechanics*, 2nd ed. [Pergamon Press, Oxford (1987); Nauka, Moscow (1988)].
[11] L. D. Landau and E. M. Lifshitz, *Statistical Physics* [Pergamon Press, Oxford (1969); Nauka, Moscow (1964)].
[12] H. B. Callen and T. A. Welton, Phys. Rev. **83**, 34 (1951).
[13] M. L. Levin and S. M. Rytov, *Theory of Equilibrium Thermal Fluctuations in Electrodynamcis* [in Russian], Nauka, Moscow (1967).
[14] C. C. Ackermann, B. Bertman, H. A. Fairbank, and R. A. Guyer, Phys. Rev. Lett. **16**, 789 (1966).
[15] T. F. McNelly, S. J. Rogers, D. J. Chanin, R. J. Rollefson, W. M. Goubau, G. E. Schmidt, J. A. Krumhansl, and R. O. Pohl, Phys. Rev. Lett. **24**, 100 (1970).
[16] H. E. Jackson and S. T. Walker, Phys. Rev. B **3**, 1428 (1971).
[17] B. A. Danil'chenko, V. N. Poroshin, and O. G. Sarbeĭ, JETP Lett. **30**, 196 (1979).
[18] M. P. Shaskol'skaya (Ed.), *Handbook of Acoustic Crystals* [in Russian], Nauka, Moscow (1967).

Translated by Steve Torstveit

LATTICE DYNAMICS

Fractional and split crowdions in complex crystal structures

V. D. Natsik and S. N. Smirnov*

B. Verkin Institute for Low Temperature Physics and Engineering, National Academy of Sciences of Ukraine, pr. Lenina 47, 61164 Kharkov, Ukraine

E. I. Nazarenko

V. N. Karazin Kharkov National University, pl. Svobody 4, 61077 Kharkov, Ukraine

(Submitted October 6, 2000)
Fiz. Nizk. Temp. **27**, 316–332 (March 2001)

An analysis is made of the existence conditions and dynamical features of crowdion excitations in crystals with a complex structure of the crystalline field forming the crowdions in close-packed atomic rows. The crystalline matrix is assumed to be absolutely rigid, and the description of the crowdions therefore reduces to analysis of the generalized Frenkel–Kontorova model and the Klein–Gordon nonlinear differential equation corresponding to it. The cases of the so-called double-well and double-barrier potentials of the crystalline field are studied in this model: the structures of subcrowdions with fractional topological charges and of split whole crowdions are described, as is the asymptotic decay of split crowdions into subcrowdions when the double-barrier potential is transformed into a double well. The existence conditions of special types of subcrowdions are discussed separately; these conditions involve the atomic viscosity of the crystal and the external force applied to it. The qualitative analysis presented does not presuppose an exact solution of the Klein–Gordon nonlinear equation in explicit form. The results of this study generalize the conclusions reached previously in a study of certain particular cases of exactly solvable Klein–Gordon equations with complex potentials. The results of this study may be used not only in the physics of crowdions but also in other branches of nonlinear physics based on the Frenkel–Kontorova model. [DOI: 10.1063/1.1355521]

INTRODUCTION

Crowdions are nonlinear solitary waves of displacements that arise in close-packed atomic rows which are weakly coupled with the crystalline matrix surrounding these rows.[1–3] The distinguished atomic row might be an inherent part of the crystal itself or a chain of adsorbed atoms on the surface of the crystal.[4] There is reason to assume that excitations of the crowdion type also play an important role in the dynamics of linear oriented polymers, in particular, double polymer chains; in that case the ''atoms'' would be relatively rigid monomers whose internal degrees of freedom could be neglected.[5,6]

For qualitative description of the main properties of crowdions in the physics of crystals, the Frenkel–Kontorova one-dimensional crystal model is widely used. A Frenkel–Kontorova crystal is a chain of strongly interacting atoms executing one-dimensional motion on an immobile periodic substrate created by a relatively weak potential field.[3,7,8] When this model is compared with a real crystal it is assumed that the mobile chain of atoms corresponds to a distinguished atomic row, and the periodic potential of the substrate models the interaction of this rotation with the crystalline matrix. In our recently published paper[9] the problem of the structure and motion of a crowdion is treated as a dynamical problem of a complex three-dimensional crystal lattice. In the present paper we formulate the requirements that must be met by the parameters of the interatomic interaction and the geometric parameters of the crystal in order that one can do the following:

— separate out the crowdion excitations from the background of small elastic deformations of the crystal;

— reduce the description of crowdions to an analysis of solitary waves in a one-dimensional Frenkel–Kontorova crystal;

— obtain explicit expressions relating the substrate potential and the parameters of the Frenkel–Kontorova model with the interatomic interaction potentials and other microscopic characteristics of the three-dimensional crystal.

In Ref. 9 we also showed that a correct separation of nonlinear crowdion excitations and linear elastic deformations in a three-dimensional crystal is possible only in the long-wavelength approximation. This approximation corresponds to crowdions having a rather large width $\lambda \gg b$ and low velocity $V \ll c$ (b and c are, respectively, the characteristic values of the interatomic distance and the sound velocity in the crystal). If the requirements listed above are met, one can pass to the continuum limit in the equations describing the crowdions. To a first approximation one can also assume that the crystalline matrix is absolutely rigid, i.e., neglect its deformations. In that case, for the description of

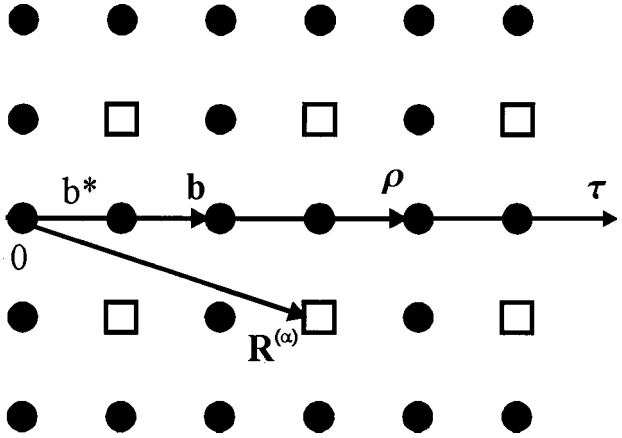

FIG. 1. Fragment of a complex crystal lattice with a distinguished atomic row (two-dimensional scheme); **b** and $\boldsymbol{\tau}$ are the elementary translation vector of the lattice and the direction vector along the distinguished atomic row, ρ and $\mathbf{R}^{(\alpha)}$ are the equilibrium positions of the atoms of the distinguished row and of the crystalline matrix surround it, respectively, and b^* is the equilibrium distance between atoms of the distinguished row.

the nonlinear dynamics of the atoms of the distinguished row it is convenient to use as the natural dynamical field variable the function $u(x,t)$, which is the field of longitudinal displacements of the atoms from their equilibrium positions in the ideal crystal and depends on the coordinate x along the chain and the time t. It is assumed that the direction of the x axis and of the displacement $u(x,t)$ is specified by the elementary translation vector **b** of the crystal along the distinguished atomic chain (Fig. 1). The energy functional corresponding to this approximation has the form

$$H=\frac{1}{b^*}\int_{-\infty}^{\infty}\left[\frac{m_a}{2}(\dot{u})^2+\frac{w}{2}(u')^2+\Phi(u)-F(x,t)u\right]dx. \tag{1}$$

Here m_a and b^* are the mass of the atoms of the distinguished row and the equilibrium distance between them, $F(x,t)$ is the external (to the crystal lattice) force acting on these atoms, w is the interatomic interaction parameter within the distinguished row, $\Phi(u)=\Phi(u+b)$ is the periodic potential of the crystalline field for atoms of the distinguished row (the ''substrate'' potential), and $\dot{u}=\partial u/\partial t$, $u'=\partial u/\partial x$.

If the interaction of two atoms of different chemical elements α and α' joined by a vector **r** is described by a pair potential $U_{\alpha\alpha'}(\mathbf{r})$, then the expressions for the parameter w and potential $\Phi(u)$ have the form[9]

$$w=\frac{1}{2}\sum_{\rho}\rho_i\rho_k\frac{\partial^2 U_{11}(\rho)}{\partial\rho_i\partial\rho_k}, \tag{2a}$$

$$\Phi(u)=\sum_{\alpha,\mathbf{R}^{(\alpha)}}[U_{1\alpha}(\mathbf{R}^{(\alpha)}-\tau u)-U_{1\alpha}(\mathbf{R}^{(\alpha)})], \tag{2b}$$

$$\tau=\frac{\mathbf{b}}{b}.$$

In these expressions the atoms of the distinguished row are assigned the chemical index $\alpha=1$, and the summation is over the equilibrium positions ρ and $\mathbf{R}^{(\alpha)}$ of these atoms and of the atoms of the matrix, respectively (Fig. 1). It is convenient to place the origin from which the vectors ρ and $\mathbf{R}^{(\alpha)}$ are measured on one of the atoms of the distinguished row, specifically, the atom with the largest binding energy with the matrix, thus ensuring that the potential is positive definite, $\Phi(u)\geqslant 0$. In the general case the parameters b and b^* have different magnitudes, but in this paper we consider the simple case when $b=b^*$. It will also be convenient to use a system of physical units in which $m_a=1$, $b=1$, and $w=1$, and keep the former notation for the dimensionless quantities. When these simplifications are taken into account, the equation of motion for the displacement field $u(x,t)$ and corresponding to energy functional (1) takes the form

$$\ddot{u}-u''+\frac{d}{du}\Phi(u)=F. \tag{3}$$

This differential equation is known in mathematical physics as the Klein–Gordon nonlinear equation. Not only is it fundamental to crowdion theory, but the analysis of many other physical problems also leads to equations of this form.[8,10–14]

From the standpoint of the physics of nonlinear phenomena, the main interest is in the solitonlike solutions of equation (3), which exist if the potential $\Phi(u)$ has a set u_p of absolute minima: $\Phi(u_p)=0$, where $u_p=p=n+\delta_i$, $n=0,\pm 1,\pm 2,...$, $0\leqslant\delta_i<1$. The numbering of the minima here takes into account both the presence of translational symmetry of the crystal and the possibility that more than one absolute minimum exists within a translational period $n\leqslant u<n+1$: the translational periods are numbered by the sequence of natural numbers n, and the absolute minima within each period by the fractional numbers $\delta_i=0,\delta_1,\delta_2,\ldots$. Stable solitonlike solutions of equation (3) in the absence of crystal forces ($F\equiv 0$) are solitary waves with a stationary profile:

$$u(x,t)=u_q(\xi),\quad \xi=x-V_q t, \tag{4}$$

which move with a constant velocity V_q and satisfy the boundary conditions

$$u_q'(\pm\infty)=0,\quad u_q(\infty)-u_q(-\infty)=\int_{-\infty}^{\infty}u_q'(\xi)d\xi=q. \tag{5}$$

Here q is a positive or negative number equal to the difference between any two adjacent numbers from the set $p=n+\delta_i$; this number is called the topological charge of the solitary wave and is an integral of the motion. If the potential $\Phi(u)$ has a single absolute minimum within a translational period (Fig. 2a and 2b) the set of numbers $p=n$ and the topological charge can assume the two values $q=s=\pm 1$, and the corresponding topological soliton is called whole (integer). Solitons for which $q=\sigma$, where $|\sigma|<1$, can exist in the case of so-called multiwell potentials (Fig. 2c) and have been given the name subsolitons (they may also be called fractional).

We note that the uniform solutions of equation (3) $u_p=p$ can be interpreted as a multiply degenerate physical vacuum for the field $u(x,t)$, in which case the solitary wave $u_q(x-V_q t)$ plays the role of a nonlinear excitation of the vacuum,[14] and it represents a moving smeared boundary, centered at the point $x_q=V_q t$, between two uniform states u_p and u_{p+q} specified at infinity.

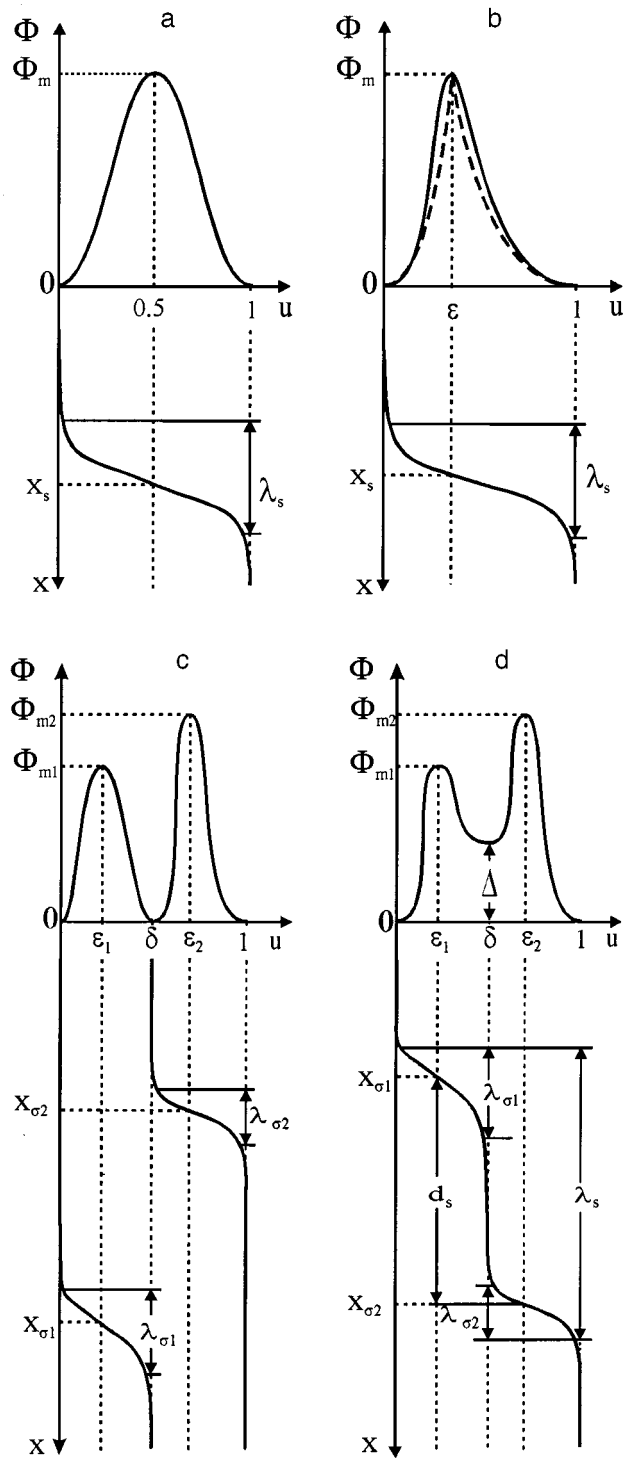

FIG. 2. Different types of crystal-field potentials $\Phi(u)$ and the kinks corresponding to them: a—symmetric single-barrier potential; b—asymmetric single-barrier potential (solid curve) and its piecewise-continuous parabolic approximation (dashed curve); c—double-well potential and fractional kinks with centers at the points $x_{\sigma i}$ and widths $\lambda_{\sigma i}$ $(i=1,2)$; d—double-barrier potential and a split kink consisting of two virtual subkinks with centers at the points $x_{\sigma i}$ and widths $\lambda_{\sigma i}$; λ_s is the width of a whole kink, and d_s is the width of a stacking fault.

As we have said, the energy functional (1) and the equation of motion (3) are the first (fundamental) approximation in the description of crowdions. In this approximation the atomic structure and dynamical properties of the crowdions are determined primarily by the shape and parameters of the potential $\Phi(u)$.[1)] In the classic paper by Frenkel and Kontorova and in the existing theory of crowdions the extremely simple sinusoidal potential $\Phi(u)=\Phi_m \sin^2(\pi u)$ is considered. For such a crystal-field potential $p=n$ and $q=s=\pm 1$; under the inequality $\Phi_m \ll 1$ the crowdion excitation has the form of a simple crowding together (or spreading apart) of the atoms in the distinguished row, the width of this being of the order of $\lambda_s=\sqrt{(1-V_s^2)/2\Phi_m} \gg 1$, and on the graph of the function $u_s(x-V_s t)$ this excitation is represented by an isolated kink centered at the point $x_s V_s t$ (Fig. 2a). The topological charge $s=-1$ corresponds to a delocalized interstitial atom (crowdion), while $s=1$ corresponds to a delocalized vacancy (anticrowdion).

A recent series of studies, starting with Refs. 13, 15, and 16, has explored the effect of a substantial deviation from a sinusoidal form of the potential $\Phi(u)$ on the soliton structure and parameters and on the corresponding kinks in the generalized Frenkel–Kontorova model (the results of these studies are reviewed in Ref. 8). Of greatest interest, in our opinion, are the cases of multiwell (Fig. 2c) and multibarrier (Fig. 2d) potentials $\Phi(u)$: the multiwell potential admits the existence of subkinks with fractional topological charge $q=\sigma$, where $|\sigma|<1$ (e.g., $|\sigma|=\delta$, $1-\delta<1$); in the case of a multibarrier potential a whole kink with integer topological charge $q=s=\pm 1$ has an internal ''fine'' structure and can be regarded as split into fragments, similar to subkinks, which are uniquely interrelated.

The potentials $\Phi(u)$ derived (or chosen as models) in the previously studied problems of nonlinear physics have been completely specified symmetric double-well and double-barrier potentials, which for certain values of their parameters go over to a sinusoidal potential and admit exact solution of the Klein–Gordon equation (3) in explicit form. One of the simplest concrete examples is a function $\Phi(u)$ of[17,18]

$$\Phi(u)=\Phi_m[\sin^2(\pi u)+\gamma \sin^2(2\pi u)]. \tag{6}$$

For $\gamma=0$ this function goes over to the classical Frenkel–Kontorova potential, and for $\gamma>1/4$ it is a symmetric double-barrier potential with an intermediate minimum at the point $\delta=1/2$. The function (6) can be interpreted formally as the approximation of a more complex periodic function by the first terms of the Fourier series.

However, in an analysis of crowdions in complex crystal structures, especially in oriented polymers, the potential $\Phi(u)$ can turn out to be extremely complex and far from a simple approximation of the form (6), and therefore the use of approximations of this kind does not allow one to describe the many interesting and important properties of real crowdion excitations. The main problem of the present study is to analyze qualitatively the structure and dynamical properties of crowdions in the case of multiwell and multibarrier crystal-field potentials without explicitly specifying the form of the function $\Phi(u)$ and without obtaining exact solutions of the Klein–Gordon equation (3) in explicit form. The existing ideas about subkinks and the splitting of whole kinks will be cast in a more general form and applied to the description of crowdions with allowance for their specifics. In addition, certain new properties of crowdions in complex crystals will be described. The results of this study can of course be used not only in the theory of crowdions but also

in other branches of the physics of nonlinear phenomena whose description reduces to analysis of the solutions of the Klein–Gordon nonlinear equation. Some of the results of our analysis are analogous, from a general physical standpoint, with results obtained earlier in the theory of magnetic solitons.

1. WHOLE AND FRACTIONAL CROWDIONS

Let us first turn to a description of the structure and dynamics of crowdions without specifying the exact form of the potential $\Phi(u)$ but only assuming that this potential is periodic and has a set of absolute minima, $u_p=p=n+\delta_i$ $(\Phi(u_p)=0)$ and a set of the the same number of maxima of various heights at the points $u_m=m=n+\varepsilon_i$ $(\Phi(u_m)=\Phi_{mi})$, where $n=0,\pm1,\pm2,...$, $0\leqslant\delta_i$, $\varepsilon_i\leqslant1$. In the absence of external forces $(F\equiv0)$ the first and second integrals of equation (3), which describe solitary waves $u_q(x-V_qt)$ satisfying boundary conditions (5) with an arbitrary value of q, can be written in the form

$$u_q'=\mathrm{sgn}(q)\left(\frac{2\Phi(u_q)}{1-V_q^2}\right)^{1/2}, \tag{7}$$

$$\int_{\varepsilon_i}^{u_{qi}}\frac{du}{\sqrt{2\Phi(u)}}=\mathrm{sgn}(q_i)\,\frac{x-V_{qi}t}{\sqrt{1-V_{qi}^2}}. \tag{8}$$

The choice of the lower limit of integration ε_i in Eq. (8) defines the center of the crowdion (kink) $x_{qi}=V_{qi}t$ as the point at which the absolute value of the crowdion deformation reaches its maximum value:

$$\max|u_{qi}'|=\left(\frac{2\Phi_{mi}}{1-V_{qi}^2}\right)^{1/2}. \tag{9}$$

Our definition of the centers of the crowdions and their numbering faithfully reflects the circumstance that an individual type of crowdion is uniquely associated with one of the maxima of the potential $\Phi(u)$. It is easy to see from Eqs. (7) and (8) that the details of the internal structure of the crowdion excitation (kink) are determined by the form of the potential profile $\Phi(u)$ on the interval joining two neighboring absolute minima; this interval specifies the value of the topological charge q_i. We note immediately that the applicability of the formulas obtained above for the description of crowdion excitations in real crystals is restricted by the requirement $\max|u_{qi}'|\ll1$, which justifies the use of the continuum limit. This requirement, according to Eq. (9), reduces to the condition $1-V_{qi}^2\gg2\Phi_{mi}$, which is violated if the crowdion velocity approaches the limiting value $V=1$ (in the original system of units, the value $c=\sqrt{w/m_a}$), and the analysis of such a fast-moving excitation requires taking lattice effects into account.

As an example, let us first consider a symmetric single-well potential with a maximum at $\varepsilon=1/2$ (Fig. 2a), which, over rather wide neighborhoods of the minimum $|u|<u^*$ and maximum $|u-1/2|<u^*$, admits a quadratic approximation[3]

$$\Phi(u)=\begin{cases}\dfrac{1}{2}\Phi''(0)u^2, & |u|<u^*,\\[2ex] \Phi_m+\dfrac{1}{2}\Phi''\left(\dfrac{1}{2}\right)\left(u-\dfrac{1}{2}\right)^2, & \left|u-\dfrac{1}{2}\right|<u^*.\end{cases} \tag{10}$$

If one is not considering ''exotic'' potentials, the parameter u^* that determines the domains of applicability of the approximations in (10) can be estimated as $u^*\simeq1/4$. This potential admits the existence of only whole crowdions with integer topological charge $q=s$. Using Eqs. (8) and (10), we easily obtain the asymptotic formulas describing the structure of the crowdion (shape of the kink) far from and close to its center $x_s=V_st(\xi=0)$:

$$u_s(\xi)=\begin{cases}1-u^*\exp\left(\dfrac{\lambda_c-s\xi}{\lambda_0}\right), & s\xi>\lambda_c;\\[2ex] \dfrac{1}{2}+\lambda_m'\sin\left(\dfrac{s\xi}{\lambda_m}\right), & |\xi|<\lambda_c;\\[2ex] u^*\exp\left(\dfrac{\lambda_c+s\xi}{\lambda_0}\right), & s\xi<-\lambda_c.\end{cases} \tag{11}$$

The shape of the kink is characterized by a set of four parameters λ_0, λ_m, λ_m^*, and λ_c, which have dimensions of length:

$$\lambda_0=\left(\frac{1-V_s^2}{\Phi''(0)}\right)^{1/2},\quad \lambda_m=\left(\frac{1-V_s^2}{|\Phi''(1/2)|}\right)^{1/2},$$

$$\lambda_m^*=\left(\frac{2\Phi_m}{|\Phi''(1/2)|}\right)^{1/2},\quad \lambda_c=\lambda_m\arcsin\left(\frac{1-2u^*}{2\lambda_m^*}\right). \tag{12}$$

The parameter λ_c determines the half-width of the central part of the kink, while λ_0 specifies the extent of its ''wings''; therefore, the characteristic kink width λ_s can be represented by the sum

$$\lambda_s=2(\lambda_0+\lambda_c)=2\lambda_0\left[1+\frac{\lambda_m}{\lambda_0}\arcsin\left(\frac{1-2u^*}{2\lambda_m^*}\right)\right]. \tag{13}$$

Analysis shows that for a wide class of potentials $\Phi(u)$ satisfying the condition of applicability of the continuum approximation $\max|u_s'|\ll1$ [see Eq. (9)] but differing in the curvature at the minimum and maximum, the parameters λ_0 and λ_c are of the same order of magnitude, which depends substantially on the barrier height Φ_m:

$$\lambda_c-\lambda_0\simeq\frac{\lambda_s}{4},\quad \lambda_s=\left(\frac{1-V_s^2}{2\Phi_m}\right)^{1/2}. \tag{14}$$

For barriers with a ''sharpened'' crest $(u^*\to0,\ |\Phi''(1/2)|\to\infty)$ the central part of the kink is absent, and its width is determined mainly by the barrier height Φ_m and the value of the derivative $\Phi''(0)$. In those cases where $\Phi''(0)\to0$ while the barrier height Φ_m remains finite, the width of the kink increases anomalously, and the exponential asymptotic behavior of the displacement field $u_s(\xi)$ gives way to a power-law behavior at large distances from the center of the kink. Such kinks have been studied previously[14] and are called power-law or algebraic kinks.

It should be noted that crowdion excitations in real three-dimensional crystals have the feature that taking the

elastic compliance of the crystalline matrix into account leads to a power-law asymptotic behavior of the crowdion strain field at large distances from the center of the crowdion for any shape of the potential $\Phi(u)$.[9,19–21] Therefore, in the case of a crowdion in a three-dimensional crystal the parameter λ_s has the meaning of the characteristic size of its core.

Of special interest is the case of an asymmetric single-well potential $\Phi(u)$ (Fig. 2b): such a potential can arise in crystals that do not have a center of inversion. In this case the structure of the field of displacements of a whole crowdion (the shape of the kink) near its center is asymmetric. As we saw above, the value of the derivative of the potential $\Phi(u)$ in the neighborhood of the maximum does not materially affect the structure of the crowdion; therefore, the asymmetry indicated above is conveniently illustrated by considering as an approximation the piecewise continuous function[2)]

$$\Phi(u)=\begin{cases}\dfrac{\Phi_m}{\varepsilon^2 u^2}, & 0\leqslant u\leqslant\varepsilon,\\[2ex] \dfrac{\Phi_m}{(1-\varepsilon)^2}(u-1)^2, & \varepsilon\leqslant u\leqslant 1.\end{cases}$$

In this approximation one can obtain exact expressions for the displacement field $u_s(\xi)$ in explicit form:

$$u_s(\xi)=\begin{cases}\varepsilon\exp\left(\dfrac{s\xi}{\lambda_\varepsilon}\right), & s\xi\leqslant 0,\\[2ex] 1-(1-\varepsilon)\exp\left(-\dfrac{s\xi}{\lambda_{1-\varepsilon}}\right), & s\xi\geqslant 0.\end{cases} \tag{15}$$

In this case the central part of the kink consists of two parts with dimensions of the order of λ_ε and $\lambda_{1-\varepsilon}$, and the width of the kink is $\lambda_s=\lambda_\varepsilon+\lambda_{1-\varepsilon}$:

$$\begin{pmatrix}\lambda_\varepsilon\\ \lambda_{1-\varepsilon}\end{pmatrix}=\begin{pmatrix}\varepsilon\\ 1-\varepsilon\end{pmatrix}\lambda_s,\quad \lambda_s=\left(\frac{1-V_s^2}{2\Phi_m}\right)^{1/2}. \tag{16}$$

If the asymmetric potential $\Phi(u)$ has a rather extended crest with a small curvature, there will be yet another distinguished fragment with a half width of λ_c [see formulas (12)].

According to the well-known ideas of nonlinear mechanics,[3,14] any stable solitary wave (in our case, crowdion excitation) can be regarded as a particle with certain values of the self field energy E_s and effective rest mass m_s. A general expression for the energy and mass of an excitation in the case $F\equiv 0$ is easily obtained by substituting the displacement field $u_s(x-V_st)$ into the energy functional (1) and using relation (7) at $q=s$:

$$E_s=\frac{1}{\sqrt{1-V_s^2}},\quad m_s=I, \tag{17}$$

$$I=\int_0^1\sqrt{2\Phi(u)}\,du. \tag{18}$$

We will not analyze in detail the dependence of E_s and m_s on the shape and parameters of the potential $\Phi(u)$, since this question is discussed quite thoroughly in the review by Braun and Kivshar.[8] We note only that when a crowdion in a real crystal is considered with allowance for the elastic compliance of the crystalline matrix, formula (17) can be used only for making order-of-magnitude estimates of its energy and mass, while the exact values of these parameters depend not only on the potential $\Phi(u)$ but also on the elastic properties of the crystalline matrix.[9]

Let us now turn to an analysis of the properties of crowdions (kinks) for more-complex forms of the potential $\Phi(u)$. As we said in the Introduction, in complex crystal structures the periodic function $\Phi(u)$ can have several wells (absolute minima) within a period $0\leqslant u<1$ of the structure, and the same number of barriers (maxima) separating them. In this case the stable stationary solution of the Klein–Gordon equation (3) corresponds to kinks with fractional topological charges $q=\sigma$, where $-1<\sigma<1$: these kinks join uniform states fixed at infinity by any pair of adjacent wells of the potential $\Phi(u)$, separated by a distance $|\sigma|$. We describe the fractional kinks for the particular example of a asymmetric double-well potential $\Phi(u)$ (Fig. 2c) having two sets of absolute minima: $u_n=n$ and $u_\nu=\nu=n+\delta$, where $n=0,\pm 1,\pm 2,\ldots,0<\delta<1$. We denote the two sets of maxima of such a potential by the symbols $u_{m1}=m_1$ and $u_{m2}=m_2$, where $m_1=n+\varepsilon_1$, $m_2=n+\varepsilon_2$, $0<\varepsilon_1<\delta<\varepsilon_2<1$. In the general case the barriers between wells can have different heights $\Phi_{m1}=\Phi(u_{m1})$ and $\Phi_{m2}=\Phi(u_{m2})$.

In the absence of external forces ($F\equiv 0$) Eq. (3) has two sets of spatially uniform stable solutions $u_n=n$ and $u_\nu=\nu$, corresponding to the wells of the potential $\Phi(u)$: $\Phi(u_n)=\Phi(u_\nu)\equiv 0$. In this case the physical vacuum for the field $u(x,t)$ consists of two inequivalent sets of spatially uniform states u_n and u_ν, the degeneracy of which is twice that for a single-well potential $\Phi(u)$. The fractional crowdions (subkinks) $u_\sigma(x-V_\sigma t)$ are nonlinear solitonlike excitations of such a vacuum: an individual excitation is a smeared boundary between neighboring uniform states of different sets, separated by intervals $|\sigma_i|$: the parameter σ can take values $\sigma_1=+\delta$ and $\sigma_2=\pm(1-\delta)$ (Fig. 2c). The increase in the degree of degeneracy of the vacuum leads to growth of the number of independent elementary excitations: in the case under study, two types of crowdions and two types of anticrowdions can exist.

The displacement field $u_\sigma(x-V_\sigma t)$ of a fractional crowdion describes localized crowding together or spreading apart of atoms in a close-packed row and for any specified value of σ_i is determined by relations (7) and (8). The internal structure of fractional crowdions is analogous to that of whole crowdions: it is governed by the shape of the potential $\Phi(u)$ on the intervals σ_i joining adjacent minima [see formulas (9)–(16)]. The characteristic value of the width of a fractional crowdion, $\lambda_{\sigma i}$, can be estimated by the formula

$$\lambda_{\sigma i}=|\sigma_i|\left(\frac{1-V_{\sigma i}^2}{2\Phi_{mi}}\right)^{1/2},\quad i=1,2. \tag{19}$$

Fractional crowdions, like whole ones, have pseudoparticle properties with self-energies $E_{\sigma i}$ and effective rest masses $m_{\sigma i}$, which are given by the expressions

$$E_{\sigma i}=\frac{I_{\sigma i}}{\sqrt{1-V_{\sigma i}^2}},\quad m_{\sigma i}=I_{\sigma i}; \tag{20}$$

$$I_{\sigma i}=\int_0^{|\sigma_i|}\sqrt{2\Phi[u-(i-1)|\sigma_i|]}\,du, \quad i=1,2. \tag{21}$$

2. SPLIT CROWDIONS

The multiwell lattice potential $\Phi(u)$ considered at the end of the previous Section is obviously exclusive and rarely encountered in real situations. Both in the physics of crowdions and in some other branches of physics one is much more likely to have a multibarrier potential $\Phi(u)$.[8,10–13,17,18,24] The qualitative representation of the fine structure of a whole crowdion with topological charge $s=\pm 1$ in crystals with a multibarrier potential $\Phi(u)$ is given by formula (7) for $q=s$: the value of the crowdion-created deformation $u_s'(\xi)$ of the close-packed row of atoms has maxima and minima corresponding to the extrema of $\Phi(u)$, and the graph of the displacement field $u_s(\xi)$ takes the form of a multikink consisting of a set of fine kinks. The number of such kinks is equal to the number of maxima of $\Phi(u)$ on the interval (0, 1), and their height is of the order of the width of the potential barriers. This structure can be interpreted as the splitting of a solitary wave with integer topological charge $u_s(\xi)$ into a set of intercoupled solitary waves moving with a single velocity V_s and having fractional topological charges σ_i: here $\mathrm{sgn}(\sigma_i)=\mathrm{sgn}(s)$ and $\Sigma_i\sigma_i=s$. It is important to emphasize that the individual fragments of the multikink, which are similar to subkinks, are not independent: their shape and the distance between them are uniquely specified and are interrelated. In order to distinguish these formations from free subscrowdions, from now on we shall call them partial (or virtual) crowdions. A rigorous analytical description of a multikink as a sum of partial kinks has been obtained[8,11,12] for a number of specific potentials $\Phi(u)$, e.g., for the potential (6). The qualitative analysis proposed below allows one to establish the conditions under which a whole crowdion (kink) can be represented approximately as a set of coupled subcrowdions in those cases when it is not possible to obtain an explicit solution of the Klein–Gordon equation.

In this Section we consider a double-barrier potential $\Phi(u)$ of arbitrary shape, having within a period $0\leqslant u<1$ two minima of different depths, separated by two barriers (Fig. 2d). We denote the minima and maxima of the potential $\Phi(u)$ we use the symbols u_n, u_ν, u_{m1}, and u_{m2} introduced in the previous Section. The absolute minima u_n are numbered by integers $n=0,\pm 1,\pm 2,...$; the local minima u_ν by the fractional numbers $\nu=n+\delta$, where $0<\delta<1$; the maxima u_{mi} $(i=1,2)$ by fractional numbers $m_i=n+\varepsilon_i$, where $0<\varepsilon_1<\delta<\varepsilon_2<1$. By definition $\Phi(u_n)\equiv 0$, and a local minimum will be characterized by the parameter $\Phi(u_\nu)=\Delta$; the heights of the barriers separating the valleys of the potential $\Phi(u)$ are denoted $\Phi(u_{mi})=\Phi_{mi}$. It is clear that in the limit $\Delta\to 0$ we arrive at the previously investigated case of the double-well potential.

The double-barrier potential under consideration admits the existence of a solitonlike excitation $u_s(x-V_st)$ with an integer topological charge $s=\pm 1$, which is specified by the corresponding boundary conditions. In this case it is convenient to take the center of the crowdion (kink) as the point $x_s=V_st$ at which the displacement has the value $u_s(0)=\delta$, i.e., coincident with the local minimum. Under this condition the second integral of equation (3) in the absence of external forces $(F\equiv 0)$ has the form

$$\int_\delta^{u_s}\frac{du}{\sqrt{2\Phi(u)}}=s\,\frac{x-V_st}{\sqrt{1-V_s^2}}. \tag{22}$$

According to relation (7), on the axis $\xi=x-V_st$ there also exist two maxima ξ_i of the modulus of the deformation $|u_s'(\xi)|$:

$$\xi_i=s\sqrt{1-V_s^2}\int_\delta^{\varepsilon_i}\frac{du}{\sqrt{2\Phi(u)}}, \quad i=1,2. \tag{23}$$

It is easy to see that outside the interval (ξ_1,ξ_2) the displacement field $u_s(\xi)$ has a structure described by the upper and lower lines of formula (11), and the characteristic extent λ_0 of the wings of the kink is determined by the value of the derivative $\Phi''(0)$. We note only that in this case as a standard estimate for the parameter u^* one can take the value $u^*\simeq 1/8$ if $\delta\simeq 1/2$.

The central part of the kink has an extent $d_s=\xi_2-\xi_1$:

$$d_s=\sqrt{1-V_s^2}\int_{\varepsilon_1}^{\varepsilon_2}\frac{du}{\sqrt{2\Phi(u)}}. \tag{24}$$

To obtain an idea of the structure of the displacement field $u_s(\xi)$ near the center of the kink $(\xi=0)$ and to estimate the characteristic value of the parameter d_s, we use a quadratic approximation of the potential $\Phi(u)$ in the neighborhood of the local minimum, on a certain interval $2u^*<\varepsilon_2-\varepsilon_1$:

$$\Phi(u)\simeq\Delta+\frac{1}{2}\Phi''(\delta)(u-\delta)^2, \quad |u-\delta|\leqslant u^*. \tag{25}$$

Substituting (25) into (22) and doing some straightforward calculations, we arrive at the following expressions:

$$u_s(\xi)=\delta+\left(\frac{2\Delta}{\phi''(\delta)}\right)^{1/2}\sinh\left(\frac{s\xi}{\lambda_c^*}\right), \quad \xi\to 0; \tag{26}$$

$$\lambda_c^*=\left(\frac{1-V_s^2}{\Phi''(\delta)}\right)^{1/2}.$$

Let us discuss the question of how the width d_s of the central part of the kink depends on the parameters of the potential $\Phi(u)$. If the parameter Δ and the barrier heights Φ_{mi} are of the same order of magnitude, then the integral in (24) can be evaluated using the theorem of the mean:

$$d_s=\sqrt{1-V_s^2}\sum_{i=1}^{2}|\delta-\varepsilon_i|\left(\frac{C_i}{\sqrt{2\Phi_{mi}}}+\frac{1-C_i}{\sqrt{2\Delta}}\right),$$

$$0<C_1, \quad C_2<1. \tag{27}$$

Of special interest is the limiting case of a very deep local minimum of the potential $\Phi(u)$, when $\Delta\to 0$. In this case the extent of the central part of the kink increases anomalously according to the asymptotic estimate

$$d_s\gtrsim d_c=\lambda_c^*\ln\left[\frac{2(u^*)^2\Phi''(\delta)}{\Delta}\right], \quad \Delta\to 0. \tag{28}$$

It should be noted that the unbounded growth of $d_s(\Delta)$ as $\Delta\to 0$ does not occur only in the case of an ''exotic''

double-barrier potential and the double-well corresponding to it in the limit $\Phi''(\delta)=\infty$. For example, suppose that on the interval $\varepsilon_1<u<\varepsilon_2$ the potential $\Phi(u)$ admits the approximation

$$\Phi(u)=\Delta+\frac{\Phi_{mi}}{|\varepsilon_i-\delta|^{\gamma}}|u-\delta|^{\gamma},\quad 1<\gamma<2,\quad i=1,2. \tag{29}$$

Then the width $d_s(\Delta)$ of the central part of the kink remains finite as $\Delta\to 0$, but it increases anomalously as $\gamma\to 2$:

$$d_s(0)=\frac{2}{2-\gamma}\sum_{i=1}^{2}|\varepsilon_i-\delta|\left(\frac{1-V_s^2}{2\Phi_{mi}}\right)^{1/2}. \tag{30}$$

Thus at sufficiently small Δ the central part $d_s(\Delta)$ of the kink joins two fragments centered at the points ξ_1 and ξ_2 and having shapes close to those of subkinks with topological charges $\sigma_1=\pm\delta$ and $\sigma_2=\pm(1-\delta)$ and widths $\lambda_{\sigma i}$ (19). At the center of the crowdion, at an interval d_s, the atoms of the close-packed row occupy positions close (with exponential accuracy) to the local minima, and the potential energy of each of these atoms has a value close to Δ. This fragment of the crowdion is a sort of stacking fault of the atomic rows—a one-dimensional analog of the planar stacking faults or antiphase boundaries well known[2,25] in the physics of crystals[3)]

Turning to an analysis of the self-energy of the crowdion in the case of a double-barrier potential with a rather deep local minimum, we write the function $\Phi(u)$ in the form of a sum of a double-well potential $\Phi^{(DW)}(u)(\Phi^{(DW)}(0)=\Phi^{(DW)}(\delta)=0)$ and a rather small positive definite function $\varphi(u)$ that goes to zero at the ends and outside the interval between maxima $(\varepsilon_1,\varepsilon_2)$:

$$\Phi(u)=\Phi^{(DW)}(u)+\varphi(u). \tag{31}$$

Let $\max\varphi(u)=\varphi(\delta)=\Delta\ll\Phi_{m1},\Phi_{m2}$; then at small values of Δ one may use the expansion

$$\sqrt{\Phi(u)}\simeq\sqrt{\Phi^{(DW)}(u)}+\frac{\Delta}{2\sqrt{\Phi^{(DW)}(u)+\Delta}}.$$

In this approximation the energy of a whole crowdion (17) is given by

$$E_s\simeq E_{\sigma 1}+E_{\sigma 2}+\frac{\Delta}{1-V_s^2}d_s(\Delta). \tag{32}$$

Here $E_{\sigma i}$ is the energy of a subcrowdion with topological charge σ_i, given by formula (20), and d_s is the distance between the centers of the subcrowdions, the value of which can be estimated with the aid of the integral

$$d_s(\Delta)=\sqrt{1-V_s^2}\int_{\varepsilon_1}^{\varepsilon_2}\frac{du}{\sqrt{2[\Phi^{(DW)}(u)+\Delta]}}. \tag{33}$$

The last term in Eq. (32) has the meaning of the energy of the stacking fault joining the partial crowdions.

On the basis of the above analysis we arrive at the conclusion that in the case of any double-barrier potential $\Phi(u)$ with a sufficiently deep local minimum a whole crowdion with topological charge s can be treated approximately as a set of uniquely interrelated but spatially separate subcrowdions of the same sign with fractional topological charges $\sigma_1=s\delta$ and $\sigma_2=s(1-\delta)$ joined by an extended stacking fault

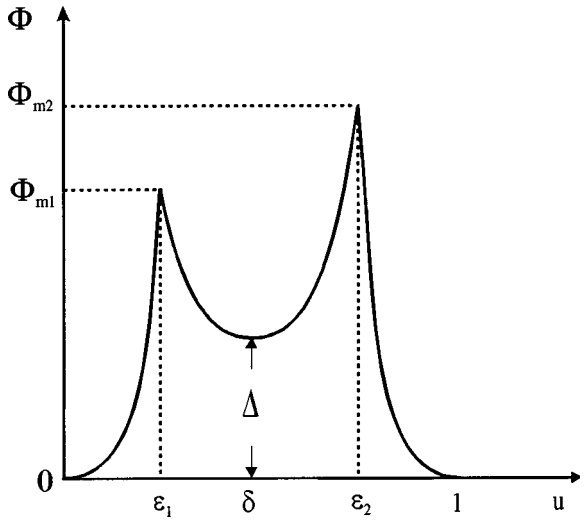

FIG. 3. Piecewise-continuous parabolic approximation of a double-barrier potential $\Phi(u)$.

d_s. Such a crowdion (or the corresponding kink) will be called split, and the subcrowdions bounding it will be called partial (or virtual) crowdions. The concepts of crowdion splitting are useful for an approximate description of crowdion excitations in crystals with a complex shape of the crystalline relief of $\Phi(u)$ and are physically justified under the inequality $\lambda_{\sigma i}\ll d_s$, which is equivalent to the inequality $\Delta\ll\Phi_{mi}$.

A rather good illustration of the general concepts formulated above is given by the explicit exact solution of the problem of a split crowdion for a piecewise continuous parabolic potential of the form (Fig. 3)

$$\Phi(u)=\begin{cases}\dfrac{1}{2}K_0^2u^2, & 0\leqslant u\leqslant\varepsilon_1;\\ \Delta+\dfrac{1}{2}K_c^2(u-\delta)^2, & \varepsilon_1\leqslant u\leqslant\varepsilon_2;\\ \dfrac{1}{2}K_0^2(u-1)^2, & \varepsilon_2\leqslant u\leqslant 1;\end{cases} \tag{34}$$

$$\sigma_i^2K_0^2\geqslant 2\Delta,\quad i=1,2.$$

As independent parameters of this potential we shall consider the curvatures at the minima, $K_0^2=\Phi''(0)$, $K_c^2=\Phi''(\delta)$, the depth $\Delta=\Phi(\delta)$ of the local minimum, and its position δ. Then the maxima ε_1 and ε_2 and the barrier heights Φ_{m1} and Φ_{m2} are functions of these parameters, and the corresponding relations are conveniently written in the form

$$\varepsilon_i-\delta=\frac{(-1)^i}{K_0^2-K_c^2}[|\sigma_i|K_0^2-\sqrt{\sigma_i^2K_0^2K_c^2+2(K_0^2-K_c^2)\Delta}],$$

$$\Phi_{mi}(\Delta)=\frac{1}{2}K_c^2(\varepsilon_i-\delta)^2+\Delta,\quad i=1,2. \tag{35}$$

The displacement field of the whole crowdion is given by the formulas

$$u_s(\xi)=\begin{cases}\varepsilon_1\exp\left(\dfrac{s\xi+\lambda_{c1}}{\lambda_0}\right), & s\xi\leqslant-\lambda_{c1};\\ \delta+\lambda_\Delta\sinh\left(\dfrac{s\xi}{\lambda_c}\right), & -\lambda_{c1}\leqslant s\xi\leqslant\lambda_{c2};\ ;\\ 1-(1-\varepsilon_2)\exp\left(\dfrac{\lambda_{c2}-s\xi}{\lambda_0}\right), & s\xi\geqslant\lambda_{c2}\end{cases}\tag{36}$$

$$K_0\lambda_0=K_c\lambda_c=\sqrt{1-V_s^2},\quad K_c\lambda_\Delta=\sqrt{2\Delta},$$

$$\lambda_{ci}=\lambda_c\ln\left[\frac{|\varepsilon_i-\delta|+\sqrt{\lambda_\Delta^2+(\varepsilon_i-\delta)^2}}{\lambda_\Delta}\right],\quad i=1,2.\tag{37}$$

The deformation $u_s'(x-V_st)$ in the solitary wave (36) has two extrema at the points $x_i=V_st+(-1)^i\lambda_{ci}$. The two points x_i move with a velocity V_s and can be regarded as the centers of virtual subkinks joined by stacking faults with a width

$$d_s(\Delta)=x_2-x_1=\lambda_c\ln\times\left\{\frac{[\sqrt{\Phi_{m1}(\Delta)}+\sqrt{\Phi_{m1}(\Delta)-\Delta}][\sqrt{\Phi_{m2}(\Delta)}+\sqrt{\Phi_{m2}(\Delta)-\Delta}]}{\Delta}\right\}.\tag{38}$$

This interpretation corresponds to the form of the exact expression for the energy of a whole crowdion, which is the sum of the energies of the virtual subcrowdions $E_{\sigma i}(\Delta)$ and the energy of the stacking fault:

$$E_s(\Delta)=E_{\sigma1}(\Delta)+E_{\sigma2}(\Delta)+\frac{\Delta}{1-V_s^2}d_s(\Delta),$$

$$E_{\sigma i}(\Delta)=\frac{1}{K_0K_c\sqrt{1-V_s^2}}\times\{K_0\sqrt{\Phi_{mi}(\Delta)[\Phi_{mi}(\Delta)-\Delta]}+K_c\Phi_{mi}(\Delta)\}.\tag{39}$$

In the limit $\Delta\to0$ the width of the stacking fault increases without bound according to the asymptotic law

$$d_s(\Delta)\simeq\lambda_c\ln\left[\frac{4\sqrt{\Phi_{m1}(0)\Phi_{m2}(0)}}{\Delta}\right],$$

$$2\Phi_{mi}(0)=\frac{\sigma_i^2K_0^2K_c^2}{(K_0+K_c)^2}.\tag{40}$$

Here its energy goes to zero, and the virtual subcrowdions are transformed into independent fractional crowdions with topological charges $\sigma_1=s\delta$ and $\sigma_2=s(1-\delta)$ and having widths $\lambda_{\sigma i}$ and energies $E_{\sigma i}$:

$$\lambda_{\sigma i}=|\sigma_i|\left(\frac{1-V_{\sigma i}^2}{2\Phi_{mi}(0)}\right)^{1/2},\quad E_{\sigma i}=|\sigma_i|\left(\frac{\Phi_{mi}(0)}{2(1-V_{\sigma i}^2)}\right)^{1/2},$$

$$i=1,2.\tag{41}$$

The analysis done in this Section leads us to a general conclusion of fundamental importance as to the asymptotic behavior of the solitary waves (crowdions, kinks) upon the transformation of any double-barrier potential $\Phi(u)$ to a double-well potential $\Phi^{(DW)}(u)$. In the limit $\Delta\to0$ the energy of the stacking fault goes to zero ($d_s(\Delta)\Delta\to0$), and the whole excitation asymptotically decays into fraction excitations. This means that the additional degeneracy of the physical vacuum as a result of such a transformation causes a fundamental rearrangement of the spectrum of nonlinear excitations of the system: the solitary waves with integer topological charge vanish, and the role of elementary solitonlike excitations is taken up by solitary waves with fractional topological charges. This conclusion is generalized without difficulty to the case of potentials $\Phi(u)$ with any number of barriers on the interval (0, 1).

As to the dynamics of close-packed atomic rows in crystals, the above result means that if the crystalline potential $\Phi(u)$ for them is a multiwell potential, then the insertion of an additional atom or the removal of an atom (e.g., under the influence of radiation) does not give rise to localized structural states of the interstitial atom or vacancy type but are inevitably delocalized, displacing the atomic row by an amount equal to the elementary translation vector. It is possible that in certain real crystal structures there are two mutually compensating tendencies: the tendency toward localization of the crowdions on account of the large barrier heights of the crystalline potential relief is weakened by the presence of deep local minima in it. This circumstance can prove important in interpreting the diffusion and radiation properties of complex crystals.

It should be noted, however, that this conclusion needs refinement. Remember that it was obtained in the continuum approximation for a structurally uniform crystal. If the Peierls barriers that exist because of the discreteness of the lattice structure or the potential barriers for crowdions erected by local defects and internal stress fields are taken into account, then the pinning of partial crowdions on such barriers can substantially limit the aforementioned delocalization.[4,26] The tendency of whole crowdions to decay is also weakened by spatial dispersion effects, i.e., when derivatives of higher order are taken into account in the equation of motion (3).[22]

Let us conclude this Section by remarking that the problem of split topological solitons has yet another interesting aspect—the presence of internal dynamics of such excitations,[8,18] but a discussion of those questions in reference to crowdion dynamics goes beyond the scope of this paper.

3. SPECIAL TYPES OF SUBCROWDIONS

In Sec. 1 we determined and discussed fractional crowdions, which exist only in atomic rows placed in a multiwell potential relief (Fig. 2c). However, there are some entirely real special circumstances that promote the appearance of fractional crowdions in cases of a multibarrier crystalline relief $\Phi(u)$ as well (Fig. 2d): these circumstances are the presence of external forces $F\neq0$ or the inclusion in the equation of motion for the field $u(x,t)$ the force of dynamic friction $f(\dot u)$, which in general is an odd function of the velocity of the atomic displacements, $f(-\dot u)=-f(\dot u)$.

Let us first assume that there is no friction ($f(\dot u)\equiv0$) and analyze the existence conditions for crowdions in atomic rows placed in the potential $\Phi^{(F)}(u)=\Phi(u)-Fu$, where $\Phi(u)$ is a double-barrier potential (Fig. 2d) with a rather deep local minimum Δ and $F=\text{const}$ is a constant force of a

rather small magnitude ($\Delta \ll \Phi_{mi}, |F| \ll \Phi_{mi}, i=1,2$). The force F, generally speaking, disrupts the periodicity of the potential and lifts the degeneracy of the stable energy states, thereby violating a necessary condition for the existence of stationary soliton excitations with nonzero topological charge. Therefore, at arbitrary values of F the Klein–Gordon equation (3) does not have solutions in the form of stable solitary waves with a stationary profile and with $q=s=\pm 1$ like those that exist in the absence of external forces and which are described in Sec. 2. An exception is the two distinguished critical values of the force $F=F_i(i=1,2)$ at which the potential $\Phi^{(F)}(u)$ admits the existence of stable solitary waves of stationary profile but now with a fractional topological charge $q=\sigma_i$, $|\sigma_i|<1$.

One is readily convinced of the correctness of this assertion by analyzing the different properties of the potential $\Phi^{(F)}(u)$. Under the inequalities $\Delta \ll \Phi_{mi}$ and $|F| \ll \Phi_{mi}$ the potential $\Phi^{(F)}(u)$ has two families of minima:

$$u_n(F)=n+u_0(F), \quad u_\nu(F)=(n+\delta)+u_\delta(F); \tag{42}$$

here $u_0(F)$ and $u_\delta(F)$ are, respectively, the displacements of the global and local minima of the potential $\Phi(u)$ under the influence of the force F which can be found by solving the equation $d\Phi(u)/du=F$. This means that Eq. (3) for $F\neq 0$ admits a set of locally stable uniform states $u_n(F)$ and $u_\nu(F)$ which are periodically (with period 1) arranged on the axis of displacements. The potential energies of these states, $\Phi^{(F)} \times [u_n(F)]$ and $\Phi^{(F)}[u_\nu(F)]$ for arbitrary values of the force F, generally speaking, are different, but there exist one positive value $F_1>0$ and one negative $F_2<0$ value for which the energies of pairs of neighboring states are equal (Fig. 4). These states are separated by intervals $\delta+u_\delta(F_1)-u_0(F_1)$ and $(1-\delta)+u_0)(F_2)-u_\delta(F_2)$, and the values of the force $F_i(i=1,2)$ are solutions of the equation

$$\Phi[\delta+u_\delta(F)]-\Phi[u_0(F)] + [(i-1-\delta)-u_\delta(F)+u_0(F)]F=0. \tag{43}$$

For considering the potential $\Phi^{(F)}(u)$ at the critical values of the force $F=F_i$ within the period $n=0$, we introduce the notation

$$\max[\Phi(u)-F_i u]-\min[\Phi(u)-F_i u]=\tilde{\Phi}_m^{(i)}, \tag{44}$$

$$\pm[u_0(F_i)-u_\delta(F_i)+(i-1-\delta)]=\tilde{\sigma}_i, \quad i=1,2. \tag{45}$$

The presence of two neighboring spatially uniform states $u_0(F_i)+(i-1)$ and $\delta+u_\delta(F_i)$ with the same values of the potential energy (Fig. 4) creates the necessary condition for the existence of stable solitary waves of stationary profile $u(x,t)=u_\sigma(x-V_\sigma t)$ moving with an arbitrary constant velocity V_σ. The topological charges of these waves, $\sigma=\tilde{\sigma}_i(i=1,2)$ are determined by relation (45); they can be specified by the boundary conditions, fixing the indicated uniform states at infinity. The internal structure of such excitations and the kinks corresponding to them is analogous to the structure of the fractional crowdions described in Sec. 1 (Fig. 2c). The first and second integrals of equation (3) with allowance for boundary conditions fixing the topological charge $\tilde{\sigma}_i$ are determined by expressions analogous to (7) and (8): in these expressions one must set $q_i=\tilde{\sigma}_i$, the potential $\Phi(u)$ must be replaced by the renormalized potential

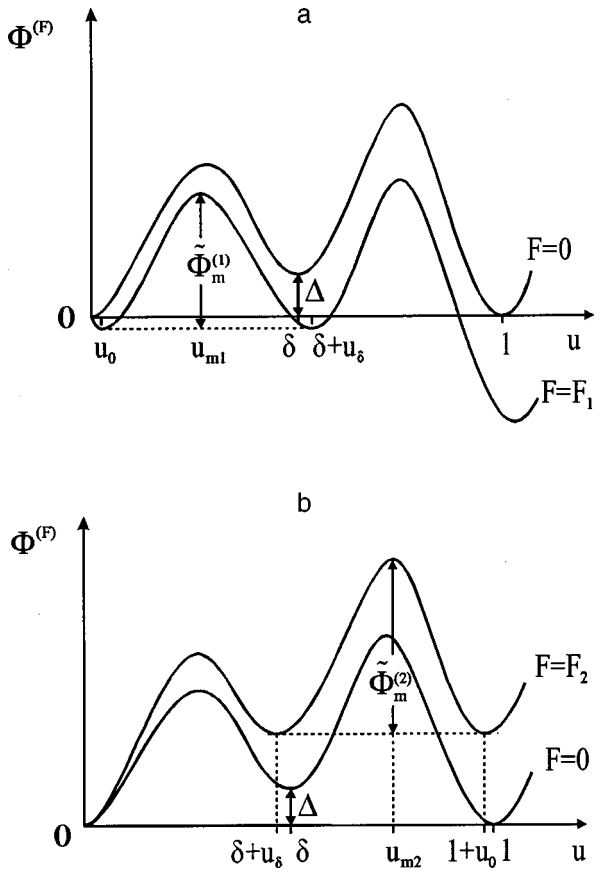

FIG. 4. Transformation of a double-barrier potential $\Phi(u)$ under the influence of a uniform external force F: a—initial ($F=0$) and critical ($F=F_1$) configurations of the total potential $\Phi^{(F)}(u)=\Phi(u)-Fu$ for positive values of the force F_1; b—the same, for negative values of the force F_2.

$$\tilde{\Phi}^{(i)}(u)=\Phi(u)-\Phi[u_0(F_i)]-[u-u_0(F_i)-(i-1)]F_i, \quad i=1,2, \tag{46}$$

and, instead of ε_i, as the lower limit of integration in (8) one should use the value u_{mi}; the location of maximum of the function $\tilde{\Phi}^{(i)}(u)$, where it has a height $\tilde{\Phi}_m^{(i)}$ given by (44) and separates the two wells of equal depth under consideration.

The energy, effective rest mass, and characteristic width of the given crowdions can be calculated using formulas (19) and (20), replacing Φ_{mi} by $\tilde{\Phi}_m^{(i)}$ and replacing the integral $I_{\sigma i}$ by

$$\tilde{I}_{\sigma i}=\int_0^{|\tilde{\sigma}_i|}\sqrt{2\tilde{\Phi}^{(i)}[u+u_0(F_i)+(i-1)(1-|\tilde{\sigma}_i|)]}du, \quad i=1,2. \tag{47}$$

It is easy to show that at sufficiently small values of the parameter Δ one has to a first approximation $u_0(F) \simeq F/\Phi''(0)$ and $u_\delta(F)\simeq F/\Phi''(\delta)$, and the solution of equation (43) for the critical force F_i and the topological charges $\tilde{\sigma}_i$ of the ''critical crowdions'' have the form

$$F_i=\frac{\Delta}{\delta+1-i}, \tag{48}$$

$$\tilde{\sigma}_i = \pm(i-1-\delta)\left[1+\frac{\Delta}{(i-1-\delta)^2}\,\frac{\Phi''(0)-\Phi''(\delta)}{\Phi''(0)\Phi''(\delta)}\right],$$

$$i=1,2. \tag{49}$$

For $\Delta\to 0$ the ''critical crowdions'' are transformed into fraction crowdions with topological charges $\sigma_1=\pm\delta$ and $\sigma_2=\pm(1-\delta)$, and at small but finite values of Δ the parameters of the critical and ordinary subcrowdions differ by small quantities proportional to Δ.

We also note that relation (48) can be given a simple physical interpretation. The quantity Δ (Δ/b in the original units) is the energy density per unit length, i.e., tension force of a semi-infinite stacking fault, which arises when an individual unstable partial crowdion appears in the crystal. This tension is equivalent to a force applied to the partial crowdion, expelling it from the crystal:

$$\mathcal{F}_{\sigma i}^{(\Delta)} = (-1)^{i+1}\,\mathrm{sgn}(\sigma_i)\Delta. \tag{50}$$

At the same time, in the presence of an external force F applied to the atoms of a close-packed row, the effective force acting on a crowdion with topological charge σ_i is (Refs. 3 and 9)[4)]

$$\mathcal{F}_{\sigma i}^{(F)} = -\sigma_i F. \tag{51}$$

It is easily verified that relation (48) agrees with the balance condition for these forces, $\mathcal{F}_{\sigma i}^{(\Delta)}+\mathcal{F}_{\sigma i}^{(F)}=0$, under which a partial crowdion is converted into a stable subcrowdion moving with an arbitrary constant velocity.

Direct experimental observation of critical subkinks is complicated by the difficulty of realizing an exact equality $F=F_i$. Therefore, from the standpoint of experiment, one is mainly interested in the anomalies of the kinetic characteristics that should arise in systems with a double-barrier potential $\Phi(u)$ when $F\to F_i$. These anomalies have been detected, e.g., in studies of the low-temperature plasticity of a number of body-centered metals with double-barrier Peierls relief for dislocations.[13,27–30]

The existence conditions for stable stationary crowdions (solitary waves) acquire an additional specific condition when, for the displacement field $u(x,t)$ in Eq. (3), one takes into account, in addition to the potential force F, the force of dynamic friction $f(\dot{u})$:

$$\ddot{u}-u''-f(\dot{u})+\frac{d}{du}\Phi(u)=F. \tag{52}$$

Let us discuss the changes that are brought about by the introduction of the dynamic friction force in the existence conditions of fractional crowdions for $F=0$. We saw above that in the case of a double-barrier potential $\Phi(u)$ (Fig. 2d), solitary waves with a stationary profile and fractional topological charge cannot exist in the absence of external forces, but the situation is fundamentally different when the friction force is taken into account. We write the double-barrier potential $\Phi(u)$ in the form of a sum (31) of a double-well potential $\Phi^{(DW)}(u)$ with an intermediate absolute minimum at the point δ (Fig. 2c) and a positive admixture $\varphi(u)$, which reaches a maximum at the point δ and, together with its first derivative, vanishes at the boundaries of the intervals $[0,1]$ and $[\varepsilon_1,\varepsilon_2]$: $\varphi(\delta)=\Delta\ll\Phi_{mi}$, $\varphi'(\delta)=\varphi(0)=\varphi(1)=\varphi(\varepsilon_i)=\varphi'(0)=\varphi'(1)=\varphi'(\varepsilon_i)=0$. Formally we shall consider the force $f(\dot{u})$ together with the potential $\varphi(u)$ to be small quantities and use perturbation theory methods for analysis of the nonlinear excitations of the field $u(x,t)$. The corresponding inequality ensuring satisfactory convergence of the perturbation theory procedure will be obtained at the end of this Section.

As the zeroth approximation of perturbation theory we choose the subcrowdions corresponding to the potential $\Phi^{(DW)}(u)$:

$$u(x,t)=u_{\sigma i}(x-Vt)+\eta(x-Vt), \tag{53}$$

$$(1-V^2)u''_{\sigma i}-\frac{d}{du_{\sigma i}}\Phi^{(DW)}(u_{\sigma i})=0, \tag{54}$$

$$\sigma_i=\pm[i-1+(3-2i)\delta], \quad i=1,2. \tag{55}$$

The perturbation $\eta(\xi)$ of the displacement field and the parameter V are unknown quantities to be determined. It is natural to assume that the dynamic friction does not affect the systematics or values of the topological charges but can only to some degree distort the structure of the central parts of the crowdions. Formally this assumption reduces to imposing boundary conditions of the following form on the perturbation $\eta(\xi)$:

$$\eta(\pm\infty)=\eta'(\pm\infty)=0. \tag{56}$$

The first approximation of perturbation theory corresponds to the equation

$$\frac{d}{du}\Phi(u)\simeq\frac{d}{du_{\sigma i}}\Phi^{(DW)}(u_{\sigma i})+\frac{d}{du_{\sigma i}}\varphi(u_{\sigma i})+\frac{d^2}{du_{\sigma i}^2}\Phi^{(DW)}(u_{\sigma i})\,\eta,$$

$$f(\dot{u})\simeq -f(Vu'_{\sigma i}).$$

As a result, we obtain a linear differential equation for the perturbation $\eta(\xi)$:

$$(1-V^2)\,\eta''-\frac{d^2}{du_{\sigma i}^2}\Phi^{(DW)}(u_{\sigma i})\,\eta=\frac{d}{du_{\sigma i}}\varphi(u_{\sigma i})+f(Vu'_{\sigma i}). \tag{57}$$

In the presence of a friction force $f(\dot{u})$ a wave with the stationary profile (53) cannot satisfy equation (52) for arbitrary values of the velocity V, and the problem therefore reduces to one of determining not only the functions $\eta(\xi)$ but also the permissible values of the crowdion velocity $V=V_{\sigma i}^{(f)}$: in general these values depend on the form and parameters of the functions $f(\dot{u})$ and $\Phi(u)$. The permissible values of the velocity can be established by using the well-known alternative theorem in the theory of linear differential equations.[31,32] The existence condition for the solution of the inhomogeneous linear equation (57) with boundary values (56) is that the right-hand side of this equation be orthogonal to the particular solution $\eta^{(0)}(\xi)$ corresponding to its homogeneous equation with the same boundary values. In finding this solution we make use of the equation of the zeroth approximation (54). Differentiating Eq. (54) with respect to the coordinate ξ, we obtain

$$(1-V^2)(u'_{\sigma i})''-\frac{d^2}{du_{\sigma i}^2}\Phi^{(DW)}(u_{\sigma i})u'_{\sigma i}=0. \tag{58}$$

Comparing Eqs. (58) and (57) and taking into according the absence of crowdion deformations at infinity, $u'_{\sigma i}(\pm\infty)=0$, we come to the conclusion that the required partial solution of the homogeneous equation (57) can be taken as $\eta^{(0)}(\xi)=u'_{\sigma i}(\xi)$. Thus the condition determined by the alternative theorem reduces to the equation

$$\int_{-\infty}^{\infty}u'_{\sigma i}(\xi)f[Vu'_{\sigma i}(\xi)]d\xi=(-1)^i\,\mathrm{sgn}(\sigma_i)\Delta. \tag{59}$$

Thus the derivative $u'_{\sigma i}(\xi)$ satisfies relation (7) with the potential $\Phi^{(DW)}(u)$ and $q=\sigma_i$, and the friction force is assumed to be an odd function of velocity, $f(-\dot{u})=-f(\dot{u})$; then the left-hand side of Eq. (59) can be expressed in terms of the potential $\Phi^{(DW)}(u)$ and as

$$\mathcal{F}_{\sigma i}^{(f)}(V)+(-1)^{i+1}\,\mathrm{sgn}(\sigma_i)\Delta=0, \tag{60}$$

$$\mathcal{F}_{\sigma i}^{(f)}(V)=\int_0^{|\sigma_i|}f\left[\frac{V\sqrt{2\Phi^{(DW)}[u-(i-1)|\sigma_i|]}}{\sqrt{1-V^2}}\right]du. \tag{61}$$

Thus, if the atoms of the distinguished row are acted upon by dynamic friction, a necessary condition for the existence of stationary crowdion excitations with fractional topological charges is the presence of real solutions $V=V_{\sigma i}^{(f)}$ of equation (60). We also note that Eq. (60) allows us to interpret the quantity $F_{\sigma i}^{(f)}(V)$ as an effective force of dynamic drag on the crowdion due to the dissipative properties of the individual atoms. In such an interpretation, Eq. (60) represents the balance of two forces: the drag force $\mathcal{F}_{\sigma i}^{(f)}(V)$ (61) and the force of linear tension $\mathcal{F}_{\sigma i}^{(\Delta)}$ (50) of a semi-infinite stacking fault, which arises at infinity when a partial crowdion appears in the crystal if $\Delta\neq 0$.

As an example which admits solution of this problem in explicit form, let us consider the case of a linear drag on the atoms: $f(\dot{u})=-\beta\dot{u}$, where β is the coefficient of atomic viscosity. In this case

$$\mathcal{F}_{\sigma i}^{(f)}(V)=-\frac{I_{\sigma i}\beta V}{\sqrt{1-V^2}},$$

$$I_{\sigma i}=\int_0^{|\sigma_i|}\sqrt{2\Phi^{(DW)}[u-(i-1)|\sigma_i|]}du, \tag{62}$$

and the velocity of steady motion of a fractional crowdion with topological charge σ_i is

$$V_{\sigma i}^{(f)}=\frac{(-1)^{i+1}\,\mathrm{sgn}(\sigma_i)\Delta}{\sqrt{\Delta^2+\beta^2I_{\sigma i}^2}}. \tag{63}$$

Analysis of Eq. (57) for the perturbation $\eta(\xi)$ near the centers ξ_i of the fractional crowdions with allowance for the above stipulations as to the properties of the potential $\varphi(u)$ and for relation (63) yields an estimate of the characteristic values of the perturbation:

$$\eta(\xi_i)=\frac{(-1)^i\Delta\sqrt{2\Phi_{mi}}}{I_{\sigma i}|\Phi''(\varepsilon_i)|}. \tag{64}$$

Consequently, the condition of applicability of the continuum approximation, $V_{\sigma i}^{(f)}\ll 1$, and the condition of convergence of the above perturbation theory procedure, $\eta(\xi_i)\ll u_{\sigma i}(\xi_i)=i-1+(3-2i)\varepsilon_i$, reduces to two inequalities:

$$\Delta\ll\beta I_{\sigma i},\quad \Delta\ll[i-1+(3-2i)\varepsilon_i]\frac{|\Phi''(\varepsilon_i)|I_{\sigma i}}{\sqrt{2\Phi_{mi}}}. \tag{65}$$

We note that the specific dynamic crowdion with fractional topological charge described above, which exists in a viscous crystalline matrix, is analogous from a general physical standpoint to a well-known entity in the theory of magnetic solitons: π domain walls, which move with a constant velocity in a dissipative magnetic medium under the influence of a uniform magnetic field (the so-called Walker regime of domain-wall motion).

The above analysis of two particular cases is easily generalized to the case when both an external force $F\neq 0$ and a force of friction $f\neq 0$ are simultaneously present in Eq. (52). In this case the double-barrier potential $\Phi(u)$ (Fig. 2d) with a sufficiently deep intermediate minimum ($\Delta\ll\Phi_{mi}$) also admits the existence of stable solitary waves with stationary profile and fractional topological charges $\sigma_i\simeq\pm\delta,\pm(1-\delta)$. The velocity $V_{\sigma i}^{(F,f)}$ of these waves depends on both the forces F and f and the parameters of the potential $\Phi(u)$. In an approximation linear in Δ and F the values of $V_{\sigma i}^{(F,f)}$ are solutions of the balance equation between the tension force of the stacking fault (50), the external force (51), and the force of friction (61):

$$\mathcal{F}_{\sigma i}^{(\Delta)}+\mathcal{F}_{\sigma i}^{(F)}+\mathcal{F}_{\sigma i}^{(f)}(V)=0. \tag{66}$$

If the drag on the atoms is of a linear character, then the velocity $V_{\sigma i}^{(F,f)}$ is found to be

$$V_{\sigma i}^{(F,f)}=(-1)^{i+1}\,\mathrm{sgn}(\sigma_i)\frac{(-1)^i|\sigma_i|F+\Delta}{\sqrt{[(-1)^i|\sigma_i|F+\Delta]^2+\beta^2I_{\sigma i}^2}},$$

$$i=1,2. \tag{67}$$

In the numerator of this expression is the total force exerted on the kink by the stacking fault and the external force field; the correctness of this result is conditional on a sufficiently small value of this force. When this force is equal to zero, a nonzero friction force ($\beta\neq 0$) admits the existence of static fractional crowdions only.

CONCLUSION

The main goal of this study was to apply to the description of crowdions in complex crystal structures the concepts of fractional and split topological solitons—concepts which were formulated previously in the study of other problems of nonlinear mechanisms.[8] In the Introduction we set forth the main prerequisites that allow the problem of the dynamics of crowdion excitations in a three-dimensional crystal to be reduced to analysis of the one-dimensional Frenkel–Kontorova model with a complicated substrate potential $\Phi(u)$ and the Klein–Gordon nonlinear equation (3) corresponding to that model. In Sec. 1 of this paper we mainly set forth the known concepts of the theory of topological solitons: what was original was that the exposition was couched in the most general form possible, permitting a unified description of the

structure and properties of solitons (crowdions) for any complicated form of the potential profile $\Phi(u)$ and for arbitrary values and signs of the topological charges. A comparative analysis was made of the characteristics of solitons with integer and fractional topological charges as independent stable nonlinear excitations of a multiply degenerate physical vacuum, and the commonalities and differences of the properties of whole solitons and subsolitons were noted.

In Sec. 2 the splitting of whole solitons (crowdions) into partial solitons and the conditions for this effect, which takes place in the case of a so-called multibarrier potential $\Phi(u)$, were described in the most general form possible. Previously the splitting effect had been described for certain types of specific symmetric double-barrier potentials $\Phi(u)$ admitting explicit solution of the Klein–Gordon equation. In contrast to the earlier studies, our analysis did not presuppose obtaining exact solutions of the Klein–Gordon equation in explicit form. Here we have described the qualitative prerequisites that permit the introduction of the concept of partial (virtual) topological solitons and the stacking fault joining them, and we also obtained analytical asymptotic expressions for the geometric and energy characteristics of the individual fragments of a split soliton in the case of a double-barrier potential $\Phi(u)$ of arbitrary form. A qualitative description was given for the asymptotic decay of a whole topological soliton into free subsolitons when the double-barrier potential is transformed into a double well. We have also obtained in explicit form an exact solution of the problem of the splitting and decay of a whole solitons for the particular example of an asymmetric piecewise-continuous parabolic potential $\Phi(u)$. We have briefly discussed the analogies between split crowdions and split dislocations and the possible physical effects due to the splitting of crowdions in crystals with a complex structure.

In Sec. 3 we discussed the special types of fractional topological solitons (crowdions) that can arise in the case of a multibarrier potential $\Phi(u)$ in the presence of external or dynamic friction forces acting on the atoms of a close-packed row in a complex crystal. The necessary condition for transforming a partial crowdion into a free stable subcrowdion is the balance of three forces: the external force, the force of friction, and the tension force of a semi-infinite stacking fault. We briefly discussed the possibility of observing solitons of this type in experiments and noted their analogy with the π domain walls that exist in magnets in a uniform external magnetic field.

The authors are sincerely grateful to A. S. Kovalev and M. M. Bogdan for a discussion of the problems addressed in this paper and for some constructive criticism.

*E-mail: smirnov@ilt.kharkov.ua

1) The next approximation of crowdion theory is to take into account the elastic compliance and deformation of the crystalline matrix. That leads to a certain renormalization of the crowdion characteristics without altering the qualitative ideas about the crowdion excitation.[9]

2) A piecewise parabolic approximation of the potential $\Phi(u)$ is often used in the analysis of topological solitions in various physical models.[12,14,22,23]

3) In the physics of crystals the analogy between topological solitons in the Frenkel-Kontorova one-dimensional crystal model and dislocations in a three-dimensional crystal is often discussed. From this standpoint the partial (virtual) crowdions described above and the atomic-row stacking faults joining them are one-dimensional analogs of partial dislocations and atomic-plane stacking faults.

4) Unfortunately, as a result of a technical error the sign of this force was indicated incorrectly in Ref. 9.

[1] H. R. Paneth, Phys. Rev. **80**, 708 (1950).
[2] J. Friedel, *Dislocations* [Pergamon Press, Oxford (1964); Mir, Moscow (1967)].
[3] A. M. Kosevich, *Theory of the Crystal Lattice* [in Russian], Vishcha Shkola, Kharkov (1988).
[4] I. F. Lyuksutov, A. G. Naumovets, and V. L. Pokrovskiĭ, *Two-Dimensional Crystals* [in Russian], Naukova Dumka, Kiev (1988).
[5] G. Kaush, *Destruction of Polymers*, Moscow, Mir (1981).
[6] V. R. Regel', A. I. Slutsker, and É. E. Tomashevskiĭ, *Kinetic Nature of the Strength of Solids* [in Russian], Nauka, Moscow (1974).
[7] Ya. I. Frenkel', *Introduction to the Theory of Metals* [in Russian], Nauka, Leningrad (1972).
[8] O. M. Braun and Yu. S. Kivshar, Phys. Rep. **306**, 1 (1998).
[9] V. D. Natsik and E. I. Nazarenko, Fiz. Nizk. Temp. **26**, 283 (2000) [Low Temp. Phys. **26**, 210 (2000)].
[10] K. Lonngren and A. Scott (Eds.), *Solitons in Action* [Academic Press, New York (1978); Mir, Moscow (1981)].
[11] R. K. Bullough and P. J. Caudrey (Eds.), *Solitons* [Springer-Verlag, Berlin (1980); Mir, Moscow (1983)].
[12] R. K. Dodd, J. C. Eilbeck, J. Gibbon, and H. C. Morris, *Solitons and Nonlinear Wave Equations* [Academic Press, New York (1982); Mir, Moscow (1988)].
[13] P. Guyot and J. E. Dorn, Can. J. Phys. **45**, 983 (1967).
[14] A. M. Kosevich and A. S. Kovalev, *Introduction to Nonlinear Physical Mechanics* [in Russian], Naukova Dumka, Kiev (1989).
[15] M. Peyrard and M. Remoissenet, Phys. Rev. B **26**, 2886 (1982).
[16] M. Remoissenet and M. Peyrard, Phys. Rev. B **29**, 3153 (1984).
[17] K. Maki and P. Kumar, Phys. Rev. B **14**, 118, 3920 (1976).
[18] S. Burdick, M. El-Batanouny, and C. R. Willis, Phys. Rev. B **34**, 6575 (1986).
[19] A. M. Kosevich and A. S. Kovalev, ''Theory of the dynamic crowdion in a three-dimensional highly anisotropic medium,'' in *Dynamics of Dislocations*, Naukova Dumka, Kiev (1975).
[20] A. S. Kovalev, A. D. Kondratyuk, A. M. Kosevich, and A. I. Landau, Phys. Rev. B **48**, 4122 (1993); Phys. Status Solidi B **177**, 177 (1993).
[21] A. I. Landau, A. S. Kovalev, and A. M. Kosevich, Phys. Status Solidi B **179**, 373 (1993).
[22] M. M. Bogdan, A. M. Kosevich, and G. A. Maugin, Condens. Matter Phys. **2**, 255 (1999).
[23] O. K. Dudko and A. S. Kovalev, Fiz. Nizk. Temp. **26**, 821 (2000) [Low Temp. Phys. **26**, 603 (2000)].
[24] A. Hubert, *Theorie der Domänenwände in Geordneten Medien* [Springer-Verlag, Berlin (1974); Mir, Moscow (1977)].
[25] J. P. Hirth and J. Lothe, *Theory of Dislocations* [McGraw-Hill, New York (1967); Atomizdat, Moscow (1972)].
[26] P. Tchofo Dinda and C. R. Willis, Phys. Rev. E **51**, 4958 (1995).
[27] E. Kuramoto, Y. Aono, and T. Tsutsumi, Cryst. Res. Technol. **19**, 331 (1984).
[28] B. V. Petukhov and Yu. I. Polyakov, Kristallografiya **32**, 1324 (1987) [Sov. Phys. Crystallogr. **32**, 778 (1987)].
[29] T. Suzuki, H. Koizumi, and H. O. K. Kirchner, Acta Metall. Mater. **43**, 2177 (1995).
[30] A. N. Diulin, G. I. Kirichenko, V. D. Natsik, and V. P. Soldatov, Fiz. Nizk. Temp. **24**, 595 (1998) [Low Temp. Phys. **24**, 452 (1998)].
[31] R. Courant and D. Hilbert, *Metods of Mathematical Physics, Vol. I* [Interscience, New York (1953), (1962); Gostekhteorizdat, Moscow, Leningrad (1933)].
[32] E. Madelung, *Die Mathematischen Hilfsmittel des Physikers*, 6th ed. [Springer-Verlag, Berlin (1957); Fizmatgiz, Moscow (1960)].

Translated by Steve Torstveit

LETTERS TO THE EDITOR

Effect of argon on the thermal expansion of fullerite C_{60} at helium temperatures

A. N. Aleksandrovskii, V. G. Gavrilko, V. B. Esel'son, V. G. Manzhelii, B. G. Udovidchenko, and V. P. Maletskiy

B. Verkin Institute for Low Temperature Physics and Engineering of the National Academy of Sciences of Ukraine, Lenin Ave. 47, 61164, Kharkov, Ukraine

B. Sundqvist

Umea University, Department of Experimental Physics, 90187, Umea, Sweden
(Submitted December 26, 2000)
Fiz. Nizk. Temp. **27**, 333–335 (March 2001)

The linear thermal expansion of compacted Ar-doped fullerite $C_{60}(Ar_xC_{60})$ is investigated at 2–12 K using a dilatometric method. The thermal expansion of Ar_xC_{60} is also studied after partial desaturation of argon from fullerite. It is revealed that argon doping resulted in a considerable change of the temperature dependence of the thermal expansion of fullerite. An explanation of the observed effects is proposed. © *2001 American Institute of Physics.*
[DOI: 10.1063/1.1355522]

We have previously reported the detection and investigation of a negative linear thermal expansion coefficient α of fullerite C_{60} at helium temperatures.[1,2] The effect was tentatively attributed to tunneling transitions between energetically equivalent orientations of C_{60} molecules. To test this assumption, we have studied the thermal expansion of Ar-doped C_{60} at liquid helium temperatures. The results of these studies are presented in this communication. In a fullerite crystal each C_{60} molecule is associated with two tetrahedral and one octahedral interstitial cavities[3] whose average linear dimensions are about 2.2 Å and 4.2 Å, respectively.[4] According to x-ray[5] and neutron diffraction[6,8] data, the Ar atoms, with a gas-kinetic diameter 3.405 Å,[7] occupy only the octahedral cavities. It should also be noted that at 15 K the lattice parameter of a saturated Ar_xC_{60} solution is 0.006 Å smaller than that of fullerite.[6] We assumed that the Ar atoms occupying the octahedral interstices would increase the potential barrier impeding rotation of the C_{60} molecules and thus diminish the probability of rotational tunnel transitions and consequently the tunneling splitting of the ground state of the molecules.[2] If this assumption is correct, the total negative thermal expansion $\int \alpha\, dT$ should decrease and the region of negative expansion should shift towards lower temperatures after doping.

An Ar-doped C_{60} sample was studied at 2–12 K using a high-sensitivity capacitive dilatometer[9] and with the same procedure as was applied to pure C_{60} earlier.[1,2] The sample was prepared by compacting high-purity (not worse than 99.98% C_{60}) powder under about 1 kbar. The grain sizes were 0.1–0.3 mm. The resulting C_{60} sample was a cylinder 9 mm high and 10 mm in diameter. The thermal expansion coefficient along the cylinder axis was first measured at 2–12 K before doping. The evacuated sealed measuring cell with the sample was then warmed to room temperature and filled with argon under atmospheric pressure. The doping lasted for 19 days.

When the doping process was completed, the Ar-filled measuring cell with the sample was slowly cooled to helium temperatures. In this case both the phase transitions of C_{60} (at 260 and 90 K) occurred in an Ar atmosphere. Figure 1 shows the measured coefficients before (curve *1*) and after (curve *2*) Ar-doping. It is seen that the doping not only leads to the expected decrease in the negative thermal expansion and its shift towards lower temperatures but that is also reduces strongly the (positive) thermal expansion coefficient above 5.5 K.

It seems natural to assume that the Ar-induced increase in the barrier impeding rotational motion of the C_{60} molecules should also enhance the angular dependence of the noncentral forces acting upon the C_{60} molecules. As a result,

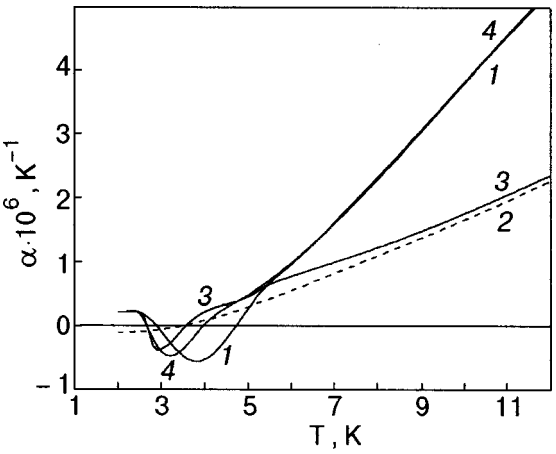

FIG. 1. Temperature dependences of the thermal expansion of compacted fulletite C_{60}: pure fullerite before doping (*1*); Ardoped fullerite (*2*); fullerite after evacuation of Ar for 3 days (*3*) and for 45 days (*4*).

the frequencies of the orientational oscillations of the molecules should increase, and hence the normal (positive) thermal expansion coefficient dependent on these oscillations should decrease. This is what we observed experimentally at $T > 5.5$ K. The experimental results can thus be explained qualitatively by proceeding from the assumption that the atomic Ar impurity introduced to the octahedral interstices of C_{60} suppresses the splitting of the ground state of the C_{60} molecules and modifies the orientational oscillation spectrum of the molecules.

It appears that dissolved Ar atoms influence the thermal expansion very strongly even though they are able to move quite freely inside the octahedral lattice interstices. We should also bear in mind that in our experiment the Ar atoms occupy only a part of the octahedral interstices. We did not estimate the quantity of the dissolved Ar. According to Morosin *et al.* [10] neon occupies only 21% of the octahedral interstices under identical conditions (room temperatures, atmospheric pressure). Taking into account that in a simple cubic lattice each of C_{60} molecules is surrounded by six octahedral interstices, the 21% occupancy implies that with randomly distributed impurity atoms, about 75% of the C_{60} molecules have Ar atoms nearby. However, because the Ar atoms are larger than Ne atoms, this number must be considered an upper limit of occupancy only.

Another important consideration here is that we believe that only a small fraction of the C_{60} molecules (the so-called ''defects'') for which the rotation-impeding barrier U_φ is quite low contributes to the negative thermal expansion of fullerite.[2] Correspondingly, the doping-induced change in the negative thermal expansion is determined only by the Ar atoms neighboring these ''defects.'' At the same time, the positive thermal expansion is affected by all the dissolved Ar atoms.

To obtain more information, we studied how the thermal expansion coefficient changed when the doping atoms were removed from the sample. For this purpose, the measuring cell with the sample was warmed to room temperature and evacuated to 1×10^{-3} mm Hg. The gas evacuation at room temperature lasted for 3 days. The thermal expansion was then measured at low temperatures. The results are shown in Fig. 1 (curve *3*). It is seen that the thermal expansion coefficient changes only slightly above 5 K, but below 3.5 K the negative thermal expansion again has the minimum typical for undoped C_{60}. The measuring cell with the sample was warmed again to room temperature and gas evacuation was continued for 42 days. The thermal expansion coefficient was then measured with the results shown in Fig. 1 (curve *4*). Note, in particular, that after a total of 45 days evacuation of argon the ''high-temperature'' part of the thermal expansion coefficient was restored completely. The negative thermal expansion in the range 2.5–5 K, however, still differed from that of the initial pure sample.

This can be accounted for assuming the following. The octahedral voids adjacent to defects, i.e., C_{60} molecules with low U_φ barriers, form deeper potential wells for the impurity atoms than the regular octahedral interstices do. It is therefore more difficult to remove the impurities from these near-defect regions, and the residual impurities concentrated around defects are precisely those responsible for the negative thermal expansion of fullerite. There is also another fact supporting this assumption. The thermal expansion coefficients α of all our C_{60} samples, both those used in Refs. 1 and 2 and in this study, agree quite well above 5 K but differ considerably in the temperature region where α is negative. These samples were prepared under different conditions and vary in quality and in the amount of residual impurities.

The proposed qualitative explanation of the effect observed cannot replace a consistent theoretical interpretation. Several interesting ideas have been published to date, which are concerned with a tentative mechanism of the negative thermal expansion of molecular crystals.[11] In the case of fullerite, we decide in favor of our explanation since it accounts for the unusually high Grüneisen coefficients, which were observed experimentally.

We wish to thank Yu. A. Freiman, V. M. Loktev, V. D. Natsik, A. I. Prokhvatilov, and M. A. Strzhemechny for participation in the discussion of the results.

The authors are indebted to the Science and Technology Center of Ukraine and the Royal Academy of Sweden for support.

[1] A. N. Aleksandrovskii, V. B. Esel'son, V. G. Manzhelii, A. Soldatov, B. Sundqvist, and B. G. Udovidchenko, Fiz. Nizk. Temp. **23**, 1256 (1997) [Low Temp. Phys. **23**, 943 (1997)].
[2] A. N. Aleksandrovskii, V. B. Esel'son, V. G. Manzhelii, A. Soldatov, B. Sundqvist, and B. G. Udovidchenko, Fiz. Nizk. Temp. **26**, 100 (2000) [Low Temp. Phys. **26**, 75 (2000)].
[3] P. A. Heiney, J. Phys. Chem. Solids **53**, 1333 (1992).
[4] C. H. Pennington and V. A. Stenger, Rev. Mod. Phys. **68**, 855 (1996).
[5] G. E. Gadd, M. James, S. Moricca, P. J. Evans and R. L. Davis, Fullerene Sci. Technol. **4**, 853 (1996).
[6] G. E. Gadd, S. J. Kennedy, S. Moricca, C. J. Howard, M. M. Elcombe, P. J. Evans, and M. James, Phys. Rev. B **55**, 14794 (1997).
[7] V. G. Manzhelii, A. I. Prokhvatilov, I. Ya. Minchina, and L. D. Yantsevich, in *Handbook of Binary Solutions of Cryocrystals* [Begell House Inc., New York; Wallingford (UK) (1996)].
[8] G. E. Gadd, P. J. Evans, D. J. Hurwood, J. Wood, and M. James, Chem. Phys. Lett. **261**, 221 (1996).
[9] A. M. Tolkachev, A. N. Aleksandrovskii, and V. I. Kuchnev, Cryogenics **9**, 547 (1975).
[10] B. Morosin, J. D. Jorgenson, S. Short, G. H. Kwei, and J. E. Shirber, Phys. Rev. B **53**, 1675 (1996).
[11] V. M. Loktev, Fiz. Nizk. Temp. **25**, 1099 (1999) [Low Temp. Phys. **25**, 823 (1999)].

This article was published in English in the original Russian journal. Reproduced here with stylistic changes by AIP.